INSTITUT CHARLES SADRON

UNIVERSITÉ DE STRASBOURG

THÈSE

présentée pour obtenir le grade de

DOCTEUR de l'UNIVERSITÉ DE STRASBOURG

par

Ting LIANG

Supramolecular Polymers of Triarylamines: Studies in Aqueous Medium and Covalent Capture of Their Self-assemblies

Soutenue publiquement le 13 janvier 2017 devant le jury composé de:

Docteur Olivier Colombani (SRSMC UMR 7565, Le Mans) – Rapporteur externe

Professeur Patrice Woisel (CNRS UMR 8207-Universite Lille 1) – Rapporteur externe

Professeur Nicolas Giuseppone (ICS, Université de Strasbourg – CNRS, Strasbourg) – Directeur de thèse

Docteur Emilie Moulin (ICS– CNRS, Strasbourg) – Co-directeur de thèse

Discipline : chimie organique

ABSTRACT

Based on the unique directionality and reversibility of non-covalent interactions, supramolecular self-assembly works as an elegant methodology to construct multifunctional hierarchical architectures. Inspired by nature, where water provides a vital environment for biological process such as biomacromolecular folding, water-soluble supramolecular polymers have been prepared and studied so as to mimic related biological systems. On the other hand, owing to the dynamic nature of their non-covalent bonds, supramolecular polymers often lack mechanical robustness. Thus, cross-linking strategies have been developed in order to combine highly ordered molecular arrangement inherent to the sef-assembly and mechanical robustness of the covalent backbone, which might bee promising to reach functional materials for practical applications.

In this thesis, we focus on well-designed triarylamine molecules which are known to self-assemble into supramolecular polymers with excellent physical properties, as discovered by our group. In particular, molecules studied in this manuscript are based on tris-amide triarylamine scaffold known to produce self-assemblies with metallic conductivity and self-healing behavior. First, we studied the self-assemblies of three novel tris-amide triarylamine derivatives decorated with either poly(ethylene glycol) (PEG), peptide or cyanine dyes side chains on the three amide positions in polar solvents, *i.e.* either water or methanol. Characterizations by various physico-chemical techniques (NMR, UV-Vis absorption, fluorescence, infrared spectroscopies, microscopies, scatterings) demonstrated the formation of fibrillar aggregates for all molecules in such polar environments. Overall, this study suggest that the triarylamine core act as the main driving force for the self-assembly into columnar aggregates while side chains ensure solubility in these solvents and/or favor the formation of chiral architectures. In a second study, we investigated the formation of tris-amide triarylamine supramolecular polymers decorated with norbornene and siloxane end side chains, which could be further used to freeze the self-assembled structures by ring opening metathesis polymerization and sol-gel methods, respectively. While physical and mechanical properties of the chemical gels obtained by sol-gel methodologies remain to be analyzed, first studies on chemical gels obtained by ring opening metathesis polymerization suggested increased robustness and similar optical properties compared to their physical equivalents (supramolecular gels). We believe that these cross-linking strategies could become useful to build up mechanically robust materials with physical properties inherent to the supramolecular polymerization of the molecular building blocks.

Overall, this work extends the current knowledge on triarylamine molecules. In particular, it shows a) that the hydrophobic triarylamine core can be used to drive self-assembly processes in polar solvents such as water similarly to well-known benzenetrisamide (BTA) moieties and b) that physical properties associated with the formation of triarylamine supramolecular polymers can be preserved in their covalent counterpart as soon as the proper pilling of the molecular units remains intact. We believe that these studies could broaden the current applications of triarylamine supramolecular polymers as functional materials.

Résumé en Français

1) Introduction

Pour contrôler les systèmes chimiques complexes, les outils de la Chimie Supramoléculaire s'avèrent puissants et représenteront certainement une des technologies clef du 21e siècle.[1] En effet, la réversibilité intrinsèque des liaisons chimiques impliquées dans la formation d'assemblages supramoléculaires apporte à ces systèmes un caractère "adaptatif", capable de réorganiser leur structure en fonction des conditions environnementales.[2] En 2010, l'équipe du Prof. Giuseppone a découvert les propriétés d'auto-assemblage uniques d'un motif triarylamine spécifique sous l'influence d'un stimulus lumineux.[3] Ce comportement s'avère totalement inédit malgré le grand nombre d'études effectuées sur cette famille de molécules du fait de ses propriétés photoactives.[4] Au cours des dernières années, notre groupe a synthétisé de nombreux dérivés de triarylamines (TAAs), qui ont été utilisés pour produire des architectures supramoléculaires multifonctionnelles.[5] En fonction des différents groupements qui substituent ce coeur TAA, diverses morphologies ont pu être observées et les propriétés physiques de ces auto-assemblages produits dans des solvants non polaires tels que les solvants chlorés ou le toluène se sont également révélées variées (propriétés cristal-liquide,[5] conductrices,[6] plasmoniques[5]...).

A partir de ces travaux, mon projet de thèse consistait en deux objectifs: a) étudier l'auto-assemblage et les propriétés de ces composés TAA dans des solvants polaires comme l'eau ou le méthanol. Pour cela, comme tenu du caractère hydrophobe des TAAs, il s'avérait nécessaire de synthétiser de nouvelles molécules incorporant des groupements latéraux favorisant la solubilité dans de tels solvants; b) stabiliser les auto-assemblages de triarylamine par polymérization covalente et étudier les propriétés physiques associées à ces nouvelles structures. Pour cela, il convenait de synthétiser de nouvelles molécules incorporant des groupements polymérisables sur les chaines latérales, qui n'influençaient pas les propriétés d'auto-assemblages des TAAs.

2) Résultats et discussions

a) Auto-assemblage de triarylamines dans l'eau

L'eau fonctionne comme un micro-environnement spécial pour les auto-assemblages supramoléculaires car elle fournit des liaisons hydrogène et des interactions hydrophobes

---

[1]Lehn, J.-M. *Supramolecular Chemistry: Concepts and Perspectives* VCH, 1995, New York.

[2](a) Aida, T. Meijer, E. W. and Stupp, S. I. Functional Supramolecular Polymers. *Science* **335,** 813–817 (2012); (b) Busseron, E. Ruff, Y. Moulin, E. and Giuseppone, N. Supramolecular self-assemblies as functional nanomaterials. *Nanoscale* **5,** 7098 (2013).

[3]Moulin, E. Niess, F. Maaloum, M. Buhler, E. Nyrkova, I. and Giuseppone, N. The hierarchical self-assembly of charge nanocarriers: A highly cooperative process promoted by visible light. *Angew. Chemie - Int. Ed.* **49,** 6974–6978 (2010).

[4]Ning, Z. and Tian, H. Triarylamine: a promising core unit for efficient photovoltaic materials. *Chem. Commun.* **414,** 5483 (2009).

[5](a) Armao, J. J. Maaloum, M. Ellis, T. Fuks, G. Rawiso, M. Moulin, E. and Giuseppone, N. Healable supramolecular polymers as organic metals. *J. Am. Chem. Soc.* **136,** 11382–11388 (2014); (b) Busseron, E. Cid, J. J. Wolf, A. Du, G. Moulin, E. Fuks, G. Maaloum, M. Polavarapu, P. Ruff, A. Saur, A. K. Ludwigs, S. and Giuseppone, N. Light-Controlled Morphologies of Self-Assembled Triarylamine-Fullerene Conjugates. *ACS Nano* **9,** 2760–2772 (2015); (c) Domoto, Y. Busseron, E. Maaloum, M. Moulin, E. and Giuseppone, N. Control over nanostructures and associated mesomorphic properties of doped self-assembled triarylamine liquid crystals. *Chem. - A Eur. J.* **21,** 1938–1948 (2015); (d) Armao, J. J. Rabu, P. Moulin, E. and Giuseppone, N. Long-Range Energy Transport via Plasmonic Propagation in a Supramolecular Organic Waveguide. *Nano Lett.* **16,** 2800–2805 (2016).

[6]Faramarzi, V. Niess, F. Moulin, E. Maaloum, M. Dayen, J. F. Beaufrand, J. B. Zanettini, S. Doudin, B. and Giuseppone, N. Light-triggered self-construction of supramolecular organic nanowires as metallic interconnects. *Nat. Chem.* **4,** 485–490 (2012).

pour le processus de polymérisation supramoléculaire.[7] Dans une étude fondamentale, le groupe de Meijer a étudié la polymérisation supramoléculaire d'une série de dérivés du benzène-1,3,5-tricarboxamide (BTA) dans l'eau (Figure 1a).[8] Afin de comprendre l'influence des interactions hydrophobes sur le processus d'auto-assemblage, le cœur BTA a été fonctionnalisée avec des chaînes amphiphiles constituées d'un espaceur hydrophobe de différentes longueurs (10-12 CH_2) et d'une extrémité de type tétraéthylène glycol. Fait intéressant, seuls les dérivés de BTA incorporant des espaceurs undecyle et dodécyle ont formé des polymères supramoléculaires stables dans l'eau, comme en témoignent les études de spectroscopies optiques et l'imagerie Cryo-TEM. Des systèmes de copolymères supramoléculaires constitués des dérivés de BTA amphiphiles et des dérivés de BTA marqués avec Cy3 ou Cy5 (5% en moles) ont été utilisés pour confirmer l'apparition du processus de polymérisation grâce au phénomène de transfert d'énergie par résonance Forster (FRET). Cet exemple souligne l'importance de l'ajustement des interactions non covalentes afin d'induire le processus de polymérisation. Dans notre groupe, nous avons synthétisé une série de monomères à base de bis-urée hydrophobes décorés soit de résidus peptidiques bioactifs hydrophiles, soit de colorants de type cyanine fluorescents (Figure 1b).[9] Le monomère peptidique s'est auto-assemblé en un polymère supramoléculaire avec une structure en forme de plaque tandis que le monomère fluorescent a produit un polymère supramoléculaire présentant une structure en forme de ruban. Cependant, les co-auto-assemblages dérivés de mélanges équimolaires de monomères avec différentes chaînes latérales ont conduit à un copolymère supramoléculaire ayant la morphologie similaire à celle observée pour le polymère contenant les chaines latérales fluorescentes.
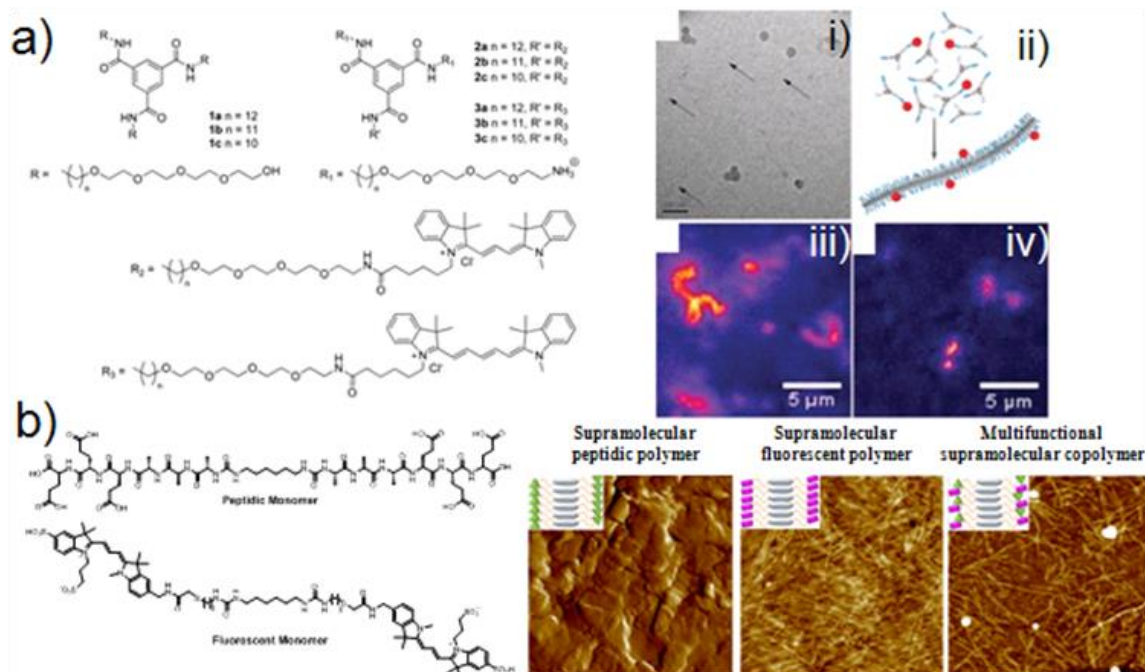
Figure 1: a) Structure chimique des dérivés de la BTA **1a-c**, **2a-c**, **3a-c** et i) Image cryo-TEM de **1b** dans l'eau; ii) représentation schématique du mélange d'une petite quantité de BTA marqués au colorant avec des BTA non marquées avant l'injection dans l'eau, pour permettre l'assemblage des BTA en fibres marquées par fluorescence. Instantanés des films observes par microscopie de fluorescence; iii) fibres formées par **1a** avec 5% de **3a** et iv) fibres formées par **1b** avec 5% de **3b** avec des longueurs proches de la limite de résolution; b) Structures des

[7]Chandler, D. Interfaces and driving force of hydrophobic assembly. *Nature* **437**, 640-647 (2005).

[8]Leenders, C. M. A. Baker, M. B. Pijpers, I. A. B. Lafleur, R. P. M. Albertazzi, L. Palmans, A. R. A. and Meijer, E. W. Supramolecular polymerisation in water; elucidating the role of hydrophobic and hydrogen-bond interactions. *Soft Matter* **12**, 2887–2893 (2016).

[9]Xiang, Y. Moulin, E. Buhler, E. Maaloum, M. Fuks, G and Giuseppone, N. Hydrogen-Bonded Multifunctional Supramolecular Copolymers in Water. *Langmuir* **31**, 7738–7748 (2015).

monomères peptidiques et de monomères fluorescents et images de microscopie à force atomique (AFM) de polymère peptidique supramoléculaire, de polymère fluorescent supramoléculaire et de copolymère supramoléculaire multifonctionnel.

A partir de ces travaux,[9] Nous avons ainsi envisagés la synthèse de trois composés **TAPEG**, **TAPeptide** et **TACy3** incorporant respectivement des groupements latéraux de type poly(éthylène glycol), séquence peptidique et fluorophore de type cyanine soluble en milieu aqueux (Figure 2).

La synthèse du dérivé **TAPEG** a été réalisée en deux étapes (réduction, amidation) avec de bons rendements à partir du composé *N,N*-bis(4-nitrophenyl)benzene-1,4-diamine[5] et du dérivé commercial MeO-PEG$_{16}$-NHS. Le composé **TAPeptide** a été obtenu grâce aux techniques de synthèse peptidique sur support solide (l'étape de couplage du coeur triarylamine sur les chaines peptidiques étant elle-même réalisée sur le support) et à une purification finale par HPLC préparative en phase inverse. Enfin, pour la molécule **TACy3**, nous avons d'abord synthétisé le dérivé cyanine fluorescent **Cy3**[10] à l'échelle du gramme (4 étapes à partir du composé potassium 2,3,3-trimethyl-3H-indole-5-sulfonate) qui a ensuite été couplé à un dérivé triarylamine tris-thiolé[11] pour produire 300 mg de dérivé **TACy3** après purification par HPLC en phase inverse.
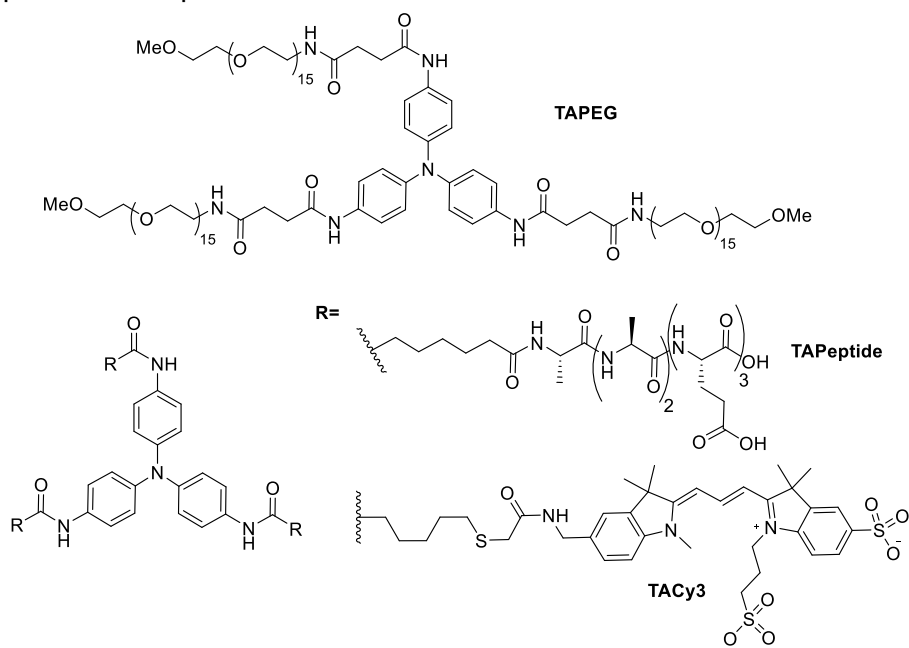
Figure 2: Structures des dérivés triarylamines **TAPEG**, **TAPeptide** et **TACy3** étudiés en solvants polaires.

Ces trois molécules présentent une bonne solubilité dans l'eau et le méthanol, ce qui nous a permis d'étudier leur auto-assemblage par différentes techniques physico-chimiques telles que les spectroscopies optiques, les techniques de diffusion du rayonnement et de microscopie (Figures 3 and 4). Les spectres de fluorescence du composé **TAPEG** présentent des intensités différentes et indiquent donc la formation de structures différentes dans ces deux solvants (Figure 3a). Dans le chloroforme, la bande d'absorption située aux alentours de 800 nm, qui correspond à la présence de radicaux triarylammonium cations,[3] voit son

[10]Tauk, L. Schröder, A. P. Decher, G. and Giuseppone, N. Hierarchical functional gradients of pH-responsive self-assembled monolayers using dynamic covalent chemistry on surfaces. *Nat. Chem.* **1,** 649–656 (2009).

[11]Armao, J. J. Domoto, Y. Umehara, T. Maaloum, M. Contal, C. Fuks, G. Moulin, E. Decher, G. Javahiraly, N. and Giuseppone, N. Supramolecular Organic Nanowires as Plasmonic Interconnects. *ACS Nano* **10,** 2082–2090 (2016).

intensité augmenter sous l'effet de l'irradiation lumineuse (Figure 3d). Cette observation suggère la formation de polymères supramoléculaires pour le dérivé **TAPEG** dans les solvants chlorés *via* des interactions de type transfert de charge. Dans l'eau et le méthanol, des fagots de fibres bien définis ont pu être observés par microscopie électronique à transmission (TEM) avec des longueurs atteignant 1.5 µm dans l'eau et 2.4 µm dans le méthanol (Figure 4a, d).

Figure 3: a) Spectres de fluorescence du composé **TAPEG** dans l'eau (noir) et dans le méthanol (rouge) à une concentration de $5*10^{-5}$ M, excitation à λ = 339 nm, b) Spectres de fluorescence du composé **TAPeptide** dans l'eau (noir) et dans le méthanol (rouge) à une concentration de $5*10^{-5}$ M, excitation à respectivement λ = 318 nm et 305 nm, c) Spectres d'absorption UV-vis du composé **TACy3** dans l'eau (noir) et dans le méthanol (rou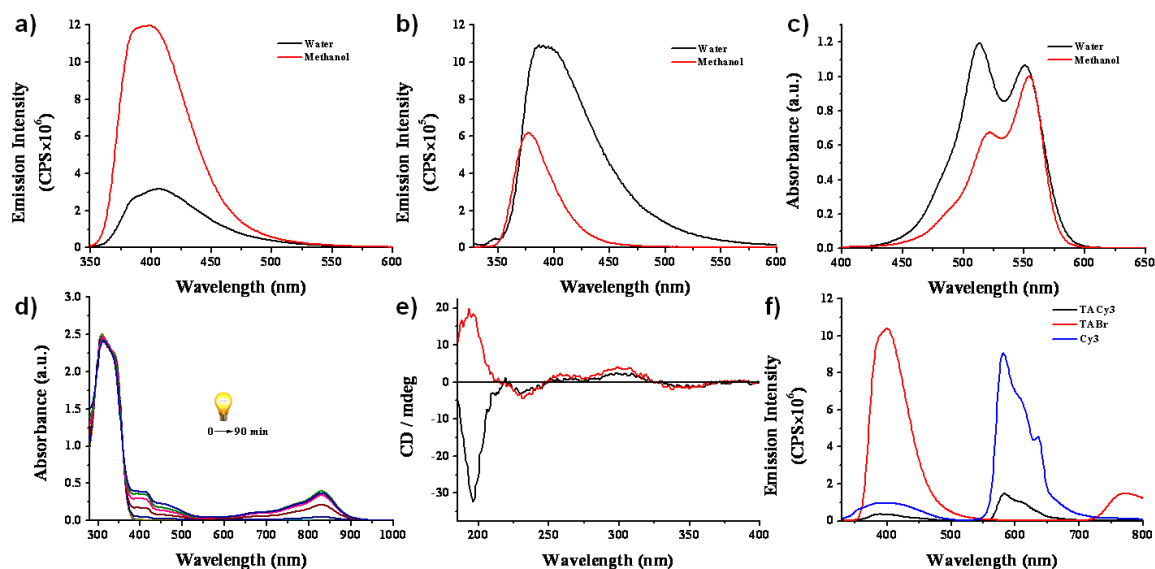ge) à une concentration de $5*10^{-5}$ M, d) Spectres d'absorption UV-vis du composé **TAPEG** dans le chloroforme sous irradiation lumineuse à une concentration de 10^{-4} M, e) Spectre CD du composé **TAPeptide** dans l'eau (noir, [**TAPeptide**] = 10^{-3} M) et dans le méthanol (rouge, [**TAPeptide**] = 10^{-4} M), f) Spectres de fluorescence des composés **TACy3** (10^{-4} M)**, TABr** (10^{-4} M) et **Cy3** ($3*10^{-4}$ M) dans le méthanol, excitation à respectivement λ = 319 nm, 322 nm and 319 nm.

Le spectre de dichroïsme circulaire obtenu pour l'auto-assemblage du composé **TAPeptide** indique la formation d'une structure en feuillets β dans le méthanol, qui peut être induite par les cœurs triarylamines chiraux, alors qu'une structure de type "random coil" est observée pour la même molécule dans l'eau (Figure 3e). Le spectre d'émission de ce composé dans le méthanol présente une intensité plus faible et un maximum d'émission à une longueur d'onde plus petite quand on le compare à celui obtenu dans l'eau (Figure 3b). Cette observation suggère que des structures auto-assemblées différentes sont formées dans ces deux solvants. Cependant, les études de microscopie (TEM) n'ont, pour l'instant, pas mis en évidence de telles différences puisque, aussi bien dans l'eau que dans le méthanol, des structures rigides et similaires sont observées (Figure 4b, e). Compte tenu de la sensibilité au pH du squelette peptidique, nous avons également étudié l'impact du pH sur les morphologies des agrégats par microscopie TEM (Figure 4g and h). Dans le tampon pH = 2 ou pH = 4, des structures micrométriques correspondant à de longues fibres ont été observées, bien que des fibres plus courtes et souples soient enregistrées à pH = 2 par rapport à pH = 4. Ce résultat est en accord avec les observations effectuées par AFM (Figure 4i).

Enfin, une étude de spectroscopie UV-Vis-NIR a mis en évidence un maximum d'absorption décalé vers le bleu pour le composé **TACy3** dans l'eau par rapport au méthanol, démontrant ainsi la formation d'agrégats de type H dans l'eau et l'absence d'agrégation des dérivés

cyanine dans le méthanol (Figure 3c). De plus, pour ce même composé dans le méthanol, une forte diminution de l'intensité de fluorescence associée aux deux unités électro-actives est observée, suggérant qu'il existe un phénomène de transfert d'énergie ou d'électron entre le cœur triarylamine et les dérivés cyanines (Figure 3f). Il est alors intéressant de noter que ces différences spectroscopiques ont pu être corrélées avec la formation d'auto-assemblages présentant des morphologies différentes. En effet, des études de microscopie TEM ont montré la formation de structures en rubans dans l'eau et de vésicules dans le méthanol (Figure 4c, f).
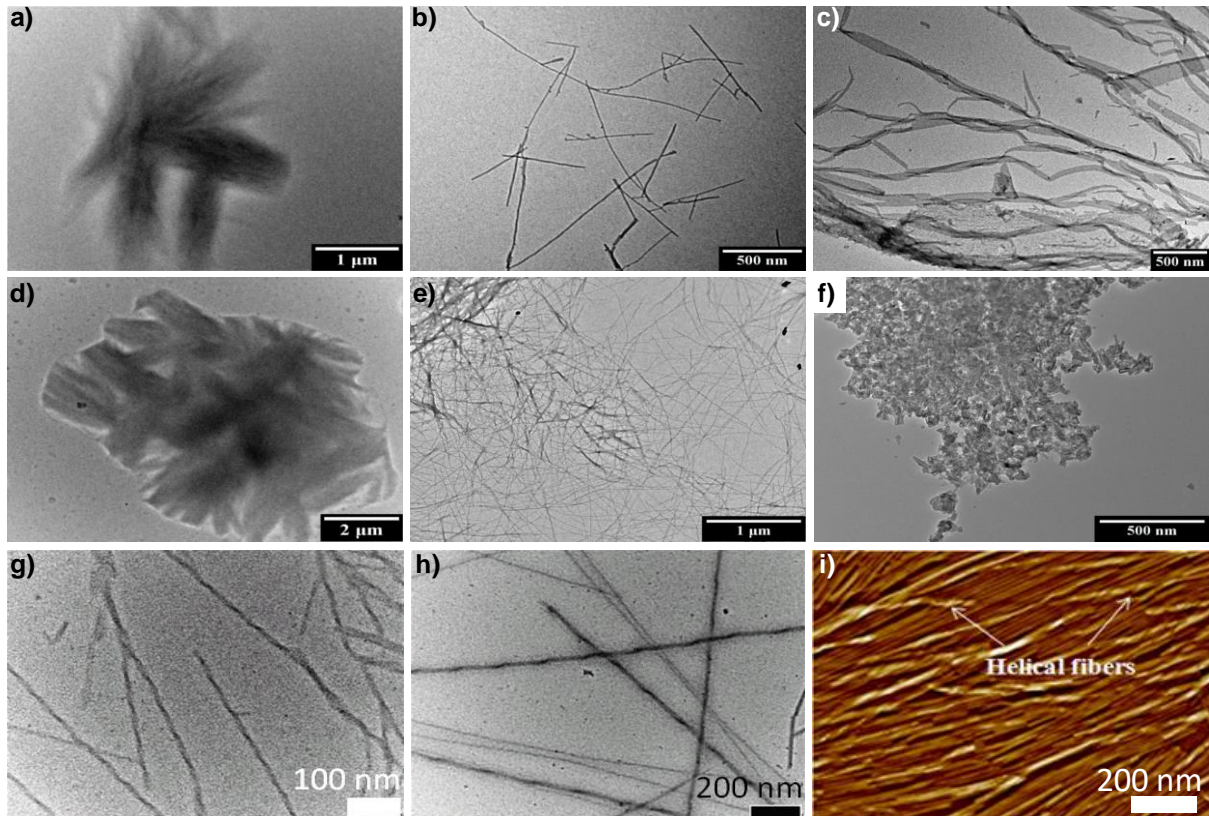
Figure 4: Images TEM obtenues pour les composés a) **TAPEG** dans l'eau, b) **TAPeptide** dans l'eau, c) **TACy3** dans l'eau, d) **TAPEG** dans le méthanol, e) **TAPeptide** dans le méthanol, f) **TACy3** dans le méthanol, g) **TAPeptide** dans le tampon pH=2, h) **TAPeptide** dans le tampon pH=4 et image AFM de i) **TAPeptide** dans le tampon pH=2.

Afin de déterminer précisément les structures des auto-assemblages, notamment l'arrangement local de nos molécules dans les objets auto-assemblés et une détermination plus précise de la taille et de la structure de nos agrégats, nous avons réalisé, en collaboration avec le groupe Prof. Buhler (Université Paris Diderot), une série d'expériences de diffusion de lumière et de neutrons. Dans l'eau et le méthanol, les courbes de diffusion du composé TAPEG suggèrent la formation de structures mono-colonnaires, qui s'agrègent en structures denses par enchevêtrement des chaines latérales PEG. Pour le composé TAPeptide, les données dans l'eau indiquent la présence de polymères enchevêtrés avec une section dont la taille correspond à la formation d'agrégats mono-colonnaires. Cependant, la faible intensité de diffusion enregistrée dans le méthanol n'a pas permis l'identification précise des auto-assemblages de TAPeptide obtenus dans ce milieu. La faible intensité diffusée par le composé TACy3 dans le méthanol indique l'absence d'auto-assemblage dans ce milieu et un signal de diffusion correspondant à celui des monomères. Dans l'eau, la courbe de diffusion pourrait être associée à la formation de chaînes gaussiennes ou à des objets 2D

lisses, mais une étude plus poussée des données s'avère nécessaire pour élucider leur auto-assemblage précis.

Figure 5: Spectres de SANS de a) **TAPEG** dans l'eau (10⁻² M, rouge) et dans le methanol (10⁻² M, bleu), b) **TAPeptide** dans l'eau (10⁻³ M, rouge) et dans le methanol (10⁻⁴ M, bleu), et c) **TACy3** dans l'eau (10⁻² M, rouge) et dans le methanol (10⁻³ M, bleu).

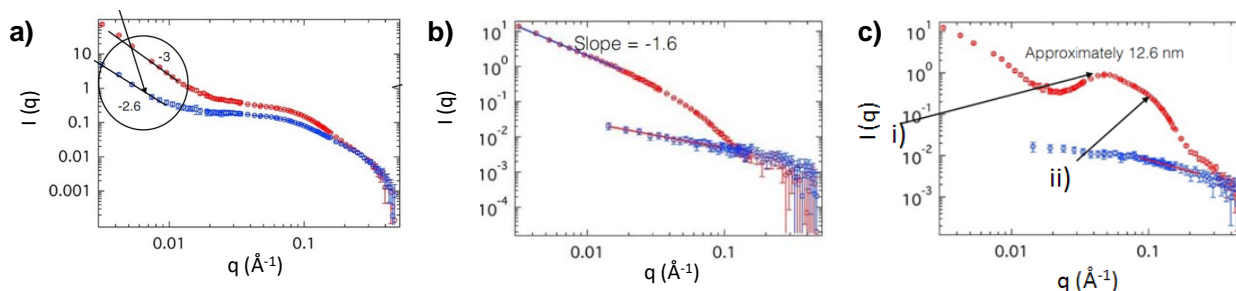Compte tenu de potentiels effets de surface lors des études microscopiques et afin de déterminer précisément les structures des différents auto-assemblages obtenus, nous avons réalisé des études de diffusion des neutrons et de la lumière sur les diverses solutions. Ce travail, en collaboration avec le groupe du Prof. Buhler (Université Paris Diderot), confirme, pour chacune des molécules, la formation de structures différentes dans l'eau et dans le méthanol. Cependant, une analyse plus précise des résultats est en cours de finalisation afin de déterminer précisément l'arrangement local de nos molécules au sein des auto-assemblages ainsi que leur forme et taille précise. Cette étude nous permettra de déterminer si les cœurs TAAs sont empilés de façon similaire à ce qui est observé en solvants non polaires, empilement qui est à l'origine des propriétés remarquables observées au cours de ces dernières années dans notre équipe.[12]

b) Stabilisation de structures auto-assemblées par polymérisation covalente

Les polymères contenant des fragments pi-conjugués sont prometteurs pour construire des dispositifs opto-électroniques en raison de la longue portée des leurs structures ordonnées à l'échelle nanométrique.[13] Cependant, l'essence même des interactions non-covalentes conduit à des polymères supramoléculaires plus fragiles que leurs homologues covalents mais facilite leur mise en œuvre au sein de dispositifs. Dans les processus d'auto-assemblage, certains intermédiaires cinétiques peuvent afficher des propriétés plus intéressantes que les structures finales et il peut donc s'avérer intéressant de les piéger au sein de polymères covalents pour en étudier les propriétés. Le groupe du Prof. Aida a utilisé la polymérisation par ouverture de cycle (ROMP) pour piéger les auto-assemblages thermodynamiquement et cinétiquement favorisés d'un amphiphile hexabenzocoronene (HBC) décoré avec des unités norbornène (Figure 6a).[14] Alors que des structures de type nanocoils sont principalement observées à 15 °C, elles évoluent progressivement vers des

[12]Nyrkova, I. Moulin, E. Armao, J. J. Maaloum, M. Heinrich, B. Rawiso, M. Niess, F. Cid, J. J. Jouault, N. Buhler, E. Semenov, A. N. and Giuseppone, N. Supramolecular self-assembly and radical kinetics in conducting self-replicating nanowires. *ACS Nano* **8,** 10111–10124 (2014).

[13](a) Nalluri, S. K. M. Shivarova, N. Kanibolotsky, A. Zelzer, M. Gupta, S. Frederix, P. W. J. M. Skabara, P. J. Gleskova, H. Ulijn, R. V. *Langmuir* **30**, 12429-12437 (2014); (b) Abbel, R. Grenier, C. Pouderoijen, M. J. Stouwdam, J. W. Leclere, P. E. L. G. Sijbesma, R. P. Meijer, E. W. and Schenning, A. P. H. J. White-Light Emitting Hydrogen-Bonded Supramolecular Copolymers Based on π-Conjugated Oligomers. *J. Am. Chem. Soc.* **131,** 833–843 (2009); (c) Zhang, W. Jin, W. Fukushima, T. Saeki, A. Seki, S. and Aida, T. Supramolecular Linear Heterojunction Composed of Graphite-Like Semiconducting Nanotubular Segments. *Science (80-.).* **334,** 340–343 (2011).

[14]Yamamoto, T. Fukushima, T. Yamamoto, Y. Kosaka, A. Jin, W. Ishii, N. and Aida, T. Stabilization of a kinetically favored nanostructure: Surface ROMP of self-assembled conductive nanocoils from a norbornene-appended hexa-peri-hexabenzocoronene. *J. Am. Chem. Soc.* **128,** 14337–14340 (2006).

nanotubes après plusieurs jours comme le montrent des études par microscopie SEM. Les deux types de structures ont été réticulés par ROMP en utilisant le catalyseur de Grubbs de seconde génération permettant d'accroître la stabilité thermique des deux nano-agrégats. En outre, le processus de post-polymérisation a permis de déterminer la conductivité des nanocoils réticulés (1×10^{-4} S.cm^{-1}), alors que celle des structures auto-assemblées équivalente n'a pas pu être déterminée du fait de leur destruction sous l'effet du dopage. Ce travail illustre une stratégie de post fonctionnalisation pour capturer des structures fonctionnelles thermodynamiquement défavorisées lors du processus d'auto-assemblage supramoléculaire. La réaction sol-gel a également été utilisée par le groupe de Shinkai afin de geler les structures auto-assemblées dans la phase organogel (Figure 6b).[15] Un monomère à base de porphyrine décoré avec quatre groupes siloxane à sa périphérie a démontré sa capacité à s'auto-organiser en nanofibres et à former un gel en présence de Cu^{2+} dans les solvants aromatiques. Après polycondensation *in situ* au sein de la structure auto-assemblée, un gel solide constitué de faisceaux d'agrégats de porphyrine 1-D a été obtenu. Fait intéressant, la température de transition du gel réticulé résultant a été fortement augmentée (160°C) indépendamment de la concentration et son module de stockage G' a été amélioré d'un facteur 14 par rapport aux gels avant polycondensation sol-gel. Ce travail a clairement démontré la puissance de polymérisation covalente pour obtenir des matériaux avec une robustesse accrue.
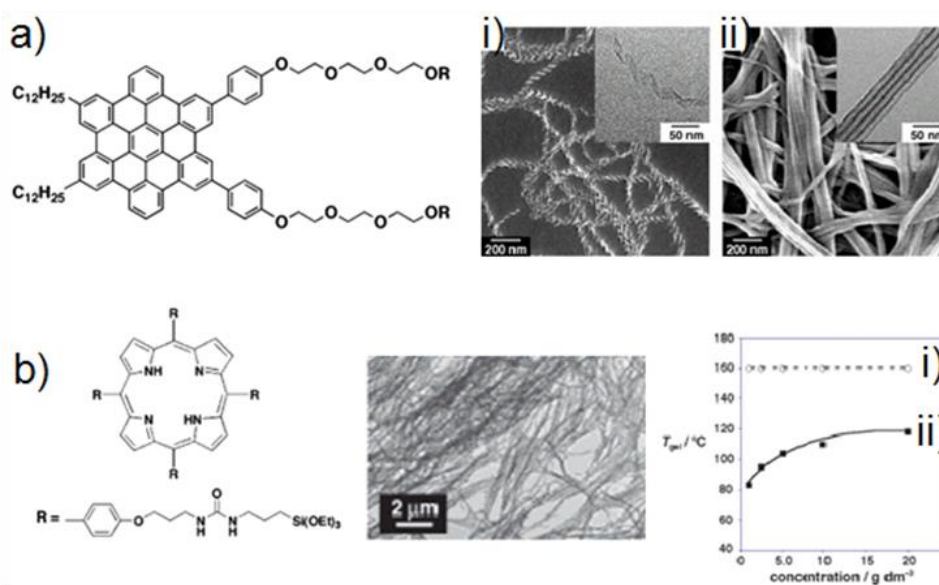
Figure 6: a) Structure moléculaire d'un HBC amphiphile décoré par un groupe norbornène polymérisable en bout de chaine (R). Images SEM et TEM (encadré) de i) nanocoils polymérisés et ii) nanotubes polymérisés par post-ROMP; b) Structure d'un dérivé de porphyrine modifié par des groupements triéthoxysilyl, image TEM du xérogel correspondant après polycondensation sol-gel induite par l'anisole et évolution de la témpérayure de transition T$_{gel}$ en fonction de la concentration du complexe Cu correspondant   ii) avant et i) après polycondensation sol-gel en utilisant l'anisole.

Pour ce second projet, trois nouveaux dérivés triarylamines décorés sur les chaines latérales pour des groupements norbornene ou siloxane ont été envisagés afin de pouvoir réticuler les nanostructures auto-assemblées par polymérisation par ouverture de cycle par métathèse (ROMP)[16] ou par méthodes de type sol-gel[17] (Figure 7).

---

[15]Kishida, T. Fujita, N. Sada, K. and Shinkai, S. Sol-gel reaction of porphyrin-based superstructures in the organogel phase: Creation of mechanically reinforced porphyrin hybrids. *J. Am. Chem. Soc.* **127,** 7298–7299 (2005).

[16]Luh, T. Y. Ladderphanes: A new type of duplex polymers. *Acc. Chem. Res.* **46,** 378–389 (2013).
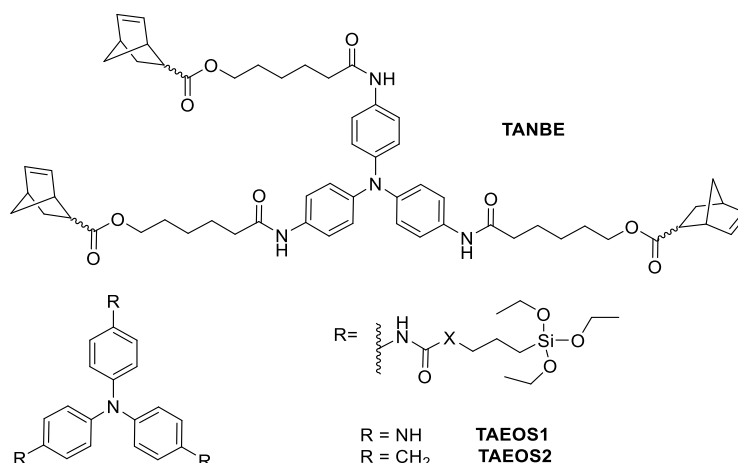
Figure 7: Structures des dérivés triarylamines **TANBE**, **TAEOS1** et **TAEOS2** étudiées pour la stabilisation de structures auto-assemblées par polymérisation covalente

La synthèse du composé **TANBE** a été réalisée en trois étapes (réduction, amidation et substitution nucléophile) avec de bons rendements à partir du composé N,N-bis(4-nitrophenyl)benzene-1,4-diamine.5 Le composé **TAEOS1** a été obtenu en une étape à partir du composé N,N-bis(4-aminophenyl)benzene-1,4-diamine5 et du composé commercial 3-(triethoxysilyl)propyl isocyanate. La synthèse du composé **TAEOS2** s'est avérée plus difficile mais a pu être réalisée en trois étapes. Tout d'abord, le chlorure de 4-pentenoyle a réagi avec le composé N-hydroxysuccimide pour fournir l'ester correspondant, qui a alors été engagé dans une réaction de silylation avec le triethoxysilane en présence de catalyseur de Karstedt pour fournir l'ester activé silylé. Enfin, ce composé a été couplé au dérivé N,N-bis(4-aminophenyl)benzene-1,4-diamine en utilisant la diisopropylethylamine comme catalyseur pour fournir la molécule **TAEOS2**. Toutes ces synthèses ont permis l'obtention de plusieurs centaines de milligrammes, ce qui est important si l'on souhaite étudier les propriétés macroscopiques de ces molécules. Les auto-assemblages de ces trois composés ont alors été étudiés dans des solvants apolaires tels que le toluène ou un mélange dichlorométhane/méthanol (9:1).

Le composé **TANBE** s'auto-assemble sous la forme d'un gel dans le toluène du fait de la formation d'un réseau de fibres entrelacées, comme cela a pu être observé par microscopie TEM (Figure 8a-b). De plus, l'épaisseur d'une fibre a pu être déterminée à 1 nm par microscopie à force atomique (AFM), suggérant ainsi la formation d'agrégats sous la forme de simples colonnes comme nous avons pu l'observé précédemment5 (Figure 8c). Nous avons ensuite utilisé le catalyseur de Grubbs III[18] pour polymériser par ROMP les gels physiques irradiés et non-irradiés. Les images obtenues par microscopie SEM ont mis en évidence la formation de fibres longues et larges qui produisent un dense réseau (Figure 8d-e). Une comparaison des Figures 8e et 8d nous tend à estimer que l'alignement des fibres se fait sur de plus longues distances lorsque le gel a été soumis à un stimulus lumineux. Ces observations doivent cependant être corrélées par des études structurales des gels par diffusion du rayonnement.

[17]Mizoshita, N. Tani, T. and Inagaki, S. Syntheses, properties and applications of periodic mesoporous organosilicas prepared from bridged organosilane precursors. *Chem. Soc. Rev.* **40,** 789–800 (2011).
[18]Lu, H. Wang, J. Lin, Y. and Cheng, J. One-pot synthesis of brush-like polymers via integrated ring-opening metathesis polymerization and polymerization of amino acid N-carboxyanhydrides. *J. Am. Chem. Soc.* **131,** 13582–13583 (2009).
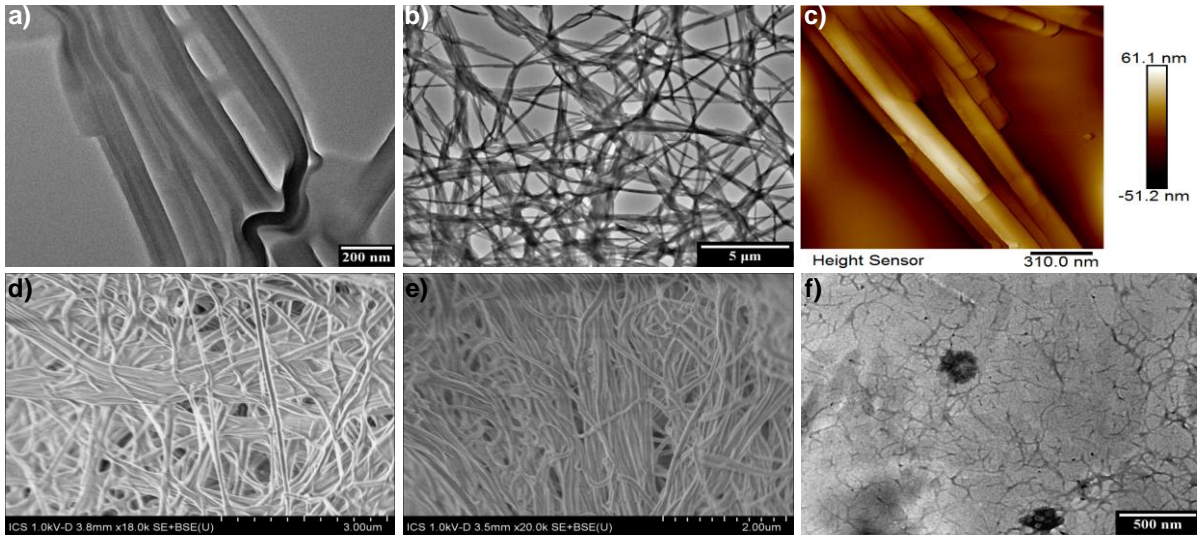
Figure 8: a-b) Images TEM du composé **TANBE** dans le toluène, c) image AFM du composé **TANBE** dans le toluène, d-e) Images SEM des gels de **TANBE** polymérisés d) avant et e) après irradiation lumineuse, et f) image TEM du composé **TAEOS1** dans un mélange dichlorométhane/méthanol (9:1).

Les différents gels (avant/après polymérisation, avant/après irradiation lumineuse) ont également été caractérisés par spectroscopies RMN ^{1}H, IR et UV-vis. Comparé au monomère, les gels polymérisés laissent apparaitre une forte diminution de la bande vibrationnelle à 1335 cm^{-1}, ce qui indique que les oléfines cycliques ont été converties en oléfines acycliques, synonyme de succès de la polymérisation par ROMP (Figure 9d).
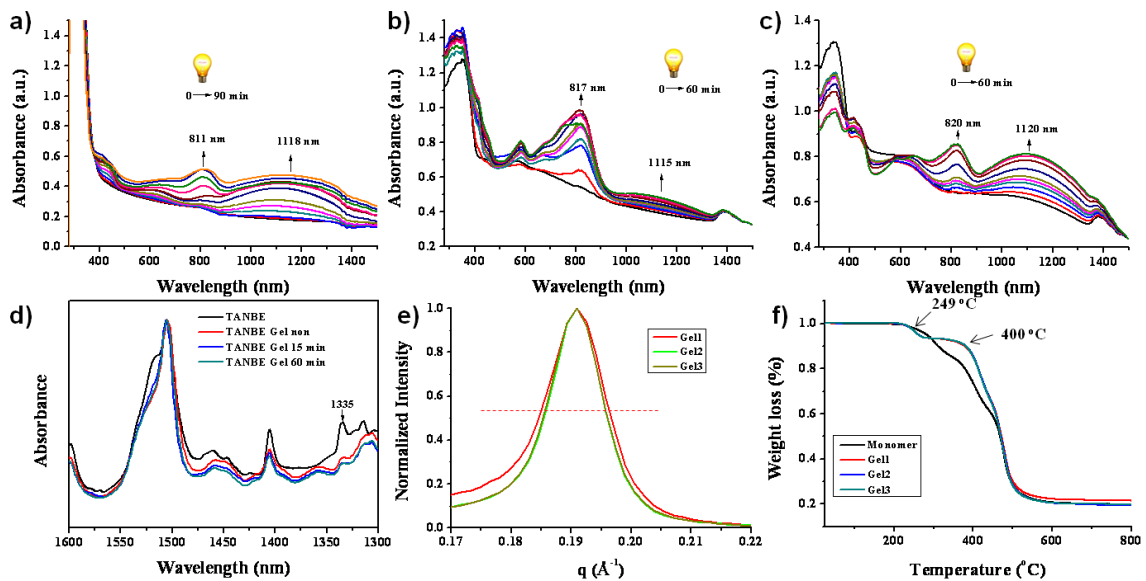
Figure 9: a-c) Spectres d'absorption UV-vis-NIR sous irradiation lumineuse dans un mélange toluene/10% tétrachloroéthane a) du gel non-polymérisé **TANBE** (15 mM), b) du gel polymérisé **TANBE** (15 mM, sans irradiation avant polymérisation) et, c) du gel polymérisé **TANBE** (15 mM, irradié durant 15 min avant polymérisation), d) Spectre IR du monomère **TANBE** et des gels polymérisés **TANBE** (non-irradié, irradiés durant 15 min et 60 min), e) Pics de diffraction des rayons X normalisés à 0.191 Å-1 pour les gels polymérisés **TANBE** (non-irradié (Gel 1), irradiés durant 15 min (Gel 2) et 60 min (Gel 3)), f) Courbes d'analyse thermogravimétrique pour les gels polymérisés **TANBE** (non-irradié (Gel 1), irradiés durant 15 min (Gel 2) et 60 min (Gel 3)).

Pour les gels physiques de **TANBE** dans un mélange toluene/10% tétrachloroéthane, les spectres UV-Vis-NIR laissent tous apparaitre une bande d'absorption à environ 811 nm qui indique la présence de radicaux cations et une bande d'absorption à 1118 nm qui correspond à un phénomène de transfert de charge intermoléculaire comme nous avons déjà pu

l'observer (Figure 9a).5 Ces observations suggèrent que les groupements norbornene n'affectent pas les propriétés d'auto-assemblages des triarylamines. Il est intéressant de remarquer qu'après polymérisation, une bande d'absorption très large est observée dans le proche infrarouge et que, sous irradiation lumineuse, les bandes à ~ 810 et 1110 nm augmentent. Ces expériences suggérent que les molécules **TANBE** au sein des gels polymérisés sont empilées en mono-colonnes, ce qui permet un transfert de charge efficace entre les atomes d'azote centraux. Les premières études de rhéologie ont permis de démontrer la robustesse des gels polymérisés par rapport aux gels physiques qui se comportent comme des liquides (Figure 9e). Des études complémentaires sont en cours, notamment en ce qui concerne la conductivité des gels polymérisés.

Pour tous les gels réticulés, un fort pic de diffusion à 0.191 Å-1 témoigne d'un arrangement de type smectique avec une périodicité de 32.9 Å le long de la structure auto-assemblée à une dimension comme cela a déjà pu être observé par notre groupe (Figure 9e). Afin d'étudier l'effet de l'irradiation de lumière sur les nanostructures, un ajustement gaussien a été réalisé pour ces pics de diffusion et une diminution de la largeur du pic à mi-hauteur pour les gels Gel2 et Gel3 irradiés, contrairement à Gel1, suggère une diminution des défauts au sein de la structure lors du processus d'irradiation lumineuse. Des analyses thermogravimétriques démontrent que le monomère **TANBE** commence à se décomposer vers 249 ℃ tandis que les gels polymérisés correspondant commencent à se décomposer vers 400 ℃, indiquant une stabilité thermique améliorée après polymérisation (Figure 9f). Des expériences de rhéologie ainsi que des mesures de conductivité sont en cours afin de déterminer les propriétés mécaniques et électroniques de nos gels polymérisés de façon covalente.

En ce qui concerne les dérivés silylés **TAEOS1** et **TAEOS2**, des structures fibrillaires ont été observées par microscopie TEM (Figure 8f) pour le gel obtenu par catalyse acide à partir de **TAEOS1**. Cependant, il nous a été difficile de reproduire ces gels et, par manque de temps, nous avons pas pu explorer de nouvelles méthodes de polymérisation.

3) Conclusion générale

Au cours de ce travail, nous avons synthétisé trois nouveaux dérivés triarylamine solubles en milieu aqueux et les polymères supramoléculaires correspondant ont été caractérisés dans l'eau et dans le méthanol. Ce travail représente le premier exemple d'auto-assemblages de triarylamines dans l'eau et démontre qu'en choisissant des substituants appropriés, les composés TAA conservent leur capacité à s'auto-assembler même dans des solvants hautement polaires. Par ailleurs, nous avons également synthétisé trois composés triarylamine présentant des groupements polymérisables. Les polymères supramoléculaires obtenus à partir du composé **TANBE** tendent à former des gels physiques qui peuvent être polymérisés de façon covalente par ROMP. Bien que l'étude des propriétés de conduction reste à être réalisée, il semble que l'utilisation tandem d'un phénomène d'auto-organisation supramoléculaire et d'une polymérisation covalente s'avère une stratégie prometteuse pour produire des matériaux organiques innovants, c'est-à-dire qui combinent les propriétés physiques associées à l'auto-organisation à l'échelle nanométrique et la robustesse du polymère covalent. L'ensemble de ce travail démontre le potentiel du synthon triarylamine comme unité de structure pour produire des polymères supramoléculaires dans une large gamme de solvants et pour conduire à des matériaux fonctionnels robustes pour des applications futures dans le domaine de l'électronique et/ou de la plasmonique.

Acknowledgements

ABBREVIATIONS AND SYMBOLS

Å	ångström
AcOH	acetic acid
Ac_2O	acetic anhydride
AFM	atomic force microscopy
Boc	*tert*-butyloxycarbonyl
BTA	1,3,5-benzenetrisamide
°C	celsius degree
COSY	correlation spectroscopy
CD	circular dichroism
CV	cyclic voltammetry
δ	chemical shift
DCM	dichloromethane
DIPEA	diisopropylethylamine
DMF	dimethylformamide
DMSO	dimethylsulfoxide
DLS	dynamic light scattering
DSC	differential scanning calorimetry
EPR	electron paramagnetic resonance
ESI-MS	mass spectrometry with electrospray ionization
EtOAc	ethyl acetate
FRET	Förster Resonance Energy Transfer
FT-IR	Fourier Transform InfraRed
GPC	gel permeation chromatography
h	hour
HOMO	highest occupied molecular orbital
HPLC	high performance liquid chromatography
HRTEM	High resolution transmission electron miscroscopy
ITC	isothermal titration calorimetry
J	coupling constant
K	Kelvin
K_d	dissociation constant
L	liter
L_c	Contour length
LC/MS	liquid chromatography coupled to mass spectrometry
MALDI	Matrix Assisted Laser Desorption Ionisation
λ_{max}	maximum of emission/absorption wavelength
µL	microliter
µm	micrometer

mL	milliliter
μmol	micromole
mmol	millimole
MS	mass spectrometry
nm	nanometer
NMR	nuclear magnetic resonance
NMP	*N*-methylpyrrolidinone
NIR	near infrared
PA	Peptide amphiphile
ppm	parts per million
PEG	poly(ethylene glycol)
R_f	retardation factor
R_g	gyration radius
R_H	hydrodynamic radius
ROMP	ring opening metathesis polymerization
r.t.	room temperature
SAS	small angle scattering
SANS	small angle neutron scattering
SAXS	small angle X-ray scattering
SEM	scanning electronic microscopy
SLS	static light scattering
SPPS	solid phase peptide synthesis
T	temperature
TBAHFP	tetrabutylammonium hexafluorophosphate
TEA or NEt_3	triethylamine
TEM	transmission electronic microscopy
TFA	trifluoroacetic acid
TGA	thermogravimetric analysis
THF	tetrahydrofuran
TIPS	triisopropylsilane
TLC	thin layer chromatography
UPLC	ultra performance liquid chromatography
UV	ultra-violet
Vis	visible
WAXD	Wide angle X-ray diffraction
XRD	X-ray diffraction

GENERAL INTRODUCTION AND OBJECTIVES

Triarylamine-type molecules are very efficient functional units widely used as photoconductors and charge carriers. In particular, they display appreciably high hole-transport mobility and are thus inserted in a number of electro-optical devices even as photoconductors for the Xerox® process in laser printers and photocopiers, but also to a lesser extend in organic light emitting diodes (OLEDs). Recently, we discovered that well-defined triarylamine (TAA) molecules can give rise to a firmly new kind of self-assembly that is produced by the non-covalent polymerisation of catalytic amounts of triarylammonium radicals, which stack with their neutral counterparts (Figure A). We demonstrated that a simple irradiation by visible light of a solution of these molecules in chloroform can generate supramolecular triarylamine nanowires (STANWs) which at higher concentrations aggregate into larger fibers (typically 10-50 nm in width and 50-1000 nm in length, Figure Ab) via a highly synergistic process.
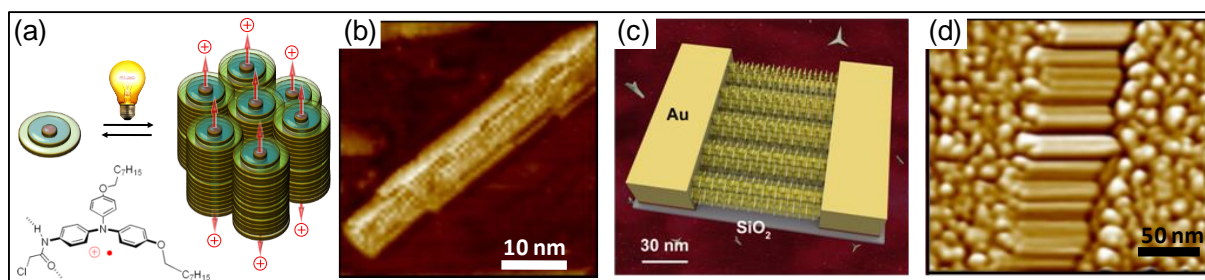
Figure A | Light-triggered self-construction of supramolecular organic nanowires as conducting interconnects. (a) Nucleation of the fibers by supramolecular associations of a modified triarylamine upon light irradiation; (b) AFM image of the self-assembled fiber; (c) directed growth and insertion of the 100 nm fibers addressed by the electric field within electrodes; and (d) corresponding AFM image of the nanowires displaying high conductivity characteristics.

We then probed their conductivity using 100 nm width nanotrenches. Interestingly, upon light irradiation, a spectacular rise by 6 orders of magnitude of the current was observed, attaining values in the mA range and conductance values ranging from several tens to several hundreds of mS. AFM imaging revealed that the wires length exactly matches the electrode gap, with orientations following the electric field applied during assembly (Figure Ad). I/V measurements on these two-terminal devices demonstated their ohmic resistive behavior related to high conductivity values (more than 5.10^3 S.m^{-1}) and an impressive interface resistance (10^{-2} Ω.cm). Recently, we also described a second generation of tris-amide triarylamines which formed soft physical gels made of long micrometric fibers in chloroform, without the need of light. Notably, upon light irradiation, an improved ordering of the fibers

was observed by both X-ray scattering and AFM, resulting in self-healing properties and self-optimization of the conduction properties. Thanks to the unique formation of through-space mixed valence charge-transfer complexes, charge-transport characteristics similar to those observed in conducting conjugated polymers were also determined for these self-assemblies. Furthermore, we have also shown that TAAs molecules can be chemically tailored, while keeping their structuring properties, to reach various mesophases upon light irradiation in chlorinated solvents.

The first objective of this thesis was to study the self-assembly behavior of tris-amide triarylamine derivatives in polar medium such as water or methanol. This work required the design and synthesis of new triarylamine structures with side chains such as polyethylene glycol, peptidic units, or cyanine dyes, which can be used as solubilizing units in water and methanol. The resulting solutions were then examined by various physico-chemical characterization techniques so as to determine the influence of molecular structure and solvent on the structures and properties of the corresponding supramolecular polymers.

The second objective was to prepare both robust and functional triarylamine-based polymers by taking advantage of the self-assembling properties of tris-amide triarylamine derivatives. There, we designed and studied the self-assembly and the corresponding physical properties of new triarylamine molecules with polymerizable side chains such as siloxane or norbornene units. We then examined how covalent polymerization processes such as ring opening metathesis polymerization or sol-gel methodologies affect the physical and mechanical properties of the corresponding covalent networks.

We expect that these studies will extend the actual knowledge on the potential of the triarylamine scaffold as structuring unit to produce supramolecular polymers in a wide range of solvents and as functional materials for further applications in electronics and/or plasmonics.

BIBLIOGRAPHICAL PART

Chapter I: Generalities on supramolecular polymers

1. Supramolecular polymers

a. Definitions

In 1987, the nobel prize in chemistry was awarded to C. J. Pedersen, J. M. Lehn and D. J. Cram for their pioneering work on supramolecular chemistry. In the nobel lecture of J. M. Lehn, supramolecular chemistry was defined as "organized entities of higher complexity that result from the association of two or more chemical species held together by intermolecular forces".[19] As early as in the 19th century, J. D. van der Waals started to pay attention to non-covalent interactions when he studied the state of real gases. Compared to traditional covalent forces, these supramolecular intermolecular forces correspond to non-covalent interactions such as hydrogen bond, metal-ligand complexes, π-π stacking, host-guest interactions, hydrophobic interactions, van der Waals and so on.[20] Table 1 shows various supramolecular interactions and their corresponding association constants. In general, metal-ligand complexes and electrostatic interactions display the strongest binding constants while hydrogen bond, π-π stacking, host-guest and hydrophobic interactions are located at the middle range and van der Waals forces are the weakest one. Thanks to these non-covalent interactions, supramolecular chemistry has become an important tool to build complex matter at the interface with biology and physics.[21] In particular, by combing polymer science and supramolecular chemistry, a new research area has emerged in the early 90's.[22] Through the use of reversible and highly directional secondary interactions, monomeric units arrange into polymeric arrays in solution or in solid state, which behave in agreement with the theories of polymer physics and lead to the formation of supramolecular polymers.[23] In contrast with conventional polymers, they exhibit high reversibility due to the non-covalent character of their interactions, which offers the possibility to fabricate materials which can respond to environmental stimuli, such as temperature, solvent, pH and redox reactions. However, the strength of the different non-covalent interactions involved will affect the degree of polymerization, the lifetime of polymer chain and the nature of the architectures, which result in general in weaker polymers compared to covalent ones. Hence, a rational choice of the

---

[19]Lehn, J.-M. Supramolecular Chemistry—Scope and Perspectives Molecules, Supermolecules, and Molecular Devices (Nobel Lecture). *Angew. Chem. Int. Ed.* **27,** 89–112 (1988).

[20]Lehn, J.-M. Toward Self-Organization and Complex Matter. *Science (80-.).* **295,** 2400–2403 (2002).

[21]Lehn, J. M. Perspectives in chemistry - Aspects of adaptive chemistry and materials. *Angew. Chemie - Int. Ed.* **54,** 3276–3289 (2015).

[22]Lehn, J. M. Dynamers: Dynamic molecular and supramolecular polymers. *Aust. J. Chem.* **63,** 611–623 (2010).

[23]Brunsveld, L. Folmer, B. J. B. Meijer, E. W. and Sijbesma, R. P. Supramolecular Polymers. *Chem. Rev.* **101,** 4071–4098 (2001).

non-covalent interactions involved in the supramolecular polymerization process will allow to modulate the dynamics of the polymer and ultimately its properties. Another feature related to the directionality of some non-covalent interactions such as hydrogen bond, π-π stacking and metal coordination is the possibility to produce one-dimensional supramolecular polymers with properties inherent to this unidimensional character.

Synthetic supramolecular polymers can be categorized according to different criteria, such as the physical nature of the intermolecular non-covalent driving forces as reported in Table 1, the structural unit used as building block or the thermodynamics of the self-assembly process. Another classification can be established on the type of monomer, such as a single A monomer unit and an A-B type monomer with complementary A:B interactions, or even a two component A, B system with complementarity between single A and B monomers. In this manuscript, supramolecular polymers will be classified mainly based on the non-covalent interactions involved in the polymerization process but also according to their structural unit.
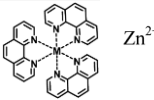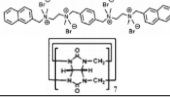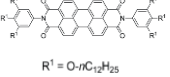
Non-covalent interactions	Examples	Binding constants
Hydrogen bond		$K = 10^7\ M^{-1}$ in $CHCl_3$
Metal-ligand	Zn^{2+}	$K = 10^{17}\ M^{-3}$ in aqueous KNO_3
Host-guest		$K \approx 10^9\ M^{-1}$ in sodium acetate buffer pH=4.75
π-π	$R^1 = O\text{-}nC_{12}H_{25}$	$K = 1.5 \times 10^7\ M^{-1}$ in methylcyclohexane

Table 1 | Typical examples of supramolecular interactions and their binding constants (Reproduced from[24]).

Supramolecular polymerization is a non-covalent assembly process controlled by both thermodynamic and kinetic parameters. The evolution of the Gibbs free energy during the supramolecular polymerization process is of high importance for mechanistic studies. Indeed, according to this evolution, the growth mechanism of supramolecular polymers can be

---

[24](a) Yang, L., Tan, X., Wang, Z. and Zhang, X. Supramolecular Polymers: Historical Development, Preparation, Characterization, and Functions. *Chem. Rev.* **115,** 7196–7239 (2015); (b) Biedermann, F. and Schneider, H. J. Experimental Binding Energies in Supramolecular Complexes. *Chem. Rev.* **116,** 5216–5300 (2016); (c) Chen, Z. Fimmel, B. and Würthner, F. Solvent and substituent effects on aggregation constants of perylene bisimide π-stacks – a linear free energy relationship analysis. *Org. Biomol. Chem.* **10,** 5845 (2012); (d) Huang, Z. Yang, L. Liu, Y. Wang, Z. Scherman, O. A. and Zhang, X. Supramolecular polymerization promoted and controlled through self-sorting. *Angew. Chemie - Int. Ed.* **53,** 5351–5355 (2014).

classified in three different paths: isodesmic, nucleation-elongation and ring-chain polymerization processes (Figure 1).[25]
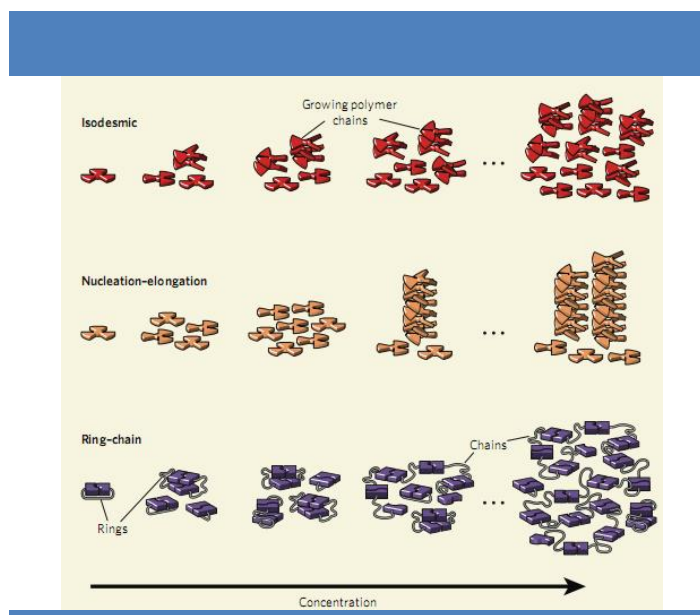
Figure 1 | Three main mechanism of supramolecular polymerization (Reproduced from[26]).

Similar to step growth polymerization in covalent polymers, the isodesmic growth is characterized by a single binding constant between monomers whatever the length of the polymer. Such behavior features the absence of critical temperature or concentration of monomer in an isodesmic polymerization. The nucleation-elongation mechanism, which is called cooperative polymerization as well, involves two steps that are a thermodynamically unfavorable nucleation step followed by a more rapid elongation step. In such mechanism, the binding constant for the first step is larger than the one related to the growth step, cooperatively promoting the supramolecular polymerization event. For such growth, a minimum temperature and/or concentration are necessary for the supramolecular polymers to dominate over the monomeric units. Therefore, a good method to distinguish the different supramolecular polymerization mechanisms is to investigate changes in UV-vis absorption, circular dichroism or ^{1}H NMR as a function of concentration and temperature. Finally, the ring-chain growth mechanism is usually used to explain systems with ditopic monomeric units, which is a special case of supramolecular polymerization. In this self-assembly pathway, cyclic monomer and oligomers are in equilibrium with their linear counterpart. Below a certain concentration, the end groups of monomers tend to attach with each other thus generating a closed ring while above a particular concentration monomers form linear

[25]De Greef, T. F. A. Smulders, M. J. Wolffs, M. Schenning, A. P. H. J. Sijbesma, R. P. and Meijers, E. W. Supramolecular Polymerization. *Chem. Rev.* **109,** 5687–5754 (2009).

[26]De Greef, T. F. A. and Meijer, E. W. Q & A Supramolecular polymers. *Nature* **453,** 171–173 (2008).

main-chain polymers rapidly.

Recently, living supramolecular polymerization was named by analogy with covalent polymer and features a controlled chain growth and a narrow polydipersity. Takeuchi and co-workers reported the first living supramolecular polymer based on a porphyrin system.[9a] While porphyrin derivatives self-assemble into kinetically trapped J-aggregates in solution through an isodesmic pathway, thermodynamically stable H-aggregates were formed from these J-aggregates through a cooperative mechanism, as demonstrated by UV-Vis experiments. Importantly, short H-aggregate seeds obtained by sonication could initiate the transformation of J-aggregates into H-aggregates with a narrow polydispersity of around 1.1, as demonstrated by AFM images. Some years later, Würthner and co-workers proposed a more general seeded living supramolecular polymerization approach for a variety of π-conjugated molecules to self-assemble into novel supramolecular architectures.[27b] A perylene bisimide-based derivative PBI-1 was synthesized, consisting of amide groups and solubilizing alkyl chains incorporated at the imide positions. As demonstrated by temperature-dependent UV-vis spectroscopy, this monomer self-assembled into elongated nanofibers through a cooperative nucleation-growth process, which showed a thermal hysteresis during a cycle of assembly and disassembly (Figure 2a). Furthermore, a seeded supramolecular polymerization could be achieved by adding a small amount of PBI-1 seeds into a fresh monomer solution under appropriate conditions (303 K).
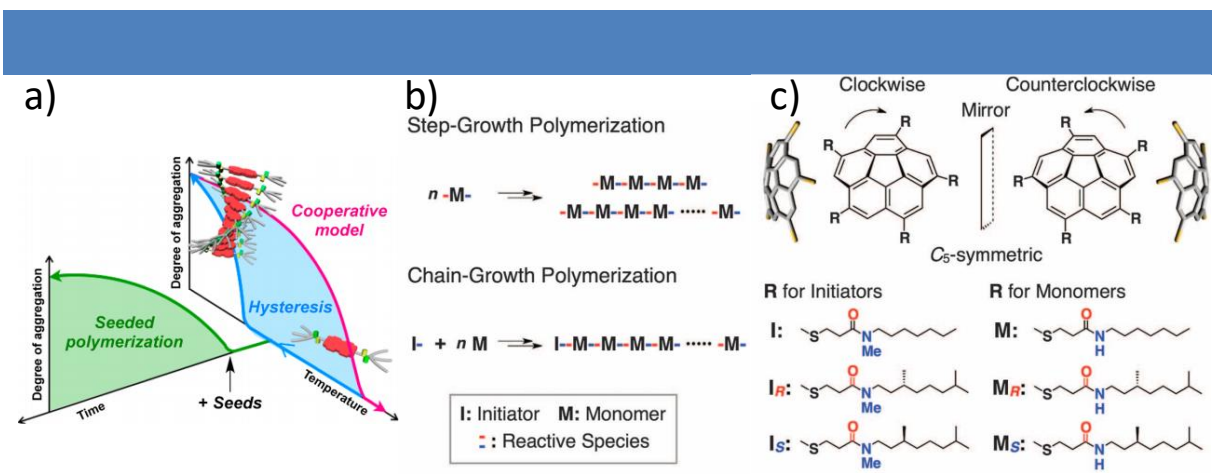
Figure 2 | a) Schematic representations of the cooperative model and seeded polymerization of a perylene bisimide; b) Schematic representations of step-growth (upper) and chain-growth (lower) polymerizations; c) Chemical structures of C$_5$-symmetric corannulene-based chiral initiators and monomers and schematic representation for the bowl-to-bowl corannulene intersion. The arc-shaped arrows represent tentative definitions of the clockwise and counterclockwise H → R substituent arrays

[27](a) Ogi, S., Sugiyasu, K., Manna, S., Samitsu, S. & Takeuchi, M. Living supramolecular polymerization realized through a biomimetic approach. *Nat. Chem.* **6**, 188–195 (2014); (b) Ogi, S. Stepanenko, V. Sugiyasu, K. Takeuchi, M. and Würthner, F. Mechanism of self-assembly process and seeded supramolecular polymerization of perylene bisimide organogelator. *J. Am. Chem. Soc.* **137**, 3300–3307 (2015).

along the corannulene periphery (Reproduced from[27b,28]).

More recently, Aida and co-workers reported the chain-growth supramolecular polymerization of non-planar bowl-shaped corannulene molecules decorated with five thio alkyl chains functionalized with either tertiary or secondary amide unit (Figure 2b-c).[28] These C_5-symmetric molecules with secondary amide chains (M, M_R, M_S) are likely to form cage-like structures by intramolecular H-bonding in methylcyclohexane at room temperature, while upon heating these monomers would undergo 1-D chain growth spontaneously. Furthermore, when the hydrogens from the amides on side chains were substituted with methyl groups, intramolecular hydrogen bonding was inhibited. However, methyl-substituted amides can be used as proton acceptor unit for non-covalent interactions with secondary amides. Thus, the author checked wether these methyl-substituted molecules (I, I_S, I_R) could be used as initiators for the chain growth polymerization. Interestingly, when a catalytic quantity of the initiator with specific chiral side chains (right or left handed) was mixed with its respective monomer, the corresponding helical polymer was formed with narrow polydispersity (1.2-1.3). Overall, the recently developed living supramolecular polymerization approach appears as a useful and powerful tool to precisely construct diverse complex architectures with potentially unprecedented physical properties.

b. Examples

The first example of main-chain supramolecular polymers was reported by the group of Lehn in 1990.[29] Two monomers based on tartartic acids bearing either two diaminopyridines or two uracil derivatives as end groups were designed and synthesized. A supramolecular liquid crystalline polymer was formed from these two units by triple hydrogen bonding, presenting a thermotropic mesophase over a wide temperature range (from below room temperature to above 200 ºC). Since then, supramolecular polymers have been extensively studied and the strategies developed toward their synthesis have impressively progressed in the following decades.[30] For instance, inspired by biological systems, such as the tobacco mosaic virus, which arises from the self-assembly of biomacromolecules associated by multiple non-covalent interactions in an orthogonal manner, scientists have developed innovative supramolecular polymers built in a cooperative fashion by several non-covalent forces. Here,

---

[28]Kang, J. Miyajima, D. Mori, T. Inoue, Y. Itoh, Y. and Aida, T. A rational strategy for the realization of chain-growth supramolecular polymerization. *Science (80-.).* **347,** 646 (2015).

[29]Fouquey, C. Lehn, J.-M. and Levelut, A.-M. Molecular Recognition Directed Self-Assembly of Supramolecular Liquid Crystalline Polymers from Complementary Chiral Components. *Adv. Mater.* **2,** 254–257 (1990).

[30]Stupp, S. I. and Palmer, L. C. Supramolecular Chemistry and Self-Assembly in Organic Materials Design. *Chem. Mater.* **26,** 507–518 (2013).

I want to briefly select some examples of supramolecular polymers on the basis of various non-covalent interactions such as hydrogen bond, π-π stacking, host-guest interaction and charge transfer interaction. We will also show how the cooperative use of several supramolecular interactions could give rise to polymeric structures in a controlled manner.

Because of its directionality and versatility, hydrogen bond interaction is a prominent candidate to build up supramolecular polymers. However, considering their moderate strength as single interaction, they are usually used in arrays or in combination with other non-covalent interactions to produce robust polymers. For instance, Stupp and co-workers innovatively designed a peptide-amphiphile composed of five parts for biomineralization: a hydrophobic nonpolar alkyl tail was followed by four cysteine residues used for cross-link; the third part then consisted in a flexible linker attached to a single phosphorylated serine residue designed to direct the mineralization of hydroxyapatite; finally a RGD residue was introduced for biorecognition.[31] This molecule was described to self-assemble into discrete nanofibers by controlling the pH. After cross-linking by disulfide bonding between intermolecular cysteine residues, the fibers were reinforced and could direct the mineralization of hydroxyapatite to generate a composite material analoguous to collagen fibrils and hydroxyapatite crystals in bone, suggesting potential applications in tissue engineering. In another example, the same group presented a series of terthiophene-peptide conjugates which self-organized into diverse architectures including flat spicules, nanotubes, spiral sheets and giant flat sheets depending on the dipeptidic sequence made of a hydrophobic amino-acid (G, V, I, or L) and a glutamic acid residue.[32] This example highlights how small changes in the chemical structure can affect the self-assembling properties of the monomer. The group of Meijer has also an important contribution to the formation of supramolecular polymers based on hydrogen bonding interactions. For example, they reported the formation of one-dimensional columnar aggregates based on *N,N',N''*-trialkylbenzene-1,3,5-tricarboxamides (BTAs) through strong, threefold α-helix-type hydrogen bond.[33] Interestingly, they showed that chirality derived from simple D/H isotope substitution is sufficient to induce the preferential formation of a helical conformer through a nucleation growth mechanism as determined by CD and UV-Vis experiments. Finally, recently, Colombani *et al.* synthesized hydrogen bonding tris(urea) units substituted with polymeric side chains of different lengths obtained by atom transfer radical

---

[31]Hartgerink, J. D. Beniash, E. and Stupp, S. I. Self-Assembly and Mineralization of Peptide-Amphiphile Nanofibers. *Science (80-.).* **294,** 1684–1688 (2001).

[32]Lehrman, J. A. Cui, H. G. Tsai, W. W. Moyer, T. J. and Stupp, S. I. Supramolecular control of self-assembling terthiophene-peptide conjugates through the amino acid side chain. *Chem. Commun.* **48,** 9711–9713 (2012).

[33]Cantekin, S. Balkenende, D. W. R. Smulders, M. M. J. Palmans, A. R. and Meijer, E. W. The effect of isotopic substitution on the chirality of a self-assembled helix. *Nat. Chem.* **3,** 42–6 (2011).

polymerization.[34] These tris(urea) derivatives were found to self-assemble in cyclohexane into supramolecular bottle brushes, which size was influenced by the degree of polymerization and chemical nature of the polymeric side chains. Furthermore, the critical solubility temperature of the supramolecular aggregates was found to be for the first time quite lower than that of covalent polystyrene. Thus, this example demonstrated that supramolecular polymers can be an alternative to covalent polymers in order to reach unusual physical properties.
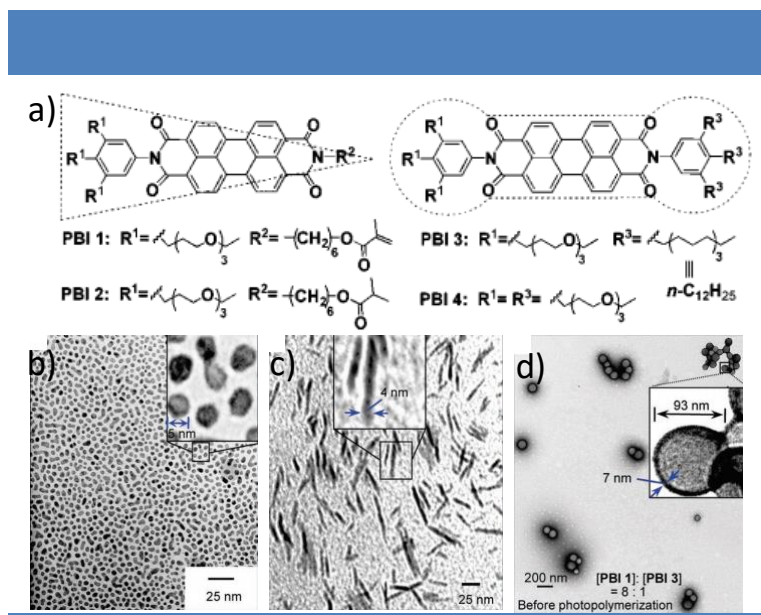
Figure 3 | a) Molecular structures of wedge- and dumbbell-shaped amphiphilic perylene bisimide; TEM images of self-assembled PBI 1 b), PBI 4 c) and co-aggregates of PBI 1 and PBI 3 in a 8:1 molar ratio d) (Reproduced from[35]).

Numerous studies have also been reported on the self-assembly of well-designed π-conjugated molecules such as perylene bisimide (PBI) and hexabenzocoronene (HBC). As shown in Figure 3a), Würthner and co-workers studied the self-assemblies and co-assemblies in aqueous solutions of four perylene bisimide amphiphiles.[35] Spherical micelles were observed for wedge-shaped monomers PBI **1** and PBI **2** (Figure 3b) individually whereas dumbbell-shaped PBI **4** was found to aggregate into nanorods (Figue 3c). Interestingly, co-aggregates made of PBI **1** and PBI **3** were shown to produce hollow vesicles which could be further photopolymerized *in situ* thanks to the presence of methacylate unit (Figure 3d). This group has been very active in the development of supramolecular polymers based on perylene bisimide going from very fundamental studies to applications as nanocarriers or in

---

[34] Catrouillet, S. Bouteiller, L. Nicol, E. Nicolai, T. Pensec, S. Jacquette, B. Bohec, M. L. and Colombani, O. Self-assembly and critical solubility temperature of supramolecular polystyrene bottle-brushes in cyclohexane. *Macromolecules* **48,** 1364–1370 (2015).
[35] Zhang, X. Chen, Z. and Würthner, F. Morphology control of fluorescent nanoaggregates by co-self-assembly of wedge- and dumbbell-shaped amphiphilic perylene bisimides. *J. Am. Chem. Soc.* **129,** 4886–4887 (2007).

the field of supramolecular electronics.[36] Another pioneering example was reported by the group of Aida, who synthesized a width controlled supramolecular nanotube with a high aspect ratio from the self-assembly in THF of an amphiphilic hexa-peri-hexabenzocoronene.[37] Two layers of π-stacked coronenes formed the wall of the nanotube with a thickness of around 3 nm while the hydrophilic triethylene glycol chains decorated both exterior and interior surfaces of the nanotube. After oxidation with $NOBF_4$, a single nanotube placed between platinum nanogap electrodes displayed an ohmic behavior and an electrical conductivity of 2.5 MΩ at 285 K, which was comparable to that of inorganic semiconductor nanotube. Since this example, supramolecular polymers based on π-π interactions have found numerous applications as optoelectronic materials, as described in section III. b. of this chapter.

Charge-transfer (CT) interactions which could be considered as a particular case of π-π interactions, force an aromatic donor to assemble alternatively with an electron acceptor. Because of their relative weakness and low directionality, these interactions have been used in a cooperative way with other interactions to construct supramolecular polymers. For instance, Zhu and co-workers reported a new tetrathiafulvalene (TTF) decorated with a urea side chain, which behaves as an organogelator in 2-propanol, cyclohexane and 1,2-dichloroethene.[38] In cyclohexane, upon addition of 7,7,8,8-tetracyanoquinodimethane (TCNQ), its internal nanostructure evolved from fibers to tubular object while the gel structure remained but its color changed to deep green as a result of CT complexation. Importantly, when the gel was oxidized either chemically or electrochemically, disruption of the gel occurred suggesting that the generated radical cation ($TTF^{\bullet+}$) interferes with H-bonds involved in the polymerization process. In a more recent example, Ghosh and Das reported the self-assembling properties of an electron-deficient naphthalene diimide molecule. In methylcyclohexane, thanks to orthogonal H-bonding through hydrazide and hydroxyl groups and aromatic stacking, this compound was shown to produce reverse vesicles (Figure 4a).[39] Interestingly, when this building block was co-assembled with a pyridine-functionalized pyrene donor, the presence of intramolecular CT interactions induced the formation of reverse micelles (Figure 4b). Overall, these examples highlight how the nature and the dynamics of non-covalent interactions influence the morphologies of the resulting supramolecular polymers.

[36]Würthner, F. Saha-Moller, C. R. Fimmel, B. Ogi, S. Leowanawat, P. and Schimt, D. Perylene Bisimide Dye Assemblies as Archetype Functional Supramolecular Materials. *Chem. Rev.* **116,** 962–1052 (2016).

[37]Hill, J. P. Jin, W. Kosaka, A. Fukushima, T. Ichihara, H. Shimomura, T. Ito, K. Hashizume, T. Ishii, N. and Aida, T. Self-Assembled Hexa-peri-hexabenzocoronene Graphitic Nanotube. *Science (80-.).* **304,** 1481–1483 (2004).

[38]Wang, C. Zhang, D. and Zhu, D. A low-molecular-mass gelator with an electroactive tetrathiafulvalene group: Tuning the gel formation by charge-transfer interaction and oxidation. *J. Am. Chem. Soc.* **127,** 16372–16373 (2005).

[39]Das, A. and Ghosh, S. Stimuli-responsive self-assembly of a naphthalene diimide by orthogonal hydrogen bonding and its coassembly with a pyrene derivative by a pseudo-intramolecular charge-transfer interaction. *Angew. Chemie - Int. Ed.* **53,** 1092–1097 (2014).
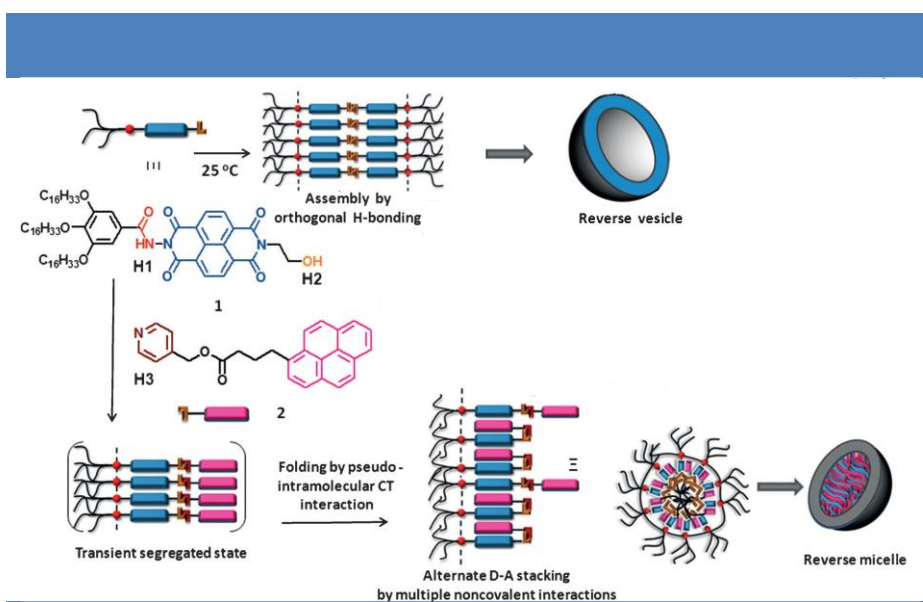
Figure 4 | Schematic representation of the self-assembly of 1 and its co-assembly with 2 (Reproduced from[39]).

A large number of supramolecular polymers based on host-guest recognition motifs have also been reported. Such motifs always arise from the combination of a receptor and a ligand which are hold together by a combination of several non-covalent interactions. Host molecules are usually macrocyclic molecules including cyclodextrins, crown ethers, cucurbit[8]urils and calixarenes while guest molecules should be able to enter inside these host cavities. For instance, Woisel *et al.* reported a well-defined reversible pillar-based supramolecular self-assemblis in both organic and aqueous media.[40] The host pillar[5]arene end-functionalised with poly(dimethylacrylamide) (MePilla-PDMAC) was shown to bind to a pyridinium guest molecule at its α-chain-end to construct a supramolecular complex. As observed by ^{1}H NMR and cryo-TEM experiment, the MePilla-PDMAC self-assembled into micelle-like aggregates in water which remain stable upon heating but can reversibly release an encapsulated molecule such as an electron deficient guest at elevated temperature.

2. Characterizations of supramolecular polymers

Because of the dynamic and reversible nature of non-covalent interactions, characterization of supramolecular polymers is not easy. Indeed, a slight change in concentration, temperature or external stimuli might affect the self-assemblies to a large degree. In most cases, supramolecular polymers cannot be comprehensively studied by a single characterization technique. Hence, a combination of several characterization methods

---

[40]Laggoune, N. Delattre, F. Lyskawa, J. Stoffelbach, F. Guigner, J. M. Ruellan, S. Cooke, G. and Woisel, P. Synthesis, binding and self-assembly properties of a well-defined pillar[5]arene end functionalised polydimethylacrylamide. *Polym. Chem.* **6,** 7389–7394 (2015).

ranging from NMR and optical spectroscopies, microscopies, viscometry to light scattering and so forth is required to fully analyze the complex structures and properties of supramolecular polymers.[41] Thereafter, we have selected some examples of supramolecular polymers which characterization required particular techniques to elucidate their structure, self-assembly mechanism or properties.

In 2012, our group reported the self-assembly of poly(ethylene glycol)-perylene diimides in aqueous solutions, whose structures and dynamical properties were characterized by a combination of TEM microscopy, small-angle X-ray scattering (SAXS) and static and dynamic light scattering experiment (SLS and DLS).[42] Whereas SAXS was used to elucidate the local structure and molecular packing of the nanometic aggregates observed by DLS and TEM imaging, SLS and DLS were subsequently used to demonstrate that these stacks gradually grow into large spherical structures due to interpenetration of PEG chains. The bimodal distribution observed by dynamic light scattering experiments further demonstrated that the large globular self-assemblies release free primary stacks with time but which could be reincorporated by shaking. In another example, our group reported the formation of muscle-like metallosupramolecular polymers based on [c2]daisy chains in the mixture of chloroform and acetonitrile.[43] From small-angle neutron scattering (SANS) and SLS measurements, the relative change in linear mass density between the extended supramolecular polymer and contracted counterpart could be estimated to $\Delta M_L = (250 \pm 25)$ g mol^{-1} nm, indicating a change of the polymer contour length $\Delta L_C = (6.4 \pm 0.7)$ µm upon contraction. Overall, these examples highlight the importance of scattering experiments in determining the precise local arrangement of the molecular unit in the polymer but also the degree of polymerization which is not accessible by conventional size exclusion chromatography due to the relative lability of non-covalent interactions.

In 2007, Bouteiller and co-workers reported the synthesis and characterization of bis-urea based supramolecular polymers in a wide range of solvents from water to toluene (Figure 5a).[44] Viscosity measurements indicated that the urea groups and the hydrophobic alkylene spacers were necessary to induce the self-assembly process (Figure 5b). According to SANS experiment, all aggregates in water, acetonitrile and toluene consisted in elongated

[41](a) Liu, Y. Wang, Z. and Zhang, X. Characterization of supramolecular polymers. *Chem. Soc. Rev.* **41,** 5922–5932 (2012); (b) Yu, G. Yan, X. Han, C. and Huang, F. Characterization of supramolecular gels. *Chem. Soc. Rev.* **42,** 6697–722 (2013).

[42]Jouault, N. Xiang, Y. Moulin, E. Fuks, G. Giuseppone, N. and Buhler, E. Hierarchical supramolecular structuring and dynamical properties of water soluble polyethylene glycol–perylene self-assemblies. *Phys. Chem. Chem. Phys.* **14,** 5718 (2012).

[43]Du, G. Moulin, E. Jouault, N. Buhler, E. and Giuseppone, N. Muscle-like supramolecular polymers: Integrated motion from thousands of molecular machines. *Angew. Chemie - Int. Ed.* **51,** 12504–12508 (2012).

[44]Obert, E. Bellot, M. Bouteiller, L. Andrioletti, F. Lehen-Ferrenbach, C. and Boue, F. Both water- and organo-soluble supramolecular polymer stabilized by hydrogen-bonding and hydrophobic interactions. *J. Am. Chem. Soc.* **129,** 15601–15605 (2007).

filaments with an elliptical cross-section, which size prove to be dependent on the solvent, similarly to the degree of polymerization and linear mass density (Figure 5c). Finally, isothermal titration calorimetry (ITC) was used to investigate the thermodynamic parameters of the supramolecular polymers (Figure 5d). Quantitative analysis indicated that the self-assemblies in water were entropy driven with hydrophobic interactions being the main driving force while, in organic solvents, self-assemblies were enthalpy driven owing to hydrogen bond interactions. Overall, combination of several characterization techniques allowed for a fine understanding of the self-assembly process.
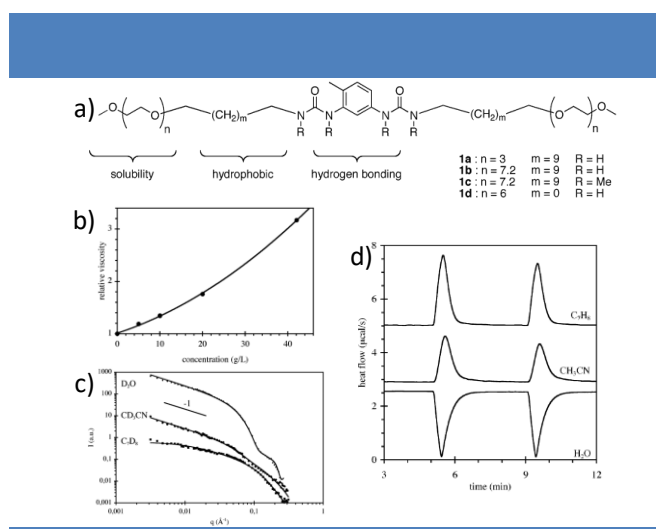
Figure 5 | a) Design and structures of bis-ureas; b) Relative viscosity (η/η_0) of water solutions versus concentration of 1b (at 25 ^{o}C); c) SANS intensity (I) versus scattering vector (q) for solutions of 1b in D$_2$O, d$_3$-acetonitrile, and d$_8$-toluene at 5 g/L (4 mM) and 22 ^{o}C; d) Heat effect produced by injecting aliquots of solutions of 1b in a given solvent into the same pure solvent (T= 25 ^{o}C). Toluene and acetonitrile, 10 µL injections at 4 mM; water, 8 µL injections at 33 mM (Reproduced from[44]).

Würthner and co-workers reported the self-assembling and gelation properties of perylene bisimide directed by hydrogen bond and π-π interactions.[45] Solvent and temperature dependent UV-Vis and circular dichrosim (CD) spectroscopies were employed to investigate the influence of different peripheral alkyl substituents on the self-assembly mechanism. From UV-Vis measurements, PBI derivatives modified with linear alkyl side chains produce H-type stacks and red gels whereas J-type stacks and green gels are observed for PBI with branched alkyl chains. CD experiments suggested that PBI derivatives containing chiral side chains lead to self-assemblies with a preferential helicity. Additionally, chiral solvents like (R)- or (S)-limonene could effectively direct the formation of one-handed helical fibers from non-chiral building blocks as confirmed by AFM studies. Thus, optical spectroscopies are convenient techniques to determine the occurrence of a self-assembly process when building

---

[45]Ghosh, S. Li, X. Q. Stepanenko, V. and Würthner, F. Control of H- and J-type π stacking by peripheral alkyl chains and self-sorting phenomena in perylene bisimide homo- and heteroaggregates. *Chem. - A Eur. J.* **14,** 11343–11357 (2008).

blocks have characteristic absorption and/or emission properties. However, these techniques preclude any characterization of the shape and size of the aggregates, which can be accessed by microscopy techniques. More recently, the same group studied the formation of supramolecular block copolymers in water by TEM, 2D NMR and optical spectroscopy.[46] A flat unsubstituted perylene bisimide dye and a twisted tetrabay-substituted one were co-self-assembled into a supramolecular block copolymer, which slowly transformed into thermodynamically stable self-sorted homopolymers upon heating. Importantly, precise arrangement of the dyes at the molecular scale was determined by ROESY NMR experiment which revealed an intermolecular face-to-face stacking between the two different PBI molecules.

Sanchez *et al.* reported a systematic investigation of the supramolecular polymerization mechanisms of oligo(phenylene ethynylene)-based tricarboxamides molecules in different solvents. [47] Techniques including variable-temperature circular dichroism (VT-CD) spectroscopy, concentration dependent ^{1}H NMR spectroscopy and isothermal titration calorimetry (ITC) were employed. Whereas ITC revealed the isodesmic nature of the polymerization process in chloroform, VT-CD experiment indicated a nucleation-growth process in apolar solvents such as toluene or methylcyclohexane. The elucidation of the self-assembly mechanism could be correlated with the gelation properties in the different solvents, which remained qualitative.

Rheological studies have also been performed on supramolecular polymers providing information on their physical properties but also their arrangement at the mesoscale. For instance, the groups of Creton and Callies studied the linear viscoelastic properties of supramolecular polymers built from poly(n-butyl) acrylate chains of various M_n decorated with a triurea moiety offering six hydrogen bonds.[48] As shown from Figure 6, a dissipative rheological behavior was observed at high frequency whereas a viscoelastic behavior indicated a relaxation of the side chains depending on their length in the middle frequency range. Interestingly, at low frequency, a good alignment of the rod like supramolecular polymers into large domains was observed for relatively small side chains, and in agreement with the formation of a gel-like structure.

---

[46]Görl, D. Zhang, X. Stepanenko, V. and Würthner, F. Supramolecular block copolymers by kinetically controlled co-self-assembly of planar and core-twisted perylene bisimides. *Nat. Commun.* **6,** 7009 (2015).

[47]Aparicio, F. García, F. and Sánchez, L. Supramolecular polymerization of C3-symmetric organogelators: Cooperativity, solvent, and gelation relationship. *Chem. - A Eur. J.* **19,** 3239–3248 (2013).

[48]Callies, X. Vechambre, C. Fonteneau, C. Pensec, S. Chenal, J. -M. Chazeau, L. Bouteiller, L. Ducouret, G. and Creton, C. Linear Rheology of Supramolecular Polymers Center-Functionalized with Strong Stickers. *Macromolecules* **48,** 7320–7326 (2015).
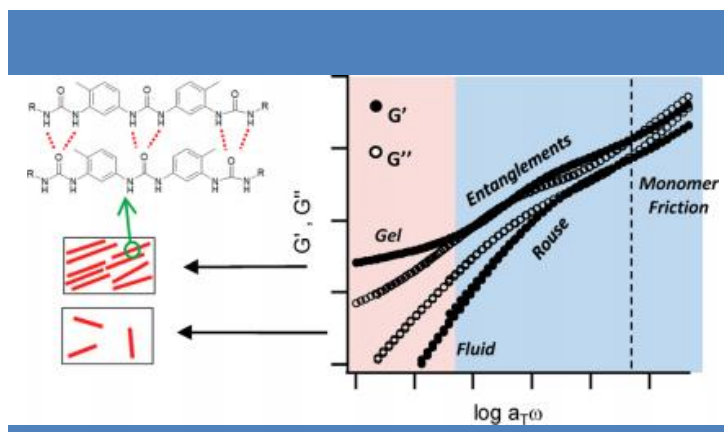
Figure 6 | Schematic chemical structure of the PnBA3U supramolecular polymer and schematic of the frequency and temperature dependence of the viscoelastic moduli for linear polymers functionalized by strong stickers in the middle. The colors indicate the molecular origin of the different zones identified in the plots (Reproduced from[30]).

Overall, a variety of physico-chemical techniques can be used to characterize supramolecular polymers, their self-assembly mechanism and their properties. In general, such experiments provide important information on the possible applications of the self-assembled structures.

3. Applications of supramolecular polymers

The development of supramolecular polymers has attracted more and more attention from researchers in the field of material science. [49] Indeed, reversible non-covalent interactions are providing supramolecular polymers with dynamic behavior that covalent polymers cannot achieve.[50] Another important advantage of supramolecular polymers is related to their highly ordered internal structure due to the unidirectionality of secondary interactions. Herein, I would like to illustrate some examples of functional supramolecular polymers with respect to their self-healing, optoelectronic, biomedical and catalytic properties.

a. Self-healing materials

Self-healing materials can be defined as materials which are able to heal a mechanical damage caused by an external force thanks to physical and/or chemical processes initiated by

---

[49](a) Aida, T. Meijer, E. W. and Stupp, S. I. Functional Supramolecular Polymers. *Science (80-.).* **335,** 813–817 (2012); (b) Moulin, E. Cormos, G. and Giuseppone, N. Dynamic combinatorial chemistry as a tool for the design of functional materials and devices. *Chem. Soc. Rev.* **41,** 1031–49 (2012); (c) Busseron, E. Ruff, Y. Moulin, E. and Giuseppone, N. Supramolecular self-assemblies as functional nanomaterials. *Nanoscale* **5,** 7098 (2013).

[50]Liu, K. Kang, Y. Wang, Z. and Zhang, X. 25th Anniversary article: Reversible and adaptive functional supramolecular materials: "noncovalent interaction" matters. *Adv. Mater.* **25,** 5530–5548 (2013).

the stress itself.[51] Such materials are inspired by biological systems and are expected to solve problems such as lifetime of the product, availability of resources, and costs. The particular features of non-covalent interactions, such as reversibility, directionality and stimuli-responsiveness make supramolecular polymers potential candidates for self-healing polymeric materials. As early as in 2000, Meijer *et al.* synthesized telechelic polymers consisting of linear polymeric chains dimerized by quadruple hydrogen bonding units between 2-ureido-4[1H]-pyrimidinones.[52] The resulting polymers showed the characteristics of a soft rubber with a storage modulus of around 10^6 Pa as revealed by dynamic oscillatory shear measurements. Interestingly, the zero shear melt viscosity of this polymer was temperature dependent, indicating reversibility due to non-covalent interactions. Leibler and co-workers prepared a supramolecular network from di- and tritopic fatty acids and ureas which behave as a self-healing and thermoreversible rubber.[53] Stress-strain experiment demonstrated the possibility to stretch this network up to 500% before breaking. One remarkable property of this system is its self-healing properties at room temperature by simply bringing together two pieces of the materials. Importantly, the self-healed materials showed similar deformation properties compared to their initial counterpart thanks to the dynamic properties of hydrogen bond interactions. Host-guest interactions were also employed to form redox-responsive and self-healing supramolecular hydrogels by the group of Harada.[54] In this system, a host poly(acrylic acid) (pAA) polymer decorated on its lateral chains by β-cyclodextrine (β-CD) hosts and a guest pAA modified polymer with ferrocene units were mixed to generate a supramolecular hydrogel (Figure 7a). A redox stimulus was used to control the sol-gel phase transition of the supramolecular hydrogel as oxidation leads to the formation of ferrocenium ions which have a low affinity for β-CD. Interestingly, macroscopic self-healing properties of the gel were observed after bringing together two pieces of gels and standing for 24 h. Such behavior was ascribed to host-guest interactions between ferrocene and β-CD as an oxidized piece of pAA-Fc gel could never reattach to a piece of pAA-β-CD (Figure 7b). A more recent example reported by the group of Bao describes a highly stretchable and self-healing elastomer based on a network of poly(dimethylsiloxane) chains cross-linked using 2,6-pyridine- dicarboxamide ligands and

---

[51](a) Yang, Y. and Urban, M. W. Self-healing polymeric materials. *Chem. Soc. Rev.* **42,** 7446–67 (2013); (b) Herbst, F. Döhler, D. Michael, P. and Binder, W. H. Self-healing polymers via supramolecular forces. *Macromol. Rapid Commun.* **34,** 203–220 (2013).

[52]Folmer, B. J. B. Sijbesma, R. P. Versteegen, R. M. Van Der Rijt, J. A. J. and Meijer, E. W. Supramolecular polymer materials: Chain extension of telechelic polymers using a reactive hydrogen-bonding synthon. *Adv. Mater.* **12,** 874–878 (2000).

[53]Cordier, P. Tournilhac, F. Soulié-Ziakovic, C. and Leibler, L. Self-healing and thermoreversible rubber from supramolecular assembly. *Nature* **451,** 977–80 (2008).

[54]Nakahata, M. Takashima, Y. Yamaguchi, H. and Harada, A. Redox-responsive self-healing materials formed from host–guest polymers. *Nat. Commun.* **2,** 511 (2011).

iron (II) metal ions.[55] As shown from Figure 7c, a healing time as long as 48 hours led to repaired films exhibiting a relatively high stretching ability with a healing efficiency of $90 \pm 2\%$ at room temperature compared with the low efficiencies for the short time healed samples.
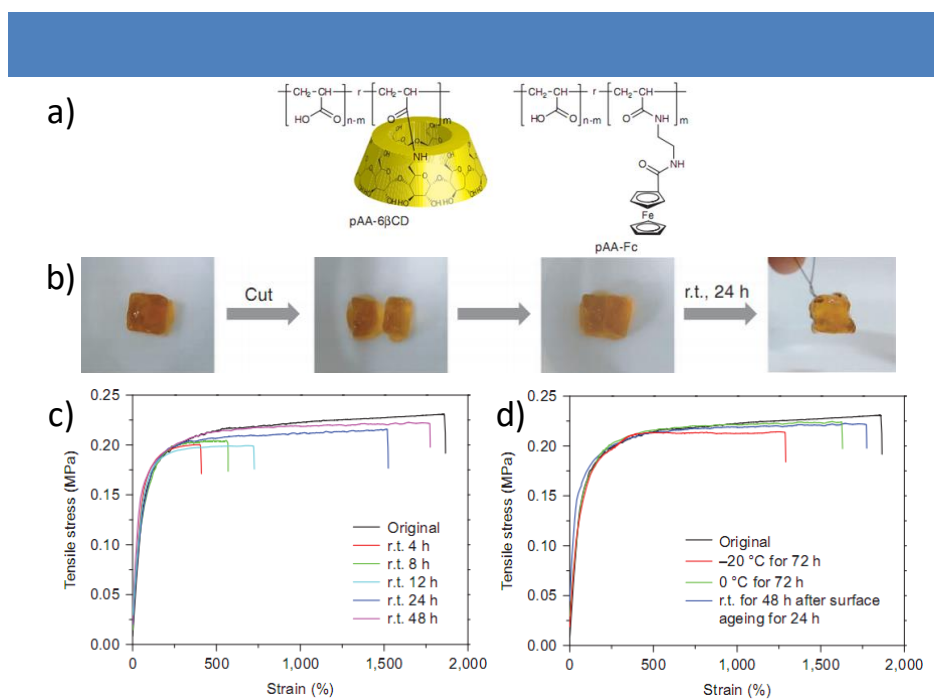

Figure 7 | a) Chemical structures of host and guest pAA polymers; b) After standing for 24 h, two cut hydrogel pieces were rejoined, and the crack sufficiently healed to form one gel; c) Stress-strain curves of a film made of a PDMS supramolecular polymer healed at room temperature (r.t.) for different lengths of time; d) Stress-strain curves of the same film healed at -20 and 0 ℃ for 72 hours, and at room temperature for 48 hours after surface ageing for 24 hours (Reproduced from[54,55]).

The stress-strain curves at different temperatures and aging times demonstrated that temperature played a more important role than aging time (Figure 7d). When a high electric field (17.2 mV.m^{-1}) was applied, the elastomer could expand 3.6% without any electric breakdown, showing potential applications as mimic of artificial muscles. Overall, these examples demonstrate that a large variety of non-covalent interactions can be involved in self-healing processes owing to their dynamic character.

b. *Optoelectronic materials*

Supramolecular self-assemblies of π-conjugated molecules showing long distance ordered structures have appeared as promising platforms for applications as conducting 1-D materials or in optoelectronic devices.[56] Aida and co-workers reported a nanotubular

[55]Li, C.-H. Wang, C. Keplinger, C. Zuo, J. Jin, L. Sun, Y. Zheng, P. Cao, Y. Lissel, F. Linder, C. You, X. and Bao, Z. A highly stretchable autonomous self-healing elastomer. *Nat. Chem.* **8,** 618–624 (2016).

[56](a) Schenning, A. P. H. J. & Meijer, E. W. Supramolecular electronics; nanowires from self-assembled pi-conjugated systems. *Chem. Commun. (Camb).* 3245–58 (2005); (b) Babu, S. S. Prasanthkumar, S. and Ajayaghosh, A. Self-assembled gelators for organic electronics. *Angew. Chemie - Int. Ed.* **51,** 1766–1776 (2012); (c) Moulin, E. Cid, J. J. and Giuseppone, N. Advances in supramolecular electronics - From randomly self-assembled nanostructures to addressable self-organized interconnects. *Adv. Mater.* **25,** 477–487 (2013); (d) Jain, A. and

supramolecular p-n junction produced by co-assembling sequentially a hexa-peri-hexabenzocoronene derivative bearing two bipyridine units as side chains (HBC-BiPy) and a tetrafluoro-HBC derivative (4F-HBC).[57] As transmission electron microscopy-energy dispersive X-ray spectroscopy can be used to map elements and bipyridine ligands can accommodate with copper ions, this technique was used to determine the formation of nanotubes with HBC-BiPy on one side and 4F-HBC on the other one. To date, this supramolecular block copolymer is the only example from small molecules that exhibits long living charge carriers up to 5 times that of their individual components, as measured by flash-photolysis time-resolved microwave conductivity. Wasielewski *et al.* exploited a zinc tetrabenzotetraphenyl porphyrin decorated with four perylenediimide acceptor units on its periphery.[58] The monomer self-assembled in toluene into a cofacial dodecamer with a finite size and narrow polydispersity. Transieny EPR and absorption spectroscopies revealed that a radical ion pair in π-stacked self-assembly having a 26 Å separation distance showed a much longer lifetime of 169 ± 0.5 ns than that of the monomer. Ulijn and Kinloch reported the formation of peptide nanotubes produced by enzyme-triggered self-assembly of 9-fluorenylmethoxycarbonyl-tri-leucine molecule (Figure 8a). Upon addition of a hydrolytic enzyme, the non-assembling monomer aggregated into a hydrogel. TEM and cryo-TEM imaging of the corresponding xerogel demonstrated the formation of nanotubular structures with an inner diameter of ~ 9 nm and an external one of ~ 24 nm (Figure 8i and ii). The electrical performance of the xerogel was shown to exhibit a sheet resistance of 0.1 MΩ/sq in air and 500 MΩ/sq in vacuum at room temperature, with its resistance increasing as the content of water decreased (Figure 8a).[59] In 2009, Meijer and Schenning reported the synthesis and optical properties of three different π-conjugated oligomers, namely a blue-emitting oligofluorene core, a green-emitting oligo(phenylene vinylene) core and a red-emitting perylene bisimide core.[60] These monomers could be individually self-assembled into supramolecular polymers in solution, which could be easily spin-coated as thin films without phase separation giving rise to light emitting films (Figure 8b). Importantly, when these monomers were mixed at an optimum ratio and the resulting solution was spin-coated,

George, S. J. New directions in supramolecular electronics. *Mater. Today* **18,** 206–214 (2015).

[57]Zhang, W. Jin, W. Fukushima, T. Saeki, A. Seki, S. and Aida, T. Supramolecular Linear Heterojunction Composed of Graphite-Like Semiconducting Nanotubular Segments. *Science (80-.).* **334,** 340–343 (2011).

[58]Roznyatovskiy, V. V. Carmieli, R. Dyar, S. M. Brown, K. E. and Wasielewski, M. R. Photodriven charge separation and transport in self-assembled zinc tetrabenzotetraphenylporphyrin and perylenediimide charge conduits. *Angew. Chemie - Int. Ed.* **53,** 3457–3461 (2014).

[59]Xu, H. Das, A. K. Horie, M. Shaik, M. Smith, A. M. Luo, Y. Lu, X. Collins, R. Liem, S. Y. Song, A. Popelier, P. L. A. Turner, M. L. Xiao, P. Kinloch, I. A. and Ulijn, R. V. An investigation of the conductivity of peptide nanotube networks prepared by enzyme-triggered self-assembly. *Nanoscale* **2,** 960–6 (2010).

[60]Abbel, R. Grenier, C. Pouderoijen, M. J. Stouwdam, J. W. Leclere, P. E. L. G. Sijbesma, R. P. Meijer, E. W. and Schenning, A. P. H. J. White-Light Emitting Hydrogen-Bonded Supramolecular Copolymers Based on π-Conjugated Oligomers. *J. Am. Chem. Soc.* **131,** 833–843 (2009).

white emission was observed upon excitation of the oligofluorene energy donor. This approach provided a useful strategy to fabricate pure organic white light emitting diodes as an alternative to currently existing technologies.
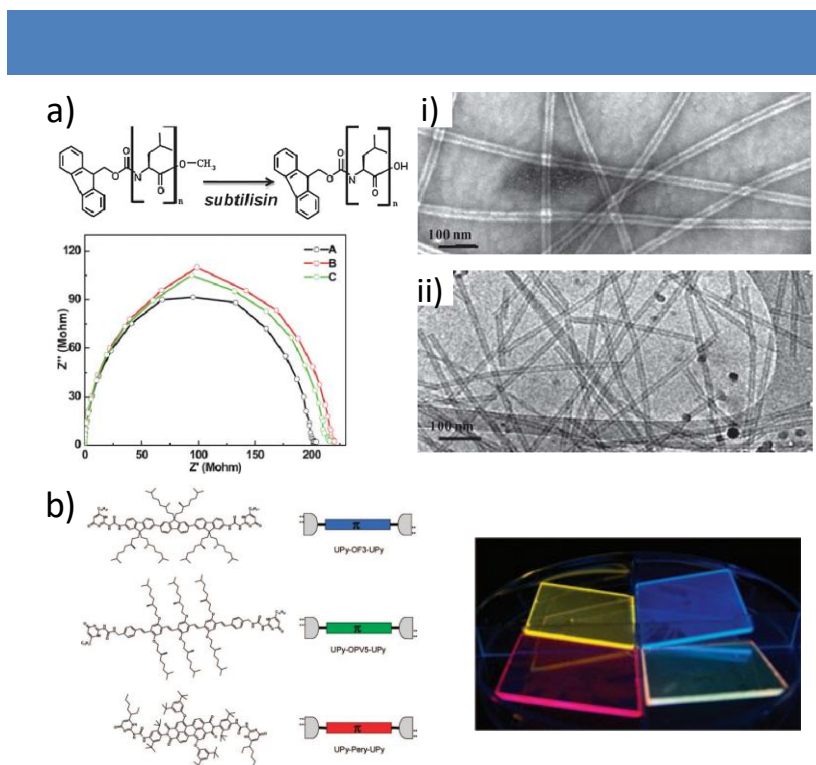
Figure 8 | a) Enzymatic hydrolysis of fluorenylmethoxycarbonyl-L-leucine-L-leucine-L- leucine methyl ester (Fmoc-L3-OMe) to Fmoc-L3 and complex impedance plot data for Fmoc-L3 film at different times in vacuum. A-day 0, B-day 2, C-day 4; i) TEM image of Fmoc-L3 (sample was negatively stained with 2% uranyl acetate); ii) cryo-TEM micrograph of Fmoc-L3 hydrogel; b) Chemical structures of the di-UPy functionalized chromophores used in this study and spin coated films of pure di-UPy chromophores and a mixture under UV irradiation (365 nm) (Reproduced from[59,60]).

Overall, these selected examples highlight how supramolecular polymers can be used to produce materials with advanced optoelectronic properties that can rival the ones observed in their covalent counterpart.

c. *Biomedical applications*

Inspired by structures found in living systems, supramolecular polymers offer several appealing advantages due to their order and dynamics associated to the presence of reversible non-covalent interactions. Over the last decades, supramolecular materials with inherent degradation properties, rapid responsiveness to biological stimuli, tunable mechanical properties and ease to deliver or bind bioactive agents *in vivo* have demonstrated great potential for biomedical applications.[61] Thereafter, we will describe some selected examples

---

[61](a) Boekhoven, J. and Stupp, S. I. 25th anniversary article: Supramolecular materials for regenerative medicine. *Adv. Mater.* **26,** 1642–1659 (2014); (b) Webber, M. J. Appel, E. A. Meijer, E. W. and Langer, R. Supramolecular biomaterials. *Nat. Mater.* **15,** 13–26 (2015);

related to novel therapies, tissue engineering or even biomedical devices. The group of Stupp has produced an enormous contribution to the field of supramolecular polymers with biomedical applications.[62] For instance, they reported the formation bioactive peptide amphiphile (PA) nanofibers by co-assembling of PA molecules containing RGDS end-chain as bioactive epitope and a tripeptide molecule used to increase the biological adhesion of bone-marrow mononuclear cells (BMNCs) (Figure 9a and b).[63]
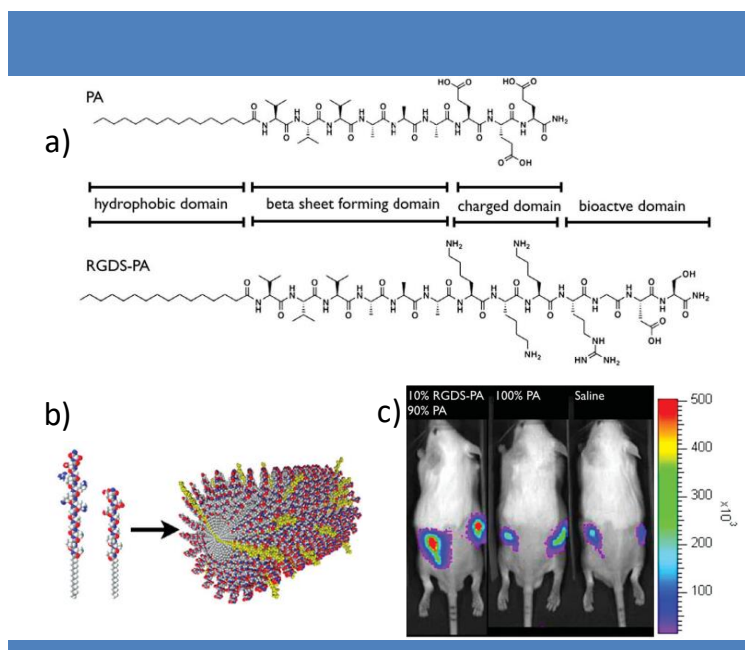

Figure 9 | a) Molecular structures of a typical PA and RGDS-PA that consist of 4 domains: a hydrophobic domain, a β-sheet forming domain, a charged domain and a bioactive domain; b) PA and RGDS-PA coassemble to form fibers expressing the RGDS bioactive cue; c) Bioluminescent images reveals an increase in bioluminescence after four days for cells encapsulated in gels of 10% RGDS-PA as a result of an increase in cell number (Reproduced from[63]).

The viability and proliferation of these cells *in vitro* were enhanced when they were embedded in the nanofiber network made by this bicomponent system, and which can serve as a supportive matrix for transplanted BMNCs. By subcutaneously injecting this binary system in mice, the supramolecular polymers can give rise to the survival of BMNCs as demonstrated by bioluminescent imaging of the transplanted mices (Figure 9c). In another example, the group of Stupp developed a new cell-free therapy for ischemic cardiovascular disease by designing a peptide amphiphile assigned to mimic the activity of vascular endothelial growth factor (VEGF).[64] A peptide amphiphile was designed to incorporate a well-known peptide

(c) Dong, R. Zhou, Y. Huang, X. Zhu, X. Lu, Y. and Shen, J. Functional supramolecular polymers for biomedical applications. *Adv. Mater.* **27,** 498–526 (2015).

[62]Cui, H. Webber, M. J. and Stupp, S. I. Self-Assembly of Peptide Amphiphiles: From Molecules to Nanostructures to Biomaterials. *Biopolym. (Peptide Sci.)* **94,** 1–18 (2010).

[63]Webber, M. J. Tongers, J. Renault, M. Roncalli, J. G. Losordo, D. W. and Stupp, S. I. Development of bioactive peptide amphiphiles for therapeutic cell delivery. *Acta Biomater.* **6,** 3–11 (2010).

[64]Webber, M. J. Tongers, J. Newcomb, C. J. Marquardt, K. Bauersachs, J. Losordo, D. W. and Stupp, S. I. Supramolecular nanostructures that mimic VEGF as a strategy for ischemic tissue repair. *Proc. Natl. Acad. Sci.* **108,** 13438–13443 (2011).

sequence that mimics VEGF. The resulting cylindrical nanostructures displaying a high-density of VEGF-mimetic peptide at their surfaces enhance the migration, proliferation and survival of endothelial cells compared to the VEGF-mimetic peptide alone. Interestingly, these PA nanofibers were shown to promote an angiogenic response *in vivo* in two models of cardiovascular disease mainly due to the regeneration of blood microcirculation. Meijer and co-workers developed bioactive supramolecular materials constructed by co-assembling a UPy-based oligocaprolactone with two UPy-based peptidic sequences, namely UPy-GRGDS which promotes the adhesion of cells *via* integrin receptors and UPy-PHSRN which is known to mediate cell adhesion.[65] *In vitro* experiments indicated that the presence of both UPy-peptides in the material is mandatory to observe cell adhesion and spreading of fibroblasts. Interestingly, *in vivo*, the supramolecular material was shown to induce cell signaling and angiogenesis, thus holding promises for use in tissue engineering. Yui and co-workers reported RGD-functionalized polyrotaxane block copolymer through host-guest interaction.[66] As indicated by surface plasmon resonance (SPR) measurements, this supramolecular polymer had the ability to interact with integrin β_1 molecules rapidly and dynamically compared to the the random copolymers with RGD side chains. SPR and quartz crystal microbalance-dissipation (QCM-D) measurements demonstrated that the random copolymer showed the initial time lag followed by a growth of the dissipation factor value while RGD-functionalized polyrotaxane block copolymer interact with the cells from the beginning. Overall, these examples demonstrate how supramolecular polymer with peptidic biorecognition units can be used for tissue engineering but also as biological sensors.

d. *Supramolecular catalysis*

Supramolecular catalysis has been a prevailing field in supramolecular chemistry and several approaches have been reported to date.[67] Supramolecular architectures have been utilized as nanoreactors or catalytic capsules and supramolecular assemblies could also lead to chirality amplification during the catalytic processes. Besides, the reversible nature of supramolecular polymers offers the opportunities to build up stimuli-controlled catalytic systems.

Parquette and Lee explored the use of supramolecular nanotubes self-assembled from a

---

[65]Dankers, P. Y. W. Harmsen, M. C. Brouwer, L. A. van Luyn, M. J. A. and Meijer, E. W. A modular and supramolecular approach to bioactive scaffolds for tissue engineering. *Nat. Mater.* **4,** 568–74 (2005)

[66]Seo, J. H. Kakinoki, S. Inoue, Y. Yamaoka, T. Ishihara, K. and Yui, N. Inducing rapid cellular response on RGD-binding threaded macromolecular surfaces. *J. Am. Chem. Soc.* **135,** 5513–5516 (2013).

[67]Singh, N. Tena-Solsona, M. Miravet, J. F. and Escuder, B. Towards Supramolecular Catalysis with Small Self-assembled Peptides. *Isr. J. Chem.* **55,** 711–723 (2015).

proline-lysine dipeptide conjugated to a naphthalene diimide unit in aqueous media to catalyze an aldol reaction in water thanks to the presence of hydrophobic microenvironments.[68] Conversions up to 97% were recorded for the aldol reaction between various benzaldehydes and cyclohexanone using a small loading (max. 10% mol) of this supramolecular nanostructure as catalyst. Whereas a slight decrease of the catalytic efficiency was observed after several catalytic cycles (recovery by ultracentrifugation) the enantioselectivity of the reaction increased by almost 10% after five cycles. Very recently, the groups of Escuder and Van Esch reported a series of self-sorted catalytic supramolecular hydrogels to catalyze one-pot deacetalization-aldol reactions.[69] Two hydrogelators were synthesized: one bolaamphiphilic structure with two carboxyl groups as termini and one amphiphilic dipeptide with an L-proline residue at its N-terminus. The co-assembly of these two monomers resulted in a self-sorting phenomenon as two kinds of fibers corresponding to the single component self-assembly could be imaged by AFM and further confirmed by DSC and wide angle X-ray diffraction (WAXD) experiments. This self-sorted hydrogel was then used in the aforementioned tandem catalytic process between benzaldehyde dimethyl acetal and cyclohexanene with up to 85% conversion and 90% enantiometic excess. These results suggest that the self-sorted gel maintained the catalytic activity of each network without interfering one with the other. Raynal and co-workers reported the co-assembly of an enantiopure BTA-based monomer with an achiral BTA ligand into chiral supramolecular helices.[70] In the presence of rhodium and because of efficient chirality transfer between the different BTA monomers, asymmetric hydrogenation of dimethyl itaconate was achieved with up to 85% enantiomeric excess in the presence of the supramolecular nanostructure. The enantioselectivity of the catalytic reaction was maintained even when substoichiometric amounts of the chiral BTA monomer were used compared to the achiral BTA ligand as a result of chirality amplification effects. Importantly, the authors demonstrated that the chirality and net helicity of the supramolecular aggregates are responsible for the formation of a preferential enantiomer and the selectivity of the catalytic reaction.

[68]Lee, K. S. and Parquette, J. R. A self-assembled nanotube for the direct aldol reaction in water. *Chem. Commun.* **51,** 15653–15656 (2015).
[69]Singh, N. Zhang, K. Angulo-Pachon, C. A. Mendes, E. van Esch, J. H. and Escuder, B. Tandem reactions in self-sorted catalytic molecular hydrogels. *Chem. Sci.* **7,** 477–482 (2016).
[70]Desmarchelier, A. Caumes, X. Raynal, M. Vidal-Ferran, A. van Leeuwen, P. W. N. M. and Bouteiller, L. Correlation between the Selectivity and the Structure of an Asymmetric Catalyst Built on a Chirally Amplified Supramolecular Helical Scaffold. *J. Am. Chem. Soc.* **138,** 4908–4916 (2016).

Chapter II: Supramolecular polymers in aqueous medium

Water plays a pivotal role in nature, providing a medium for biological processes such as protein and DNA folding, membrane formation and substrate binding.[71] In an aqueous environment, hydrophobic interactions are occurring predominantly during molecular self-assembly and offer complexity, adaptability and structural robustness to supramolecular polymers.[72] Rational molecular design and controlled polymerization pathway allow the design of diverse nanostructures including spheres, micelles, vesicles, nanorods, nanofibers, nanoribbons, nanotubes and so forth, having potential for various applications as stated in the previous chapters.[73] In this chapter, recent advances regarding supramolecular polymers in water will be reviewed according to the main non-covalent interactions involved.

1. Hydrogen bonding supramolecular amphiphiles

Although hydrogen bonds are greatly weakened in aqueous environments, strategies including multiple hydrogen bonds motifs, hydrophobic shielding and combination with other non-covalent interactions contribute to the preparation of supramolecular polymers in such polar media.

In a fundamental study, Meijer *et al.* investigated the supramolecular polymerization of a series of benzene-1,3,5-tricarboxamide (BTA) derivatives in water.[74] In order to study the influence of hydrophobic and hydrogen-bonding interactions on the self-assembly process, the BTA moiety was functionalized with amphiphilic chains consisting of a methylene spacer of various lengths (10-12 CH_2) and a tetraethylene glycol end chain. Interestingly, only BTA derivatives incorporating undecyl and dodecyl spacers formed stable supramolecular polymers in water, as evidenced by optical spectroscopies and Cryo-TEM imaging. Supramolecular copolymer systems consisting of the amphiphilic BTA derivatives and of BTA derivatives labeled with either Cy3 or Cy5 (5 mol%) were used to confirm the

---

[71](a) Krieg, E. Bastings, M. M. C. Besenius, P. and Rybtchinski, B. Supramolecular Polymers in Aqueous Media. *Chem. Rev.* **16,** 2414–2477 (2016); (b) Oshovsky, G. V. Reinhoudt, D. N. and Verboom, W. Supramolecular chemistry in water. *Angew. Chemie - Int. Ed.* **46,** 2366–2393 (2007).

[72](a) Ma, X. and Tian, H. Stimuli-Responsive Supramolecular Polymers in Aqueous Solution. *Acc. Chem. Res.* **47,** 1971–1981 (2014); (b) Zayed, J. M. Nouvel, N. Rauwald, U. and Scherman, O. a. Chemical complexity--supramolecular self-assembly of synthetic and biological building blocks in water. *Chem. Soc. Rev.* **39,** 2806–2816 (2010).

[73](a) Krieg, E. and Rybtchinski, B. Noncovalent water-based materials: Robust yet adaptive. *Chem. - A Eur. J.* **17,** 9016–9026 (2011); (b) Du, X. Zhou, J. Shi, J. and Xu, B. Supramolecular Hydrogelators and Hydrogels: From Soft Matter to Molecular Biomaterials. *Chem. Rev.* **115,** 13165–13307 (2015).

[74]Leenders, C. M. A. Baker, M. B. Pijpers, I. A. B. Lafleur, R. P. M. Albertazzi, L. Palmans, A. R. A. and Meijer, E. W. Supramolecular polymerisation in water; elucidating the role of hydrophobic and hydrogen-bond interactions. *Soft Matter* **12**, 2887–2893 (2016).

occurrence of the polymerization process thanks to Forster resonance energy transfer (FRET). This example highlights the importance of fine-tuning non-covalent interactions in order to induce the polymerization process. Esch and co-workers reported a supramolecular amphiphilic system whose morphologies can be programmed and controlled by small molecules which act as molecular chaperone analogues (Figure 10b). [75] A 1,3,5-cyclohexyltrisamide are decorated with three hydrophobic phenylalanine amino acids bearing a tetraethylene glycol tail for 2 residues and a tetraethylene glycol mono-octyl ether for the third Phe residue, was shown to assemble into a tape-like structure *via* hydrogen-bonding and hydrophobic interactions (Figure 10b i)). When a surfactant such as CTAB (cetyl trimethyl ammonium bromide) was added to the amphiphile, native fibrilar objects were observed by TEM due to the absence of hydrophobic interactions (Figure 10b ii)). When HFIP or urea were added to gels made of tape-like structures, a gel-sol transition occurred, which was accompanied by a morphological evolution into small spherical micelles as a result of the disruption of hydrogen bonding. These programmed morphological transitions can be regarded as a new approach for the construction of smart stimuli-responsive supramolecular polymers by using molecular chaperone analogues.
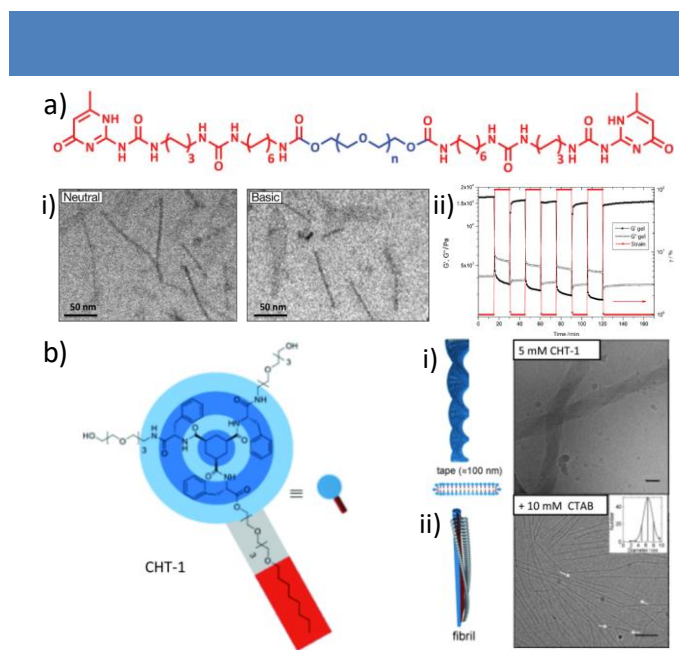
Figure 10 | a) Structure of UPy-hydrogelators with the hydrophilic PEG block in blue and the UPy-alkyl-urea end groups in red. i) Cryo-TEM of 1 wt% solution of UPy-20k demonstrates the existence of elongated fibers in both neutral and basic environment. ii) Dynamic stain amplitude test of 10 wt% UPy-10k gel at 37 °C; b) Structure of the multisegmented amphiphile CHT-1. Schematic representation and TEM images of the i) tape and ii) fiber morphologies. Scale bars are 100 nm (Reproduced from[75,76]).

[75]Boekhoven, J. Brizard, A. M. van Rijin, P. Stuart, M. C. A. Eelkema, R. and van Esch, J. H. Programmed morphological transitions of multisegment assemblies by molecular chaperone analogues. *Angew. Chemie - Int. Ed.* **50,** 12285–12289 (2011).

Dankers and co-workers developed a supramolecular hydrogel prepared from four-fold hydrogen bonding ureido-pyrimidinone (UPy) units as end chains and polyethylene glycol chains as bridging chain (Figure 10a).[76] In both neutral and basic condition (from pH 7 to 8.5), rigid and elongated fibers were observed by Cryo-TEM (Figure 10a i) and ii)). At pH > 8.5, the supramolecular hydrogel transited into a liquid. Because of its low viscosity, this liquid could flow through a 1-m long catheter and further gelate as soon as it met with a tissue. In addition, the hydrogels can also behave as liquids which recover their gel-like properties within several minutes when the strain is released. The hydrogel was also reported to carry and release growth factors in order to cure infarct scar in a pig myocardial infarction model, potentially providing a new therapeutic approach for the treatment of ischemic heart disease.

The structural versatility, water solubility and strong ability for self-assembly make peptides and proteins important building blocks for water-soluble supramolecular polymers. As mentioned in the previous section, Stupp and co-workers reported plenty of work regarding the self-assembly of linear peptide amphiphiles. For instance, in a very fundamental study, they described the influence of amino-acid sequences of peptide amphiphiles on the mechanical properties of the resulting supramolecular gels.[77] Rheological measurements showed that increasing the number and/or fraction of valine residues could improve the mechanical stiffness of the gel while alanines would weaken it. These observations were correlated with CD and FT-IR experiments, which revealed that strong gels are favored by PA which sequence leads to the formation of ordered β-sheets. Similar to the example reported by Meijer, this work highlights the importance of peptide molecular design on the physical properties of the supramolecular polymers such as the mechanical stiffness of peptide amphiphile matrices. Hybridization of peptidic sequences with π-conjugated molecular units was employed to produce a large variety of hierarchical nanostructures, having outstanding optoelectronic properties. For instance, Fry and co-workers reported the co-self-assembly of well-designed peptide amphiphiles with metalloporphyrin zinc protoporphyrin IX.[78] In basic conditions, the octa peptide amphiphile c16-AHL$_3$K$_3$-CO$_2$H was shown to self-assemble into long fibrillar aggregates thanks to β-sheet structure. Upon mixing with the porphyrin unit, fibrillar objects remained but appeared much more entangled. Finally, optical spectroscopies confirmed the incorporation of the optically-achieve compound thanks to the presence of a

[76]Leenders, C. M. A. Baker, M. B. Pijpers, I. A. B. Lafleur, R. P. M. Albertazzi, L. Palmans, A. R. A. and Meijer, E. W. Supramolecular polymerisation in water; elucidating the role of hydrophobic and hydrogen-bond interactions. *Soft Matter* **12,** 2887–2893 (2016).
[77]Pashuck, E. T. Cui, H. and Stupp, S. I. Tuning Supramolecular Rigidity of Peptide Fibers through Molecular Structure. *J. Am. Chem. Soc.* **132,** 6041–6046 (2010).
[78]Fry, H. C. Garcia, J. M. Medina, M. J. Ricoy, U. M. Gosztola, D. J. Nikiforov, M. P. Palmer, L. C. and Stupp, S. I. Self-Assembly of Highly Ordered Peptide Amphiphile Metallo- porphyrin Arrays. *J. Am. Chem. Soc.* **134,** 14646–14649 (2012).

histidine residue able to bind to the metalloporphyrin core. Tovar and co-workers have also an important contribution to this topic.[79] For instance, they reported a simple on-resin dimerization method to introduce peptidic sequences onto π-conjugated units, which then self-assembled into ribbon-like supramolecular polymers under aqueous environment thanks to a combination of π-π interactions and hydrogen bonding.[80] Electronic delocalization within 1-D nanostructures was revealed by optical spectroscopy. Similarly to this approach, Maggini *et al.* synthesized two oligo(*p*-phenylenevinylene) based amphiphiles coupled with two pentaamino-acid sequences known to form β-sheet.[81] The resulting supramolecular polymers were found to gelate reversibly upon pH modulation thanks to the formation of helical fibers in a complex network. Recently, the group of Tovar reported supramolecular donor-acceptor peptidic systems under aqueous medium wherein photoinduced electron transfer occurred.[82] The peptide amphiphiles were built from π-conjugated tetrathiophene (OT4) electron donor cores and naphthalene diimide (NDI) electron acceptors were introduced by imidation of the lysine residues located at different distances from the cores. Transient absorption spectroscopy demonstrated that electrons are transferred from the thiophene core to the NDI acceptors upon excitation of the donor. Charge-separation lifetimes increased by up to 100 times, i.e. up to the nanosecond scale in the self-assembled nanostructures compared to the non-assembled monomers. In the co-assembled systems made of donor-acceptor dyads and donor-only molecules, steady-state quenching of donor photoluminescence and transient spectral responses suggested that delocalization occurred through the self-assembly over up to four donor units. Overall, these examples illustrate the potential of water-soluble hydrogen-bonding supramolecular polymers for applications in biomedicine and optoelectronics.

2. π-π stacking supramolecular amphiphiles

Aromatic molecules decorated with hydrophilic motifs can also self-assemble in an aqueous medium into a variety of hierarchical nanostructures mainly through the mutual combination of hydrophilic and π-π interactions.[83] Although their structures are more

---

[79](a) Tovar, J. D. Supramolecular construction of optoelectronic biomaterials. *Acc. Chem. Res.* **46,** 1527–1537 (2013); (b) Ardona, H. A. M. and Tovar, J. D. Peptide π-Electron Conjugates: Organic Electronics for Biology? *Bioconjug. Chem.* **26,** 2290–2302 (2015)

[80]Vadehra, G. S. Wall, B. D. Diegelmann, S. R. and Tovar, J. D. On-resin dimerization incorporates a diverse array of pi-conjugated functionality within aqueous self-assembling peptide backbones. *Chem. Commun. (Camb).* **46,** 3947–3949 (2010).

[81]Mba, M. Moretto, A. Armelao, L. Crisma, M. Toniolo, C. and Maggini, M. Synthesis and self-assembly of oligo(p-phenylenevinylene) peptide conjugates in water. *Chem. - A Eur. J.* **17,** 2044–2047 (2011).

[82]Sanders, A. M. Magnanelli, T. J. Bragg, A. E. and Tovar, J. D. Photoinduced Electron Transfer within Supramolecular Donor-Acceptor Peptide Nanostructures under Aqueous Conditions. *J. Am. Chem. Soc.* **138,** 3362–3370 (2016).

[83]Görl, D. Zhang, X. and Würthner, F. Molecular assemblies of perylene bisimide dyes in water. *Angew. Chemie - Int. Ed.* **51,** 6328–6348

difficult to predict than in organic media, well-defined water-soluble supramolecular polymers containing π-conjugated segments have been considered as promising candidates for electronic, photonic and biological applications. Hirsch and co-workers synthesized a highly water-soluble tetrahedral shaped amphiphile based on a calixarene core decorated with two perylene diimide (PBI) moieties as hydrophobic part and two hydrophilic Newkome-type dendrons oriented on the opposite sides of the calixarene core (Figure 11a).[84] The amphiphile was shown to produce self-assembled structures at concentrations as low as 10^{-7} mol L^{-1} due to strong interactions of the PBI units and hydrophilicity of the dendrons at slightly basic pH. While cryo-TEM studies in pure water revealed the formation of various structures such as ribbon-like and tubular aggregates, the same technique showed, upon addition of THF, the unique formation of fibrous structures which ultimately turned into platelets aggregates after several weeks, as a result of crystallization. This example highlights how kinetic effects can affect polymer morphologies of a single monomer.
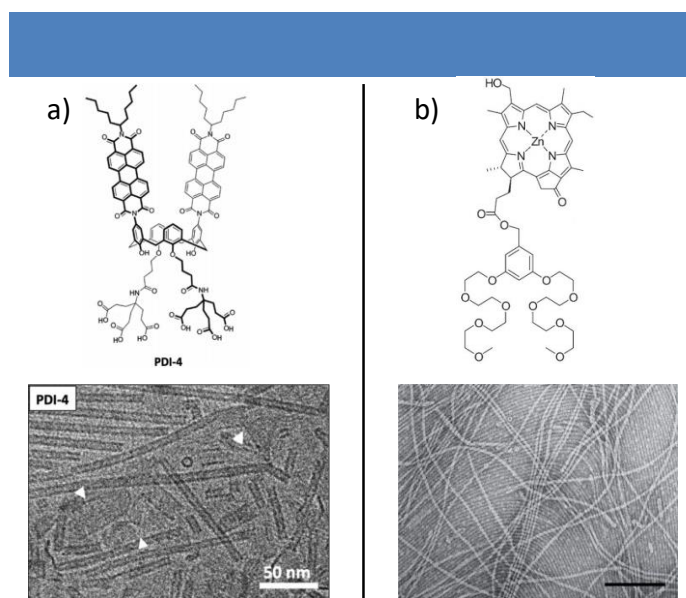

Figure 11 | a) Structure of PDI-4, and cryo-TEM image of its tubular supramolecular polymer in a water/THF mixture; b) Structure of zinc chlorin derivative and TEM image of its aggregates drop casted from a water/methanol solution (100:1; c≈10^{-5} M) and stained with 0.5% aqueous uranyl acetate at an accelerating voltage of 80 kV. Scale bar is 100 nm (Reproduced from[84,87]).

Recently, the group of Rybtchinski reported a perylene diimide amphiphile bearing a perfluorooctyl chain and poly(ethylene glycol) (PEG) chain on each bay side of the PBI core. [85] Through strong intermolecular π-π/hydrophobic interactions, this molecule self-assembled into remarkably stable supramolecular polymers with the largest association

(2012).

[84]Rodler, F. Schade, B. Jager, C. M. Backes, S. Hampel, F. Bottcher, C. Clark, T. and Hirsch, A. Amphiphilic perylene-calix[4]arene hybrids: Synthesis and tunable self-assembly. *J. Am. Chem. Soc.* **137,** 3308–3317 (2015).

[85]Krieg, E. Weissman, H. Shimoni, E. Baris, A. and Rybtchinski, B. Understanding the effect of fluorocarbons in aqueous supramolecular polymerization: Ultrastrong noncovalent binding and cooperativity. *J. Am. Chem. Soc.* **136,** 9443–9452 (2014).

constant of 1.7×10^9 M^{-1} measured in a 3:1 mixture of water/THF. Interestingly, different morphologies were observed for various THF contents suggesting that the supramolecular polymers are produced through different self-assembly mechanisms. Indeed, at THF content higher than 35%, thin fibrilar aggregates were observed as a result of cooperative polymerization, whereas for water content higher than 30% the supramolecular polymerization occurred through an isodesmic growth and led to the formation of tube-like fibers. Importantly, in pure water, the association constant was so high (~ 10^{15} M^{-1}) that neither dilution nor elevated temperature allowed the disassembly of the polymer. This work provided a useful apporach for the construction of exceptionally strong supramolecular polymers in aqueous solutions. In 2014, Würthner and co-workers investigated the supramolecular polymerization of a PBI molecule decorated with dendritic oligoethylene glycol on imide positions in water.[86] Using different characterization techniques, the morphologies of the supramolecular aggregates were found to evolve from nanorods into nanoribbons built from "side-to-side" arrangement and columnar growth of the PBI when the concentration of dyes was increased. Interestingly, the different morphologies were found to give rise to different physical properties as the quantum yield of the nanoribbon self-assemblies was 5.1% higher than that of the nanorods aggregates. Progressing towards water-soluble functional polymers, the same group prepared biosupramolecular nanostructures self-assembled from bacteriochlorophyII derivatives in water/methanol (Figure 11b).[87] TEM imaging revealed the formation of nanotubular structures in a water/methanol mixture (100:1), having diameters of approximately 6 nm and lengths ranging from 300 nm to 10 μm. As measured by pulse-radiolysis time-resolve microwave conductivity (PRTRMC) technique and conductive AFM, the supramolecular polymers exhibited charge-carrier mobilities of 0.03 cm^{2}V^{-1}s^{-1} and outstanding conductivities of 0.48 S.m^{-1}, comparable to that of semiconducting supramolecular oligomers and polymers. This example suggests that water-soluble supramolecular polymers can mimic the structure and charge-transport properties of natural chlorosomal assemblies.

Häner and co-workers designed and prepared two oligomers PO-1 and PO-2 based on three phosphodiester-linked phenanthrene units, which differ by the additional attachment of a terminal pyrene unit on PO-2.[88] Upon cooling from 90 °C to room temperature, oligomer

[86]Zhang, X. Gçrl, D. Stepanenko, V. and Würthner, F. Hierarchical growth of fluorescent dye aggregates in water by fusion of segmented nanostructures. *Angew. Chemie - Int. Ed.* **53,** 1270–1274 (2014).

[87]Sengupta, S. Ebeling, D. Patwardhan, S. Zhang, X. von Berlesch, H. Bottcher, C. Stepanenko, V. Uemura, S. Hentschel, C. Fuchs, H. Grozema, F. C. Siebbeles, L. D. A. Holzwarth, A. R. Chi, L. and Würthner, F. Biosupramolecular nanowires from chlorophyll dyes with exceptional charge-transport properties. *Angew. Chemie - Int. Ed.* **51,** 6378–6382 (2012).

[88]Winiger, C. B. Li, S. Kumar, G. R. Langenegger, S. M. and Häner, R. Long-distance electronic energy transfer in light-harvesting

PO-1 formed individual fibers of several microns, which were preserved upon co-assembly with small amounts of oligomer PO-2. While the supramolecular polymer simply made of PO-1 showed weak fluorescence, its pyrene-doped equivalent emitted intensively at 406 nm upon excitation of the phenanthrene moieties, suggesting that an energy transfer occurs between the phenanthrene units and the pyrene acceptor located in their close surrounding. Interestignly, when a very small amount (around 0.015 equiv) of pyrene acceptor was incorporated in the supramolecular fibers, complete energy transfer occurred at an energy transport distance of around 150 nm, *i.e.* corresponding to ~ 400 phenanthrene molecules. These supramolecular polymers demonstrated a new approach to fabricate artificial light-harvesting systems with dynamic properties inherent to the supramolecular interactions.

Inspired by microtubules, which can be seen as supramolecular tubes built from the protein tubulin, Lee and co-workers synthesized a bent-rod meta-linked aromatic amphiphile laterally grafted with a branched oligoether dendron group, which could self-assemble into hexameric macrocycles through π-π interactions and shape complementarity. [89] The self-assembled macrocycles composed of six amphiphilic molecules could further aggregate into helical tubules with lengths up to several microns in aqueous medium. These self-assembled nanostructures could self-dissociate into smaller aggregates (N3Nm, i.e. up to 7 stacks of hexameric macrocycles) when a silver salt was added. The reason for maintaining the supramolecular chirality in these discrete nanostructures was attributed to the conservation of the hexameric macrocyclic structure which can encapsulate the silver ion by metal ligand coordination. Using a similar approach, the same group reported the formation of responsive nematic gels from the self-assembly of a rod amphiphile made of a penta-*p*-phenylene rod laterally grafted with a dendritic oligoether chain.[90] Upon cooling, the liquid-crystaline gels made of aligned hollow nanofibers underwent a transition into a transparent solution built from soft entangled supramolecular fibers. Interestingly, myoblast cells could be incorporated inside the fibrous network, further proliferated, and subsequently be released upon cooling. These anisotropic gels give the perspective to construct artificial biomaterials for tissue engineering and drug delivery applications.

supramolecular polymers. *Angew. Chemie - Int. Ed.* **53,** 13609–13613 (2014).

[89]Kim, H. J. Kang, S. K. Lee, Y. K. Seok, C. Lee, J. K. Zin, W. C. and Lee, M. Self-dissociating tubules from helical stacking of noncovalent macrocycles. *Angew. Chemie - Int. Ed.* **49,** 8471–8475 (2010).

[90]Huang, Z. Lee, H. Lee, E. Kang, S. Nam, J. and Lee, M. Responsive nematic gels from the self-assembly of aqueous nanofibres. *Nat. Commun.* **2,** 459 (2011).

3. Supramolecular amphiphiles based on host-guest interactions

Mostly driven by the cooperativity of several non-covalent interactions, an impressive number of host-guest amphiphiles based on various macrocyclic hosts have been developed to yield well-defined nanostructures in aqueous solutions with multifunctional properties and potential applications mainly related to drug delivery.[91]

Huang *et al.* prepared a diblock copolymer based on host-guest interactions from a polyethylene oxide block bearing a bis(m-phenylene)32-crown-10 host as terminal unit (**4**) which behaves as the hydrophilic fraction and a supramolecular polymer block based on viologen/32-crown-10 ether macrocycle (**3**) host-guest motifs which behave as the hydrophobic segment (Figure 12).[92]
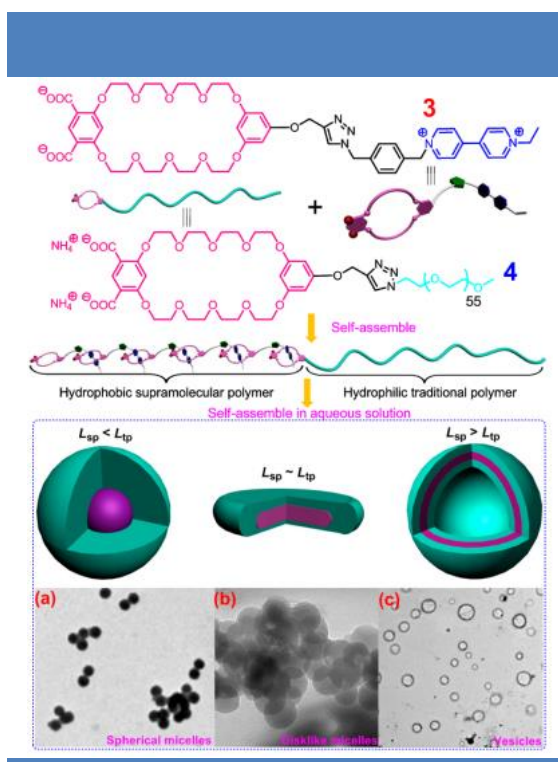

Figure 12 | Structures of building blocks 3 and 4 and cartoon representations of the diblock copolymer formation and its self-assembly in water. L_{sp} represents the extended length of the supramolecular polymer made of compound 3 and L_{tp} represents the extended length of polymer 4. TEM images of the self-assembled morphologies of the diblock copolymers in water (pH 7.0) recorded for different concentrations of 3: a) 20.0 mM; b) 30.0 mM; c) 40.0 mM, while the concentration of 4 remained constant at 1.00 mM (Reproduced from[92]).

Importantly, the supramolecular amphiphilic diblock copolymer could be produced only when the concentration of monomer **3** was higher than that of monomer **4**. The ratio of

---

[91]Yu, G. Jie, K. and Huang, F. Supramolecular Amphiphiles Based on Host-Guest Molecular Recognition Motifs. *Chem. Rev.* **115,** 7240–7303 (2015).

[92]Ji, X. Dong, S. Wei, P. Xia, D. and Huang, F. A novel diblock copolymer with a supramolecular polymer block and a traditional polymer block: Preparation, controllable self-assembly in water, and application in controlled release. *Adv. Mater.* **25,** 5725–5729 (2013).

monomers was shown to influence the chain length of the supramolecular polymer as such modification affect the proportion of hydrophobic/hydrophilic fractions, thus giving rise to different aggregate morphologies. When the chain length of the supramolecular polymer based on **3** (L_{sp}) was shorter than the chain length of polymer **4** (L_{tp}), micelles made of polymer **4** as the corona and hydrophobic host-guest supramolecular polymer based on **3** as the core block were observed. In such nanostructures, hydrophobic dye molecules could be encapsulated and subsequently released in response to pH variation. On the other hand, when L_{tp} was almost identical to L_{sp}, flatten micellar self-assemblies were observed. Finally, when the length of the supramolecular block was higher than the one of polymer **4** ($L_{sp} > L_{tp}$), vesicles with diameter of around 1 μm and wall thickness of roughly 100 nm were generated. In these nanostructures, hydrophilic molecules such as calcein could be incorporated under neutral condition and released in acidic ones. This example illustrates how different morphologies emerging from a same supramolecular polymer can lead to functional architectures with different properties. By using a different macrocyclic host such as pillar[5]arene, the same group reported a bola-type amphiphile constructed from a water-soluble pillar[5]arene and a pentaphenyl rod molecule decorated on its sides by an alkyl imidazolium chain.[93] Whereas sheet-like nanostructures with a length of 1 μm and a width of 100 nm were observed for the rod-coil molecule alone in water, the amphiphile made of one pillar[5]arene unit for one rod coil molecule aggregated into vesicular structures with an average diameter of around 200 nm. The fluorescence of vesicle was exceptionally enhanced compared to the sheet aggregates, as the pillar[5]arene units hinder electronic coupling between the pentaphenyl aromatic rings. Upon addition of paraquat which decreases pH, rapid and remarkable quenching of the fluorescence of the vesicles occurred due to the disassembly of the supramolecular host-guest system. Thus, this supramolecular polymer could find potential applications as optical sensor.

Cyclodextrins have a highly polar external surface resulting from the presence of primary hydroxyl groups and a non-polar internal cavity, which promote them as interesting hosts for host-guest chemistry in water due their high water solubility and their ease of modification. Kros and co-workers reported a stimulus-responsive system resulting from multiple orthogonal interactions (host-guest, β-sheet formation hydrophobic interactions) between an amphiphilic cyclodextrin and an adamantane-functionalized octapeptide bearing

---

[93]Yao, Y. Chi, X. Zhou, Y. and Huang, F. A bola-type supra-amphiphile constructed from a water-soluble pillar[5]arene and a rod–coil molecule for dual fluorescent sensing. *Chem. Sci.* 2778–2782 (2014).

aspartic acid residues.[94] The surface of the vesicles produced by the amphiphilic cyclodextrins could be decorated with peptidic chains behaving as random coils, *via* host-guest interactions, and without altering the self-assembled structure at pH=7.4. However, upon lowering the pH to 5.0, *i.e.* reprotonating the aspartic acid residues, the random coil domains were switched to β-sheets and concomitantly the vesicular aggregates transited into fiber-like structures. Interestingly, tetrasodium 1,3,6,8-pyrene tetrasulfonate could be encapsulated in the vesicles and further released upon decreasing the pH. In another example, Yuan and co-workers took advantage of the redox properties of ferrocene to produce stimuli-responsive delivery systems.[95] A novel supramolecular diblock copolymer constructed from poly(styrene)-β-cyclodextrin and poly(ethylene oxide)-ferrocene was shown to aggregate into vesicular structure in aqueous solution thanks to a combination of host-guest and hydrophobic interactions. Upon applying a + 1.5 V voltage, the vesicular structures disrupted thoroughly as a result of the oxidation of ferrocene and its low affinity for cyclodextrin, while, when a reductive voltage of – 1.5 V was applied to the disassembled system, similar vesicular structures were recovered. As demonstrated by fluorescent experiments, Rhodamine B could be loaded inside the hollow cavities of vesicles and released in a controlled manner by external voltage.

Calix[n]arenes offer a unique basket shape structure made of macrocyclic oligo(n) phenolic units coupled *via* methylene groups at metapositions, which promote them as important hosts to build up host-guest supramolecular amphiphiles. Li *et al.* successfully synthesized a polyrotaxane in water, which configuration can be changed reversibly by light. An α-cyclodextrin-based pseudo[3]rotaxane bearing one axially chiral 1,1'-binaphthyl unit, two photoresponsive azobenzene motifs and two 4,4'-bipyridinium units as end groups was polymerized with a bis(p-sulfonatocalix[4]arene) in water thanks to host-guest interactions.[96] As demonstrated by SEM and cryo-TEM, the supramolecular polymer can undergo a morphological transition from star-like aggregates with multiple branches to linear single helical fibers having lengths from hundreds of nanometers to micrometers upon 365 nm light irradiation for 15 min. By means of calixarene-induced aggregation, the group of Liu reported new fluorescent supramolecular nanoparticles constructed from a tetraphenylethene derivative

---

[94]Versluis, F. Tomatsu, I. Kehr, S. Fregonese, C. Tepper, A. W. J. W. Stuart, M. C. A. Ravoo, B. J. Koning, R. I. and Kros, A. Shape and release control of a peptide decorated vesicle through pH sensitive orthogonal supramolecular interactions. *J. Am. Chem. Soc.* **131,** 13186–13187 (2009).

[95]Yan, Q. Yuan, J. Cai, Z. Xin, Y. Kang, Y. and Yin, Y. Voltage-responsive vesicles based on orthogonal assembly of two homopolymers. *J. Am. Chem. Soc.* **132,** 9268–9270 (2010).

[96] Sun, R. Xue, C. Ma, X. Gao, M. Tian, H. and Li, Q. Light-driven linear helical supramolecular polymer formed by molecular-recognition-directed self-assembly of bis(p-sulfonatocalix[4]arene) and pseudorotaxane. *J. Am. Chem. Soc.* **135,** 5990–5993 (2013).

(QA-TPE) bearing tetra-ammonium side chains and mono or bis *p*-sulfonatocalix[4]arene molecules (SC4A and bis SC4A, respectively).[97] The self-assembled structures displayed an average radius of around 30 and 60 nm for SC4A+QA-TPE and bisSC4A+QA-TPE, respectively as determined by DLS experiments. The difference in size was attributed to the formation of different structures, namely multilamellar spheres for SC4A+QA-TPE and linear fibrilar structures rolled into spherical aggregates for bis SC4A+QA-TPE. While free QA-TPE did not show any fluorescence, the nanoparticles obtained from its co-dissembly with SC4A displayed aggregation-induced fluorescence (λ_{em}=480 nm, Φ=14%) as rotation of the phenyl rings from QA-TPE is hindered by the SC4A-promoted aggregation. When UV light, which lead to the cyclization of QA-TPE into a fluorescent π-conjugated system (λ_{em}=385 nm, Φ=9.3%), was shine on the SC4A+QA-TPE nanoparticles, their fluorescence was quenched by aggregation of the resulting diphenyl-phenanthrene cores. This host-guest supramolecular system with fluorescence regulated by multiple stimuli was anticipated to have potential applications in optoelectronic devices, as logic gates or fluorescent probes.

Cucurbit[n]urils (CB[n]) are macrocyclic n-glycoluril molecules, offering hydrophobic cavity for guests but they prove to be difficult to modify and are thus used as such. Scherman and co-workers reported the formation of a supramolecular peptide-amphiphile vesicle in water using CB[8] as host a pyrene-functionalized peptide as hydrophilic guest and a viologen lipid as hydrophobic guest.[98] Indeed, the size of the cavity allows for the incorporation of the viologen-pyrene complex, thus producing a supramolecular peptide-amphiphile able to generate bilayer vesicular structures with diameters ranging from 100 to 200 nm. When 2,6-dihydroxynaphthalene or 1-adamantylamine were added to the vesicles, the peptide was released due to competitive binding with CB[8] and fluorescence turned on. These supramolecular peptide amphiphiles enriched the family of stimuli-responsive self-assembled systems used for drug delivery, or peptide therapeutics. These examples demonstrate the versatilities of the structures that can be used to produced supramolecular polymers in water thanks to host-guest interactions and their potential applications as sensors and/or drug delivery systems, which are inherent to their encapsulating properties within the host.

[97] Jiang, B. P. Guo, D. S. Liu, Y. C. Wang, K. P. and Liu, Y. Photomodulated fluorescence of supramolecular assemblies of sulfonatocalixarenes and tetraphenylethene. *ACS Nano* **8,** 1609–1618 (2014).

[98] Jiao, D. Geng, J. Loh, X. J. Das, D. Lee, T. and Scherman, O. A. Supramolecular peptide amphiphile vesicles through host-guest complexation. *Angew. Chemie - Int. Ed.* **51,** 9633–9637 (2012).

4. Supramolecular amphiphilic polymers controlled by electrostatic interactions

In principle, non-covalent interactions such as hydrogen bond and aromatic stacking commonly used for self-assembly are weakened in polar media and their associated molecular units are poorly soluble in water. Hence, they are often associated with non-covalent electrostatic interactions to build up stable supramolecular polymers in aqueous solutions. Such electrostatic interactions typically involve ion-pairs made of organic anions such as sulfonate and carboxylate units and organic cations such as ammonium moieties.[99]

In 2007, Aida and co-workers reported a Gemini-shaped hexabenzocoronene amphiphile bearing water-soluble isothiouronium ion on one side and dodecyl chains on the other one.[100] These molecules were shown to self-assemble in dichloromethane into nanotubular structures, which surfaces consisted of positively charged isothiouronium ions. When this self-assembled structure was mixed with a solution of poly(4-styrenesulfonate) (PSS), a hybrid polymeric material was produced due to strong multivalent interactions between isothiouronium cations and sulfonate anions. By employing a similar strategy, the nanotubes could be decorated with densely electron deficient anthraquinone-2-carboxylate, resulting in fluorescence quenching of the self-assemblies by photoinduced electron transfer. This work provided a useful post-functionalization approach for the construction of supramolecular nanoscaffolds.

Peptides and proteins are also interesting units to generate electrostatic interactions owing to the intrinsic pH sensitivity of amino acids. For instance, Woolfson *et al.* reported the co-assembly of two peptides into long and thick protein fibers in water.[101] In order to optimize electrostatic interactions, additional aspartic acid and arginine residues were added to the peptidic sequence allowing to achieve thicker and better defined fibers by promoting longitudinal association. As demonstrated by electron microscopy, CD spectroscopy and wide-angle x-ray diffraction, the bis-peptidic co-assemblies arranged into double-stranded α-helical coiled-coil rods packed in an hexagonal lattice which further self-assemble into fibers having extended widths ($\geq$ 50 nm) and lengths ($>$ 10 μm). Additionally, the length of the peptides could be changed without affecting the formation of fibrillar aggregates but with controlling the peptidic repeat along the fiber main axis. This peptidic engineering approach

---

[99]Rehm, T. H. and Schmuck, C. Ion-pair induced self-assembly in aqueous solvents. *Chem. Soc. Rev.* **39,** 3597–3611 (2010).

[100]Zhang, G. Jin, W. Fukushima, T. Kosaka, A. Ishii, N. and Aida, T. Formation of water-dispersible nanotubular graphitic assembly decorated with isothiouronium ion groups and its supramolecular functionalization. *J. Am. Chem. Soc.* **129,** 719–722 (2007).

[101]Papapostolou, D. Smith, A. M. Atkins, E. D. Oliver, S. J. Ryadnov, M. G. Serpell, L. C. and Woolfson, D. N. Engineering nanoscale order into a designed sprotein fiber. *Proc. Natl. Acad. Sci.* **104,** 10853–10858 (2007).

offered an elegant strategy to construct nanoscale order of protein fibers. In another example, Hartgerink and colleagues synthesized a series of triblock A-B-A oligopeptides with the middle B block consisting of alternating glutamine and leucine residues, which have the tendency to form *β*-sheet structures.[102] By tuning the ratio between the size of the A and B blocks, vesicles or nanofibers of controlled size were observed by cryo-TEM. Interestingly, when a solution of $K_2(QL)_6K_2$ was subjected to increased ion concentration or pH, more viscous solutions made of infinite length fibers were observed due to the reduction of change repulsion between the peptidic fragment. Recently, the group of Besenius prepared new anionic and cationic peptide monomers, and studied their co-assembly in a 1:1 ratio (Figure 13a and b).[103]
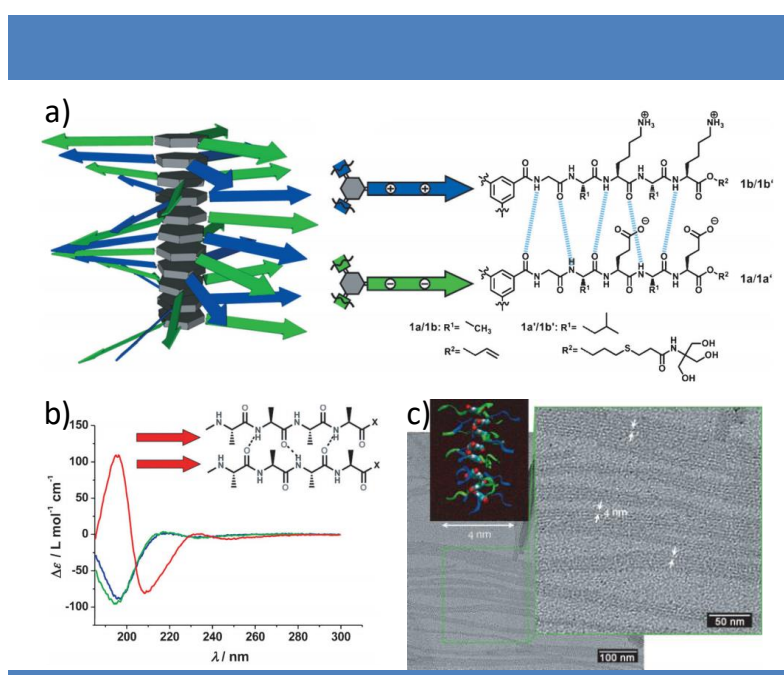
Figure 13 | a) Schematic representation of the supramolecular copolymer and the anionic/cationic β-sheet-encoded dendritic co-monomers 1a/1b and 1a'/1b'; b) CD spectra of solutions of the dendritic monomers 1a (green curve), 1b (blue curve) and a 1:1 mixture of 1a/1b (red curve); c) HRTEM images of the self-assembled dendritic peptide amphiphiles 1a and 1b [the monomers were mixed in a ratio of 1:1 at a total concentration of 0.1 mM in 20 mM phosphate buffer (pH 6.1) and then deposited onto the TEM grid] (Reproduced from[103]).

The anionic monomers consisted of a BTA core decorated by three pentapepditic strands made of alternative glutamic acid/alanine residues while cationic monomers comprised alternating lysine and alanine residues on the pentapeptide. Thanks to the cooperative combination of hydrogen bonds, Coulomb attractive interactions and hydrophobic shielding, nanorods with a width of 4 nm were recorded by HRTEM for the 1:1 supramolecular

---

[102]Dong, H. Paramonov, S. E. Aulisa, L. Bakota, E. L. and Hartgerink, J. D. Self-assembly of multidomain peptides: Balancing molecular frustration controls conformation and nanostructure. *J. Am. Chem. Soc.* **129,** 12468–12472 (2007).

[103]Frisch, H. Unsleber, J. P. Ludeker, D. Peterlechner, M. Brunklaus, G. Waller, M. and Besenius, P. PH-switchable ampholytic supramolecular copolymers. *Angew. Chemie - Int. Ed.* **52,** 10097–10101 (2013).

copolymers (Figure 13c). Interestingly, these copolymers showed a pH-sensitive on-off behavior at pH 3.6 and 8.9 due to the respective protonation of the Asp residues or deprotonation of the Lys ones. When more hydrophobic leucine residues were inserted in the sequence, the stability window of the 1:1 copolymers was expanded to pH 2.0-12.0. Finally, Hodgkiss and co-workers synthesized a set of perylene bisimides symmetrically substituted with peptidic side chains of the peptidic chain (Leu instead of Ala and Glu instead of (Glu)$_3$, respectively).[104] By tuning hydrophobic and electrostatic interactions, the self-assemblies of these derivatives were investigated. In water-rich solutions, weakly-coupled H-aggregates were formed as hydrophobic interactions are minimized in such cofacial arrangement. In acidic water (pH < 4), UV-vis absorption spectrum of the perylene bisimide aggregates demonstrated the formation of strongly coupled H-aggregates due to the absence of electrostatic repulsion. Interestingly, when divalent cations were added to water solutions of the dyes, the UV-Vis spectra evolved towards H-aggregates mostly due to coordination of the glutamate residues. These examples demonstrate how electrostatic interactions can be used to tune the morphologies of supramolecular polymers. Although non-covalent interactions are not favored in polar media, the selected examples reported in this manuscript demonstrate how molecular design is a powerful tool to achieve well-defined assemblies in water, which morphologies are related to the main self-assembling motif.

---

[104] Gallaher, J. K. Aitken, E. J. Keyzers, R. A. and Hodgkiss, J. M. Controlled aggregation of peptide-substituted perylene-bisimides. *Chem. Commun.* **48,** 7961 (2012).

Chapter III: Cross-linked supramolecular polymers

As we have seen in the previous chapters, supramolecular polymerization has been extensively studied to construct functional materials with innovative properties inherent to the dynamics of their non-covalent interactions. However, architectures built up simply by such relatively weak interactions might not be strong enough for practical applications. Therefore, cross-linking postfunctionalization strategies has been used to provide these supramolecular polymeric materials not only with thermal stability but also with mechanical robustness. On the other hand, cross-linking methods have been also utilized to capture kinetic intermediates during supramolecular polymerizations or to produce other novel supramolecular structures. To date, a variety of cross-linking methods such as olefin and ring opening metathesis polymerization, sol-gel approaches based on siloxane polymerization, photopolymerization of diacetylene units and "click" reactions have been reported to freeze supramolecular architectures. In this section, various cross-linked materials fabricated from supramolecular polymers by these different methodologies will be discussed and their properties will be highlighted.

1. Cross-linked polymers built from ring opening metathesis polymerization (ROMP)

Olefin metathesis reactions are metal-mediated bimolecular processes leading to the formation of new carbon-carbon bonds, which have a significant impact in organic synthesis and polymer chemistry. In 2005, Chauvin, Grubbs and Schrock shared the Nobel Prize in chemistry for their contributions to the development of the olefin metathesis method in organic synthesis.[105] In 1970, Chauvin proposed the rational mechanism for olefin metathesis which involves a key metallacyclobutane intermediate, and paved the way for the development of this catalytic reaction.[106] Advances related to the enhancement of the catalytic activity have been achieved independently by the group of Schrock and Grubbs, who proposed and disseminated the use of transition metal carbene complexes made from

---

[105]Grubbs, R. H. Nobel Lecture: Olefin Metathesis Catalysts for the Preparation of Molecules and Materials. *Angew. Chemie - Int. Ed.* **45,** 3760–3765 (2005).

[106]Herisson, J.-L. and Chauvin, Y. Catalyse de transformation des olefines par les complexes du tungstene. *Makromol. Chem.* **141,** 161–176 (1971)

molybdenum/tungsten and ruthenium, respectively.[105,107] The high turnover of these catalysts, their compatibility with a variety of functional groups and their possible stability to air have promoted olefin metathesis as an important tool for the synthesis of biologically relevant compounds but also for polymers. For this last application, two methodologies have been particularly developed since the mid 80's: acyclic diene metathesis (ADMET) and ring-opening metathesis polymerization (ROMP).[108] In this section, we will mainly focus on ROMP as we have used this methodology in our work.

From the kinetic point of view, ROMP is a chain growth polymerization process, meaning that the growing polymer chain is built by the stepwise addition of a monomer to its active site. In ROMP, monomers are cyclic strained olefins which react with a carbene complex catalyst to yield a metallacyclobutane intermediate, *via* a [2+2] cycloaddition thus initiating the growth of the polymer chain. The [2+2] cycloaddition of the metallacyclobutane into the metal alkylidene allows the polymerization process to propagate until all free monomers in solutions are consumed. Finally, termination of the polymerization usually occurs upon addition of a sacrificial olefin (in general, ethyl vinyl ether) to remove the metal from the polymer chain.

Over the past decades, a variety of structurally well-defined catalysts have been used for ROMP with unprecedented efficiency. In particular, various metal transitions complexes based on titanium, tungsten, molybdenum and ruthenium, and incorporating organic ligands have been developed so that reactions can be performed in homogeneous conditions. In contrast to other metals, ruthenium complexes can tolerate more polar functional groups and have thus been extensively studied. In the mid 90's, the Grubbs first-generation catalyst, synthesized from $(PPh_3)_3RuCl_2$ and diazobenzylidene followed by phosphine exchange, expanded the choice of monomers available for ROMP but proved sometimes more sensitive than Schrock catalysts (Figure 14a). In order to improve catalyst activity, a nitrogen-heterocyclic carbene (NHC) ligand, which plays a key role in the catalytic cycle, has then been incorporated to afford the Grubbs second-generation catalyst (Figure 14b). Although this catalyst shows remarkably high activity in ROMP, the obtained polymers were characterized by molecular weights and PDIs that are difficult to control.

---

[107]Schrock, R. R. Multiple metal-carbon bonds for catalytic metathesis reactions (nobel lecture). *Angew. Chemie - Int. Ed.* **45,** 3748–3759 (2006).
[108]Sutthasupa, S. Shiotsuki, M. and Sanda, F. Recent advances in ring-opening metathesis polymerization, and application to synthesis of functional materials. *Polym. J.* **42,** 905–915 (2010).
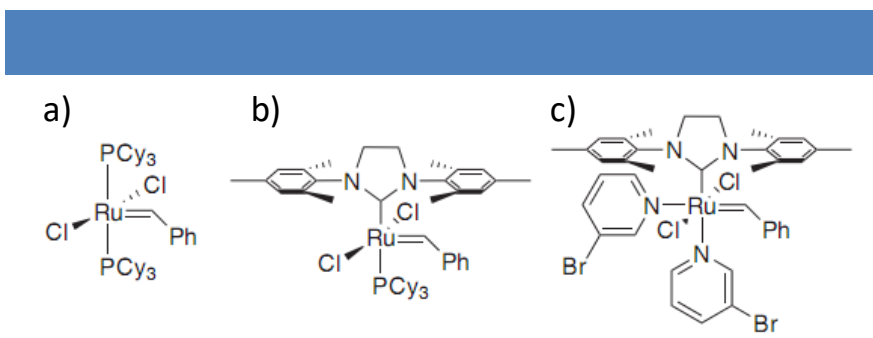
Figure 14 | a) Molecular structure of Grubbs first generation catalyst; b) Grubbs second generation catalyst and c) Grubbs third generation catalyst (Reproduced from[108]).

Finally, the Grubbs third generation catalyst, which differs from the second one by the presence of two weakly coordinating pyridine ligands, thus allowing high initiation rates, was found to provide polymers with low PDIs (<1.10) (Figure 14c). Nowadays, these three-generation Grubbs catalysts which are commercially available are commonly selected for ROMP and we will now highlight some selected examples of supramolecular polymers stabilized by ROMP using these catalysts.

In self-assembly processes, some kinetic intermediates might display more interesting properties than the thermodynamically favored aggregates and have thus to be trapped for studies. Aida and colleagues used ROMP to trap kinetically and thermodynamically favored self-assemblies of a hexabenzocoronene (HBC) amphiphile decorated with norbornene units (Figure 15a).[109] While nanocoils occurred predominantly at 15 °C, they gradually evolved towards nanotubes after standing for several days at 15 °C, as indicated by SEM microscopy. Both structures were cross-linked by ROMP using Grubbs second generation catalyst leading to enhanced thermal stabilities of both nano-aggregates (Figure 15a i) and ii)). Additionally, the post-polymerization process hampered the coil-to-tube transformation and allowed to determine the conductivity of the cross-linked nanocoils (1×10^{-4} S.cm^{-1}), which could not be determined for the nonpolymerized ones as they are disrupted upon doping. This work exemplified a postfunctionalization stategy to capture thermodynamically disfavored functional structures in the course of supramolecular self-assembly.

---

[109]Yamamoto, T. Fukushima, T. Yamamoto, Y. Kosaka, A. Jin, W. Ishii, N. and Aida, T. Stabilization of a kinetically favored nanostructure: Surface ROMP of self-assembled conductive nanocoils from a norbornene-appended hexa-peri-hexabenzocoronene. *J. Am. Chem. Soc.* **128,** 14337–14340 (2006).
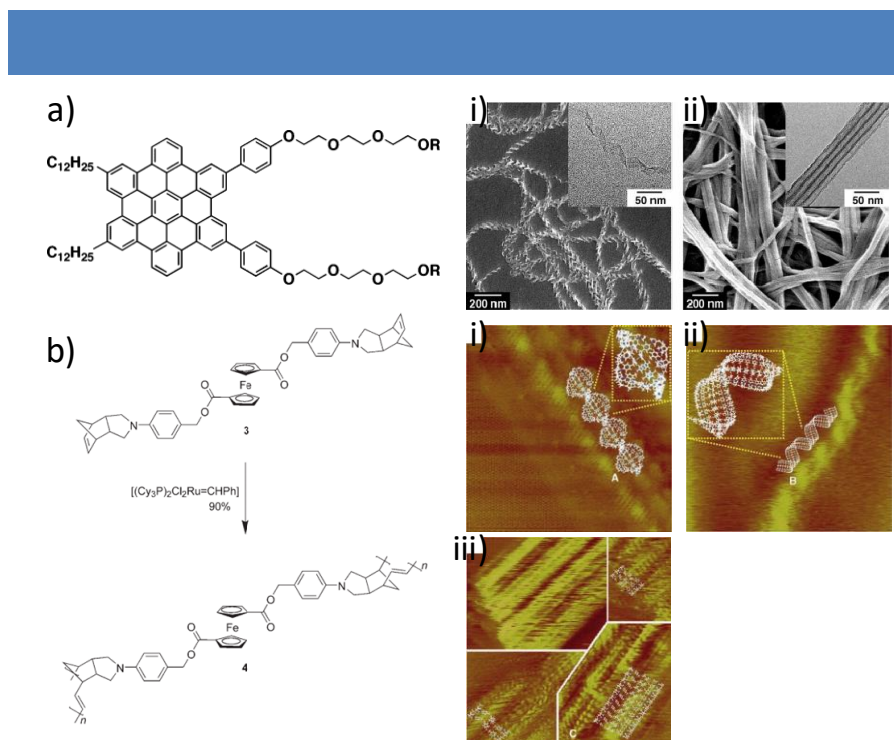
Figure 15 | a) Molecular structure of an amphiphilic HBC with polymerizable norbornene group. SEM and TEM (inset) images of i) polymerized nanocoils and ii) polymerized nanotubes by post-ROMP; b) Molecular structures of bisnorbornene derivative 3 and polymerized bisnorbornene derivative 4 through ROMP. STM images of i) helical (16.8 nm×16.8 nm), ii) supercoil (58 nm×58 nm) and iii) ladder morphologies (7.2 nm×7.2 nm) (Reproduced from[109,111]).

By employing ROMP, the research group of Luh had an important contribution to the formation of cross-linked supramolecular polymers with well-defined structures in the recent years.[110] Inspired by the double-helical structures of DNA, this group prepared an analogous double-stranded polymer constructed from a bisnorbornene derivative separated by a ferrocene linker (Figure 15b).[111] This compound with two polymerizable groups was treated with the Grubbs first generation catalyst, leading to the formation of helical, supercoil and ladder structures as precisely characterized by scanning tunneling microscopy (STM). For instance, the helical structures showed an average pitch length of 5.2 nm corresponding to 12 monomeric units and a 0.45 nm spacing between neighboring units (Figure 15b i)). The supercoiled structures were difficult to image at the molecular scale resolution but an average spacing per turn of 7.1 nm and a nominal width of around 3.0 nm could be recorded (Figure 15b ii)). As for the ladder structure, a width of 2.2 nm and a spacing between layers of around 0.5 nm were imaged, which are in agreement with parameters expected for such polynorbornene backbones (Figure 15b iii)). Subsequently, the same group reported the

[110]Luh, T. Y. Ladderphanes: A new type of duplex polymers. *Acc. Chem. Res.* **46,** 378–389 (2013).

[111]Yang, H.-C. Lin, S. Yang, H. Lin, C. Tsai, L. Huang, S. Chen, W. Chen, C. Jin, B. and Luh, T. Molecular Architecture towards Helical Double-Stranded Polymers. *Angew. Chemie - Int. Ed.* **45,** 720–730 (2006).

stepwise template polymerization of a similar unsymmetrical double stranded polymer, which can be assimilated to a replication process.[112] First, an unsymmetric ferrocene-containing monomer with one norbornene unit was polymerized by ROMP and the resulting polymer was subsequently chemically modified with a new norbornene moiety. A second round of ROMP on this polymer provided the expected double stranded network. However, in this case, only ladder shaped structures with width of 2.8 ± 0.2 nm and length of 10.5 ± 2.7 nm could be imaged by STM. These examples demonstrate different strategies to access well-defined DNA-like polymers from purely synthetic monomers using molecular design and ROMP methodologies. Subsequently, the same group took advantage of the self-assembling properties of oligoaryl monomers such as terphenylene-diethynylene or porphyrin moieties to reach polymeric ladderphanes (M_n up to 31,000 with PDIs ranging from 1.61 to 1.74) with photophysical properties associated to their monomeric units.[113] Importantly, as a result of π-π interactions between the monomers, STM imaging indicated that all polymeric structures were built with the aromatic linkers aligned perpendicular to the longitudinal axis. In terms of photophysical properties, all polymers showed absorption spectra similar to their monomers but the corresponding extinction coefficients were greatly enhanced as a result of close interactions between the electroactive units. Finally, we would like to highlight that such strategies can be used to build triple-stranded polymeric ladderphanes from C_3 symmetric planar oligoaryl linkers with C_3 symmetry through ROMP.[114] Similarly to the polymers obtained from C_2 symmetric molecules, optical properties of the triple-stranded polymers were found to be greatly affected by the ordering of the electroactive units at the nanoscale. Overall, these examples confirm that the combination of supramolecular and covalent polymerization can give rise to well-defined architectures with potentially interesting properties.

Moving in this direction, Sun and co-workers recently synthesized a new class of functional poly(bisnorbornene)-based ladderphanes incorporating perylene bisimide moieties as electroactive units.[115] As polymerization was performed with Grubbs III catalyst, triblock copolymers (ABA) with PDI of 1.4 to 1.6 and molecular weights up to 136 kDa were obtained while using difluorophenyl units as B block. Importantly, DSC experiments

[112]Lin, N. T. Lin, S. Lee, S. Chen, C. Hsu, C. Hwang, L. P. Xie, Z. Chen, C. Huang, S. and Luh, T. From polynorbornene to the complementary polynorbornene by replication. *Angew. Chemie - Int. Ed.* **46,** 4481–4485 (2007).

[113]Chou, C. M. Lee, S. Chen, C. Biju, A. T. Wang, H. Wu, Y. Zhang, G. Yang, K. Lim, T. Huang, M. Tsai, P. Lin, K. Huang, S. Chen, C. and Luh, T. Polymeric ladderphanes. *J. Am. Chem. Soc.* **131,** 12579–12585 (2009).

[114]Yang, K. W. Xu, J. Chen, C. Huang, H. Yu, T. J. Lim, T. Chen, C. and Luh, T. Triple-stranded polymeric ladderphanes. *Macromolecules* **43,** 5188–5194 (2010).

[115]Chen, J. Zhou, D. Wang, C. Liao, X. Xie, M. and Sun, R. High-performance dielectric ionic ladderphane-derived triblock copolymer with a unique self-assembled nanostructure. *RSC Adv.* **6,** 88874–88885 (2016).

demonstrated that glass transition temperatures of more than 180 $^{\circ}$C can be reached due to the rigid structure of the ladderphanes. Furthermore, the dielectric properties of the different polymers were found to be strongly related to the molecular design and arrangement of the chains. Overall, all the examples highlight the power of covalent polymerization to freeze self-assembled architectures with interesting physical properties inherent to the presence of aggregated monomers and with increased robustness.

2. Cross-linked supramolecular polymers built from sol-gel processes

The sol-gel technique is one of the important methodologies used to fabricate hybrid materials, combining organic and inorganic species on the molecular to mesoscopic scale.[116] Owing to the unique features of their inorganic moieties, hybrid materials show strikingly boosted stability and are thus promising for applications such as electroactive or controlled release materials, for instance. Compared with other types of hybrid materials, sol-gel derived silica-based materials constructed from organosilane precursors of general formula $[(RO)_3Si]_mR'$ (m$\geq$2, R' including functionalized organic units) have been widely investigated due to their ease of synthesis, good controllability and chemical stability. Sol-gel chemistry of organosilanes is typically driven by either acid or base and involves a two-step process namely hydrolysis and condensation reactions. In the first step, alkoxy groups are hydrolyzed to their hydroxyl equivalent *via* a pentacoordinate transition state in either acid or base-catalyzed environments. In general, the hydrolytic reaction is relatively slow under acidic conditions while faster under basic ones when the number of hydroxyl functions increases.[117] In the following condensation step, siloxane bonds are formed through acidic or basic catalysis. However, in basic conditions, small agglomerates in the "sol" might be produced and thus lead to colloidal gels, whereas chain-like structures are obtained and further generate network-like gels in acidic conditions. Importantly, the design of organic bridging component might allow for supramolecular self-assembly through hydrogen bonding, π-π stacking and hydrophobic interactions before polymerization, thus producing self-organized organic-inorganic materials with potentially interesting functional properties. Some selected examples will be described afterwards.

---

[116]Mizoshita, N. Tani, T. and Inagaki, S. Syntheses, properties and applications of periodic mesoporous organosilicas prepared from bridged organosilane precursors. *Chem. Soc. Rev.* **40,** 789–800 (2011).
[117]Danks, A. E. Hall, S. R. and Schnepp, Z. The evolution of 'sol–gel' chemistry as a technique for materials synthesis. *Mater. Horiz.* **3,** 91–112 (2016).

For example, Barboiu *et al.* used urea-modified macrocyclic receptors to synthesize organic-inorganic hybrid membranes *via* a sol-gel process in aprotic solvent (chloroform) under heterogeneous catalysis (Figure 16a).[118]
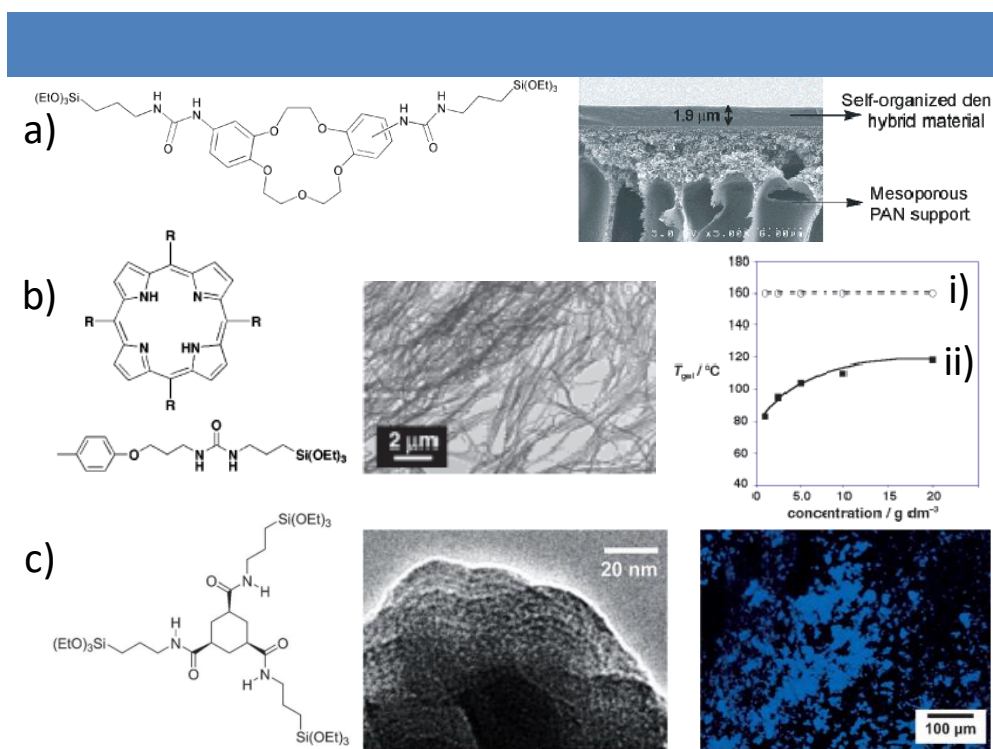

Figure 16 | a) Structure of a dipotic macrocyclic receptor and SEM image of the cross-section of the membrane obtained after the sol-gel process: the thin layer dense film is deposited onto a polymeric support; b) Structure of a triethoxysilyl modified porphyrin derivative, TEM image of the corresponding xerogel from the anisole induced sol-gel polycondensation and plots of T_{gel} versus concentration of the corresponding Cu complex ii) before and i) after sol-gel polycondensation using anisole; c) Chemical structure of a cyclohexane trisamide organosilane precursor 1 and TEM image of the corresponding periodic mesoporous organosilicas (PMO) and fluorescence micrograph of the PMO doped by a fluorescence probe (Reproduced from[118,120,122]).

The presence of urea motifs on the monomer initially drives their self-assembly in solution before alkoxysilane polymerization. As revealed by FTIR and NMR spectroscopies, hydrogen bonding interactions which promoted this self-assembly process were preserved in the silica matrix after the sol-gel process. Importantly, X-ray diffraction (XRD) and TEM experiment suggested that the macrocyclic units are arranged in a tubular structure. Furthermore, the unique supramolecular arrangement of the urea and macrocylic moieties allowed for both anion and cation transport in the membranes in a directional manner. The same group used also the sol-gel method to transfer the chirality of supramolecular polymers made of G-quadruplexes in organic-inorganic hybrid materials.[119] Using XRD and SEM

[118]Barboiu, M. Cerneaux, S. Van Der Lee, A. and Vaughan, G. Ion-Driven ATP Pump by Self-Organized Hybrid Membrane Materials. *J. Am. Chem. Soc.* **126,** 3545–3550 (2004).

[119]Arnal-Hérault, C. Banu, A. Barboiu, M. Michau, M. and Van Der Lee, A. Amplification and transcription of the dynamic supra-molecular chirality of the guanine quadruplex. *Angew. Chemie - Int. Ed.* **46,** 4268–4272 (2007).

experiments, a guaninesiloxane monomer was shown to assemble in the presence of K^+ ions into a twisted hexagonal rod-like morphology of both chiralities. Subsequently, SEM demonstrated that helical nanofibers, helical nanobundles and microsprings morphologies can be obtained for the inorganic materials upon calcination at 400 ^{o}C. These examples highlight how information such as chirality or functional properties contained in supramolecular polymers can be transferred to the mesoscopic scale using sol-gel processes, leading to new materials with programmed functions.

Sol-gel reaction was also employed by the group of Shinkai to freeze self-assembled structures made of porphyrins in the organogel phase (Figure 16b).[120] A porphyrin-based monomer decorated with four siloxane groups at its periphery was shown to self-organize into nanofibers and form gel in the presence of Cu^{2+} in aromatic solvents. Upon *in situ* sol-gel polycondensation, a robust gel made of bundles of 1-D porphyrin aggregates was obtained. Interestingly, the gel transition temperature of the resulting cross-linked gel reached up to 160 ^{o}C independently of the concentration and its storage modulus G' was enhanced 14 times compared to the gels before sol-gel polycondensation. This work clearly demonstrated the power of covalent polymerization to achieve materials with increased robustness. Similarly, Inagaki and colleagues took advantage of the π-π stacking properties of a tripodal phenylenevinylene compound functionalized with triethoxysilyl groups to form organosilica hybrid films by an acid-induced sol-gel process.[121] XRD experiments further indicated the formation of mesostructured films with a hexagonal arrangement of the channels. Furthermore, time-of-flight measurements carried out on these films indicated hole mobilities in the order of 10^{-5} cm^{2}V^{-1}s^{-1} which might be related to the molecular arrangement of the electroactive units as suggested by optical spectroscopy experiments. Some years later, the same group reported a new periodic mesoporous organosilica (POM) synthesized thanks to the cooperative self-assembly of a surfactant molecule C_{18}TMACl and hydrogen-bonded cyclohexane triamide derivative functionalized with three triethoxysilanes as pending units (Figure 16c).[122] TEM images along with XRD experiments of the hybrid materials obtained under basic catalysis revealed the presence of mesoporous structures incorporating columnar channels and with a periodicity between pores of about 5-6 nm. The porosity of this hierarchically structured material was further confirmed by nitrogen adsorption-desorption

---

[120]Kishida, T. Fujita, N. Sada, K. and Shinkai, S. Sol-gel reaction of porphyrin-based superstructures in the organogel phase: Creation of mechanically reinforced porphyrin hybrids. *J. Am. Chem. Soc.* **127,** 7298–7299 (2005).

[121]Mizoshita, N. Ikai, M. Tani, T. and Inagaki, S. Hole-transporting periodic mesostructured organosilica. *J. Am. Chem. Soc.* **131,** 14225–14227 (2009).

[122]Mizoshita, N. and Inagaki, S. Periodic Mesoporous Organosilica with Molecular-Scale Ordering Self-Assembled by Hydrogen Bonds. *Angew. Chemie - Int. Ed.* **54,** 11999–12003 (2015).

isotherm measurements. Finally, fluorescent mesoporous materials were also built from the co-assembly of the aforementioned precursor and a cyclohexane triamide decorated with these naphthyl side chains, thanks to the stabilization of the fluorophore within the walls of the material by hydrogen-bonding interactions.

Using the co-self-assembly of a diacetylene monomer decorated by siloxane groups as end chains and a surfactant, Lu and co-workers reported the two-step synthesis (sol-gel, diacetylene polymerization) of a stimuli-responsive periodic mesoporous hybrid polydiacetylene/silica material.[123] Importantly, this material proved to display thermochromic properties which are the result of the strict molecular alignment of the diacetylene units before photopolymerization. Furthermore, compared to pure polydiacetylene decomposing at 290 ºC, the organic-inorganic nanocomposite exhibited an enhanced decomposition temperature at around 500 ºC. This hybrid system, obtained by a combination of self-assembly and sol-gel approach, displays enhanced mechanical and thermal stability and, owing to the presence of conjugated optoelectronic molecules, offers possible applications in the field of sensors. Subsequently, Peng and Lu reported the formation of conducting hybrid films through the self-assembly of porphyrin-bridged silsesquioxane in THF *via* an acid catalyzed process.[124] Both TEM and XRD experiments demonstrated the mesoporous organization of the organic-inorganic hybrid materials, which displayed enhanced thermal stability compared to the film made only from the porphyrin precursor (800 ºC vs 500 ºC bulk decomposition). Upon complexation of the porphyrin units with Zn^{2+} and Fe^{2+}, the hybrid films displayed enhanced electrical conductivities of 5×10^{-4} and 4×10^{-4} S.cm^{-1} respectively at room temperature compared to the films without ion complexation ($\sim10^{-7}$ S.cm^{-1}) as a result of efficient π-π stacking of the porphyrin precursors. The same achiral porphyrin-based monomer was then reported by Peng and colleagues to form various hierarchically helical superstructures without external induction and probably due to spontaneous symmetry breaking at the air-liquid interface.[125] A combination of high resolution TEM and CD experiments suggested helical stacking for all nanostructures with the main driving force being non-covalent interactions such as π-π, hydrogen bond and Van der Waals. After carbonization at 750 ºC under argon, the ribbon-like self-assemblies showed a good electrocatalytic activity for oxygen reduction as revealed by electrochemical measurements.

[123]Peng, H. Tang, J. Yang, L. Pang, J. Ashbaugh, H. S. Brinker, J. Yang, Z. and Lu, Y. Responsive Periodic Mesoporous Polydiacetylene / Silica Nanocomposites. *J. Am. Chem. Soc.* **128,** 5304–5305 (2006).

[124]Peng, H. and Lu, Y. Squarely mesoporous and functional nanocomposites by self-directed assembly of organosilane. *Adv. Mater.* **20,** 797–800 (2008).

[125]Sun, X. Qiu, L. Cai, Z. Meng, Z. Chen, Z. Lu, Y. and Peng, H. Hierarchically tunable helical assembly of achiral porphyrin-incorporated alkoxysilane. *Adv. Mater.* **24,** 2906–2910 (2012).

Overall, these last examples highlight the potential of sol-gel techniques to fabricate cross-linked supramolecular hybrid materials with advanced optoelectronic properties.

3. Other methods to reach cross-linked supramolecular polymers

In addition to ROMP and sol-gel process, several types of polymerization have been employed to freeze supramolecular aggregates and the most common ones will be detailed afterwards.

One of the first methods that were used to reach this goal was reported in the late 90's by the group of Shinkai.[126] They prepared robust organic gels from a gelator amphiphilic molecule containing a glucosamine head group and toluene-2,4-diisocyanate which was used as the cross-linking agent. Mixing these two monomers in aromatic solvent and aging for several days yielded cross-linked gels built on urethane linkages. Importantly, the gel transition temperature of the covalent gel was doubled compared to the supramolecular one (118 $^{\circ}$C and 58 $^{\circ}$C respectively, indicating the importance of covalent linkage on robustness).

Later on, acyclic diene metathesis (ADMET) which is a powerful olefin metathesis polymerization method intensively studied to synthesize polymeric materials.[127] For instance, Aida and co-workers synthesized a Gemini-shaped HBC amphiphile similar to the one reported for ROMP bu with two cross-linkable allylic functionalities instead of norbornene units.[128] Whereas this molecule only assembled dynamically in dichloromethane, it was spontaneously cross-linked through ADMET in dichloromethane using Grubbs first generation catalyst into covalently trapped graphitic nanotubes. Compared to the non-covalent nanotubes, these ones were perfectly preserved after 24 h upon heating to 175 $^{\circ}$C and even partly after 3 days. In addition to enhanced thermal and solvent stability, this ADMET polymerization of supramolecular polymers provided nanostructures with olefinic groups on the surface, which are of particular interest for facile post-functionalization with functional groups. The group of Smith reported numerous examples of robust gels obtained *via* ADMET polymerization. For instance, they synthesized a dendritic monomer comprising four terminal alkene units in their periphery.[129] This monomer was shown to self-assemble in apolar

---

[126]Inoue, K. Ono, Y. Kanekiyo, Y. Kiyonaka, S. Hamachi, I. and Shinkai, S. Facile Preparation of Robust Organic Gels by Cross-link of a Sugar-integrated Gelator by Toluene-2,4-diisocyanate. *Chemistry Letters* 225–226 (1999).

[127]Buchmeiser, M. R. Homogeneous metathesis polymerization by well-defined group VI and group VIII transition-metal alkylidenes: Fundamentals and applications in the preparation of advanced materials. *Chem. Rev.* **100,** 1565–1604 (2000).

[128]Jin, W. Fukushima, T. Kosaka, A. Niki, M. Ishii, N. and Aida, T. Controlled self-assembly triggered by olefin metathesis: Cross-linked graphitic nanotubes from an amphiphilic hexa-peri-hexabenzocoronene. *J. Am. Chem. Soc.* **127,** 8284–8285 (2005).

[129]Love, C. S. Chechik, V. Smith, D. K. Ashworth, I. and Brennan, C. Robust gels created using a self-assembly and covalent capture strategy. *Chem. Commun. (Camb).* 5647–5649 (2005).

solvents. In toluene, at 0.5 mM, *i. e.* below the critical gelation concentration, a viscous solution was formed and subsequent polymerization using second-generation Grubbs' catalyst yielded a two-phase material composed of an insoluble part (65%) and a soluble fraction (35%). While the soluble part was made of oligomeric species as determined by GPC and MALDI experiments, the insoluble material did not show melting and decomposition at even 210 ºC, suggesting the formation of a covalently cross-linked network. In 2009, the same group expanded this work to the formation of insoluble cross-linked materials thanks to the diffusion of Grubbs second generation catalyst through the supramolecular gel (Figure 17a and b).[130] The dried cross-linked materials made of micrometer-long nanofibers as imaged by SEM could reswell to a great extent (up to 830% in DMSO) in originally compatible solvents but remained incompatible with solvents where gelation did not occur. The co-assembly of this monomer with a non-cross-likable gelator resulted in the formation of two independent nanostructures, as a consequence of self-sorting. The unreacted gelator could be easily washed out of the material while the fibrillar network resulting from ADMET remained frozen. While such materials might found applications in catalysis or regenerative medicine, they have, to the best of our knowledge, not yet been considered.
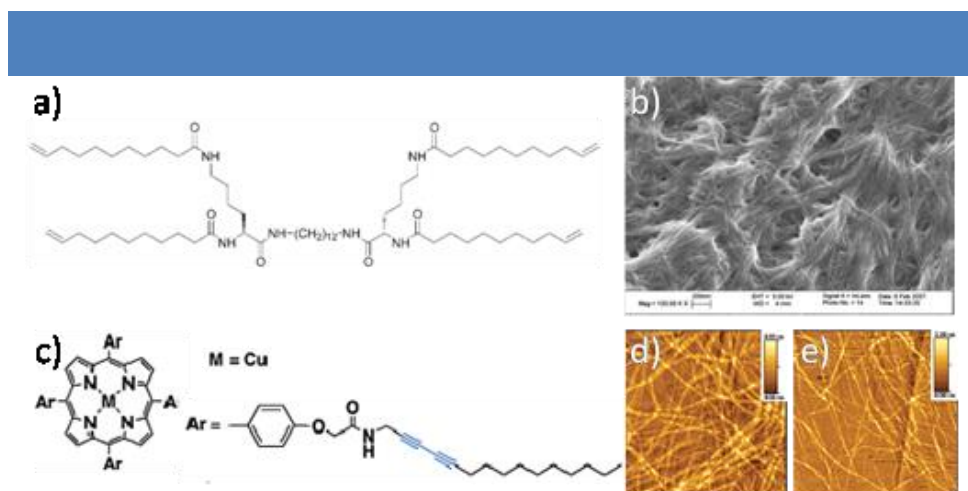
Figure 17 | a) Structure of a gelator containing four terminal alkenes; b) SEM image of the xerogel formed by the gelator reported in a) and dried from toluene under ambient conditions. Scale bar = 200 nm and average fiber diameter = ca. 20 nm; c) Chemical structure of porphyrin-based gelator containing diacetylene units; AFM images of the decalin gel of this porphyrin derivative d) before and e) after UV irradiation and chloroform rinsing (Reproduced from[130,131]).

Photopolymerization has been reported as a powerful method to stabilize supramolecular self-assemblies without introducing external reagents which could influence the self-assembly process. The most commonly used one is probably the UV-irradiation of diacetylene

---

[130]Moffat, J. R. Coates, I. A. Leng, F. J. and Smith, D. K. Metathesis within self-assembled gels: Transcribing nanostructured soft materials into a more robust form. *Langmuir* **25,** 8786–8793 (2009).

functionalized building blocks. For example, Shinkai and co-workers synthesized porphyrin derivatives decorated with alkyl chains containing diacetylene units (Figure 17c).[131] The decalin gel of this copper-containing monomer exhibited thixotropy behavior due to the formation of thin 1-D supramolecular fibers, as imaged by AFM (Figure 17d). *In situ* photopolymerization of these 1-D structures led to the formation of straight, defect-free micrometer-long fibers with a width of about 3 nm, suggesting that the porphyrin units are arranged in unimolecularly stacked arrays. Subsequently, Frauenrath and colleagues reported the synthesis of two oligopeptides functionalized with a diacetylene side chain, one of them being further decorated with an extra NHAc termini group.[132] IR experiments indicated that these two monomers self-assembled into *β*-sheet structures with an enhanced ordering packing for the molecules incorporating NHAc group due to additional intermolecular hydrogen-bonding interactions. For this molecule, scanning force microscopy combined with XRD studies showed a right-handed double helical morphology made of two flat intertwined ribbons, arising from two parallel β-sheets supramolecular structures. A combination of UV, raman and solid state cross polarization magic angle spinning (CP-MAS) spectroscopies evidenced that this hierarchically-ordered supramolecular polymer could be effectively photopolymerized into a poly(diacetylene) polymer without disrupting the structure, whereas photopolymerization of the molecule missing the NHAc unit yielded cross-linked unordered structures. This example highlights the importance of cooperative non-covalent interactions in reaching stable and ordered nanostructures even after covalent polymerization. The group of Stupp also used diacetylene photopolymerization to cross-link supramolecular polymers constructed from peptide amphiphiles.[133] In this study, they compared the structures and properties of linear and branched peptide amphiphile photopolymerized on their hydrophobic part by using various characterization techniques. The polymerization process was found to occur with a lower efficiency in the branched self-assembled nanofibers, indicating that the internal arrangement of the structures strongly affect the photopolymerization event. This example confirms the importance of molecular design to reach stable supramolecular polymers and consequently, robust covalent nanostructures.

Very recently, the same group reported the formation of well-defined hybrid materials

---

[131]Shirakawa, M. Fujita, N. and Shinkai, S. A stable single piece of unimolecularly π-stacked porphyrin aggregate in a thixotropic low molecular weight gel: A one-dimensional molecular template for polydiacetylene wiring up to several tens of micrometers in length. *J. Am. Chem. Soc.* **127,** 4164–4165 (2005).

[132]Jahnke, E. Lieberwirth, I. Severin, N. Rabe, J. P. and Frauenrath, H. Topochemical polymerization in supramolecular polymers of oligopeptide-functionalized diacetylenes. *Angew. Chemie - Int. Ed.* **45,** 5383–5386 (2006).

[133]Hsu, L. Cvetanovich, G. L. and Stupp, S. I. Peptide amphiphile nanofibers with conjugated polydiacetylene backbones in their core. *J. Am. Chem. Soc.* **130,** 3892–3899 (2008).

built up from simultaneous covalent and supramolecular polymerization events.[134] The covalent polymer was formed through an imine condensation reaction between dialdehyde-functionalized peptide amphiphile and a diamine-decorated peptide amphiphile in a slightly acidic aqueous solution, leading to the formation of both ribbon-like and cylindrical structures as observed by cryo-TEM. Simultaneous covalent and supramolecular polymerization of the two previous peptide amphiphiles with a non-covalent polymerizable one under the same experimental conditions gave rise only to ordered cylindrical objects as opposed to the flat-ribbon structures observed for the individual supramolecular polymers. Interestingly, the non-covalently attached peptide amphiphiles could be removed from the hybrid polymer by simple dilution and dialysis and reconstituted upon addition of fresh monomers. This hybrid system appears as a new versatile platform for potential applications in drug delivery and tissue repairing.

"Click" chemistry is also a versatile approach to make covalent bonds in organic synthesis and is also widely used to build covalent polymers.[135] This type of reaction mainly includes Huisgen 1,3-dipolar azide-alkyne cycloaddition, thiol-ene reactions and Diels-Alder cycloaddition, which have been successfully applied to the synthesis of macromolecules. Because of its excellent reliability and functional group tolerance, Cu^I-catalysed azide-alkyne [3+2] cycloaddition (CuAAC) was employed to post-functionalize organic supramolecular gels. For instance, Finn and co-workers prepared cross-linked organogels by CuAAC from *trans*-1,2-diaminocyclohexane undecylamide gelators modified with azide and alkyne at both alkyl ends.[136] When these monomers were mixed with ditopic cross-linkers in the presence of a copper iodide solution, robust cross-linked gels were obtained. Importantly, by adjusting the amount of cross-linking agent and of non-polymerizable organogelator, the cross-linked gels retained their thermoreversible properties but displayed enhanced mechanical properties (increased T_{gel}, average storage G' at average loss G'' moduli). Torres and colleagues reported the synthesis of a library of low-molecular-weight organogelators (LMOG) based on steroids or bis-urea and complementary LMOG molecules containing Zn^{II}-phthalocyanine moieties.[137] These molecules were found to co-gelate in various organic solvents *via* the formation of soft and straight fiber networks. Interestingly, when these supramolecular gels

---

[134]Yu, Z. Tantakitti, F. Yu. T. Palmer, L. C. Schatz, G. C. and Stupp, S. I. Simultaneous covalent and noncovalent hybrid polymerizations. *Science (80-.).* **351,** 497–502 (2016).

[135]Espeel, P. and Du Prez, F. E. 'click'-inspired chemistry in macromolecular science: Matching recent progress and user expectations. *Macromolecules* **48,** 2–14 (2015).

[136]Diaz, D. D. Rajagopal, K. Strable, E. Schneider, J. and Finn, M. G. "Click" Chemistry in a Supramolecular Environment: Stabilization of Organogels by Copper (I)-Catalyzed Azide-Alkyne [3 + 2] Cycloaddition. *J. Am. Chem. Soc.* **128,** 6056–6057 (2006).

[137]Díaz, D. Cid, J. J. Vázquez, P. and Torres, T. Strength enhancement of nanostructured organogels through inclusion of phthalocyanine-containing complementary organogelator structures and in situ cross-linking by click chemistry. *Chem. - A Eur. J.* **14,** 9261–9273 (2008).

were mixed with "clickable" diacetylene and diazide molecules, cross-linked gels with increased thermal and mechanical properties were obtained. For instance, they showed a sol-to-gel transition temperature (T_{gel}) 15 ^{o}C higher than the non-cross-linking counterpart and a storage modulus one order of magnitude higher than the supramolecular gels although retaining their viscoelastic nature. TEM experiments further revealed a morphological transformation into dense and interwined fibrous structures upon cross-linking. Overall, all these examples offer a great future for the development of mechanically and/or thermally stabilized supramolecular structures with excellent optical and electronic properties.

Chapter IV: Supramolecular polymers based on triarylamines

Over the last decades, triarylamine derivatives have been widely studied as opto- and electro-active moieties for the construction of functional materials applied to the fields of nonlinear optics, organic photovoltaic, organic light-emitting diodes and xerography due to their excellent electron donating capability and high hole-transporting mobility.[138] However, most of these studies were related to the bulk properties of the triarylamine-containing materials and only few examples reported the use of this molecular scaffold as a structuring unit to construct well-defined architectures.[139] In 2010, our group reported the first supramolecular polymer based on triarylamines by taking advantage of their molecular design.[140] A mono-amide triarylamine derivative containing one amide motif and two long alkyl chains was successfully synthesized (**1**, Figure 19) and further self-assembled into supramolecular nanowires in chlorinated solvents upon exposure to light through a combination of non-covalent interactions (hydrogen bonding, van der Waals, π-stacking and charge transfer). Upon light excitation in a chlorinated solvent, which worked as an electronic acceptor, a catalytic quantity of triarylammonium radical cations is generated and can then form charge-transfer complexes with a neutral molecule. A combined theoretical and experimental study indicated that a nucleus formed the double-columnar arrangement of these charge-transfer complexes is then necessary to drive the elongation process into double-columnar fibrils which further self-aggregate into larger and stiffer fibers with a width of 10-50 nm and lengths up to 1000 nm.[141] High-resolution AFM imaging combined with computer modeling revealed that the triarylamine columns have an alternative handedness and a twist of 60° between one another due to intermolecular hydrogen bonding in a "snowflake" packing. Based on EPR studies, one charge was expected to stabilize around 160 triarylamine molecules in the self-assembled nanowires. Considering that the distance between consecutive molecules in these supramolecular nanostructures is around 0.5 nm, this charge is supposed to be delocalized over around 80 nm. Intrigued by the potential conducting properties of our

---

[138]Ning, Z. and Tian, H. Triarylamine: a promising core unit for efficient photovoltaic materials. *Chem. Commun.* **414,** 5483 (2009).

[139](a) Wu, P. He, C. Wang, J. Peng, X. Li, X. An, Y. and Duan, C. Photoactive Chiral Metal-Organic Framework for Light-Driven Asymmetric α -Alkylation of Aldehydes. *J. Am. Chem. Soc.* **134,** 14991–14999 (2012); (b) Hua, C. Abrahams, B. F. and D'Alessandro, D. M. Controlling Interpenetration in Electroactive Co(II) Frameworks Based on the Tris(4-(pyridin- 4-yl)phenyl)amine Ligand. *Cryst. Growth Des.* **16,** 1149–1155 (2016).

[140]Moulin, E. Niess, F. Maaloum, M. Buhler, E. Nyrkova, I. and Giuseppone, N. The hierarchical self-assembly of charge nanocarriers: A highly cooperative process promoted by visible light. *Angew. Chemie - Int. Ed.* **49,** 6974–6978 (2010).

[141]Nyrkova, I. Moulin, E. Armao, J. J. Maaloum, M. Heinrich, B. Rawiso, M. Niess, F. Cid, J. J. Jouault, N. Buhler, E. Semenov, A. N. and Giuseppone, N. Supramolecular self-assembly and radical kinetics in conducting self-replicating nanowires. *ACS Nano* **8,** 10111–10124 (2014).

aggregates, nanotrenches having a length about 80 ± 20 nm and width around 100 μm were fabricated with low leakage currents. These devices were treated with a solution of mono-amide triarylamine solution in 1,1,2,2-tetrachloroethane in the presence of an electric field and under light irradiation, leading to the formation of supramolecular triarylamine nanowires aligned and completely filling the gap between the electrodes.[142] The exceptional channel conductivity of the precisely positioned nano-objects was measured up to over 5×10^3 S.m^{-1} and with a low interface resistance per unit length of around 2×10^{-4} Ω.m, which was attributed to the large density of hole carriers. Further electrical measurements indicated an ohmic behavior of the supramolecular polymers along with an intrinsic metallic character down to 4K, as demonstrated by the decreased in resistance with decreasing temperatures. This work highlights the great potential of these chemically-designed triarylamine derivatives to produce purely organic optoelectronic materials *via* a bottom-up approach.

Subsequently, a variety of mono-amide triarylamine derivatives were designed and synthesized by our group (Figure 19). First, triarylamine molecules were modified with terpyridine ligands on the amide sides and the corresponding complexes with Zn^{2+} ions self-assembled into monodisperse spheres with an average diameter of 160 nm in chloroform upon visible light irradiation (**2-3**, Figure 19).[143]
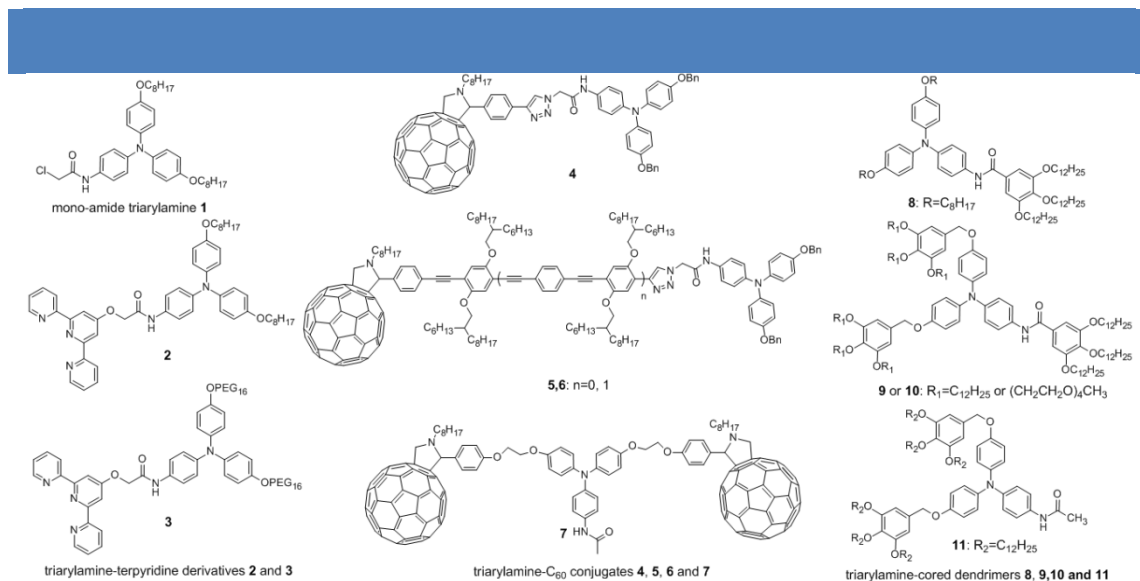
Figure 19 | Molecular structures of mono-amide triarylamine derivatives recently synthesized in our group (Reproduced from[140,143,144,145]).

Then, a set of triarylamine-fullerene conjugates incorporating all the necessary features for self-assembly were synthesized and their light-induced process was investigated in

[142]Faramarzi, V. Niess, F. Moulin, E. Maaloum, M. Dayen, J. F. Beaufrand, J. B. Zanettini, S. Doudin, B. and Giuseppone, N. Light-triggered self-construction of supramolecular organic nanowires as metallic interconnects. *Nat. Chem.* **4,** 485–490 (2012).

[143]Moulin, E. Niess, F. Fuks, G. Jouault, N. Buhler, E. and Giuseppone, N. Light-triggered self-assembly of triarylamine-based nanospheres. *Nanoscale* **4,** 6748 (2012).

chlorinated solvents (**4-7**, Figure 19).[144] Interestingly, white light irradiation of compound **4** led to micrometer-long ribbons while sunlight or UV-light gave rise to monodisperse spheres of micrometric diameters. From UV-Vis-NIR experiments, it was evidenced that the initial intensity of the light, *i.e.* the number of UV photons, is responsible for the morphological differences observed for the stacked nano-architectures, which is in agreement with the nucleation-growth mechanism model proposed for the self-assembly of triarylamine mono-amide.[141] Furthermore, our group prepared four triarylamine molecules incorporating gallic acid derivatives either on the adjacent amide moiety or on the phenolic moieties (**8-11**, Figure 19).[145] All these molecules were found to self-assemble in chlorinated solvents upon light irradiation and the resulting aggregates demonstrated aggregation-induced emission properties. When a gallate unit was present in the vicinity of the amide, stacked nanosheet structures were observed. On the other hand, when the gallate residues were only present on the phenolic moieties, packed bundles of fibrillar objects, similar to the ones observed for molecule **1**, were observed. These different nanostructures were correlated with different mesomorphic properties. For instance, triarylamine **8** showed two independent crystalline phases while compound **11** had a complex liquid-crystalline phase behavior transiting between different packing modes at room temperature. Overall, these examples highlight the importance of molecular design in the light-triggered self-assembly process of triarylamine mono-amides.

Subsequently, a second generation of C_3-symmetric triarylamines with amide groups on each phenyl unit (triarylamine tris-amide TATA) was designed and synthesized (Figure 20).[146] When a solution of molecularly dissolved molecules was subjected to light irradiation in a toluene/methanol solution containing 5vol% chloroform, disappearance of the ^{1}H NMR aromatic signals a, b and of the CH_2 signal c nearby the amide unit clearly evidenced the self-assembly of these triarylamines derivatives (Figure 20a). Upon light irradiation, a characteristic absorption band located around 1100 nm and corresponding to an intermolecular through-space charge transfer between stacked triarylamines appeared (Figure 20b). Compared to the triarylamine mono-amide, the presence of this NIR band suggests full delocalization of the radicals within the self-assembled structures, as also evidenced by EPR spectroscopy. Importantly, quenching of the fluorescence upon light irradiation also support

[144]Busseron, E. Cid, J. J. Wolf, A. Du, G. Moulin, E. Fuks, G. Maaloum, M. Polavarapu, P. Ruff, A. Saur, A. K. Ludwigs, S. and Giuseppone, N. Light-Controlled Morphologies of Self-Assembled Triarylamine-Fullerene Conjugates. *ACS Nano* **9,** 2760–2772 (2015).

[145]Domoto, Y. Busseron, E. Maaloum, M. Moulin, E. and Giuseppone, N. Control over nanostructures and associated mesomorphic properties of doped self-assembled triarylamine liquid crystals. *Chem. - A Eur. J.* **21,** 1938–1948 (2015).

[146]Armao, J. J. Maaloum, M. Ellis, T. Fuks, G. Rawiso, M. Moulin, E. and Giuseppone, N. Healable supramolecular polymers as organic metals. *J. Am. Chem. Soc.* **136,** 11382–11388 (2014).

the formation of supramolecular polarons, *i.e.* charge transfer complexes migrating through the self-assembled structures (Figure 20c).
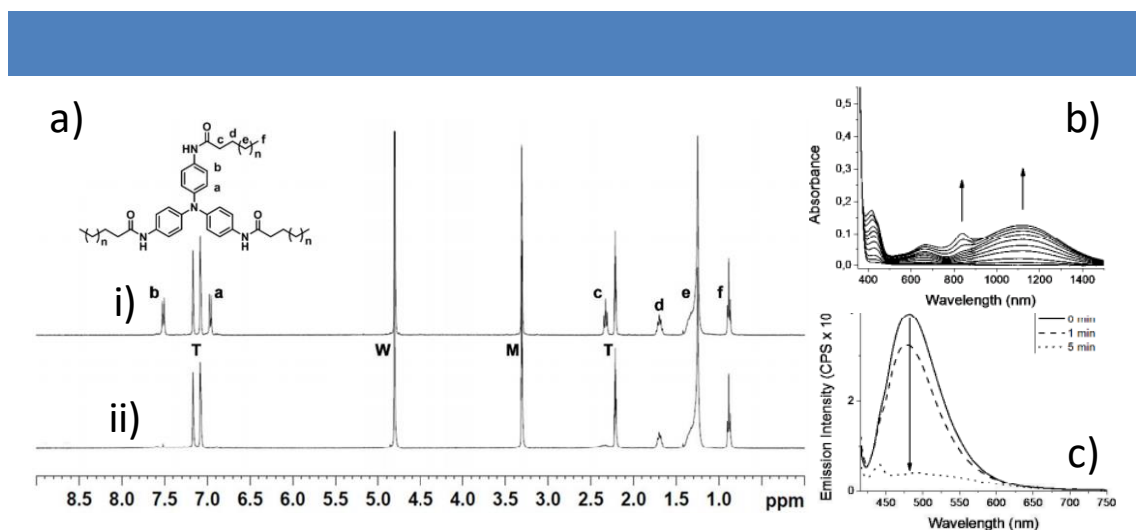
Figure 20 | a) ^{1}H NMR spectra of TATA1 (n=8) in a 5:3 Methanol-d$_4$:Toluene-d$_8$ mixture, in the presence of CDCl$_3$ (5 vol%) i) before and ii) after light irradiation (W, M, and T are the residual resonance peaks for water, methanol and toluene); b) Sequential absorbance spectra taken during light irradiation (0 → 6 min) of a 0.1 mM solution of TATA1 in CHCl$_3$; c) Fluorescence emission of TATA1 upon light irradiation showing the quenching induced by the polaron formation (Reproduced from[146]).

Compared to their mono-amide counterparts, these molecules were shown to self-assemble into mono-columnar aggregates of micrometric lengths in various organic solvents without light. However, upon light irradiation, the fibers showed improved ordering and self-healing properties because the light-induced supramolecular polarons diffusing along the fibers are fixing structural defects present in the non-irradiated self-assemblies. Whereas neutral fibers displayed semiconducting properties, these tris-amide derivatives demonstrated an ohmic behavior upon subsequent light irradiation or electrochemical oxidation in gaps as large as 4 μm. The capacity of these organic supramolecular materials to self-optimize their conducting properties by adjusting their internal structures is noteworthy for such purely organic materials, which could be used as alternative to commonly used organic metals.

In order to take advantage of the presence of metallic electrons in the supramolecular nanowires, our group then demonstrated that they could behave as subwavelength optical interconnects to bridge gold nanoparticles, leading to the formation of optical plasmonic nanocircuits.[147] First, gold nanoclusters were pre-patterned on a glass or silicon substrate *via* microphase separation of a block copolymer, and then functionalized by a monolayer of triarylamine **2** anchored by gold-sulfur bonds. These functionalized nanoclusters were

[147]Armao, J. J. Domoto, Y. Umehara, T. Maaloum, M. Contal, C. Fuks, G. Moulin, E. Decher, G. Javahiraly, N. and Giuseppone, N. Supramolecular Organic Nanowires as Plasmonic Interconnects. *ACS Nano* **10,** 2082–2090 (2016).

incubated with triarylamine trisamide nanowires to produce hybrid array of dense organic fibers between gold nanoclusters as imaged by AFM (Figure 21a). The optical conductivity of these arrays was then probed by ellipsometry and showed an increase from 259 $\Omega^{-1}\cdot cm^{-1}$ for the undoped nanowires (*i.e.* which were not lightened during incubation) to 4271 $\Omega^{-1}\cdot cm^{-1}$ for doped ones. Such enhancement of the optical conductivity could be explained by the efficient coupling of the metallic electrons of the nanowires with the plasmonic oscillations of the gold nanoclusters (Figure 21b).
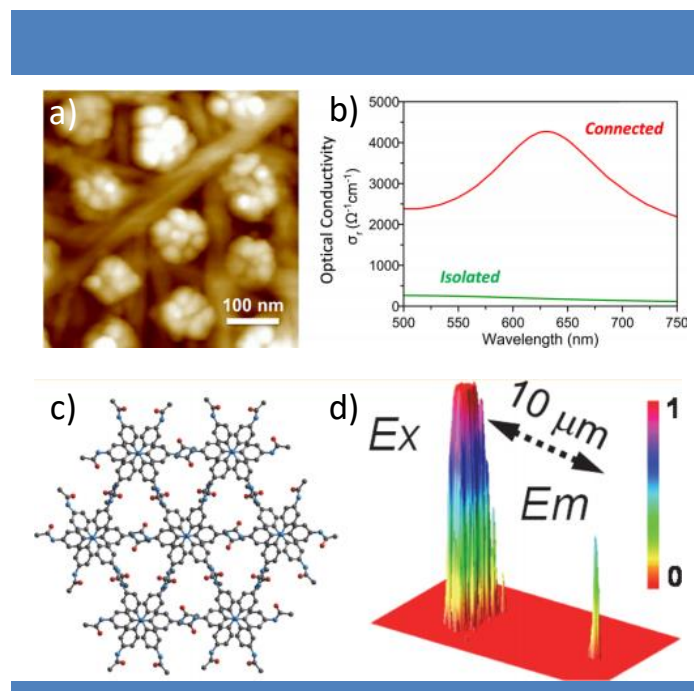
Figure 21 | a) AFM height image of the hybrid array made of organic triarylamine tris-amide fibers with gold nanoclusters; b) Overlay of the real optical conductivities, derived from ellipsometry measurements, for two connected plasmonic arrays: one with gold nanoparticles functionalized with thio-pended tris-amide triarylamine and doped fibers (red) and one with gold nanoparticles unfunctionalized with thio-pended tris-amide triarylamine and undoped fibers (green); c) Crystal structure of triarylamine tris-acetamide visualized along the direction of the columnar stacking for two layers of molecules; d) Reconstructed 3D images of light propagation in an oxidized crystal covered with indocyanine dye (crystal lengths of approximately 6 µm) (Reproduced from[147,148]).

We then showed that single needle-like crystals of triarylamine tris-acetamide, which arrange in a hexagonal pattern, could behave by themselves as supramolecular plasmonic waveguides (Figure 21c).[148] Using several techniques such as UV-Vis-NIR absorption spectroscopy and Intensity-Voltage measurements, we first showed that these crystals, when doped by light irradiation, display a high conductance with an ohmic behavior, which can be attributed to the presence of metallic electrons within their structure. We then study their potential as optical waveguide by exciting one tip of a single crystal with a laser beam, either at 532 or 785 nm. In both cases, we could observe a light output at the other tip over

[148]Armao, J. J. Rabu, P. Moulin, E. and Giuseppone, N. Long-Range Energy Transport via Plasmonic Propagation in a Supramolecular Organic Waveguide. *Nano Lett.* **16,** 2800–2805 (2016).

micrometric distance. Interestingly, we found out that both doped and undoped single crystals present optical waveguiding properties, albeit occurring through different mechanisms (active and passive, respectively). For doped crystals, the active mechanism was found to be purely plasmonic due to a strong coupling between the incident light and the metallic electrons present in the crystalline structures.

Since our seminal work in 2010, several other research groups have studied both fundamental aspects and applications of supramolecular polymers based on well-defined triarylamine molecules or closely related analogues. For instance, the group of Kim synthesized an achiral triarylamine tris-amide molecule containing diacetylene units on its side chains, which was shown to self-assemble in 1,2-dichloroethane upon visible light irradiation into micrometer-long fibrillar aggregates which consisted of bundles of nanometric fibers (Figure 22a).[149]
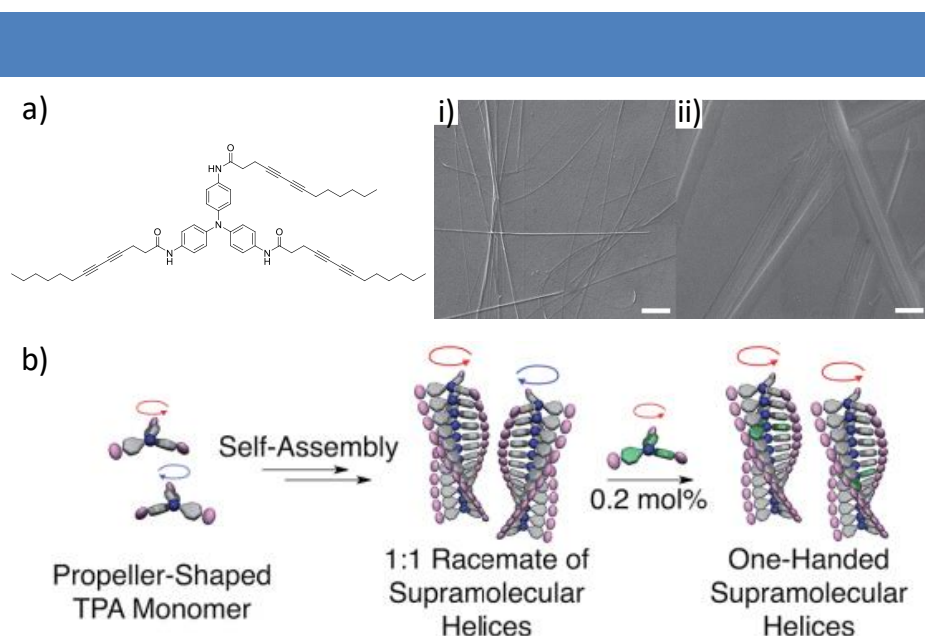
Figure 22 | a) Chemical structure of the achiral triarylamine molecule decorated with diacetylene units at the periphery. i) and ii) SEM images of the aggregates of formed by this molecule in a 1,2-dichloroethane solution (2 mg ml^{-1} concentration) upon visible light irradiation. Scale bar: i) 10 µm, ii) 500 nm; b) Schematic illustration of the self-assembly of triarylamine TPA monomers into helices and chiral amplification through the sergeants and soldiers principle. The green TPA monomer corresponds to a sergeant (Reproduced from[149,150]).

Interestingly, upon light irradiation with circularly polarized light, CD spectra of the supramolecular polymers indicated the preferential formation of a single type of helical aggregates. This light-induced supramolecular chirality could be further locked through photopolymerization of the pre-organized diacetylene units using non-polarized ultraviolet

---

[149]Kim, J. Lee, J. Kim, W. Y. Kim, H. Lee, S. Lee, H. C. Lee, Y. S. Seo, M. and Kim, S. Y. Induction and control of supramolecular chirality by light in self-assembled helical nanostructures. *Nat. Commun.* **6,** article 6959 (2015).

light as demonstrated by a marked stability of the CD activity upon irradiation with circularly polarized light of the opposite rotational direction. Importantly, conductivity measurements demonstrated that the photopolymerization process did not affect the electrical properties of the aggregates. Very recently, Miyajima and co-workers prepared several triarylamine tris-amide derivatives with various chiral or achiral alkyl chains (Figure 22b).[150] Whereas solutions of these derivatives with achiral side chains displayed silent vibrational circular dichroism (VCD) spectra, molecules with chiral side chains of opposite chiralities showed mirror-image spectra by VCD. Importantly, when a solution of achiral molecules was seeded with as low as 0.2 mol% fraction of a chiral triarylamine derivative, a full control of the handedness of the supramolecular helices was achieved. Such high control of the chirality by an incredibly low content of chiral molecules was ascribed to the propeller conformation of the triarylamine which proves to be highly dynamic.

Considering that triarylamine molecules have been extensively studied in organic photovoltaic, the group of Holmes studied the influence of the light-induced self-assembly process on the performance of triarylamine derivatives in photovoltaic devices.[151] Using triarylamine molecules decorated by two amide groups at its periphery, they showed that the device obtained from an irradiated solution displayed a significantly better efficiency than the device built from a non-irradiated one. This outcome results from the formation of a supramolecular network for the irradiated device, which enhances charge transport and disfavors recombination, as imaged by AFM. Recently, Stupp and colleagues confirmed that self-organization can be used to enhance the photovoltaic response of small molecules. Indeed, they reported a study on the self-assembly of two tripodal triarylamine-cored donor monomers bearing diketopyrrolopyrrole (DPP) side chains, which were subsequently evaluated in solution-processed bulk heterojunction organic solar cells (OSCs).[152] While the presence of branched alkyl chains on the DPP units was found to inhibit the self-assembly process, monomers incorporating linear alkyl chains were found to produce one-dimensional supramolecular nanowires, as demonstrated by AFM and grazing incidence X-ray diffraction. Such supramolecular organization was then found to have a strong influence on the performance of the solution-processed OSCs which showed a 50% increase in power conversion efficiency compared to the OSCs made from the non-self-assembling molecule.

[150]Kim, T. Mori, T. Aida, T. and Miyajima, D. Dynamic Propeller Conformation for The Unprecedentedly High Degree of Chiral Amplification of Supramolecular Helices. *Chem. Sci.* **0,** 1–6 (2016).

[151]Kumar, R. J. Churches, Q. I. Subbiah, J. Gupta, A. Ali, A. Evans, R. A. and Holmes, A. B. Enhanced photovoltaic efficiency via light-triggered self-assembly. *Chem. Commun. (Camb).* **49,** 6552–4 (2013).

[152]Aytun, T. Santos, P. J. Bruns, C. J. Huang, D. Koltonow, A. R. Cruz, M. O. and Stupp, S. I. Self-Assembling Tripodal Small-Molecule Donors for Bulk Heterojunction Solar Cells. *J. Phys. Chem. C* **120,** 3602–3611 (2016).

In a recent example, Wang and co-workers showed that such enhancement of optoelectronic performance by self-assembly can also be achieved in organic field effect transistor (OFETs).[153] Using various microscopy experiments and electron diffraction, they reported that triarylamine-C_{60} amphiphile can crystallize in two-dimensional nanosheets of well-separated C_{60} units and triarylamine columnar aggregates with a flat-on orientation. When such dual-channel structures were tested in OFET devices, an average electron mobility 2.11×10^{-4} cm^{2}V^{-1}s^{-1} of and hole mobility of 3.37×10^{-4} cm^{2}V^{-1}s^{-1}, demonstrating the ambipolar character of the TAA-C_{60} amphiphile.

Finally, we would like to mention also some recent studies performed by the group of Schmidt on a series of bridged triarylamine trisamide derivatives. Initially, a three-armed carbonyl-bridged triarylamine (CBT) decorated at its periphery by 4-(5-hexyl-2,2'-bithiophene)naphthalimides (NIBT) was shown to form transparent gels in *ortho*-dichlorobenzene at a concentration as low as 0.7 mM.[154] Interestingly, in this gel state, an energy transfer phenomenon was observed from the energy-donating CBT core to the energy-accepting NIBT units. TEM imaging of this gel further indicated the formation of a dense network of nanofibers built from the mono-columnar aggregation of the CBT molecules *via* a combination of π-π stacking, hydrogen bonding and Van der Waals interactions.[155] Importantly, confocal illumination microscopy of isolated fibers revealed their photoluminescence over their entire length, suggesting that efficient energy transport occurs, at room temperature, over distances as large as around 4 μm (i.e. over ~10,000 molecules). In collaboration with the group of Meijer, they further studied the self-assembly mechanism of CBT molecules decorated with (*S*)- or (*R*)-chiral aliphatic side chains.[156] Using a combination of optical spectroscopies, they showed that these monomers can self-assemble into either kinetically favored or thermodynamically favored helical H-aggregated supramolecular polymers depending on the followed thermal profile. Furthermore, each polymer was found to arise from a different self-assembly mechanism: isodesmic for kinetically favored polymers and nucleation-elongation for thermodynamically favored ones. Noteworthily, when mixed in a 1:1 ratio, the kinetically trapped polymer could evolve into the thermodynamically stable one, the later being used as nuclei for the polymerization process.

[153]Liang, W.-W. Huang, C. Wu, K. Wu, S. Chang, S. Cheng, Y. and Wang, C. Flat-on ambipolar triphenylamine/C $_{60}$ nano-stacks formed from the self-organization of a pyramid-sphere-shaped amphiphile. *Chem. Sci.* **7,** 2768–2774 (2016).

[154]Haedler, A. T. Beyer, S. R. Hammer, N. Hildner, R. Kivala, M. Kohler, J. and Schmidt, H. Synthesis and photophysical properties of multichromophoric carbonyl-bridged triarylamines. *Chem. - A Eur. J.* **20,** 11708–11718 (2014).

[155]Haedler, A. T. Kreger, K. Issac, A. Wittmann, B. Kivala, M. Hammer, N. Kohler, J. Schmidt, H. and Hildner, R. Long-range energy transport in single supramolecular nanofibres at room temperature. *Nature* **523,** 196–199 (2015).

[156]Haedler, A. T. Meskers, S. C. J. Zha, R. H. Kivala, M. Schmidt, H. and Meijer, E. W. Pathway Complexity in the Enantioselective Self-Assembly of Functional Carbonyl-Bridged Triarylamine Trisamides. *J. Am. Chem. Soc.* **138,** 10539–10545 (2016).

These studies demonstrate the potential of triarylamine derivatives for different applications in optoelectronic devices but also as tools to elucidate fundamental questions.

Overall, although great achievements have been reached on triarylamine-based supramolecular polymers since our seminal paper in 2010, much more developments are expected for these nanostructures, in particular, considering their promise as soft functional materials in the field of electronics and plasmonics. In the following two chapters, I will present my doctoral work in details regarding to the formation of water-soluble supramolecular polymers based on the triarylamine scaffold and the stabilization of triarylamine-based supramolecular polymers by different cross-linking methodologies.

RESULTS

Chapter V: Water-soluble supramolecular polymers based on triarylamine motifs

1. Objectives and targeted molecules

In the recent years, as already mentioned in the bibliographic part, self-assemblies of well-designed triarylamine derivatives have been intensively studied by our group. These triarylamine derivatives were demonstrated to self-assemble into various morphologies with excellent functional properties in non-polar solvents such as chlorinated solvents or toluene. However, their self-assembly in water and highly polar solvents was rarely investigated, although such amphiphilic molecules should self-organize into well-defined structures. In our group, we have recently studied the self-assembly of amphiphilic molecules made of either a bisurea or a perylene core functionalized with poly(ethylene glycol) (PEG), peptide and cyanine dyes as side chains.[157] For instance, we have demonstrated using a combination of spectroscopic scattering and imaging techniques that bisurea molecules can produce various supramolecular structures such as two-dimensional plates, twisted ribbons or branched fibers which are controlled by the chemical structure of the side chains.
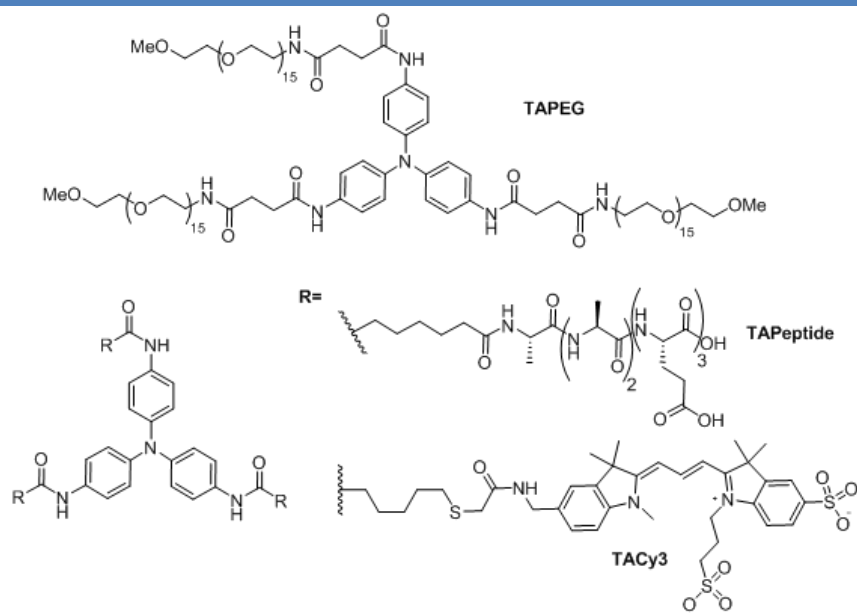
Figure 23 | Molecular structures of water-soluble triarylamines TAPEG, TAPeptide and TACy3.

---

[157]Xiang, Y. Moulin, E. Buhler, E. Maaloum, M. Fuks, G and Giuseppone, N. Hydrogen-Bonded Multifunctional Supramolecular Copolymers in Water. *Langmuir* **31,** 7738–7748 (2015).

In this chapter, we designed and studied three novel triarylamine tris-amide molecules decorated with either poly(ethylene glycol) (PEG), peptide or cyanine dyes on the three amide positions (Figure 23). We have chosen the tris-amide triarylamine core as it is known to self-assemble in columnar stacks even without oxidation of the central nitrogen atom. Furthermore, these three functional side chains were expected to endow targeted molecules with high solubility in water. In particular, a sixteen-unit PEG chain was selected as structural unit and envisioned to offer Van-der-Waals interactions for the cooperative self-assembly process. As reported by the group of Stupp[158], the sequence AlaAlaAlaGluGluGlu was chosen according to two criteria: the AlaAlaAla part was expected to form *β*-sheet structure while the GluGluGlu tripeptide is envisioned to impart solubility due to the presence of net negative charges in basic conditions. Additionally, the selected cyanine dye is water-soluble and presents a high extinction coefficient, thus offering the possibility to create a light harvesting system when connected with a suitable electron donor or acceptor moiety. After the description of the synthesis of these complex molecules, spectroscopy, microscopy and even scattering techniques were employed to characterize the different self-assemblies in either water or methanol.

2. Synthesis and characterization of triarylamine-polyethylene glycol derivative

a. Synthesis

N',N'-bis(4-aminophenyl)benzene-1,4-diamine **1a** was used as a common tris-amino triarylamine intermediate to afford all targeted molecules necessary for this project (Figure 23).[146] This triarylamine core is obtained in two steps by using a nucleophilic aromatic substitution between *p*-phenylenediamine and 1-fluoro-4-nitrobenzene followed by reduction of the nitro groups with tin chloride. As depicted in Scheme 1, the synthetic strategy to reach compound TAPEG is an amide coupling reaction between *N',N'*-bis(4-aminophenyl)benzene-1,4-diamine and commercially available *O*-[(*N*-Succinimidyl) succinyl-aminoethyl]-*O'*-methyl- polyethylene glycol (750 Dalton) which proceeds with a yield about 23%, after purification by reverse-phase HPLC.

---

[158]Pashuck, E. T. and Stupp, S. I. Direct observation of morphological tranformation from twisted ribbons into helical ribbons. *J. Am. Chem. Soc.* **132,** 8819–8821 (2010).
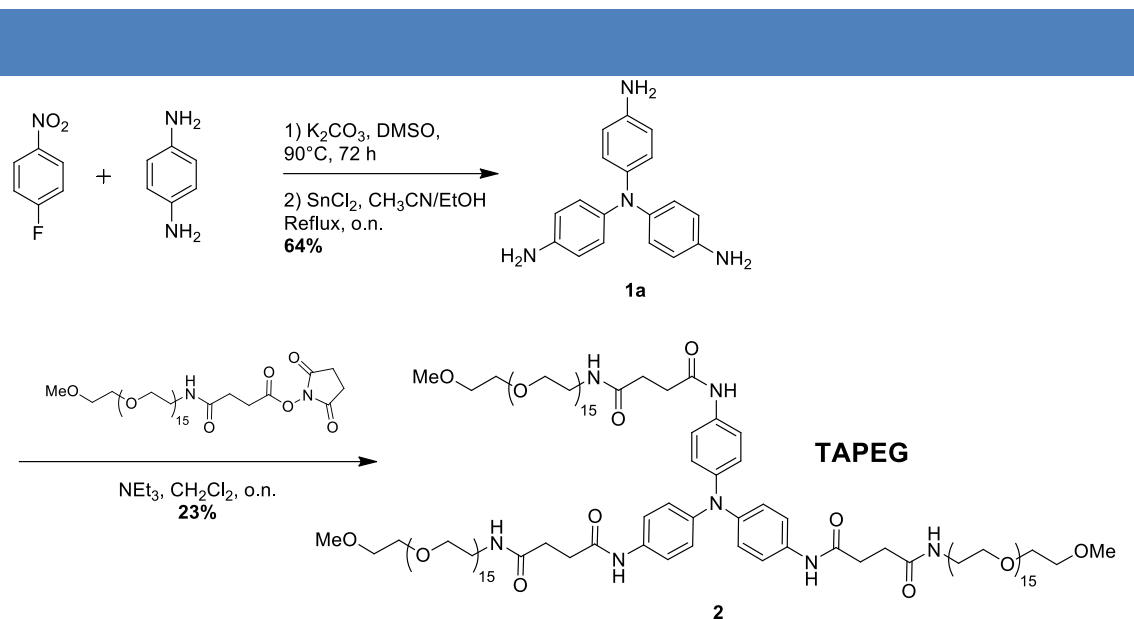
Scheme 1 | Synthetic route to water-soluble triarylamine TAPEG.

b. Characterizations

The triarylamine amphiphile TAPEG was initially investigated by ^{1}H NMR in water and methanol at a concentration of 5 mM (Figure 24). In particular, peak assignments were established by combining ^{1}H NMR with 2D-COSY NMR. This monomer showed a good solubility in water, methanol and chloroform up to 10^{-2} M. Very similar NMR spectra were observed in water and methanol and no peak broadening was observed in either solvents at this concentration (Figure 24i and ii).
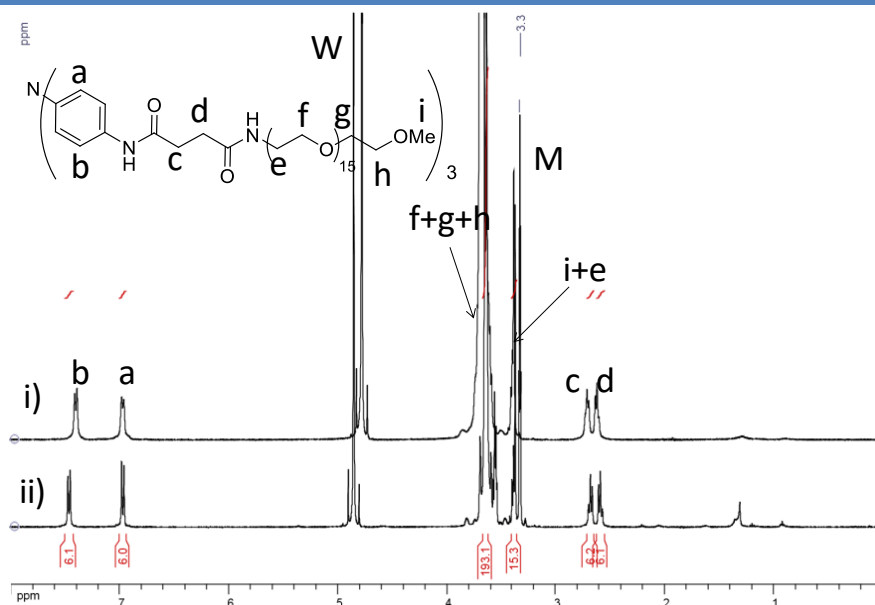
Figure 24 | ^{1}H NMR and peak assignments of TAPEG i) in deuterated water (5 mM) and ii) in deuterated methanol (5 mM) (M, W are the residual signals for methanol and water).

As shown in Figure 25, the aromatic signals a, b corresponding to the triarylamine core and the CH$_2$ signal c corresponding to the closest methylene unit to the triarylamine core disappeared upon light irradiation in chloroform, suggesting the formation of a self-assembly for TAPEG.
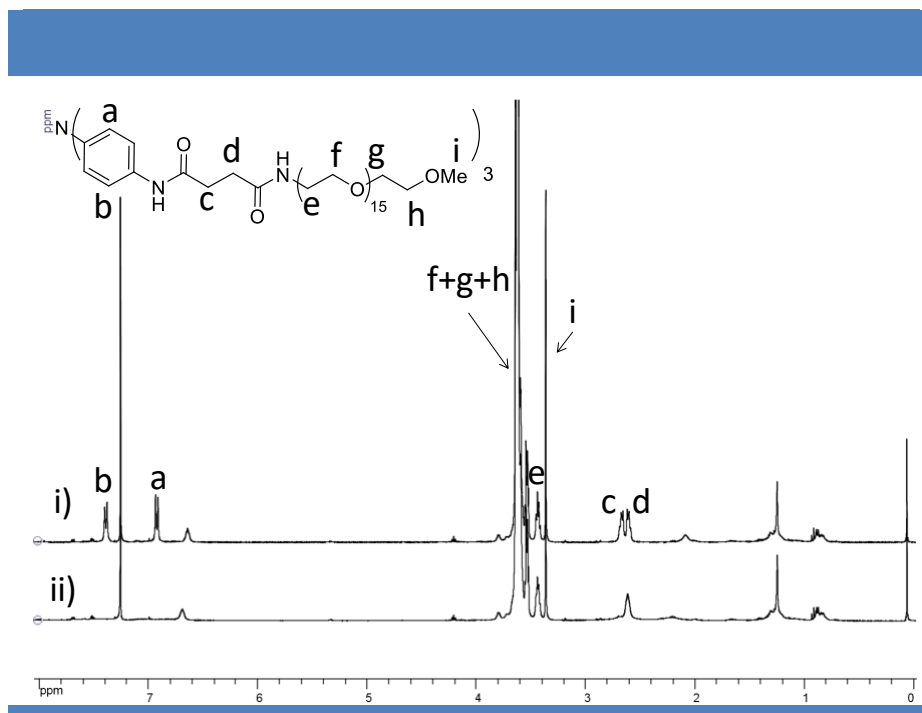
Figure 25 | ^{1}H NMR and peak assignments of TAPEG in chloroform i) before and ii) after irradiation 30 minutes with a 20 W power lamp.

In order to probe the secondary structure such as hydrogen bonding in chloroform, water, and methanol, Fourier transform infrared spectroscopy (FTIR) experiments were carried out by drop-casting a 1 mM solution on an ATR diamond probe (Figure 26). For the sample in chloroform, the presence of a sharp band at around 3297 cm^{-1} before irradiation which turned into a broad band at around 3315 cm^{-1} after light irradiation suggests the formation of hydrogen bonding interactions upon light irradiation. In the carbonyl region, the absence of a band at around 1711 cm^{-1} after light irradiation which is present for the non-irradiated sample confirm the presence of hydrogen bonds in the self-assembled structure. Interestingly, the presence of broad bands at around 3306 and 3302 cm^{-1} in water and methanol respectively are indicative of H-bonded N-H stretching vibrations. In the carbonyl region, the bands at around 1665 and 1639 cm^{-1} were assigned to C=O stretching in water and methanol respectively, demonstrating that the self-assemblies are built up *via* strong and ordered hydrogen bonds. Thus, IR experiments suggests that hydrogen bonds are preserved even in polar solvents such as water and methanol, probably due to the presence of an hydrophobic linker between the PEG chains and the triarylamine core which favors their formation.
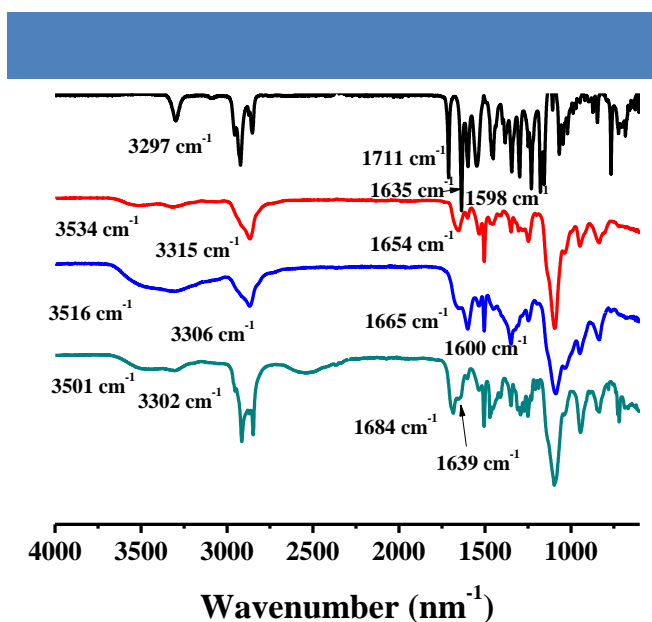
Figure 26 | FT-IR spectra of TAPEG in chloroform without irradiation (black), chloroform after irradiation (red), water (blue), methanol (green).

UV-Vis absorbance and fluorescence experiments were then employed to investigate the self-assembly process of TAPEG in chloroform, water and methanol (Figure 27).
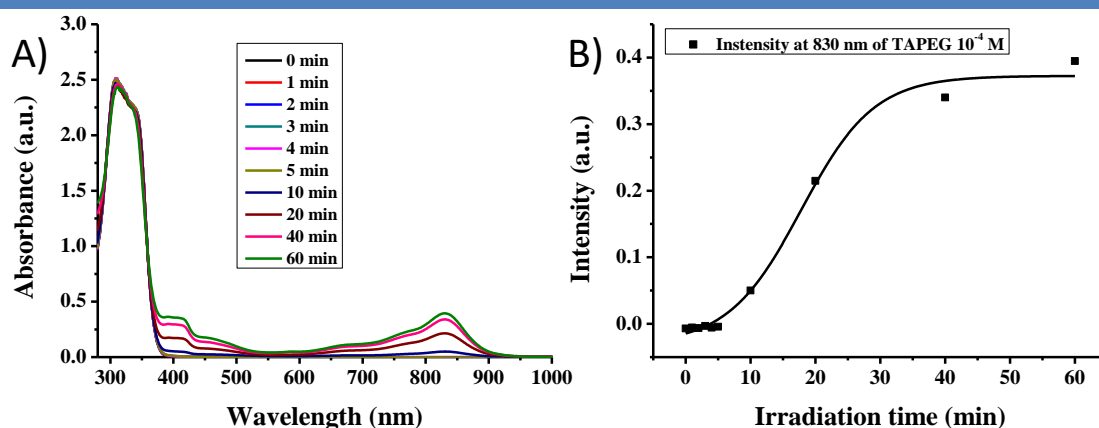
Figure 27 | a) UV-Vis-NIR spectra of TAPEG in chloroform (10^{-4} M) upon light irradiation and b) evolution of the absorbance at 830 nm with increasing irradiation time.

UV-Vis spectroscopy of TAPEG in chloroform was performed upon exposure to visible light. As described previously by our group,[140,146] light irradiation of well-designed triarylamine molecules in chlorinated solvents led to the appearance of an absorption band in the near-infrared (NIR) region, which intensity changes as a function of time. As shown in Figure 27, upon light irradiation, an absorption band at around 830 nm corresponding to the presence of localized triarylammonium radical cations was observed, the intensity of the band increased with increasing irradiation times (up to 60 minutes irradiation). Additionally, a broad band ranging from ~380 nm to 520 nm kept on increasing with light irradiation.

As shown in Figure 28, the fluorescence properties of TAPEG self-assembly in chloroform were studied as a function of time of irradiation. Upon excitation at 410 nm, a maximum emission is observed at 501 nm before light irradiation, which increases strongly after a one-minute irradiation time and then got completely quenched for prolonged irradiation time. The combination of UV-Vis-NIR and fluorescence experiments upon light irradiation suggests that TAPEG behave similarly to triarylamine trisamides and should thus lead to the formation of mono-columnar aggregates.[128]
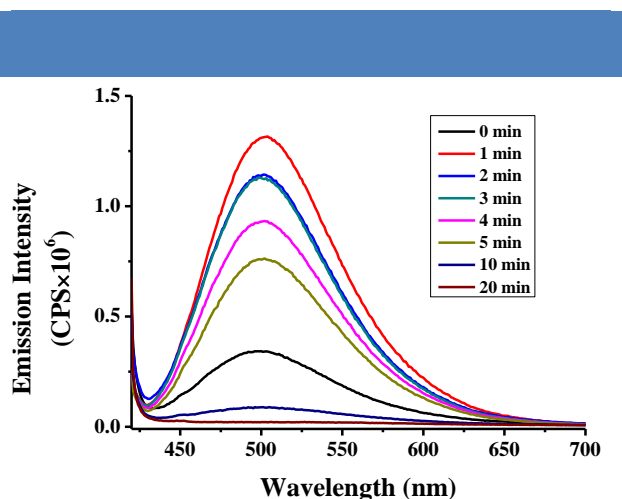
Figure 28 | Fluorescent spectra of TAPEG in chloroform at a concentration of 10^{-4} M upon light irradiation, λ_{ex}= 410 nm.

UV-Vis spectroscopy was also performed for TAPEG in both water and methanol at 10^{-4} M (Figure 29). The UV-vis spectrum from water shows a maximum absorption band at 321 nm while the spectrum from methanol exhibits a similar band with a maximum of absorption at 322 nm.
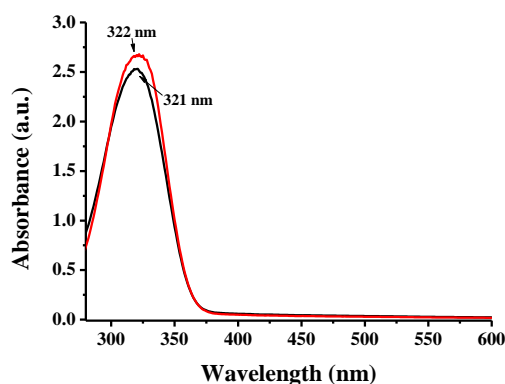
Figure 29 | UV-Vis-NIR spectra of TAPEG in a) water (10^{-4} M, black) and b) methanol (10^{-4} M, red).

Concentration-dependent fluorescence spectra of monomer TAPEG in either water or methanol were recorded (Figure 30). In water, an emission band at around 405 nm was

observed. These emission bands increased with increasing concentration increased from 10^{-8} M to 10^{-4} M, and then started to decrease until reaching a minimum at a concentration of 10^{-3} M. Similarly, the fluorescence of monomer TAPEG in methanol showed a broad band from 375 nm to 405 nm, which first increased for a concentration up to 10^{-4} M (Figure 30b). When the concentration kept on increasing, the fluorescence started to be quenched until complete quenching at 10^{-3} M. These results suggest that aggregates start to be formed in water and methanol at concentrations above 10^{-4} M. However, the presence of a shoulder band at around 380 nm suggests that several aggregates (dimers, oligomers…) might be present in solution.
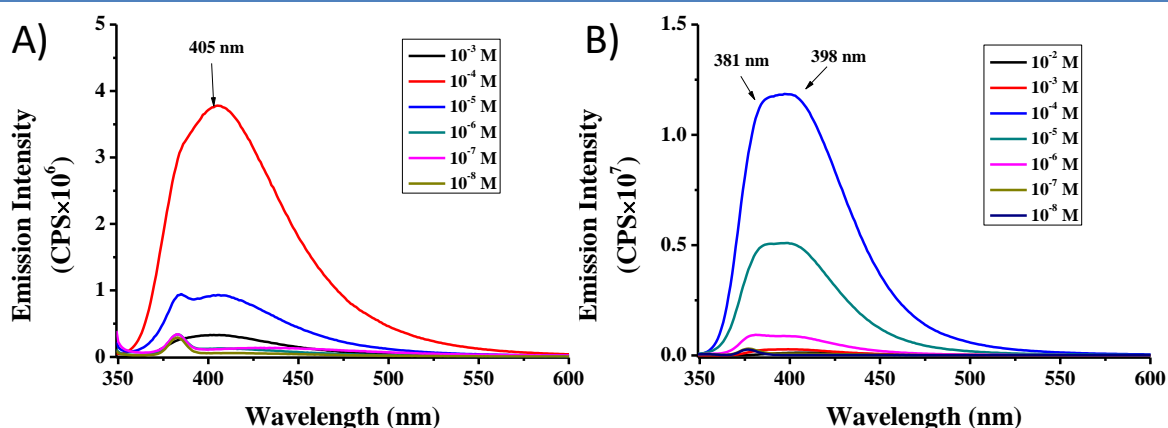
Figure 30 | Fluorescent spectra for TAPEG a) in water for concentrations ranging from 10^{-8} M to 10^{-3} M and b) in methanol for concentrations ranging from 10^{-8} M to 10^{-2} M, λ_{ex}=339 nm.

In order to determine the morphologies of these aggregates in solution, we performed SANS and LS experiments on solutions of TAPEG at 10^{-2} M. In water, the scattering curve obtained by neutron scattering exhibits the following behavior: a) a low q regime (< 0.01 Å^{-1}) in which the q-dependence of the data can be described by a power low with the exponent close to -3 such as in collapsed polymer coils or 3D aggregates, followed by; b) a Guinier regime associated with the length and cross-section of the polymers (Figure 31). This last region could be fitted using the model of a cylinder-like structure with an elliptical cross-section, providing radius a and b for the cross-section of 0.57 ± 0.03 nm and 2.5 ± 0.1 nm respectively and a length of 3.7 ± 0.2 nm. Similar to water, the scattering curve for the solution in methanol exhibits the following behavior: a) a low q regime in which the q-dependence of the data can be described by a power law with the exponent close to -2.6 which is associated with the presence of branched objects or networks, followed by b) a Guimier regime which can also be fitted with the model of a cylinder with an elliptical cross-section. Using this model, the radius a and b for the elliptical cross-section can be estimated to 0.49 ± 0.01 nm and 1.5 ± 0.1 nm respectively and the length is 5.5 ± 0.1 nm.

These results suggest that TAPEG monomer self-assembled into mono-columnar structures in polar solvents, which further aggregated into dense structures by entanglement of the lateral PEG chains.
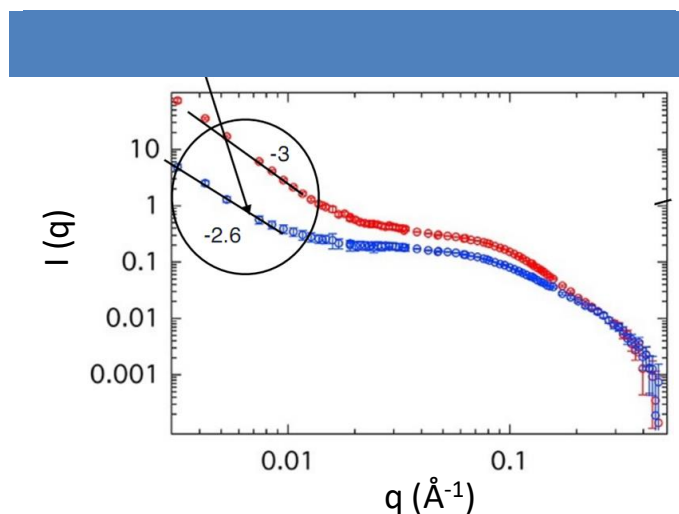
Figure 31 | SANS spectra of TAPEG in water (10^{-2} M, red) and in methanol (10^{-2} M, blue).

Then, we performed TEM imaging of TAPEG solutions in either water or methanol (Figure 32). In both cases, dense and micrometer-long fibrillar structures were observed.
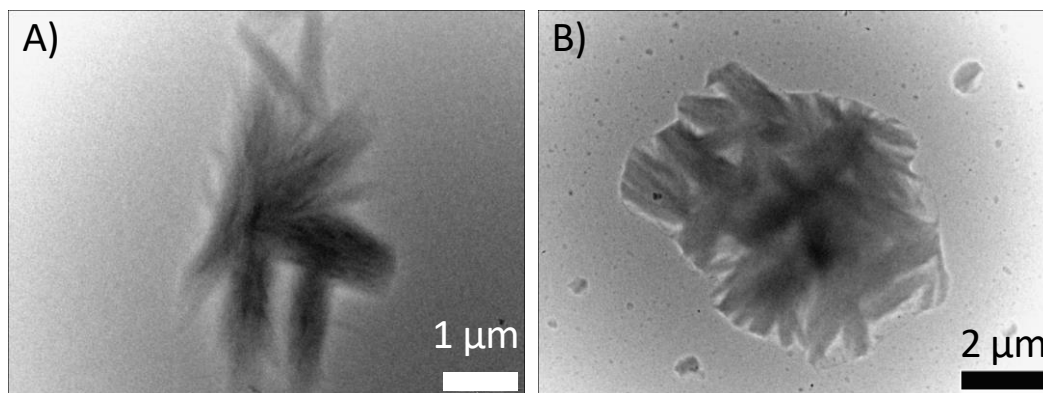
Figure 32 | TEM images of TAPEG from water (10^{-2} M) and methanol (10^{-2} M).

c. *Discussion*

Overall, a tris-amide triarylamine derivative decorated with long and flexible poly(ethylene glycol) chains was designed and synthesized. This TAPEG compound shows good solubility from polar solvents to apolar ones. While this molecule displays all the characteristic spectroscopic features of self-assembled nanostructures in chloroform upon light irradiation, its morphology remains to be determined as TEM and AFM experiments proved so far to be unsuccessful. On the other hand, in either water or methanol, spectroscopic studies revealed a similar behavior for TAPEG, which could indicate the

co-existence of monomers and oligomers at 10^{-4} M. Upon increasing the concentration to 10^{-3} M, quenching of the fluorescence suggests that triarylamine molecules are packed in dense aggregates. Such behavior is in agreement with morphologies observed by TEM and SANS behavior at low scattering vector which suggests the formation of dense aggregates. Interestingly, SANS at higher q indicates that the cross-section of these aggregates is elliptical. The difference in radius of this section between methanol and water might be attributed to a difference of solubility of PEG chains. On the other hand, the higher length observed in methanol is in agreement with the fact that hydrogen-bonding interactions are more favored than in water.

3. Synthesis and characterization of triarylamine-peptide derivative

a. Synthesis

In terms of synthetic strategies for the triarylamine-peptide amphiphile TAPEG, we envisioned to build up the structure on solid phase according to the synthetic route developed for the bis-urea molecules.[157] The peptidic segment was synthesized with the help of a standard Fmoc-based solid phase peptide synthesis (SPPS).[159] Since its initial development by Merrifield in 1963, solid phase peptide synthesis has become a routine technique to access peptides of various lengths. To date, the most used approach is the Fmoc/tBu method in which fluorenylmethoxycarbonyl (Fmoc) group protected amino acids are bound to Wang Resin. Compared with traditional liquid phase synthesis, SPPS has the advantages of rapidity, high efficiency, ease of purification and can be easily automated. From Scheme 2, the synthesis of the hexameric sequence started from Fmoc-L-Glu(OtBu)- MPPA(Wang) resin by using CEM Liberty 1 microwave synthesizer.[160] After deprotection of the Fmoc protecting group by piperidine (20%) in DMF, peptidic couplings were performed successively with Fmoc-L-Glu(OtBu)-OH two times and Fmoc-Ala-OH three times, using HBTU and DIPEA as activating mixture. Ultimate Fmoc deprotection of the compound yielded the targeted peptide sequence attached to the Wang resin, and ready for the coupling with the tris-amide triarylamine core. At the end of this solid-supported synthesis, the purity of the amino acid sequence was checked by LC/MS and ^{1}H NMR after cleavage from the solid matrix.

---

[159]Merrifield, R. B. Solid Phase Peptide Synthesis. I. The Synthesis of a Tetrapeptide. *J. Am. Chem. Soc.* **1963**, 85, 2149-2154.
[160]Fmoc Solid Phase Peptide Synthesis, A Practical Approach, (W. C. Chan, P. D. White Eds), Oxford University Press, 2000.
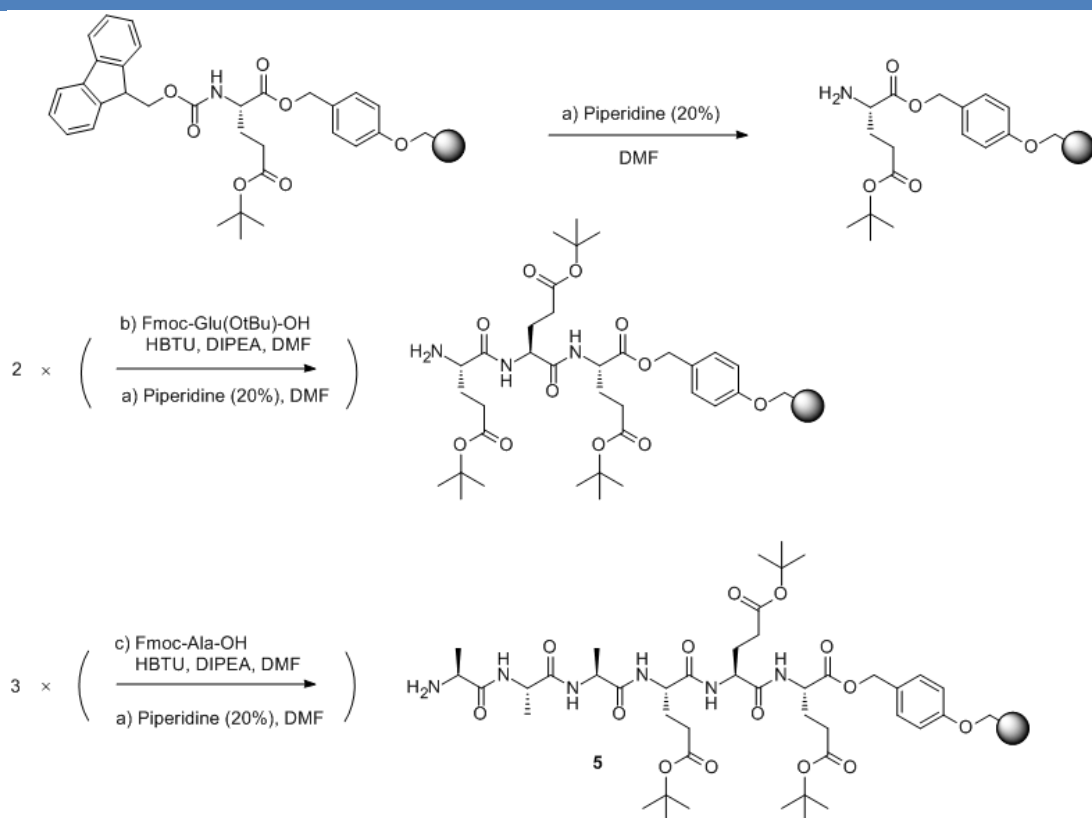
Scheme 2 | Synthetic route to solid supported peptide sequence AAAEEE.

The synthetic route followed to synthesize compound TAPeptide is depicted on Scheme 3.
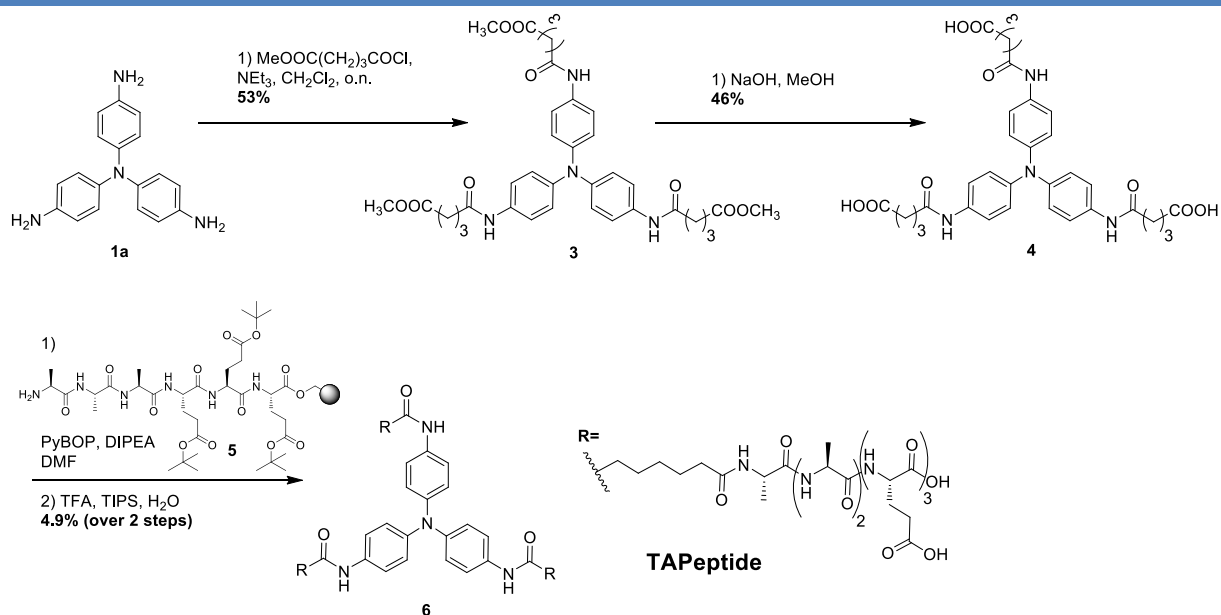
Scheme 3 | Synthetic route to water-soluble triarylamine TAPeptide.

The tris-amino triarylamine intermediate **1a** was reacted with glutaric acid monomethyl ester chloride to give compound **3** with three methyl esters as end groups. Subsequent saponification with a sodium hydroxide solution afforded compound **4** with three carboxylic acids as end groups. Solid supported triarylamine-peptide derivative was obtained by coupling this compound with the solid supported hexameric sequence **5** described previously, using PyBop as condensation agent and DIPEA as base. The reaction was monitored by UPLC after cleaving a small amount of the product from the solid support. By using a mixture of TFA/H$_2$O/TIPS (95:2.5:2.5), the final product TAPeptide was obtained albeit in low yield after concomitant release from the resin and removal of tert-butyl ester protecting groups and subsequent purification by reverse phase HPLC.

b. *Characterizations*

The molecular structure of the tris-amide triarylamine TAPeptide was demonstrated by ^{1}H NMR and COSY NMR spectra in deuterated DMF (Figures 33-34). Interestingly, proton peaks from the amide moieties of the peptidic backbone were observed between 7.8 and 8.4 ppm, suggesting that they are not hydrogen bonded in this solvent.
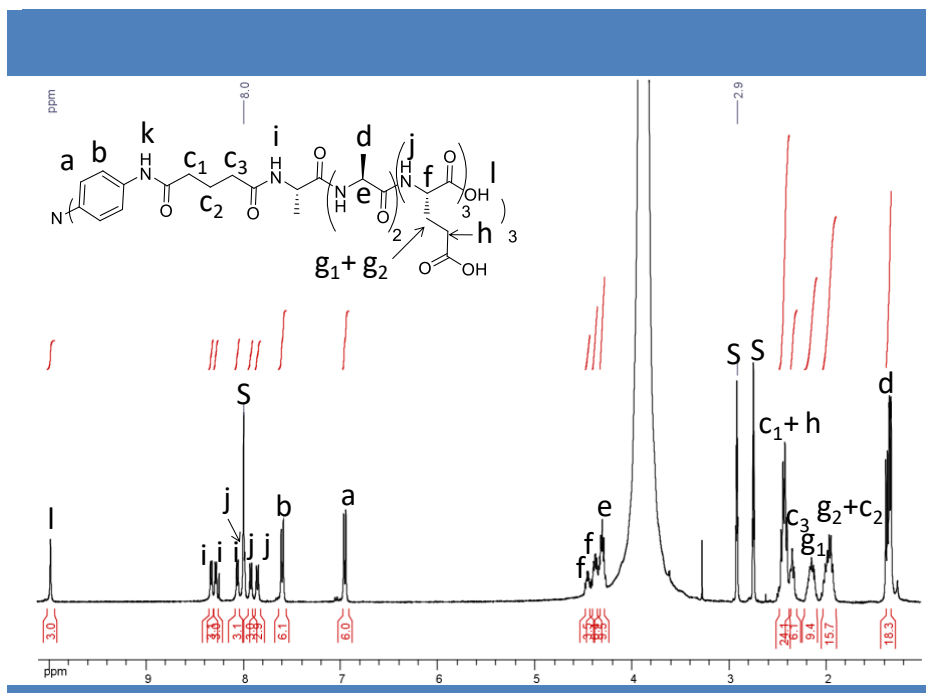
Figure 33 | ^{1}H NMR and peak assignments of TAPeptide in DMF (S is the residual signal for DMF).

As shown in Figure 34, the coupling of amide protons H$_i$ and H$_j$ with CH protons H$_e$ and H$_f$ respectively is observed in the A panel. From the correlation observed in the B panel and integrations, we could precisely determine the location of H$_e$ and H$_d$ which are assigned to the CH and CH$_3$ from the alanine moieties, respectively. Based on these amide protons, H$_i$ and H$_j$

from the A panel can be easily discriminated with H_i protons localized downfield compared to H_j protons. The coupling of protons H_f with diastereotopic protons H_{g1} and H_{g2} is illustrated in the C panel, but does not allow us to precisely discriminate both H_{g1} and H_{g2}. Then, coupling of H_{g1} and H_{g2} with methylene protons H_h is observed in the D panel. Finally, precise assignment of c_1, c_2 and c_3 was achieved by considering the remaining signals in the 2-3 ppm region and their correlation by COSY NMR.
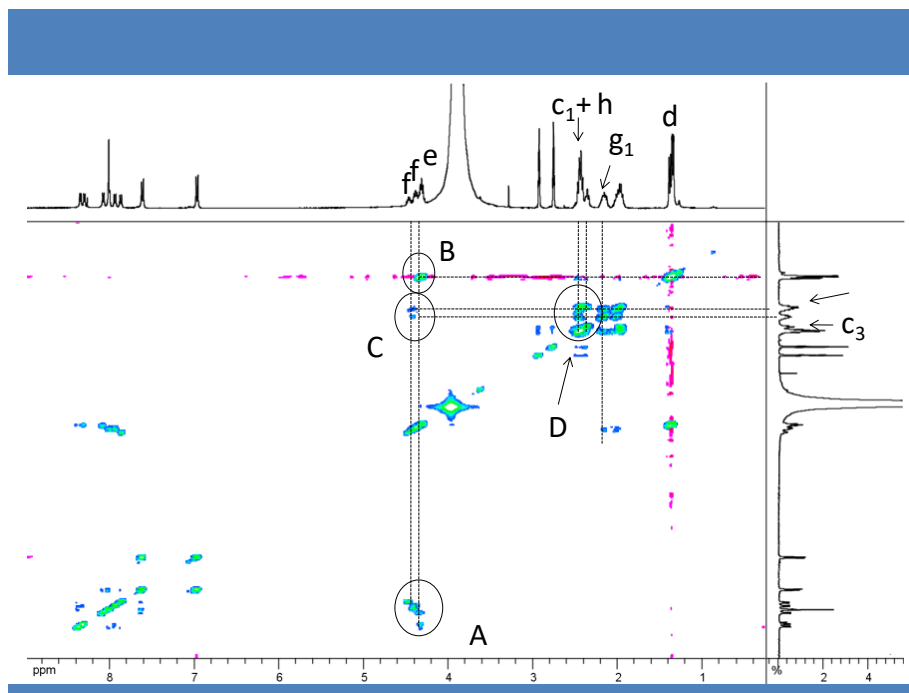
Figure 34 | ^{1}H-^{1}H COSY NMR spectrum of TAPeptide in DMF.
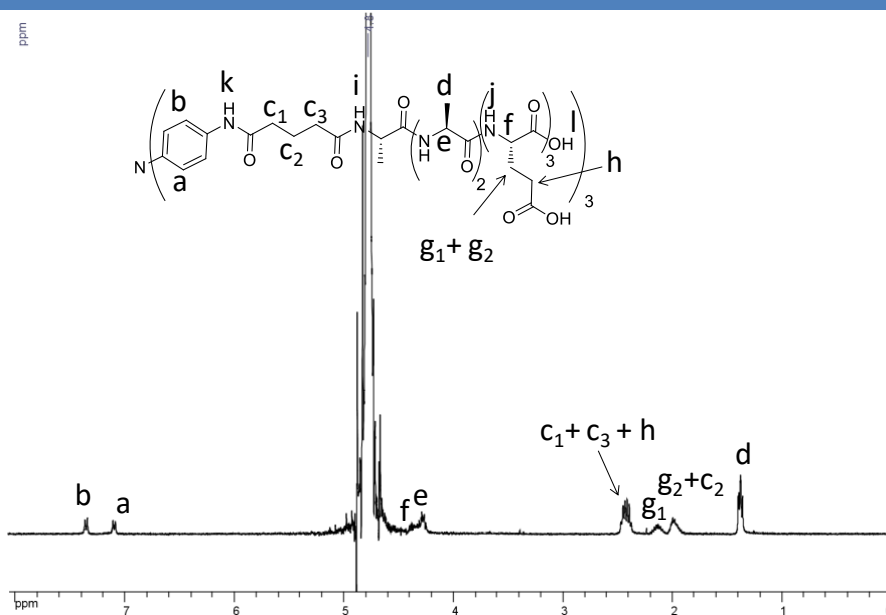
Figure 35 | ^{1}H NMR and peak assignments of TAPeptide in D$_2$O (1 mM).

This monomer also showed a good solubility in water as shown in Figure 35, however, its solubility in methanol was limited only to 10^{-4} M.

UV-Vis spectroscopy was performed for TAPeptide in either water or methanol at 10^{-4} M (Figure 36). The UV-vis spectrum from water shows a maximum absorption band at 318 nm, whereas the spectrum from methanol exhibits a maximum absorption at 305 nm. Furthermore, the concentration-dependent UV-vis spectra (10^{-8} to 10^{-4} M) for TAPeptide in either water or methanol indicate no shift of this maximum of absorption.
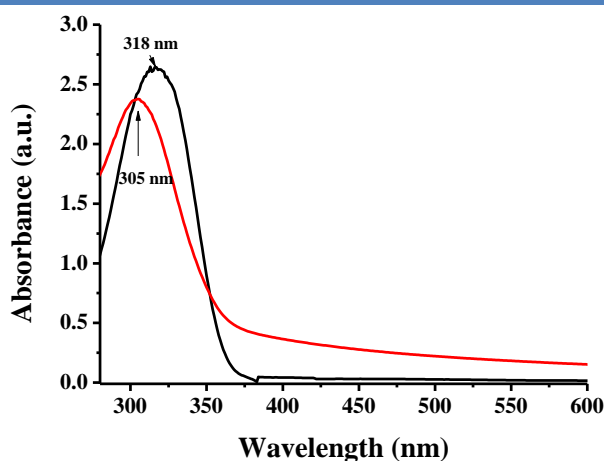
Figure 36 | UV-Vis-NIR spectra of TAPeptide in water (10^{-4} M, black) and methanol (10^{-4} M, red).

Concentration-dependent fluorescence spectra of monomer TAPeptide in either water or methanol were recorded as a function of concentration (Figure 37).
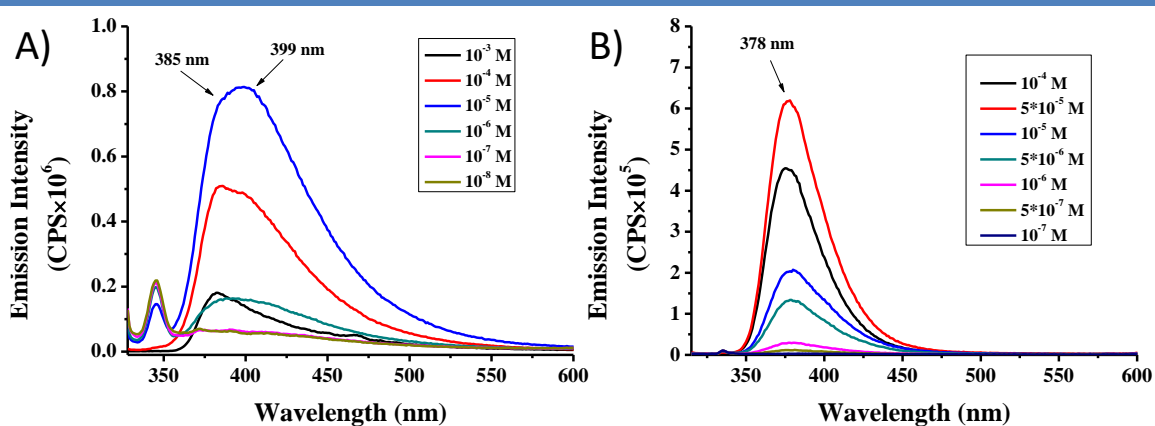
Figure 37 | Fluorescent spectra of TAPeptide a) in water for concentrations ranging from 10^{-8} M to 10^{-3} M, λ_{ex}=318 nm, slit=5 nm and b) in methanol for concentrations ranging from 10^{-8} M to 10^{-4} M, λ_{ex}=305 nm, slit=2 nm.

In water, an emission band at around 399 nm with a shoulder around 385 nm was observed. These emission bands increased with increasing concentration increased from 10^{-8}

M to 10^{-5} M, and then started to decrease until reaching a minimum at a concentration of 10^{-3} M which shows mainly an emission at 385 nm. Similarly, the fluorescence of TAPeptide in methanol showed a broad band at 378 nm, which first increased for a concentration up to 5×10^{-5} M (Figure 37b). When the concentration kept on increasing, the fluorescence started to be quenched reaching a minimum at a concentration of 10^{-4} M. Although UV-Vis experiments do not prove to be very informative, these fluorescence results suggest that aggregates start to be formed in water at concentrations above 10^{-5} M while the aggregates begin to be formed in methanol at concentrations above 5×10^{-5} M.

Circular dichroism (CD) experiments on monomer TAPeptide and peptidic sequence AAAEEE were then carried out, as shown in Figure 38a. CD spectra show weak signals for the peptidic sequence AAAEEE in both water and methanol. However, for the TAPeptide sample in either water or methanol, CD spectroscopy suggest the formation of a chiral structure in both cases, as in the triarylamine absorption region, CD spectra exhibit a weak Cotton effect. In order to compare the chirality of triarylamine motifs between water and methanol, both of the samples were recorded at 10^{-4} M in a 2 mm size cuvette (Figure 38b). In methanol, CD spectroscopy shows a strong Cotton effect for the triarylamine core, while no band is observed in this region for the sample in water. These observations suggest that the peptidic chain can induce a stronger chirality to the triarylamine motif in a methanol environment, which occurs at a lower concentration compared to water.
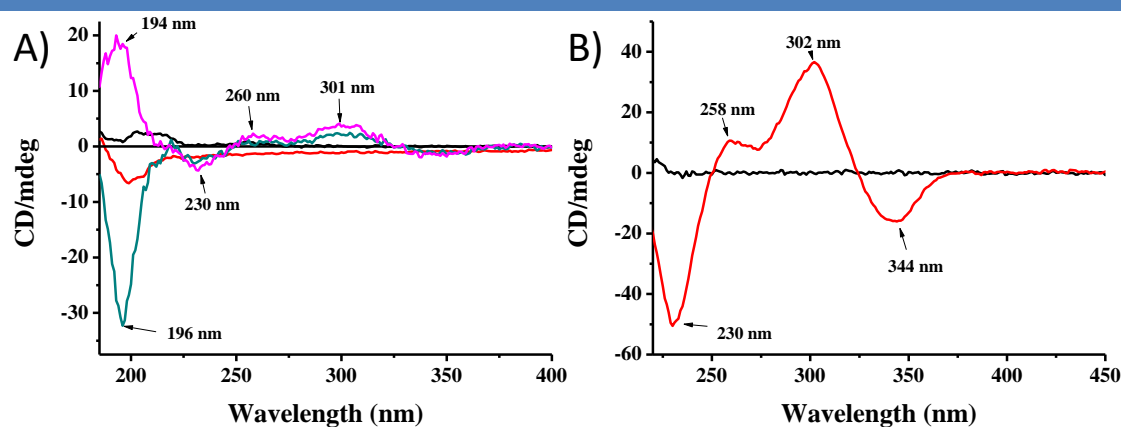
Figure 38 | a) CD spectra of AAAEEE in water (1 mM, black), AAAEEE in methanol (1 mM, red), TAPeptide in water (1 mM, green) and TAPeptide in methanol (0.1 mM, purple), cuvette: 0.1 mm; b) CD spectra of TAPeptide in water (0.1 mM, black) and methanol (0.1 mM, red), cuvette: 2 mm.

Further temperature dependent CD experiments were performed in order to confirm that this Cotton effect is derived from the chirality of the supramolecular self-assemblies (Figure 39). As the temperature increases from 10 °C to 80 °C, the intensity of band around 302 nm

decreases from 37 to 14 mdeg. In the following cooling process from 80 $^\circ$C to 10 $^\circ$C, the intensity of the band increases up to 38 mdeg, demonstrating that the Cotton effect results from the chirality of the self-assembled aggregates and that these supramolecular self-assemblies show good thermal stability. Additionally, the slight increase in the intensity observed after the heating-cooling process may suggest that more ordered structures could be formed after annealing. These CD experiments demonstrated the chiral nature of the aggregates in either water or methanol, which occur at different concentrations in agreement with fluorescent experiments.
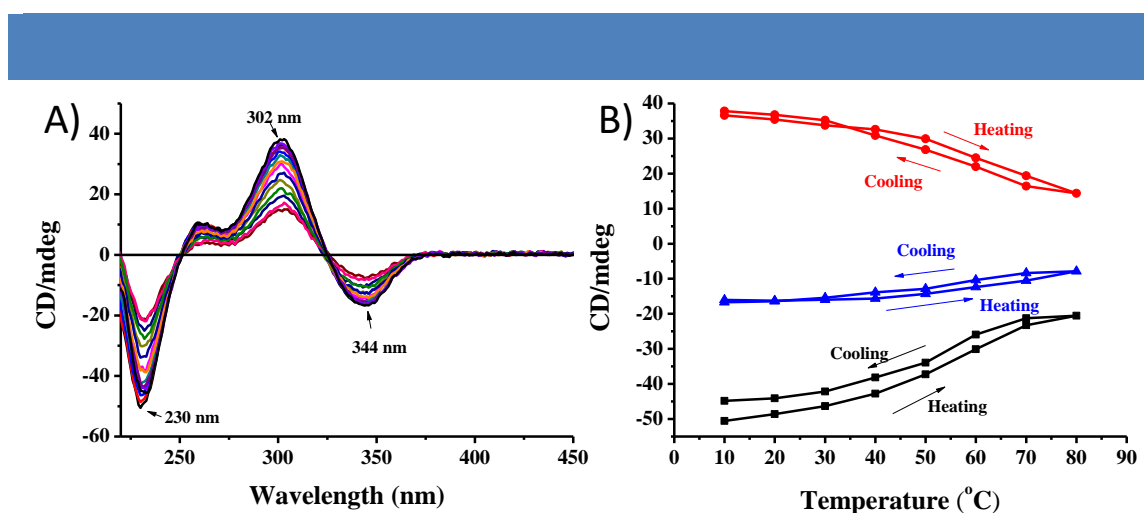
Figure 39 | a) Temperature-dependent CD spectra of TAPeptide in methanol (increased from 10 $^\circ$C to 80 $^\circ$C and then decreased to 10 $^\circ$C), cuvette: 2 mm; and b) evolutions of CD intensities at 230 nm (black), 302 nm (red) and 344 nm (blue).

FT-IR experiments were then performed by drop-casting a 10^{-3} M solution on an ATR diamond probe in order to study the self-assemblies built up from TAPeptide either in water or methanol (Figure 40).
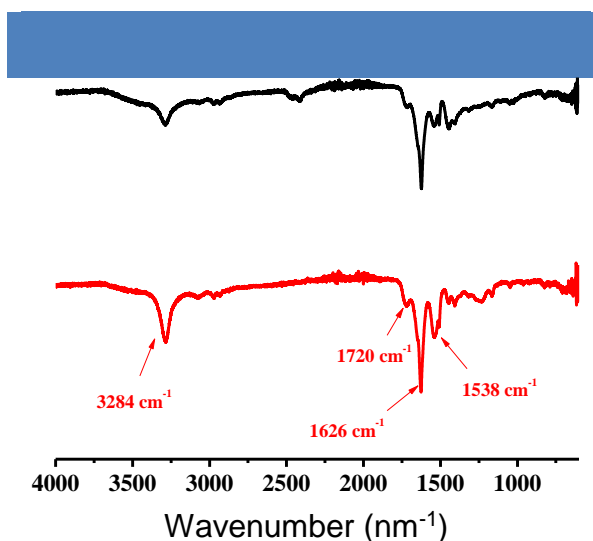
Figure 40 | FT-IR spectra of TAPeptide obtained from drop-casting a solution in water (black) and in methanol (red).

Similar spectra are observed in either solvent. In the carbonyl region, the sharp bands around 1626 cm^{-1} and 1538 cm^{-1} corresponding to amide I and amide II respectively are typical for a *β*-sheet arrangement of the peptidic backbone.[132] Furthermore, the absence of band around 1685-1695 cm^{-1} may indicate a parallel orientation of these *β*-strands. These experiments suggest that the chiral self-assembled structures are formed thanks to parallel *β*-sheet arrangement of the peptidic units in the two solvents.

SANS and LS experiments on TAPeptide in water or methanol were performed to determine the shape and characteristic dimensions of the self-assemblies (Figure 41).
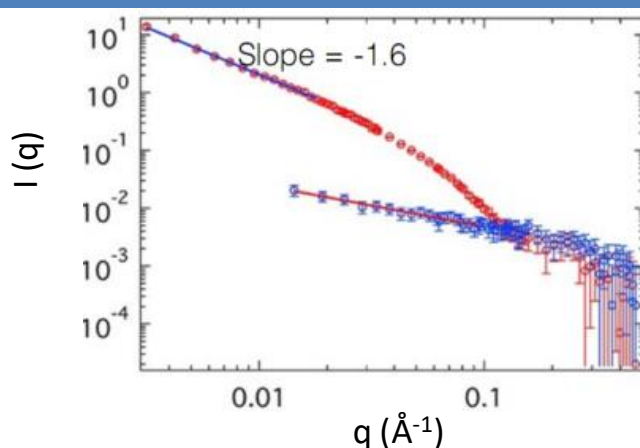
Figure 41 | SANS spectra of TAPeptide in water (10^{-3} M, red) and in methanol (10^{-4} M, blue).

In water, the scattering curve exhibits a low q regime (< 0.03 Å^{-1}) in which the q-dependance of the data can be described by a power low with the exponent close to -1.6, such as in fully swollen coils. Data were fitted using a model of flexible cylinder model, which provide a radius of the cross-section of around 2.7 ± 0.1 nm. Furthermore, SLS experiments show a q^{-3} dependance of the data for scattering vectors lower than 0.002 Å, which suggests the presence of collapsed polymer coils at larger length scales. Interestingly, due to the low solubility of the compound in methanol, only low diffusion intensity was recorded by SANS which precluded any analyses. Further DLS experiments on TAPeptide in methanol indicated the presence of aggregates which hydrodynamic radius varied between 100 and 500 nm and high polydispersity. Overall, whereas scattering techniques suggested the presence of polymer coils for TAPeptide in water with a cross-section which could correspond to the formation of monocolumnar aggregates, SANS and LS experiments could not provide meaningful information on the self-assemblies formed in methanol. Thus, we took advantage of microscopy techniques to elucidate their structures.

For TAPeptide samples in either water or methanol, rigid fibers with lengths of several micrometers were observed by TEM (Figure 42). In water, the presence of elongated fiber-like structure is in agreement with the results obtained by SANS. Statistical analysis of the TEM images indicates a mean radius of the fibers of around 3.3 nm in water which is in agreement with the radius of the cross-section determined by SANS, while the mean radius of the fibers in methanol is around 6.4 nm which could correspond to an arrangement into bundles of bis or tris columnar structures.
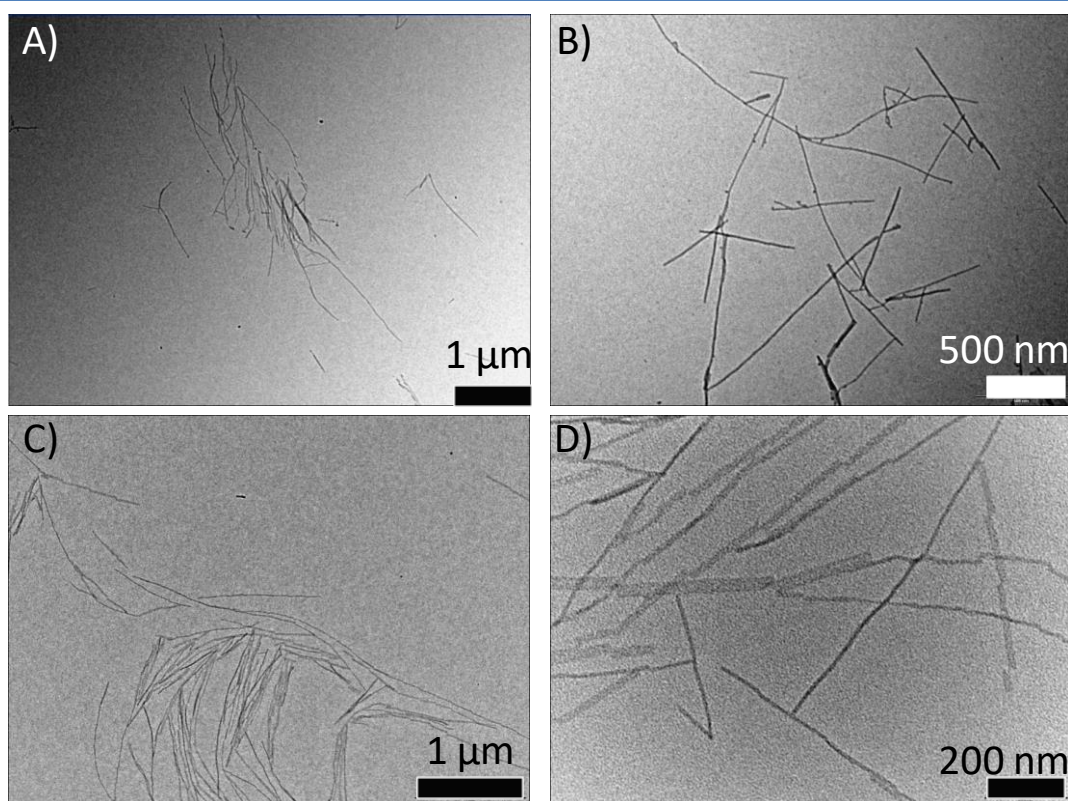
Figure 42 | TEM images of TAPeptide a-b) in water (4×10^{-4} M); and c-d) in methanol (10^{-4} M).

Considering the pH sensitivity of the peptidic backbone, we then studied the impact of the pH on the morphologies of the aggregates by TEM. The pH of a TAPeptide solution at 4×10^{-4} M in milliq water was determined to be around 3.78. For buffer pH $\geq$ 6, no self-assembly could be observed by TEM, which could be due to electrostatic repulsions and/or full solubility of TAPeptide in neutral and basic solutions thanks to the presence of deprotonated glutamate residues. In buffer pH=2 or pH=4, micrometer long fiber-like structures with a single handedness are observed, although shorter and flexible fibers are recorded at pH=2 compared to pH=4 (Figure 43). Statistical analysis of the images revealed that fibers from buffer pH=2 have a mean radius of around 8.6 nm while their mean radius from pH=4 buffer

is around 5.6 nm.
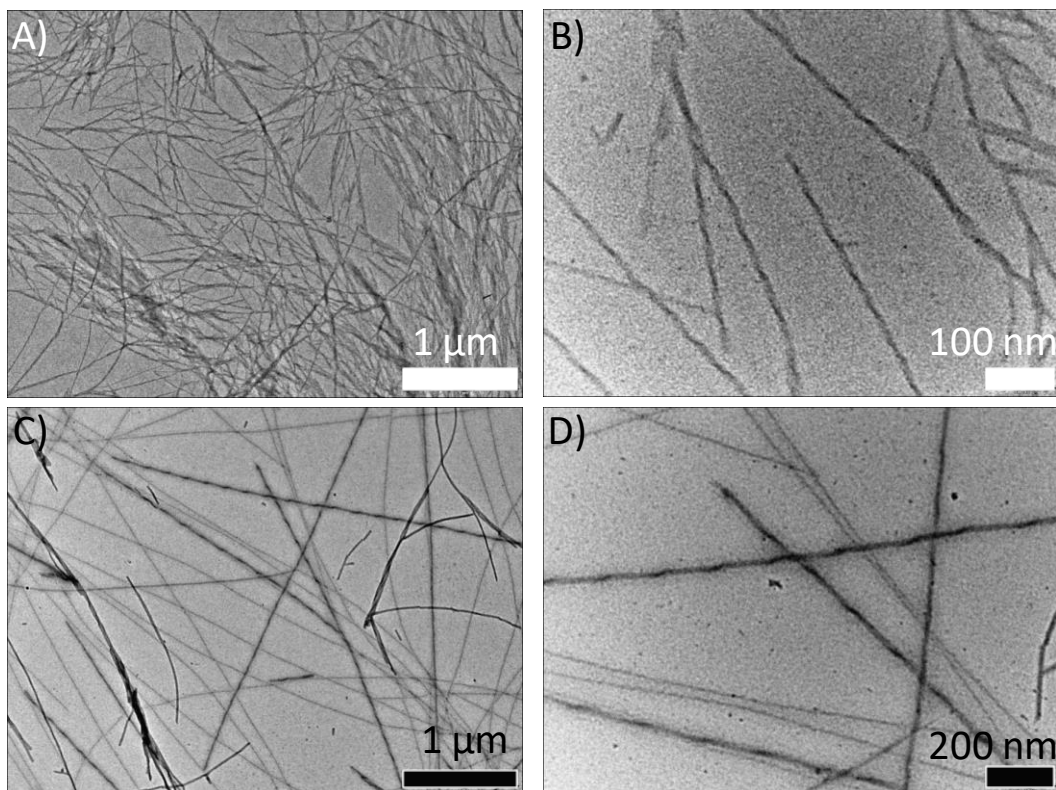
Figure 43 | TEM images of TAPeptide a-b) in buffer at pH=2 (0.1 mM) and c-d) in buffer at pH=4 (0.1 mM).

FT-IR experiments were performed on TAPeptide samples prepared in buffer at pH=2 and pH=4 (Figure 44).
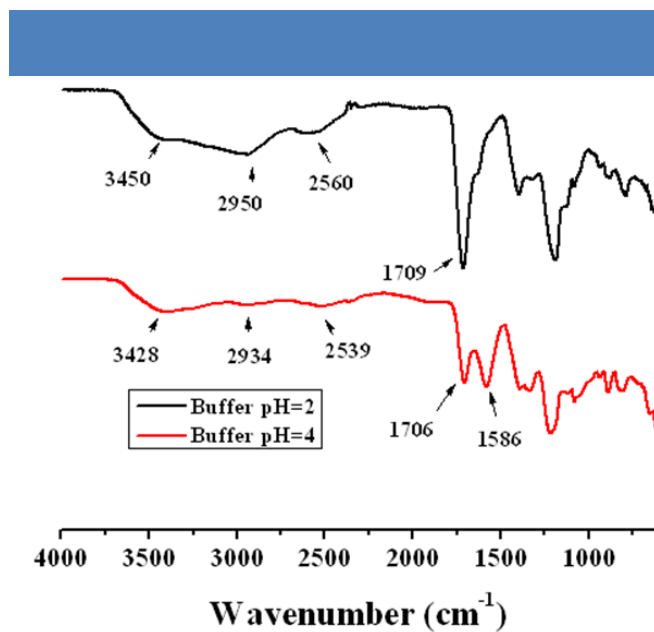
Figure 44 | FT-IR spectra of TAPeptide in buffer at pH=2 (black), and at pH=4 (red).

For both samples, the presence of bands around 1706 cm^{-1} and the broad bands in the range of 2500~3000 cm^{-1} indicate the presence of hydrogen-bonded carboxylic acid. In addition, a sharp band around 1586 cm^{-1} for TAPeptide in buffer pH=4 indicate stronger hydrogen bonds are formed within these self-assemblies in contrast to that in buffer pH=2.

c. Discussion

Overall, a tris-amide triarylamine compound decorated with three identical AlaAlaAlaGluGluGlu sequences was designed and synthesized. This TAPeptide compound shows good solubility in water, particularly at pH higher than 6, but presents a lower solubility in methanol. In both solvents, CD and FT-IR experiments suggest the formation of chiral supramolecular polymers with a parallel *β*-sheet arrangement of the peptidic backbone, but these chiral structures could currently not be imaged by TEM experiments. However, we believe that further imaging by atomic force microscopy will confirm the conclusions based on spectroscopic data. In milliq water, the micrometer long fiber-like morphologies observed by TEM are in agreement with structures determined in solution by scattering experiments. Interestingly, in buffers at pH=2 and 4, twisted fibrillar structures with a single handedness are observed by TEM imaging. However, the absence of strong IR band at around 1630 cm^{-1} suggest that the peptidic units are not arranged into *β*-sheet structures but their chirality is related to the single handedness of the aggregates. Further experiments by CD should provide us with more information on the molecular arrangement of TAPeptide molecules which lead to these observations.

4. Synthesis and characterization of triarylamine-Cy3 derivative

a. Synthesis

Scheme 4 described the synthetic route toward iodo-cyanine3 molecule **15**, which is based on the work developed by our group.[161] The synthesis is divided into two parts: a) synthesis of the indole moiety and b) synthesis of the chloroacetamide **12**. For the indole moiety, potassium 2,3,3-trimethyl-3H-indole-5-sulfonate available in a large scale in our laboratory was coupled with commercially available propane sultone in 1,2-dichlorobenzene to give compound **9** in 35% yield. This compound was then condensed with *N,N*-diphenylformamidine in a mixture of acetic acid and acetic anhydride at 120 ºC for one night to afford the secondary amide **13**, which is unstable in acidic environment and has thus

---

[161]Tauk, L. Schröder, A. P. Decher, G. and Giuseppone, N. Hierarchical functional gradients of pH-responsive self-assembled monolayers using dynamic covalent chemistry on surfaces. *Nat. Chem.* **1,** 649–656 (2009).

to be used in the next condensation reaction with compound **12** as quickly as possible.
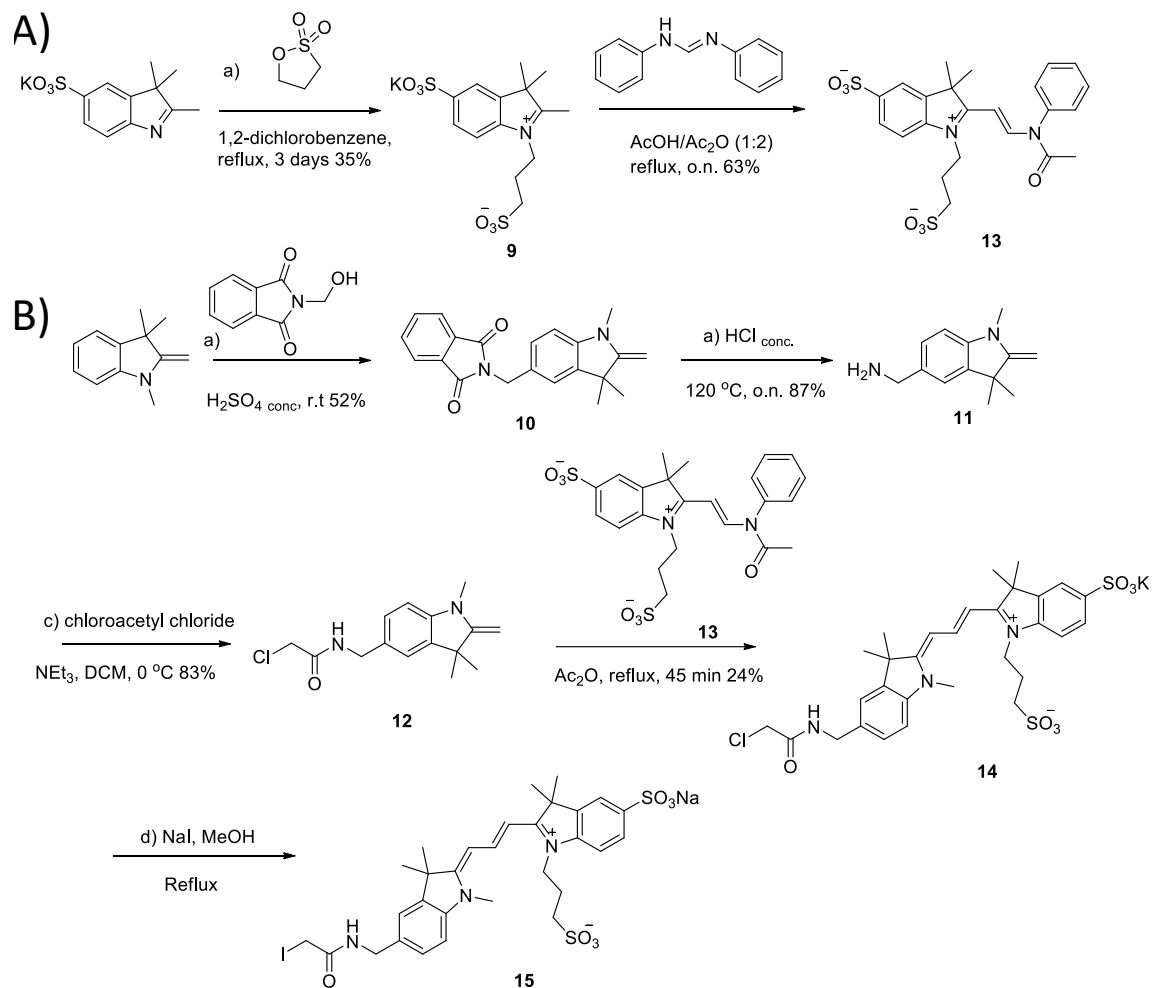

Scheme 4 | Synthetic route for Cy3-iodo molecule **15**.

For the other part, compound **10** was obtained by condensation of Fischer's base with *N*-hydroxymethylphtalimide in concentrated sulfuric acid and isolated by crystallization. After deprotection of the phtalimide unit at reflux in chlorhydric acid, amine **11** was then acylated with chloroacetyl chloride to give compound **12** in 83% yield. Condensation reaction between indoleninium bis-sulfonate **13** and chloroacetamide **12** in acetic anhydride provided pure chloro-cyanine3 **14** after purification by reverse-phase preparative HPLC. Finally, nucleophilic substitution using sodium iodide in methanol at reflux provided compound **15** which was then used freshly in the next step.

Using a synthetic strategy already reported by our group,[147] tris-amine triarylamine **1a** was acylated with 6-bromohexanoyl chloride to yield tris-amide molecule **7** with terminal bromide atoms on the alkyl chains. Nucleophilic substitution with triphenylmethane thiol at 35 ºC gave triphenylmethane protected thiol compound **8** in 55% yield. Deprotection under

argon atmosphere, using triethylsilane and trifluoroacetic acid provided compound **8b** with thiol end groups which were quickly coupled with cyanine derivative **15**. This reaction was performed in DMF in the presence of potassium carbonate for one night to give final triarylamine-cyanine derivative TACy3 in 30% yield, after purification by reverse-phase preparative HPLC.
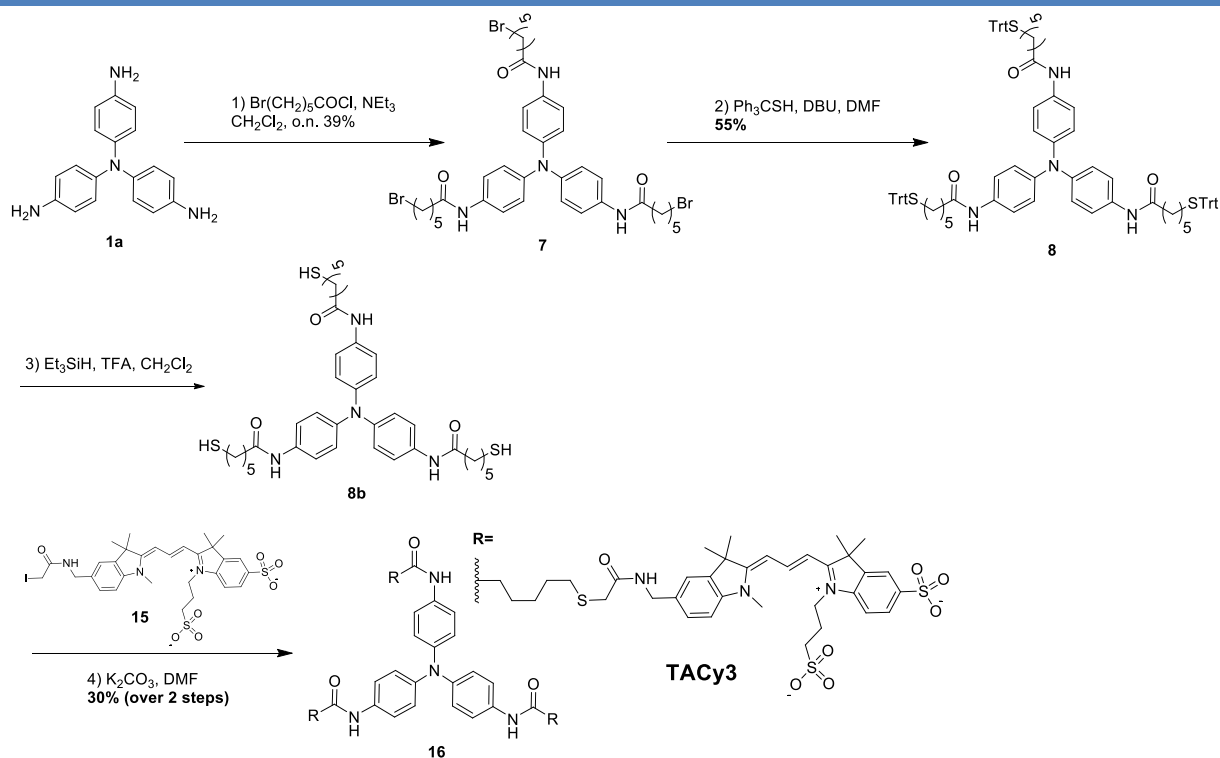
Scheme 5 | Synthetic route to access water-soluble triarylamine TACy3.

b. *Characterizations*

The molecule TACy3 shows good solubility in water (up to 10^{-2} M) and methanol (up to 10^{-3} M) (Figure 45). Confirmation of the molecular structure of TACy3 was demonstrated by ^{1}H NMR and ^{1}H-^{1}H COSY NMR in deuterated methanol. As shown from the ^{1}H NMR spectrum in deuterated water, broad proton peaks are observed, suggesting the formation of TACy3 self-assemblies in water.

FT-IR experiments were performed on TACy3 samples in both water and in methanol (Figure 46). In both solvents, the presence of a large band at around 3204 cm^{-1} along with the amide I band at ~ 1647 cm^{-1} suggest the formation of hydrogen bonds between amide groups close to the triarylamine core. The presence of a strong band at 1559 cm^{-1} in methanol might indicate that the amide moiety close to the cyanine core is free in methanol whereas it is hydrogen bonded in water.
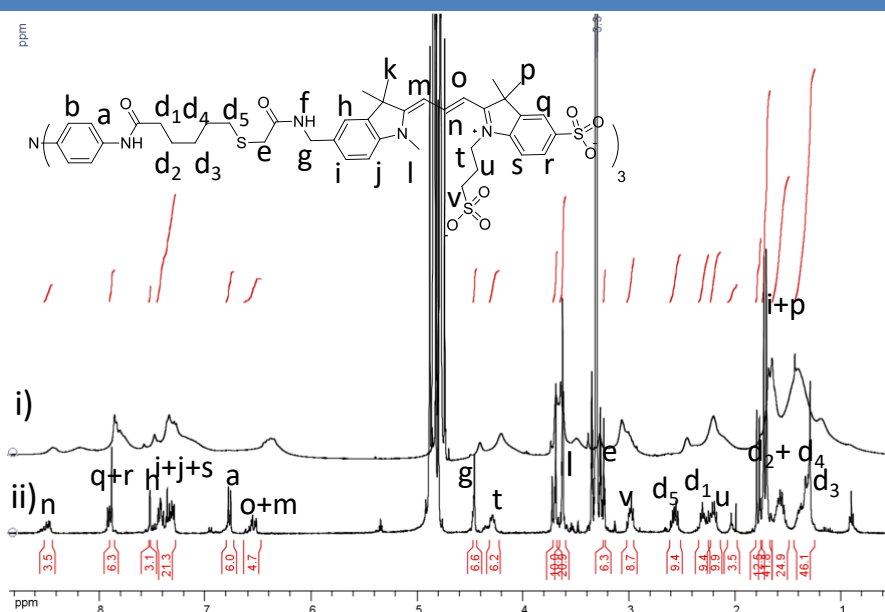
Figure 45 | ^{1}H NMR and peak assignments of TACy3 i) in D_2O (5 mM) and ii) in MeOD (1 mM).
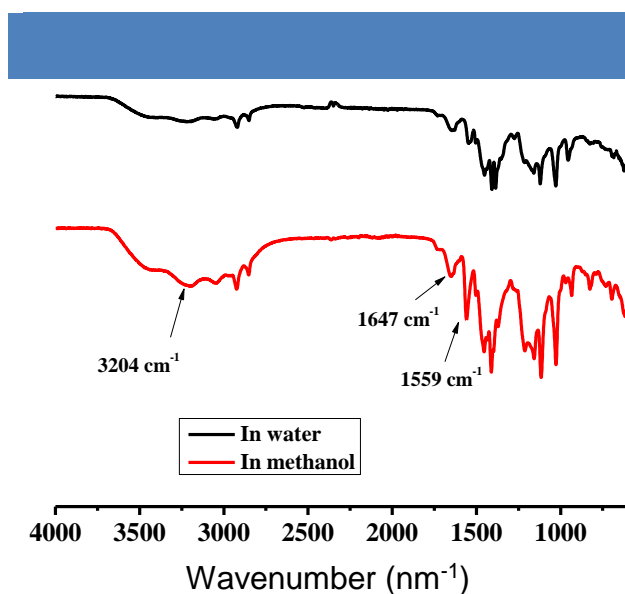
Figure 46 | FT-IR spectra of TACy3 in water (black) and methanol (red).

UV-Vis and fluorescence spectra were then employed to study the self-assembly of TACy3 in water and methanol solutions. In methanol, absorption spectra of TACy3 is almost identical to the one recorded for cyanine derivative **14** with a maximum of absorption at 553 nm (Figure 47). This observation suggests that cyanine side chains in TACy3 are not aggregated in methanol. The only difference between both compounds is related to the presence of an absorption band at 320 nm in TACy3, which corresponds to the triarylamine core. However, it is not possible to determine by absorption experiments if they are stacked or not.
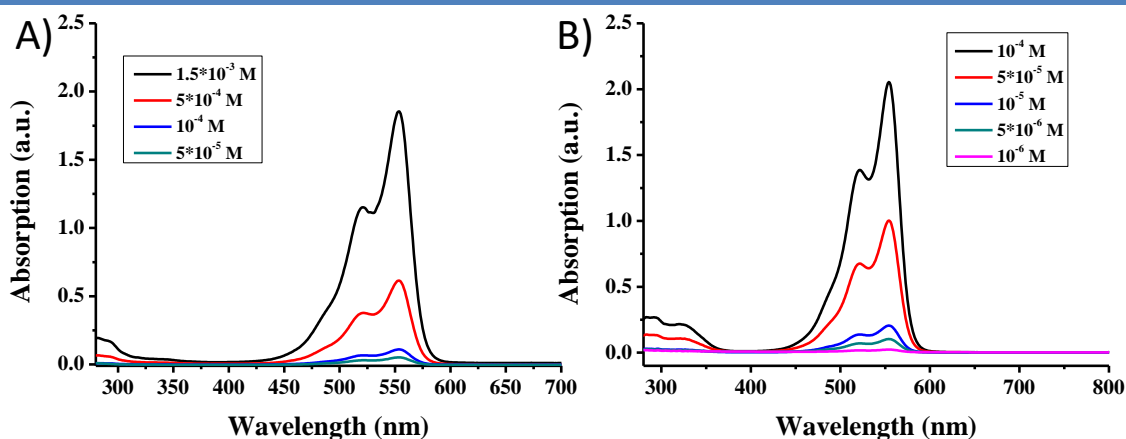
Figure 47 | UV-Vis spectra of a) cyanine3 derivative **14** in methanol at different concentrations, cuvette: 0.1 mm and b) TACy3 in methanol at different concentrations, cuvette: 1 mm.

On the other hand, as seen from the concentration-dependent absorption spectra on Figure 48a, a maximum absorption at around 513 nm is observed for TACy3 in water, which is hypsochromically shfted (547 to 513 nm) compared to Cy3 molecule **14** at similar concentrations. This blue shift of maximum absorption suggests that the Cy3 side chains of TACy3 arrange into H-aggregates were formed for TACy3 in water even at concentration as low as 5×10^{-6} M.
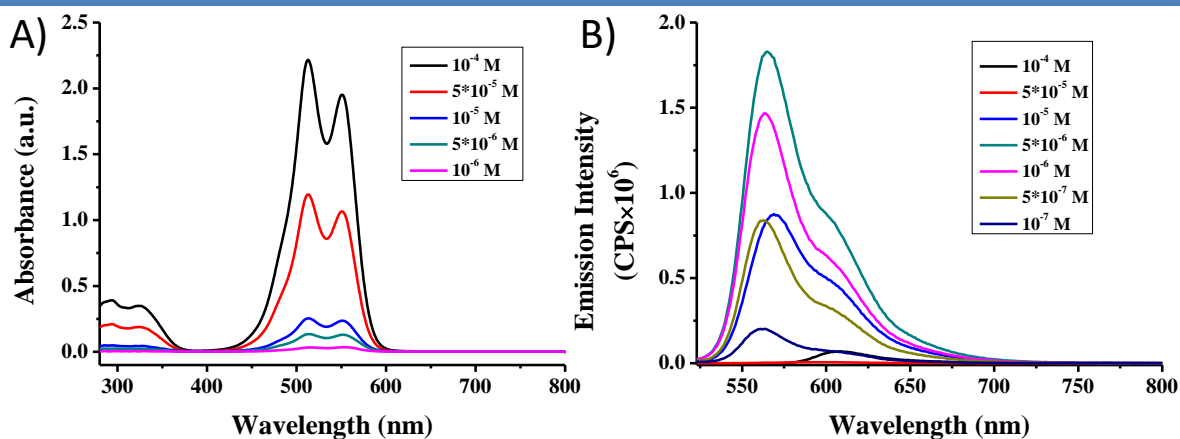
Figure 47 | a) UV-Vis spectra of TACy3 in water at different concentrations, cuvette: 1 mm; and b) fluorescence spectra of TACy3 in water for concentrations ranging from 10^{-7} to 10^{-4} M, λ_{ex}= 513 nm, slit=5 nm.

Such behavior was confirmed by fluorescence experiments on solutions of TACy3 in water at various concentrations. Upon excitation at 513 nm, a maximum emission is observed at around 561 nm, which intensity increased for concentrations to 5×10^{-6} M, and then got quenched for concentrations higher than 5×10^{-5} M (Figure 47b). These observations suggest

that the cyanine side chains of TACy3 aggregates for concentrations above 5×10^{-6} M, in agreement with UV-Vis experiments. The fluorescence spectra of TACy3 in water or methanol at different concentrations were also recorded by excitation at 322 nm or 319 nm respectively. As shown in Figure 49a, the spectra of TACy3 in water show weak emission at around 400 nm over the whole range of concentrations, suggesting the triarylamine units are stacked in the nanostructures even at low concentrations. However, for TACy3 in methanol, the increasing strong emission recorded at around 400 nm for increasing concentration indicates that triarylamine units remain free in solutions for concentrations up to 5×10^{-5} M.
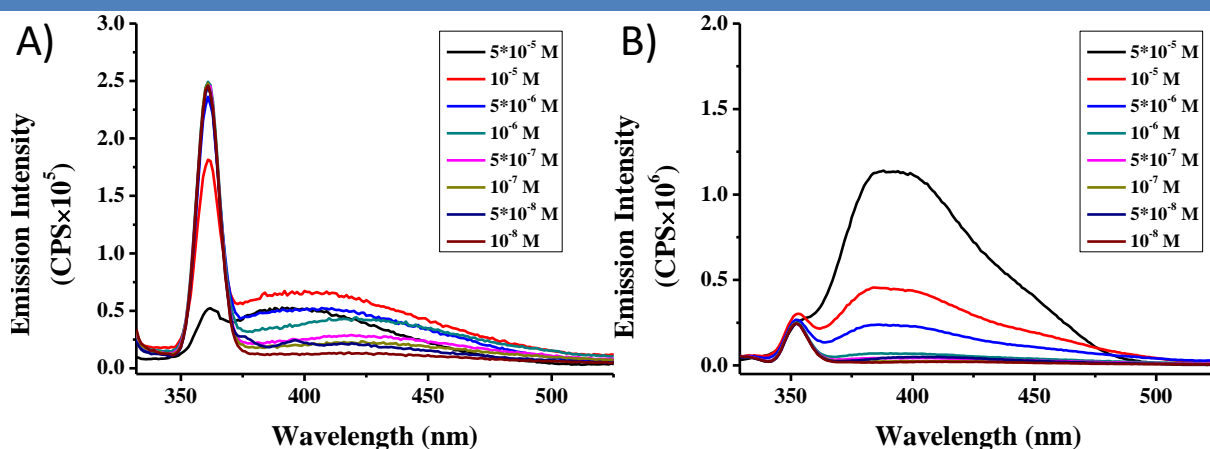
Figure 49 | Fluorescent spectra of TACy3 for concentrations ranging from 10^{-8} M to $5*10^{-5}$ M a) in water, λ_{ex}=322 nm, slit=5 nm; and b) in methanol, λ_{ex}=319 nm, slit=5 nm.

To explore whether a possible energy transfer could occur between the triarylamine core and the Cy3 moieties in TACy3 in methanol, we examined the absorption spectrum of compound **14** and the emission spectrum of compound **7** (Figure 50a). The presence of a small overlap between these two indicates that Forster resonance energy transfer (FRET) is possible from the triarylamine core to the cyanine dyes. In the molecular state, fluorescence quenching of the emission band at around 400 nm and appearance of an emission band at 568 nm are observed for TACy3 upon excitation at 319 nm compared to compound **7**. This observation suggests a very efficient deactivation of the excited state of TACy3, and energy transfer from the triarylamine core to the cyanine moieties. At higher concentration (10^{-4} M), a similar fluorescence behavior is observed although quenching of the triarylamine core proved to be less efficient. These experiments indicate that TACy3 molecules remain molecularly dissolved even at relatively high concentration and thus do not aggregate in ordered structures in methanol.
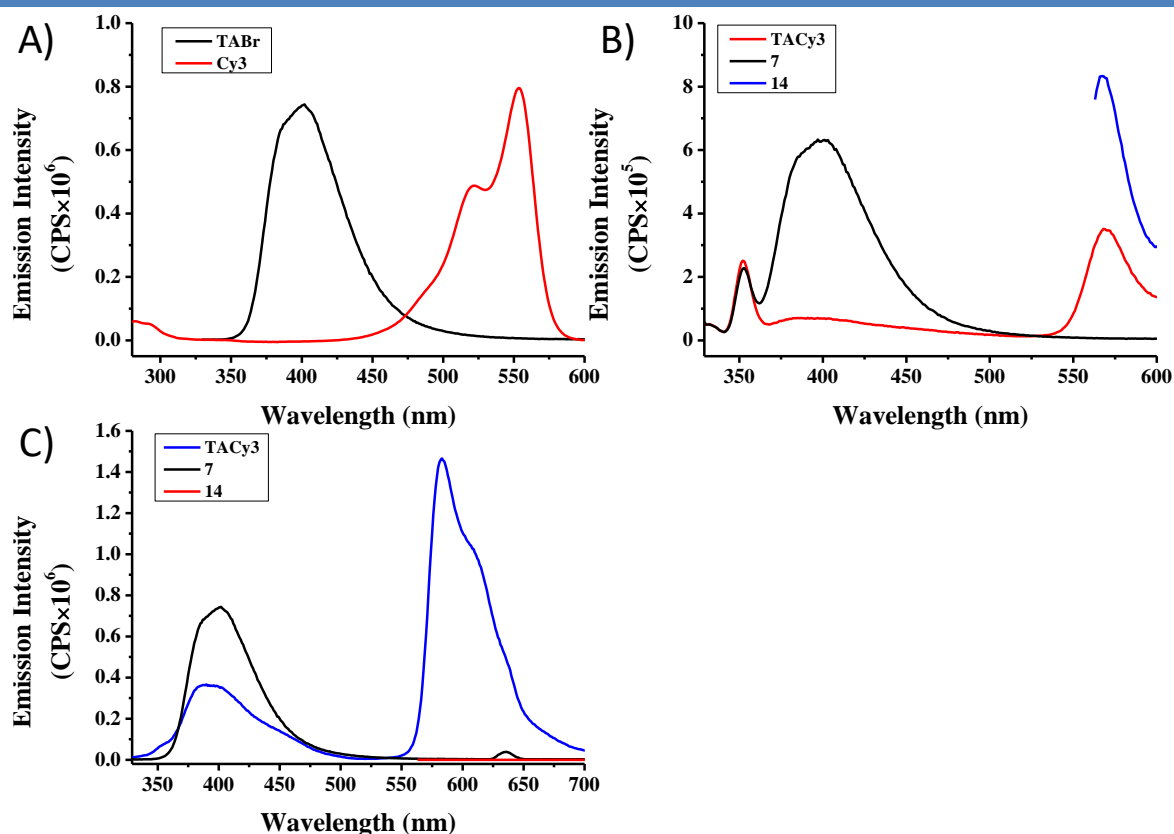
Figure 50 | a) Fluorescence spectrum of compound **7** (10^{-4} M in methanol, black), λ_{ex}=319 nm and absorption spectrum of compound **14** (10^{-4} M in methanol, red); b) fluorescence spectra in methanol of TACy3 (10^{-6} M, red), λ_{ex}=319 nm, compound **7** (10^{-6} M, black), λ_{ex}=319 nm, and compound **14** (3×10^{-6} M, blue), λ_{ex}=553 nm; c) fluorescent spectra in methanol of TACy3 (10^{-4} M, blue), λ_{ex}=319 nm, compound **14** (10^{-4} M, red), λ_{ex}=319 nm, and compound **7** (3×10^{-4} M, black), λ_{ex}=553 nm.

SANS experiments were then employed to elucidate the structure of TACy3 in water, as in methanol, we could only record a low scattered intensity which could be attributed to the diffusion of monomers (Figure 51).
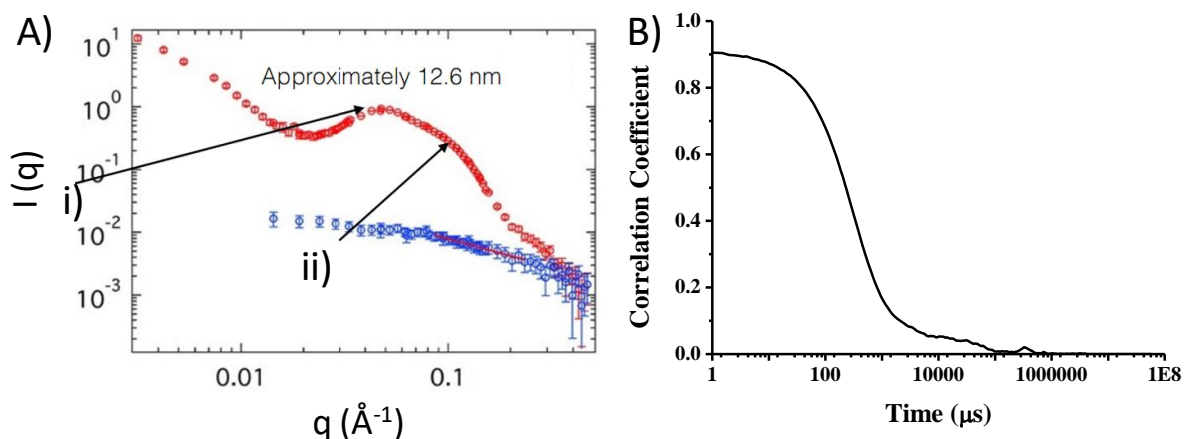
Figure 51 | SANS spectra of TACy3 in water (10 mM, red) and in methanol (1 mM, blue); and b) Zetasizer experiment performed on a 10^{-4} M solution of TACy3 in water.

In water, the scattering curve gives the following information: a) the onset of a Guinier regime in the very low q region and associated with a finite size and mass of the objects, b) a q^{-2} domain for q values up to 0.02 Å^{-1}, which could be associated to the formation of Gaussian chains or smooth 2D objects and c) a complex behavior at higher q which show a peak at a characteristic distance of 12.6 nm and a behavior similar to TAPEG for q values around 0.1 Å^{-1} (i and ii regions on Figure 51). However, more work is required to fully analyze these SANS data. Additional DLS experiments using the Zetasizer suggest the presence of one main population of objects with an average diameter of ~ 195 nm (Figure 51b). In order to evaluate the morphology of the aggregates, TEM experiments were performed by drop-casting a solution of TACy3 in water on a copper grid. TEM images of the solution in water show the presence of large 2-D ribbon-like structures while the aggregates in methanol exhibit short fiber-like structures with the length of around 200 nm (Figure 52), probably due to cystallisation of the monomers at the grid surface.
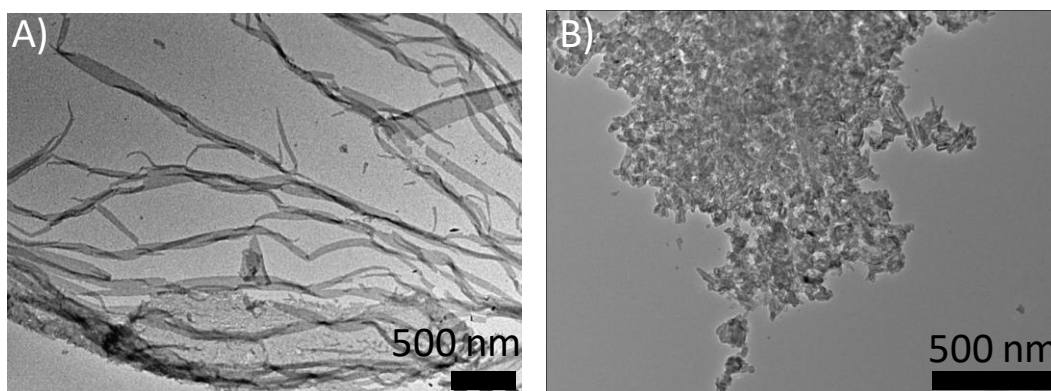
Figure 52 | TEM image of TACy3 a) in water (0.1 mM) and b) in methanol (0.1 mM).

c. *Discussion*

Overall, a tris-amide triarylamine derivative TACy3 decorated with three identical cyanine moieties as side chains was designed and synthesized. Similarly to TAPeptide, this compound displayed a better solubility in water compared to methanol. In methanol, ^{1}H NMR, optical spectroscopies and scattering techniques suggest that TACy3 is molecularly dissolved. In this solvent, fluorescence experiments suggest that energy transfer occurs between the triarylamine donor core and the cyanine acceptor moieties. Further time-resolved fluorescence measurement and transient absorption spectroscopy should be performed to investigate the process in details. In water, spectroscopies (^{1}H NMR, UV-Vis, fluorescence, FT-IR) suggest

the formation of supramolecular polymers, which structure remains to be determined precisely by completing the complex analysis of the SANS data. However, TEM imaging suggests the formation of 2-D ribbon-like structures with micrometric lengths and widths ranging from 50 to 100 nm. Further experiments such as AFM imaging and small angle X-ray scattering should be performed to determine the molecular arrangement of the TACy3 molecules within these large structures.

5. Conclusions

In this chapter, three novel water-soluble triarylamine tris-amide derivatives have been successfully synthesized. A variety of techniques were employed to characterize the self-assemblies mainly in water and methanol. For TAPEG, similar dense and large fibers are observed in water and methanol. We believe that the PEG chains preserve hydrogen bonding interactions between amide surrounding the triarylamine core leading to the formation of monocolumnar structures which further aggregate into dense structures by PEG interactions. For TAPeptide, similar elongated fibers are observed in either water or methanol. The presence of chiral peptidic side chains induces the formation of chiral supramolecular polymers with parallel β-sheet arrangement of the hexapeptides. While monocolumnar aggregates are observed in water, bundles of several fibers are recorded in methanol, arising probably from hydrogen-bonding interactions between end chain carboxylic acid units. Interestingly, in acidic aqueous conditions, the presence of twisted fibers with a single handedness, observed directly by TEM can be explained by similar molecular arrangements which have to be confirmed by additional CD experiments. Finally for TACy3, while the molecules remain molecularly dissolved in methanol, they give rise to ribbon-like structures in water thanks to the formation of H-aggregates of the cyanine moieties. The formation of large ribbon-like structures suggest an anti-parallel arrangement of the cyanine dyes which bringing together the columnar fibers produced by triarylamine self-assembly. This arrangement remains speculative and will have to be confirmed by further imaging experiments.

In conclusion, the work in this chapter describes the first triarylamine supramolecular polymers produced in aqueous media thanks to a combination of various non-covalent interactions. The triarylamine core seem to act as the main driving force for the self-assembly into columnar aggregates while side chains ensure solubility in such polar solvents and can also be used to favor the formation of chiral architectures.

Chapter VI: Cross-linked supramolecular polymers based on triarylamine motifs

1. Objectives and targeted molecules

The bottom-up supramolecular approach has been recognized as an effective way to construct soft materials with nanometric "pseudo-crystalline" electroactive domains.[56] In the past decade, supramolecular self-assemblies of π-conjugated molecules can be used to build up organic electronic devices as reported by several groups.[36,56] However, these π-electronic supramolecular polymers might be limited in terms of practical applications as a result of relatively weak non-covalent interactions. As mentioned in the bibliographical chapter, post-polymerization or cross-linking strategies would thus be interesting so as to boost the mechanical robustness and thermal stability of supramolecular architectures.

Recently, our group reported that well-designed tris-amide triarylamine can form supramolecular monocolumnar nanofibers displaying metallic behavior due to delocalized electronic states and structural repairing properties resulting from the diffusion of so called supramolecular polarons. We were wondering if a next generation of conducting nano-objects could consist in trapping the self-assembled triarylamine building blocks into a covalent framework. Ring opening metathesis polymerization (ROMP) and sol-gel process were thus considered as post-modification methodologies because they can be regarded as inert for the supramolecular polymerization and highly controllable as described in the third chapter of this manuscript. Besides, we would like to investigate the influence of amide and urea groups on the periphery of the triarylamine core on the resulting non-covalent self-assemblies. Based on these criteria, we hereafter report the synthesis of tris-amide triarylamine molecules TANBE and TAEOS1 appended with norbornene and siloxane groups respectively and, a tris-urea triarylamine molecule TAEOS2 with siloxane end groups (Figure 53), along with the characterization of their supramolecular polymers and corresponding gels by means of various techniques.
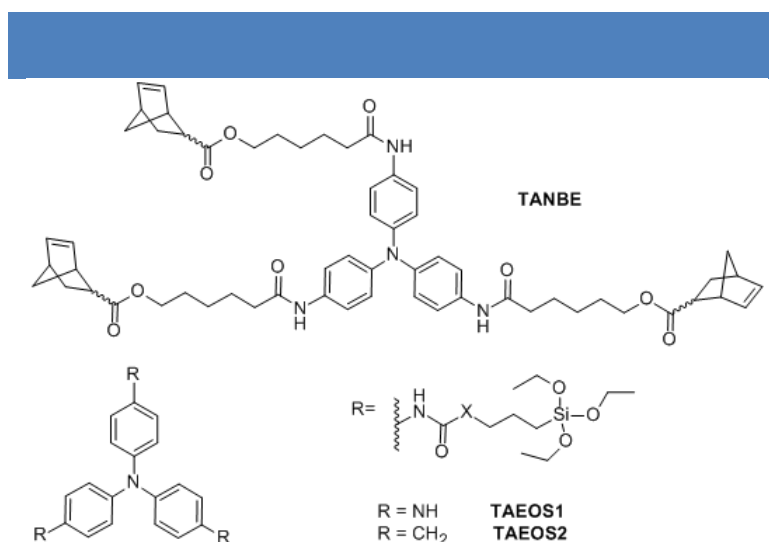
Figure 53 | Molecular structures of the targeted triarylamine derivatives TANBE, TAEOS1 and TAEOS2.

2. Synthesis

a. *Synthesis of triarylamine-urea-siloxane derivative*

The triarylamine-urea-siloxane molecule TAEOS1 was obtained by coupling *N',N'*-bis(4-aminophenyl)benzene-1,4-diamine **1a**[146] and commercially available 3-isocyanatopropyltriethoxysilane under mild conditions with a yield around 33% (Scheme 6).
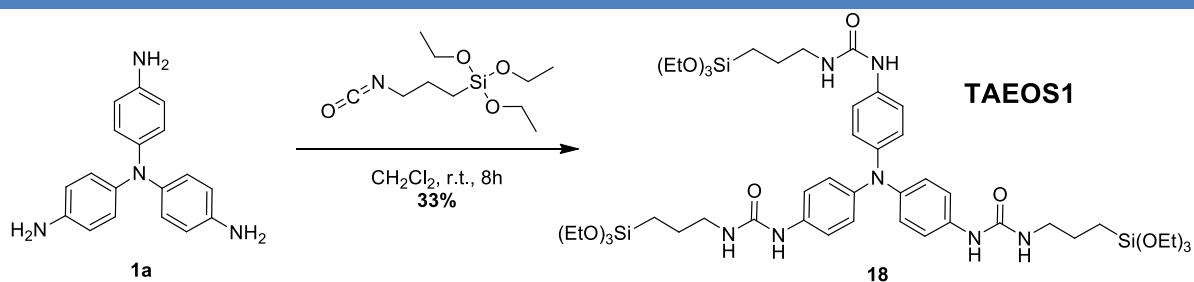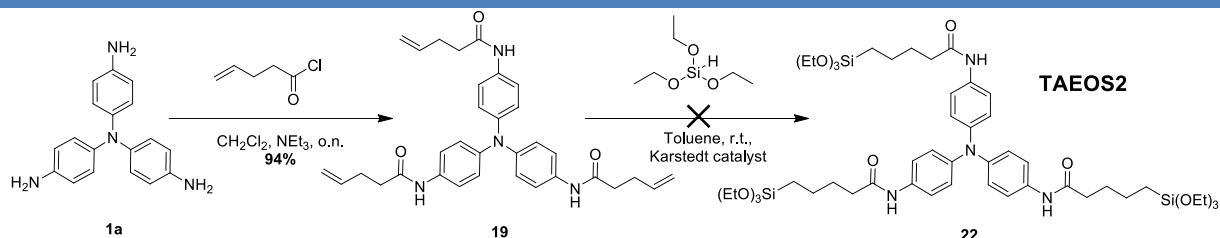

Scheme 6 | Synthetic pathway for triarylamine-urea-siloxane derivative TAEOS1.

b. *Synthesis of triarylamine-amide-siloxane derivative*

Initially, the synthetic route for molecule **22** was envisioned as depicted in Scheme 7. In the first step, the tris-amino triarylamine intermediate **1a** was acylated with three equivalents of 4-pentenoyl chloride to afford alkene-terminated triarylamine **19** in a high yield of 94%. Then, Karstedt catalyst was used for the silylation of molecule **19** in order to obtain molecule

22.[162] However, this step could not be achieved even using various reaction conditions. Hence, we changed the synthetic pathway by first synthesizing the siloxane derivative **21** as shown in Scheme 8a.

Scheme 7 | Initial synthetic pathway for triarylamine-trisamide-siloxane derivative TAEOS2.

N-hydroxysuccinimide-substituted alkene **20** was obtained in a 63% yield by reacting *N*-hydroxysuccinimide with 4-pentenoyl chloride in dichloromethane at room temperature overnight. The silylation reaction of compound **20** with triethoxysilane in the presence of Karstedt catalyst in toluene provided the siloxane derivative **21** with a yield of 68%. For the preparation of triarylamine-trisamide-siloxane derivative TAEOS2, the tris-amino triarylamine intermediate **1a** was acylated with initially three equivalents of compound **21** in tetrahydrofuran in the presence of *N,N*-diisopropylethylamine at 65 °C. The reaction was monitored by UPLC and extra compound **21** (three equivalent each time) was added portionwise into the mixture to afford compound TAEOS2 in a 53% yield (Scheme 8b).
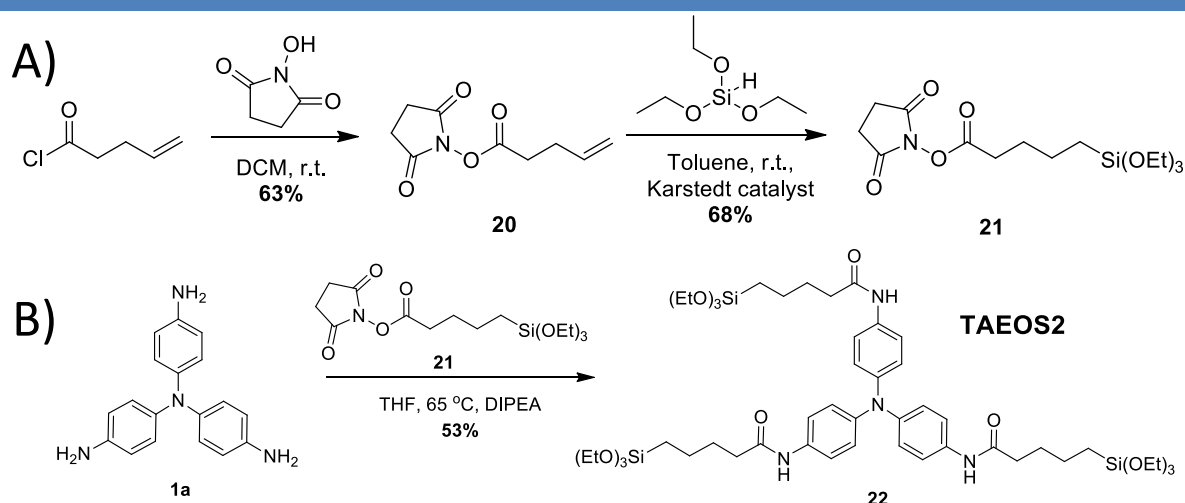
Scheme 8 | Synthetic pathways for a) siloxane derivative **21** and b) triarylamine-trisamide-siloxane derivative TAEOS2.

[162]Dickschat, A. T.Behrends, F. Surmiak, S. WeiB, M. Eckert, H. and Studer, A. Bifunctional mesoporous silica nanoparticles as cooperative catalysts for the Tsuji-Trost reaction--tuning the reactivity of silica nanoparticles. *Chem. Commun. (Camb).* **49,** 2195–7 (2013).

c. Synthesis of triarylamine-norbornene derivative

The synthetic route for triarylamine-norbornene derivative TANBE is depicted in scheme 9. The tris-amino triarylamine intermediate **1a** was acylated with commercially available 6-bromohexanoyl chloride in dichloromethane in the presence of triethylamine to give compound **7** with bromide at the termini. Nucleophilic substitution of compound **7** with commercially available 5-norbornene-2-carboxylic acid in the presence of a catalytic amount of tetrabutylammonium iodide in dimethylformamide provided compound TANBE with a yield of 50%.
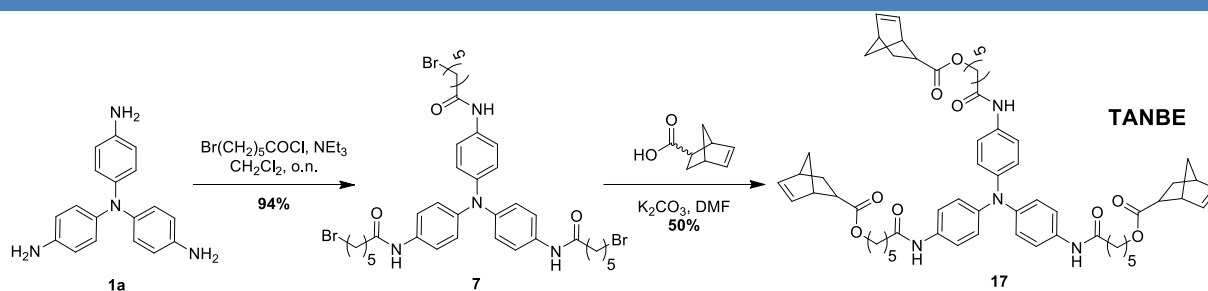
Scheme 4 | Synthetic pathway for triarylamine-norbornene derivative TANBE.

3. Characterizations

a. Characterizations of Gel-TEOS1 and Gel-TAEOS2

The self-assemblies of siloxane-triarylamine monomers in chlorinated solvents upon light irradiation were studied by means of ^{1}H NMR, UV-vis-NIR, Fluorescence spectroscopies and TEM microscopy. The molecule TAEOS1 shows a poor solubility in a single solvent, even in DMSO due to the presence of three urea groups. However, this molecule can be solubilized in a solvent mixture such as a 5:3 mixture of methanol:toluene, a 1:1 mixture of dichloromethane:methanol or tetrahydrofuran:ethanol. Hence, in a deuterated 5:3 methanol:toluene mixture with 5 vol% deuterated chloroform, the NMR spectrum of the TAEOS1 was recorded (Figure 54). After light irradiation, the resonance peaks of aromatic protons a and b and methylene proton c close to the triarylamine core disappeared due to a strong stacking of the triarylamine derivatives with a simultaneous color change from white to green. Indeed, light triggers the formation of a catalytic amount of triarylammonium radical cation in the presence of an electron acceptor such as chloroform, and the radicals nucleates at a critical concentration followed by chain growth of neutral triarylamine molecules, resulting in self-assemblies of triarylamine.[141]
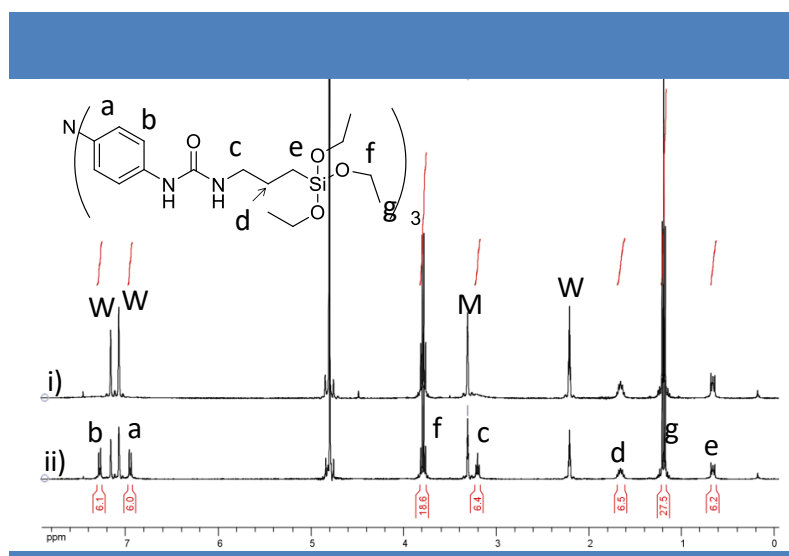
Figure 54 | ¹H NMR spectra and peak assignment of TAEOS1 in a 5:3 mixture of methanol-d4:toluene-d8, in the presence of CDCl3 (5 vol %) ii) before and i) after light irradiation for 15 minutes (M, W are the residual signals for methanol and toluene, respectively).

In contrast, the triarylamine-trisamide-siloxane derivative TAEOS2 displayed a good solubility in a wide range of organic solvents and the NMR spectra of TAEOS2 was recorded in pure deuterated chloroform (Figure 55). Similarly to the urea-based monomer TAEOS1, the disappearance of resonance signals a, b and c for monomer TAEOS2 indicated supramolecular polymerization upon light irradiation.
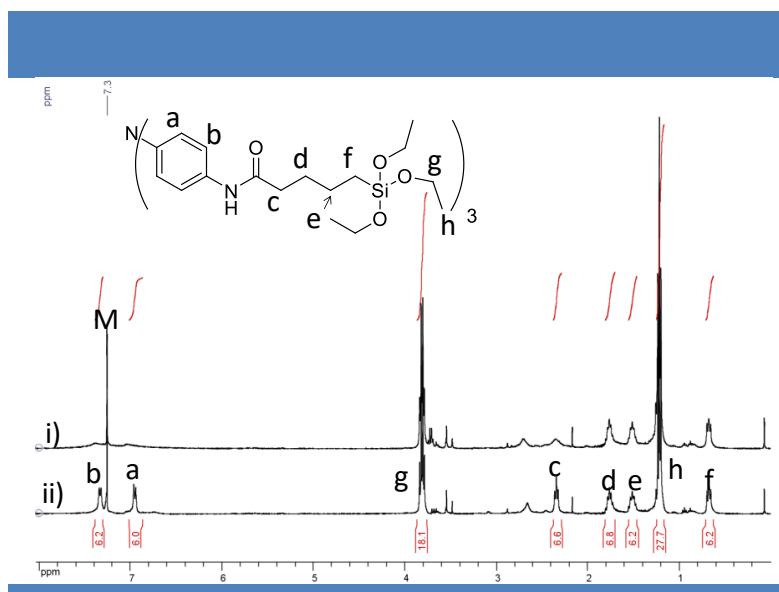
Figure 55 | ¹H NMR spectra and peak assignment of TAEOS2 in CDCl3 ii) before and i) after irradiation for 60 minutes (M is the residual signal for chloroform).

UV-Vis-NIR absorption and fluorescence experiments on a 10^{-4} M solution of compound TAEOS1 were performed to investigate the molecular self-assembly in a 5:3 methanol:toluene mixture containing 5% chloroform (Figure 56). Absorption spectra show that the band around 314 nm associated with neutral triarylamines decreases and

concomitantly bands at around 395 and 835 nm corresponding to the π-π stacking of the triarylamine aromatic cores and triarylammonium radical cations respectively increase upon light irradiation for 90 minutes (Figure 56a). The kinetic of the band at 835 nm suggests that the maximum loading of the self-assembled structure is reached after 20 minutes and that then radicals recombine and/or are quenched upon further light irradiation. Fluorescence spectra show the appearance of a weak emission band at 463 nm upon excitation at 395 nm, the intensity was almost unchanged upon light irradiation for 60 minutes (Figure 56b). All these data suggest that TAEOS1 lead to the formation of self-assembled structures upon irradiation.
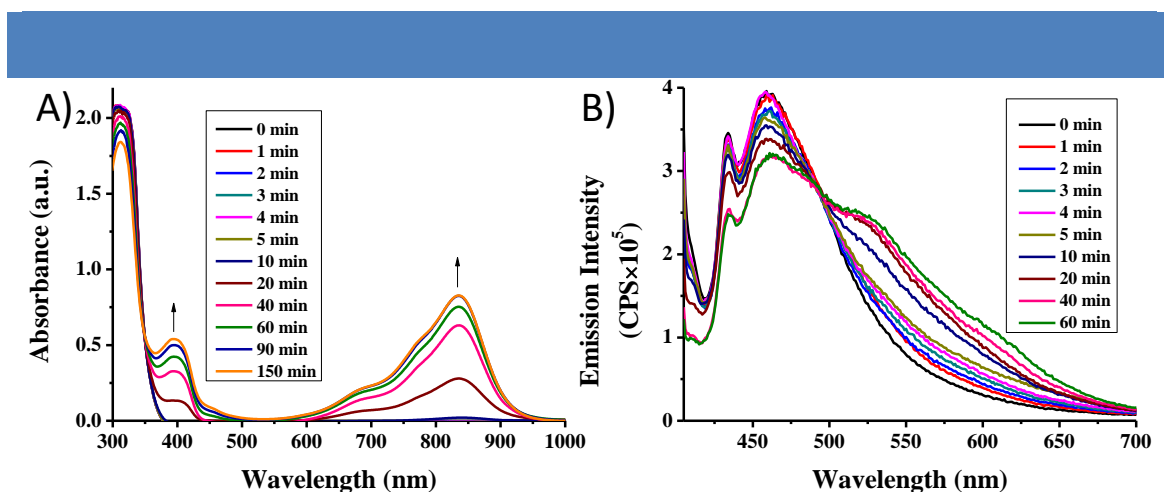
Figure 56 | Effect of light irradiation on the self-assembly of TAEOS1 in chloroform; a) UV-Vis-NIR spectra of TAEOS1 in a 5:3 mixture of methanol:toluene (5% chloroform, 10^{-4} M) upon light irradiation, and b) fluorescent spectra of TAEOS1 in a 5:3 mixture of methanol:toluene (5% chloroform, 10^{-4} M) upon light irradiation, λ_{ex}= 395 nm.

Unfortunately, only inhomogeneous structures in chloroform or 5:3 methanol:toluene were observed by transmission electron microscopy (TEM). Then, we imaged the morphology of TAEOS1 self-assemblies in a 1:1 mixture of methanol:dichloromethane. As shown on Figure 57, small and dense fibrous networks were observed for the self-assembled structures.
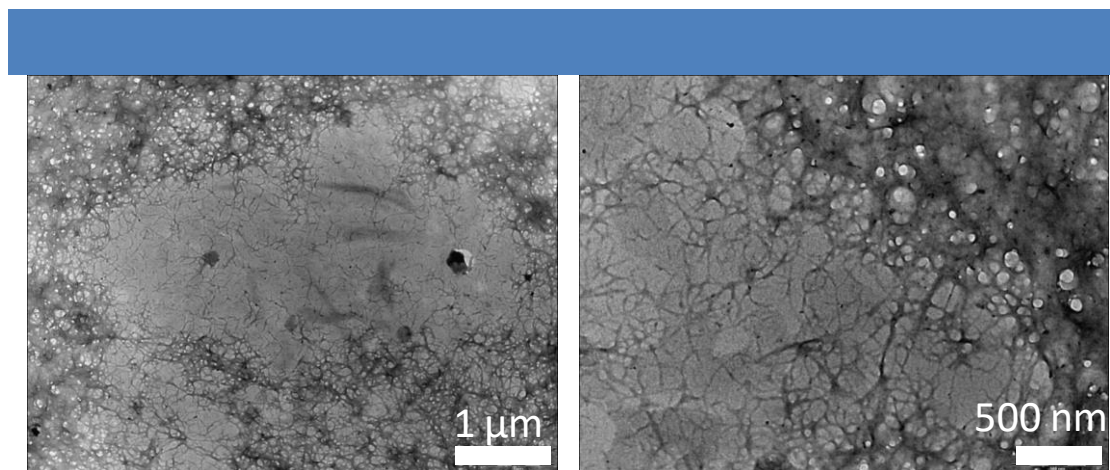

Figure 57 | TEM images of TAEOS1 in a 1:1 mixture of methanol:dichloromethane (12 mM) after light irradiation for 30 min.

Benzylamine (9 equivalents) and water (18 equivalents) were added to a solution of TAEOS1 (60 mM) in a 1:1 mixture of methanol:dichloromethane. After shaking thoroughly and incubating for several days, a strong and opaque gel was obtained (Figure 58a). On the other hand, when 1 μL water and 1.5 μL acetic acid were added, a strong and transparent gel was afforded as well albeit after incubation for months (Figure 58b).
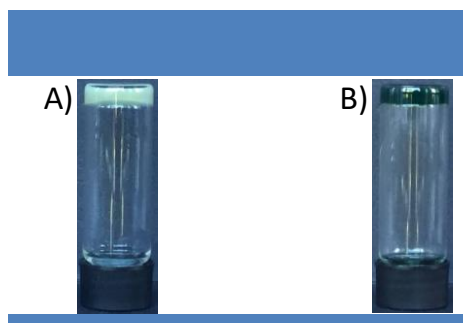

Figure 58 | Images of gels obtained under a) basic and b) acidic catalytic conditions.

While the gel obtained under basic conditions displays a pale green color, the acidic one exhibits a dark green color. This difference is attributed to the presence of benzylamine as a base which quenches part of the triarylammonium radical cations. Unfortunately, the gel derived from the acidic condition was found to be quite difficult to reproduce due to the small amount of acid needed to catalyze the gel formation and the poor solubility of the precursor in such a quantity of acid. Thus, next experiments will be related only to gels obtained under basic conditions. Scanning electron microscopy (SEM) was employed to study the morphology of the gels resulting from the polymerization under basic condition (Figure 59).
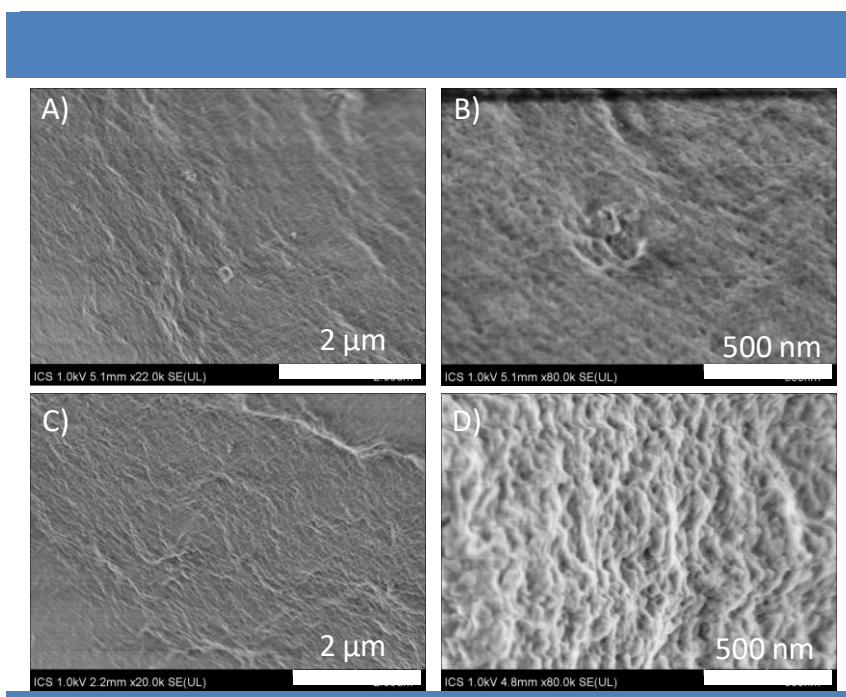

Figure 59 | SEM images of a-b) a gel made of TAEOS1 before irradiation, and c-d) a gel made of TAEOS1 after irradiation for 60 minutes.

Dense structures are observed for both non-irradiated and irradiated samples (Figure 59a and c), with small porous networks observed at higher magnification (Figure 59b and d). In order to better analyze the mesoporous structures, aerogels will be prepared for further imaging experiments. FT-IR experiments were performed to study supramolecular interactions and the presence of a silica network within the gels (Figure 60a). The presence of bands located at 3314 and 1645 cm^{-1} indicating hydrogen-bonded N-H and C=O stretching vibrations respectively, suggests that hydrogen bonds are preserved after sol-gel cross-linking. Compared with the monomer, the significantly decreased intensity of the bands located at around 2900 cm^{-1} for the gel samples are indicative of the disappearance of ethyl groups, while the broadening of the band around 1080 cm^{-1} suggests the formation of Si-O-Si network after hydrolysis and condensation of the alkylsiloxane moieties.
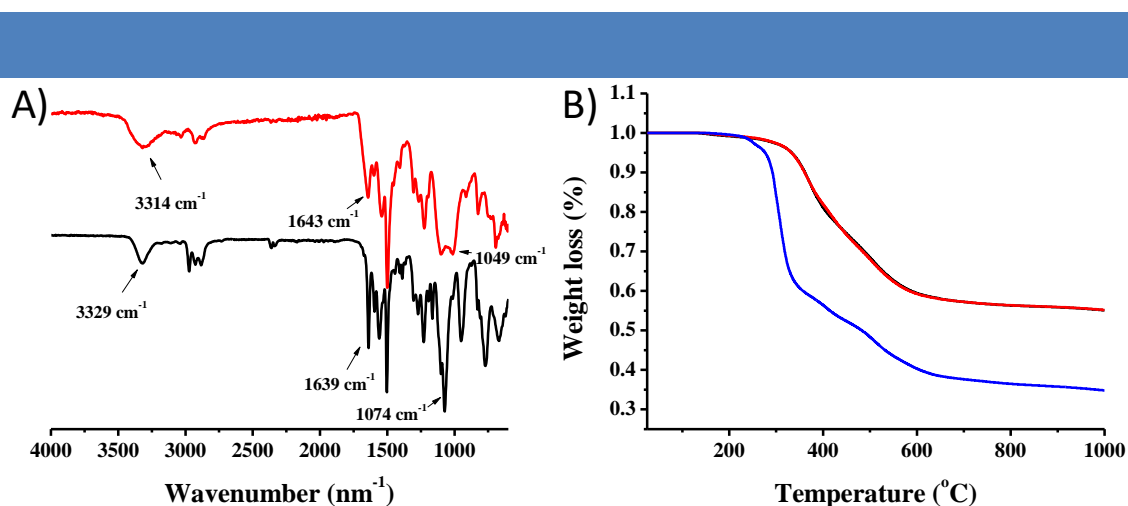

Figure 60 | a) FT-IR spectra of monomer TAEOS1 (black), 60 min irradiated gel (red) obtained under basic conditions; and b) TGA curves of monomer TAEOS1 (blue), non-irradiated gel (black) and 60 min irradiated gel (red).

The thermal stabilities of the monomer and the corresponding gels were measured by thermogravimetric analysis (Figure 60b). For the monomer, the curve undergoes two decompositions with the first one of 37.1% occuring at 337 °C and the second one occuring at 624 °C (Figure 60b). Similar curves are observed for both non-irradiated and irradiated gels with only one decomposition process about 40.9% observed at 609 °C. This improved bulk decomposition temperature can be attributed to the formation of the inorganic silica network. This set of experiments confirmed the formation of self-assembled architectures from TAEOS1 with interesting optical properties. We have then demonstrated that they can be frozen within an inorganic silica matrix which provides the material with increased robustness. However, we still need to elucidate if the optical properties associated to the formation of triarylamine self-assemblies remain stable after this sol-gel process.

UV-Vis-NIR experiments were also employed to study the self-assembly of TAEOS2 in chloroform with light irradiation (Figure 61).
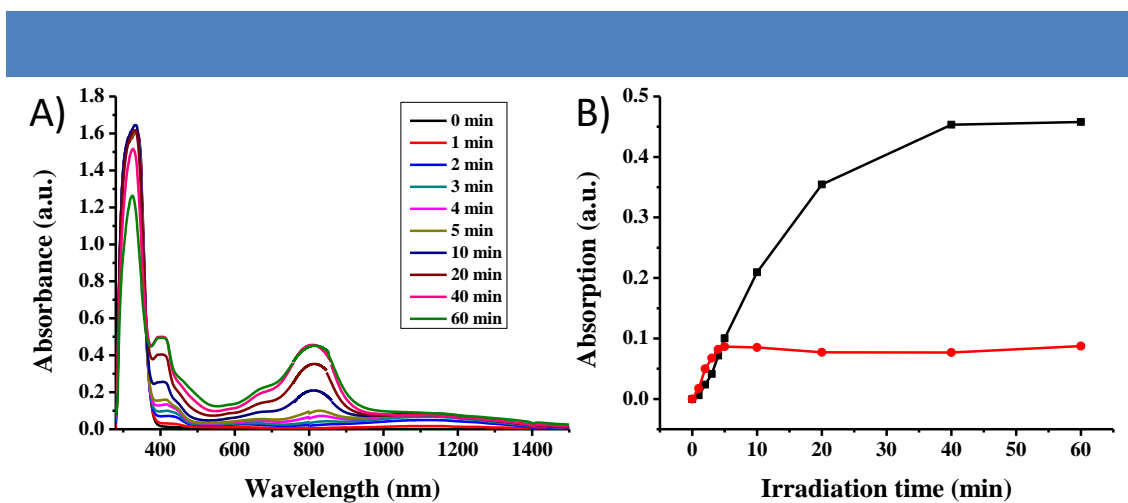

Figure 61 | Effect of light irradiation on the self-assembly of TAEOS2 in chloroform; a) UV-Vis-NIR spectra of TAOES2 in chloroform (10^{-4} M) upon light irradiation and b) kinetics recorded for the absorption bands at around 829 nm (black) and 1124 nm (red).

The spectra show that the absorption at 323 nm corresponding to neutral triarylamine molecules decreases due to their oxidation to triarylammonium radical cations while the band around 410 nm related to the aromatic stacking of triarylamines increases suggesting the formation of TAEOS2 self-assembly (Figure 61a). The absorption band around 829 nm correlated to the presence of localized radical cations increases and reaches a plateau after ~ 60 minutes of light irradiation (Figure 61b). In contrast to TAEOS1 with urea groups, the spectra of TAEOS2 with amide moieties show an absorption band at around 1124 nm for short irradiation times (~ 5 minutes) and which can be ascribed to intermolecular charge transfer, *i.e.* delocalized radicals within the self-assembled structure.[146] The spectroscopic behavior of TAEOS2 upon light irradiation is very similar to the one recorded previously by our group. We believe that the corresponding electronic and optical properties could be frozen by sol-gel processes leading to robust functional materials emerging from self-assembled structures. Such experiments however remain to be performed.

b. *Characterizations of Gel-TANBE*

In order to study the effect of light irradiation on TANBE monomer, its ^{1}H NMR was recorded in deuterated chloroform before and after light irradiation. In the absence of light, all the expected sets of signals for TANBE are observed by ^{1}H NMR as shown in Figure 62ii. The monomer corresponds to two isomers: endo and exo in a 2:1 ratio. Upon light irradiation, the disappearance of aromatic protons a and b as well as aliphatic CH_2 protons c most close to the aromatic core indicates the formation of TANBE self-assembly (Figure 62i).
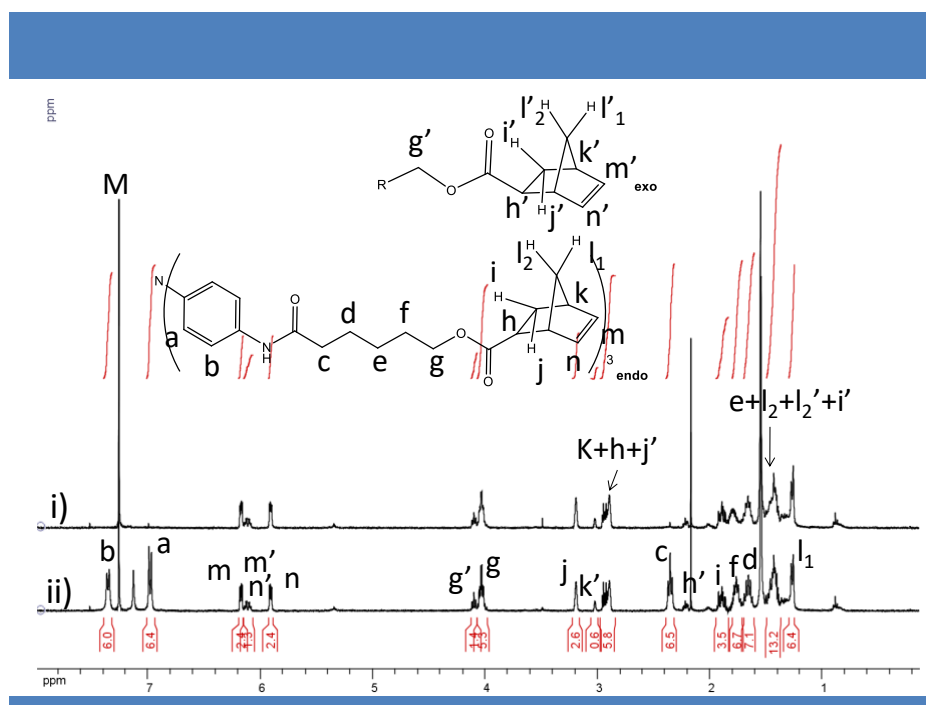
Figure 62 | ^{1}H NMR spectra and peak assignment of TANBE in CDCl$_3$ ii) before and i) after irradiation for 30 minutes (M is the residual signal for chloroform).

UV-Vis-NIR experiments were employed to study the absorption behavior of TANBE in chloroform during light irradiation. As shown in Figure 63a, the absorption band at 410 nm associated with the aromatic stacking of triarylamine increases, suggesting the formation of a self-assembled structure. The spectra show also that two bands appear at around 832 nm corresponding to the presence of localized radical cation and at around 1129 nm corresponding to delocalized radicals within the self-assembled structure (Figure 63b). As seen from the kinetics plots on Figure 63c, the intensity at 832 nm increases upon light irradiation until reaching a maximum after aroun 40 minutes while the intensity of the charge transfer band increase during the first 4 minutes of irradiation and then subsequently decreases for longer irradiation times, probably due to the generation of localized radical cations which inhibit charge transfer processes within the self-assembly. Interestingly, a broad band at around 500 nm appears upon light irradiation, which continues to increase when the radical cation band reaches its maximum and the charge transfer one at ~1100 nm decrease. This absorption band can be attributed to electron interactions between oxidized and neutral molecules within the self-assembly and suggests a highly organized structure as already observed by our group in crystals.[148] Fluorescence spectra were performed to study the emission of TANBE in chloroform during light irradiation. Before light irradiation, an emission around 484 nm was observed (Figure 63d), which immediately decreases upon light irradiation and quenches after 4 minutes. This spectroscopic behavior is identical to the

second generation of triarylamine nanowire reported by our group[146] and suggests the presence of supramolecular polarons within the self-assembled structure, and which leads to exciton quenching upon irradiation.
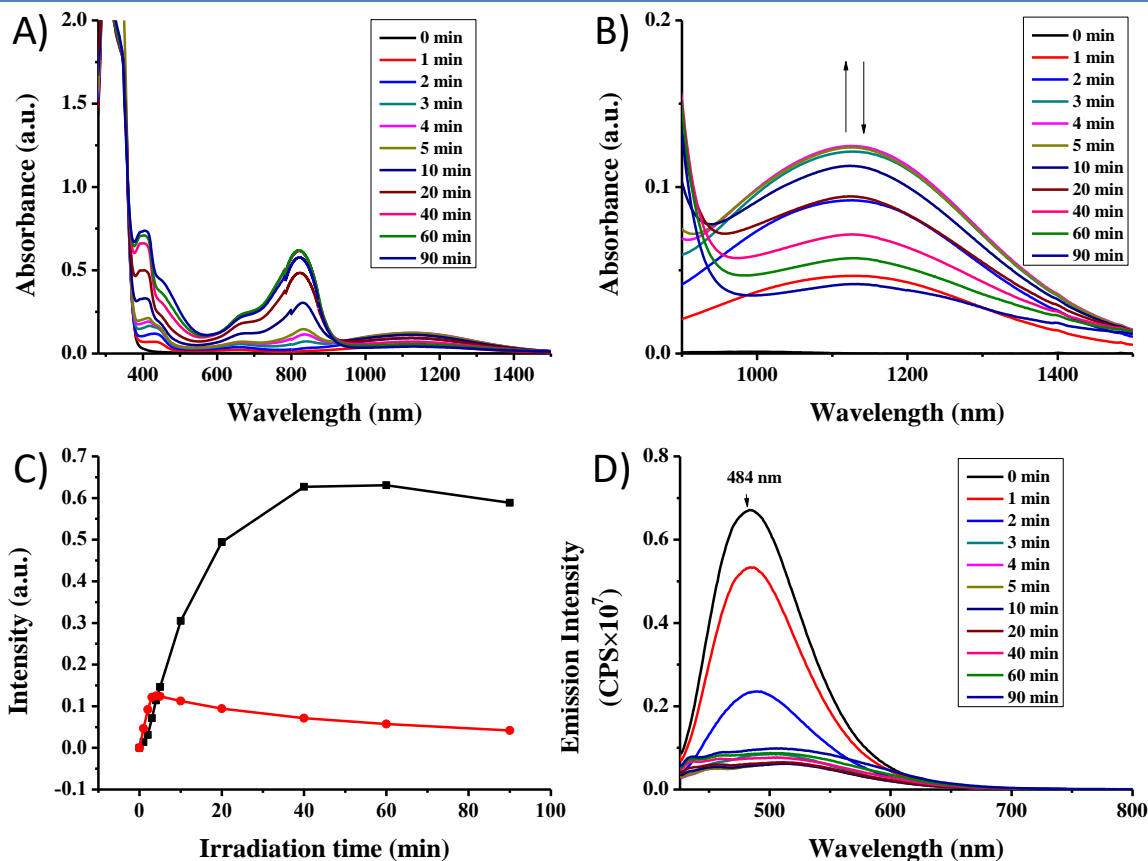

Figure 63 | Effect of light irradiation on the self-assembly of TANBE in chloroform; a) UV-Vis-NIR spectra of TANBE in chloroform (10^{-4} M) upon sequential light irradiation, b) enlarged NIR spectra of a) in the 1000-1500 nm range; c) kinetic of the absorbance at 832 nm (black) and at 1129 nm (red) upon light irradiation; d) fluorescence spectra of TANBE in chloroform (10^{-4} M) upon light irradiation, λ_{ex}= 390 nm.

However, this TANBE monomer was also found to self-assemble in toluene as demonstrated by TEM imaging, which reveals dense micrometer-long fiber-like structures (Figure 64). Unfortunately, no homogeneous morphology in pure chloroform could be imaged by TEM. Similarly, atomic force microscopy (AFM) evidenced the formation of long micrometric fibers (Figure 65), while statistical analysis revealed that the width of the fibers is around 116 nm and their thickness is around 1 nm. These observations suggest that the dense fibrillar aggregates are made of single columnar structures which further combine into large bundles. Overall, the behavior of TANBE is very similar to what we observed previously for triarylamine trisamide molecules, which encouraged us to study their covalent polymerization by ROMP using the norbornene moieties in order to reach robust functional materials.
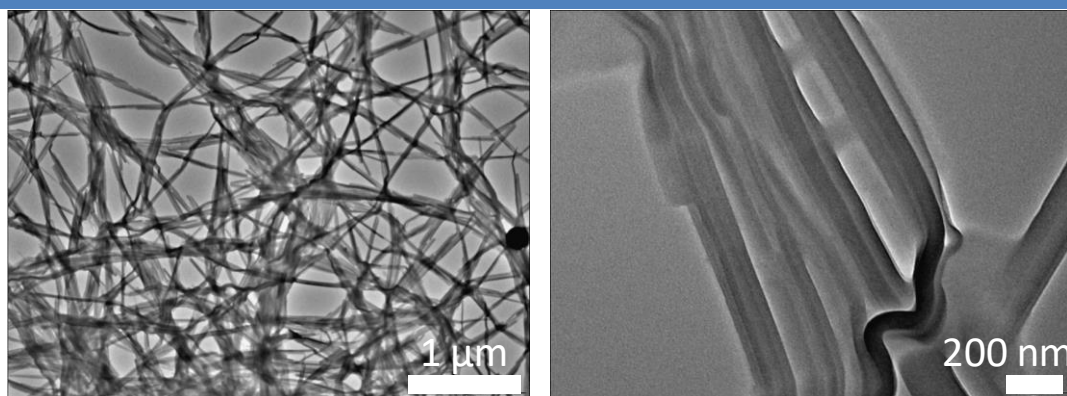
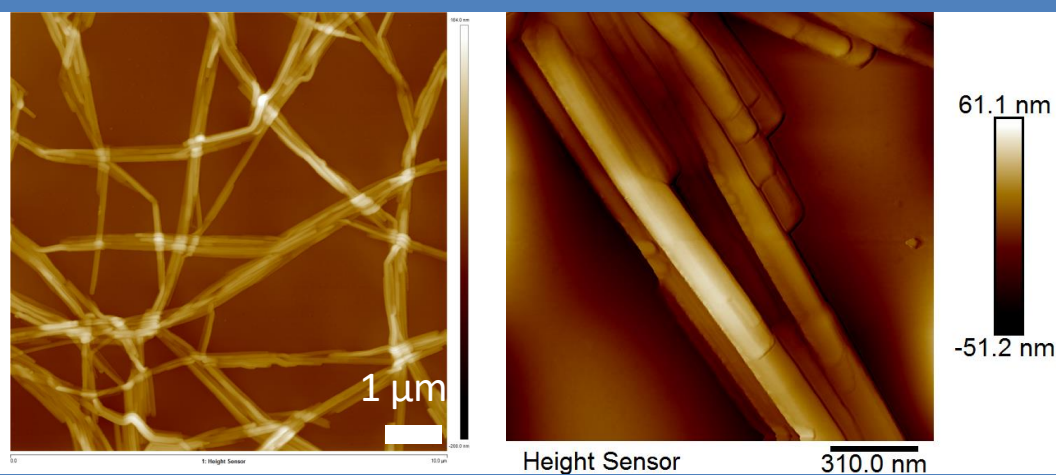**Figure 64** | TEM images of TANBE in toluene (1 mM).

Figure 65 | AFM images of TANBE in toluene (1 mM).

In order to optimize the ROMP polymerization conditions, we first attempted the polymerization in solution using various conditions: catalyst, number of equivalents of catalyst, irradiation time and solvent of the reaction (Table 2). The resulting products were characterized by ^{1}H NMR, FT-IR and gel permeation chromatography (GPC). Similar ^{1}H NMR spectra were observed for all conditions such as, for instance, the one displayed on Figure 66i for polymer PTANBE1 in deuterated THF. Compared with the ^{1}H NMR spectrum of TANBE, all proton peaks are broadened. Especially, the olefinic proton signals corresponding to the formation of polynorbornene are shifted to higher field compared to those of the monomer probably due to anisotropic shielding, and thus suggesting that the covalent polymers are formed during the reactions (Figure 66ii).
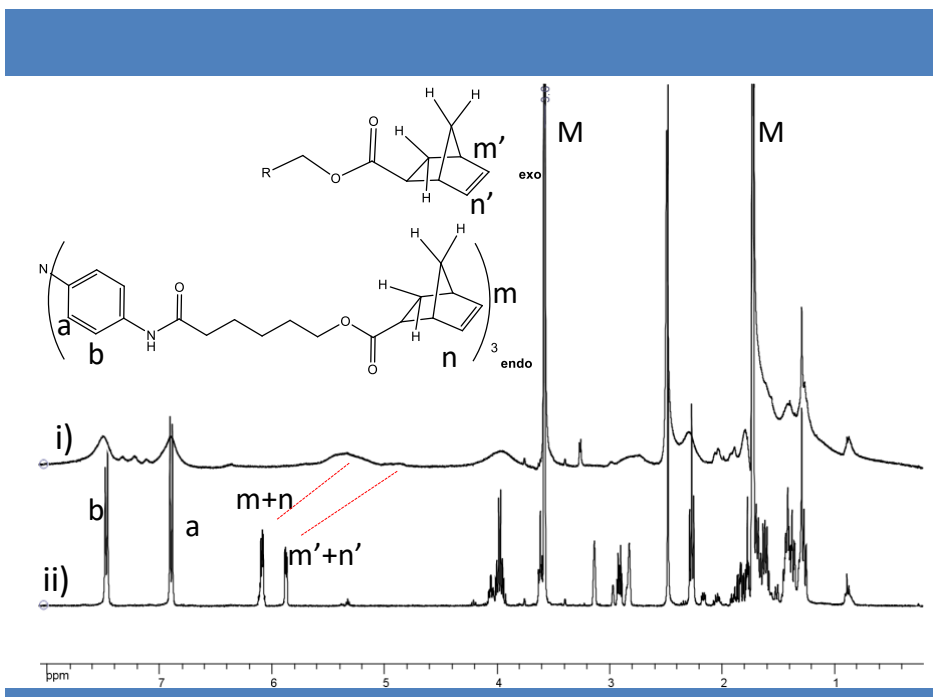
Figure 66 | ^{1}H NMR spectra of i) polymer PTANBE1 and ii) TANBE in THF-d$_8$ (M is the residual signal for tetrahydrofuran).

Additionally, FT-IR spectra were recorded to study whether the polymerization of the norbornene groups was achieved. As shown from Figure 67, the drop of the band located at 1335 cm^{-1} suggests the conversion of cyclo-olefinic double bonds into acyclic ones, confirming the formation of the polymers.[109]
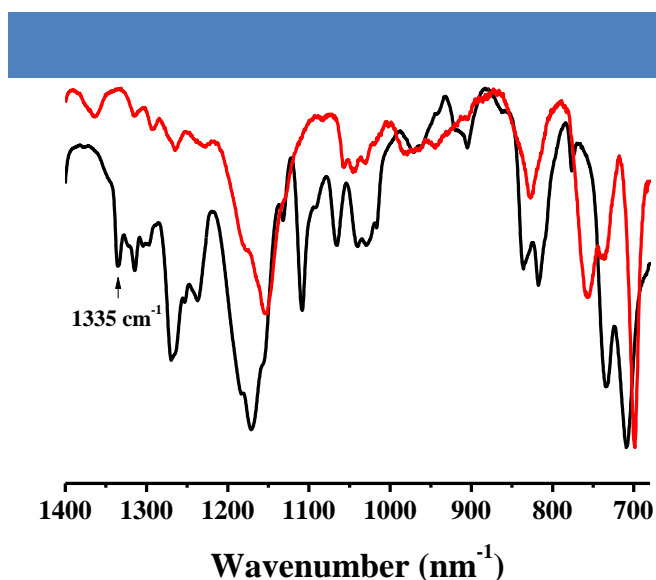

Figure 67 | Normalized FT-IR spectra of monomer TANBE (black) and polymer PTANBE1 (red).

Using Grubbs I, we first studied the influence of the solvent on the polymerization (Table 2). Toluene usually affords insoluble polymers while THF and dichloromethane usually lead to soluble polymers with larger M_w and M_n for polymers obtained by using dichloromethane compared to THF. Then, we compared how the catalyst affect the degree of polymerization

degree. First generation Grubbs catalyst (Grubbs I) usually gives polymers with large polydispersity index (PDI) (> 3) while polymers with smaller PDI (< 3) can be achieved by taking advantage of third generation Grubbs catalyst (Grubbs III).[163] On the other hand, polymers arising from concentrated reaction solutions (2 mM) in dichloromethane were found to be insoluble in THF when using Grubbs III while the ones prepared from THF showed relatively low PDI (< 2). Irradiation time seems have only slight effect on the polymerization degree. As for the reaction concentration, when it was lowered to 0.2 mM or even 0.05 mM, the polymers produced from dichloromethane start to be soluble in THF and smaller PDI (1.42) and M_w (6856) could be achieved.

Catalyst equiv	Concentration	M_w (GPC)	M_n (GPC)	PDI (GPC)	Irradiation time	Solvent	Solubility in THF	
Grubbs I 0.3	2 mM	37497	7340	5.11	non	CH_2Cl_2	S	PTANBE5
Grubbs I 0.3	2 mM	26423	5082	5.20	non	THF	S	PTANBE6
Grubbs I 0.3	2 mM	---	---	---	non	Toluene	I	PTANBE4
Grubbs I 0.3	2 mM	68128	6607	10.31	60 min	CH_2Cl_2	S	PTANBE1
Grubbs I 0.3	2 mM	14807	4540	3.26	60 min	THF/CH_2Cl_2 9/1	S	PTANBE2
Grubbs I 0.3	2 mM	---	---	---	60 min	Toluene/CH_2Cl_2 9/1	I	PTANBE3
Grubbs III 0.3	2 mM	---	---	---	60 min	CH_2Cl_2	I	PTANBE7
Grubbs III 0.3	2 mM	11279	6828	1.65	60 min	THF/CH_2Cl_2 9/1	S	PTANBE8
Grubbs III 0.3	2 mM	8552	4556	1.88	non	THF	S	PTANBE9
Grubbs III 0.3	2 mM	---	---	---	non	CH_2Cl_2	I	PTANBE10
Grubbs III 0.03	2 mM	---	---	---	60 min	CH_2Cl_2	I	PTANBE11
Grubbs III 0.3	0.2 mM	9843	4220	2.33	60 min	CH_2Cl_2	S	PTANBE12
Grubbs III 0.3	0.05 mM	6856	4816	1.42	60 min	CH_2Cl_2	S	PTANBE13

Table 2 | Polymer names, polymerization conditions, GPC results and their solubility in THF; S: soluble and I: insoluble.

UV-Vis-NIR experiments were then performed to compare the absorption of monomer

[163]Lu, H. Wang, J. Lin, Y. and Cheng, J. One-pot synthesis of brush-like polymers via integrated ring-opening metathesis polymerization and polymerization of amino acid N-carboxyanhydrides. *J. Am. Chem. Soc.* **131,** 13582–13583 (2009).

TANBE with polymer TANBE1 in a 1:9 mixture of THF:CDCl$_3$ (10^{-4} M) during light irradiation.
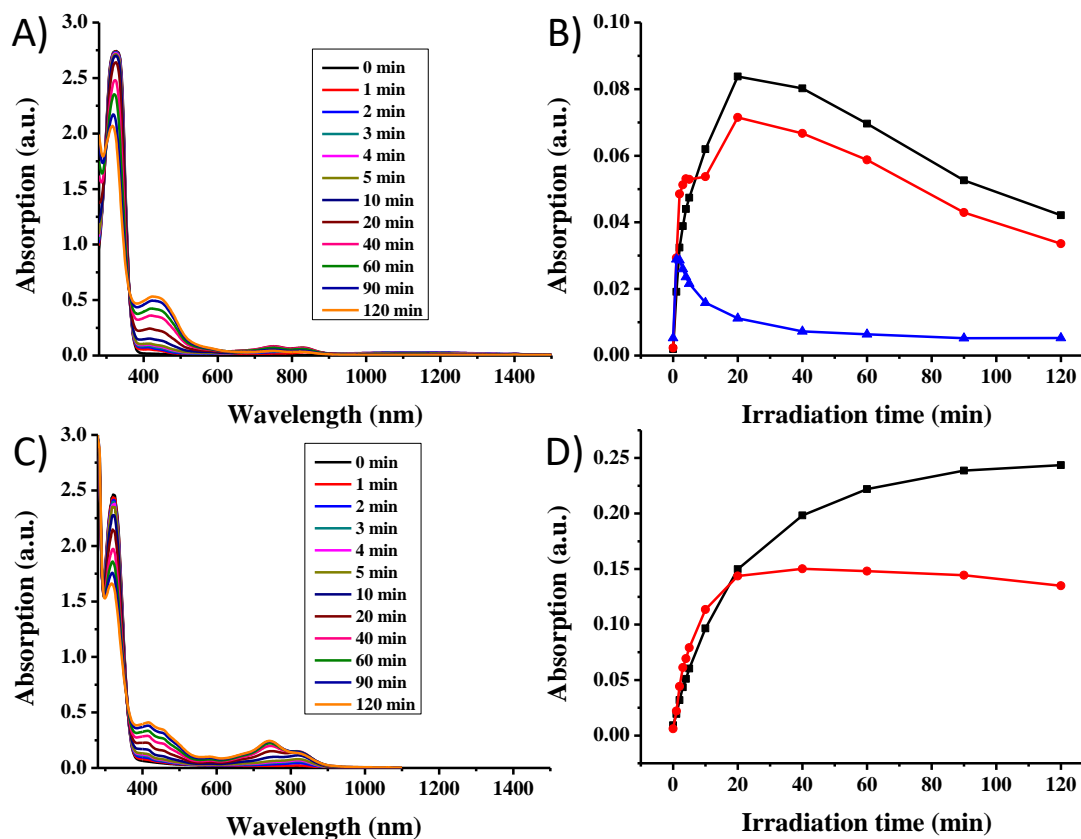

Figure 68 | a) UV-Vis-NIR spectra of monomer TANBE in a 1:9 mixture of THF:CDCl$_3$ (10^{-4} M) during light irradiation, b) evolution of the absorption at 750 nm (black), 832 nm (red) and 1148 nm (blue), c) UV-Vis-NIR spectra of polymer PTANBE1 in a 1:9 mixture of THF:CDCl$_3$ (10^{-4} M) during light irradiation and d) evolution of the absorption intensity at 742 nm (black) and 818 nm (red).

Similarly to TANBE in pure chloroform, the absorption band at around 318 nm correlated to the presence of neutral triarylamine decreases while the band at 410 nm correlated to aromatic stacking of the molecular units increases with light irradiation, indicating the formation of a self-assembly. A band at around 832 nm correlated to the presence of localized radical cations and a band located at around 1148 nm and related to intermolecular charge-transfer are observed, which show similar kinetic behavior to the one recorded in pure chloroform (Figure 68b). Additionally, a new band at 750 nm appeared, which may be due to the presence of radical cations from THF. Interestingly, spectra corresponding to polymer PTANBE1 showed similar bands at around 320, 415, 742 and 818 nm with kinetic behavior slightly different from the monomer (Figure 68c and d), and the intermolecular charge transfer band at around 1100 nm could not observed in this case. However, the large band observed at 458 nm and which spans until 520 nm is reminiscent of

the charge transfer band observed in triarylamine crystals. These UV-Vis-NIR results indicate that the electronic state of triarylamine unit is preserved after polymerization which appears particularly interesting to reach robust materials with electronic and/or optical properties reminiscent of the corresponding supramolecular polymer.

Fluorescence spectra were performed to investigate the emission of the polymer in a 1:9 mixture of THF:CDCl$_3$. Taking polymer PTANBE1 as an example, the emission at around 476 nm was found to quench partially after light irradiation for 30 minutes (Figure 69), but which remained stable after further light irradiation for another 30 minutes. These observations suggest the presence of self-assembled triarylamine within the polynorbornene backbone. However, the remaining fluorescence might also indicate the presence of more defects in the covalently polymerized material compared to its supramolecular counterpart where fluorescence got quenched shortly (less than 4 minutes) after irradiation.
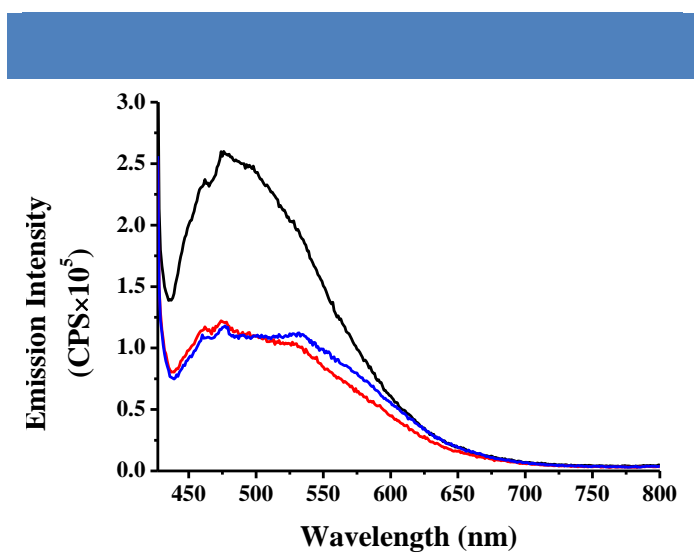

Figure 69 | Fluorescence spectra of polymer PTANBE1 in a 1:9 mixture of THF:CDCl$_3$ (10^{-4} M): before irradiation (black), after irradiation for 30 minutes (red), and for 60 minutes (blue), λ_{ex}= 417 nm.

Finally, the electrochemical behavior of monomer TANBE and polymer PTANBE1 was examined by cyclic voltammetry (CV) at a scan rate of 100 mV.s^{-1} in THF and using tetrabutylammonium hexafluorophosphate (TBAHFP) as electrolyte. The voltammogram recorded for TANBE reveals reversible one-electron oxidation peak from the neutral species to the radical cations at $E_{1/2,ox}$= +0.84 V (E_{pa}= +0.95 V, E_{pc}= +0.73 V) and which corresponds to an HOMO energy level E_{HOMO}= -5.51 eV as estimated from the onset potential (Figure 70a). Regarding polymer PTANBE1, an one-electron oxidation potential from the neutral species to the radical cation is determined to be at $E_{1/2,ox}$= +0.68 V (E_{pa}= +0.72 V, E_{pc}= +0.63 V) which corresponds to an HOMO energy level E_{HOMO}= -5.43 eV, which is slightly higher than that obtained for the monomer probably due to the electronic delocalization after
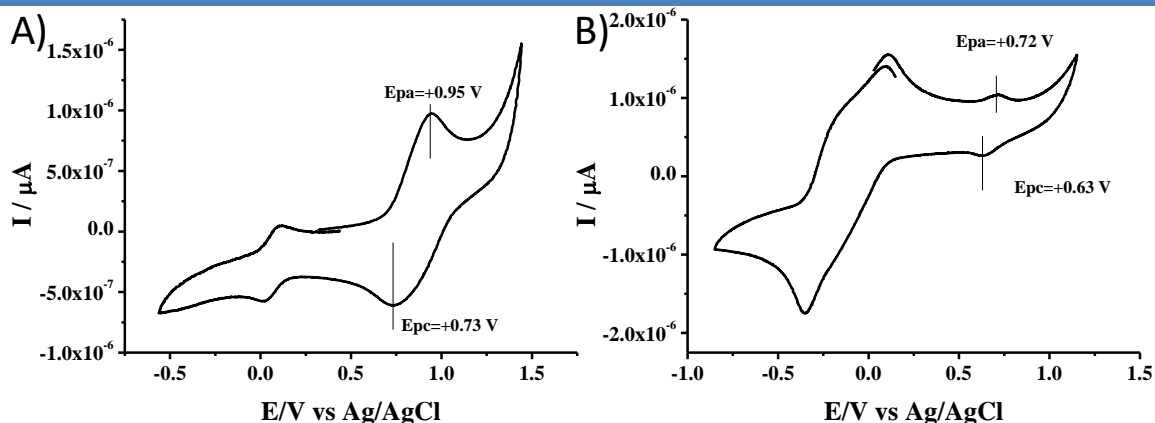
polymerization upon light irradiation (Figure 70b).

Figure 70 | Cyclic voltammograms of a) monomer TANBE using decamethylferrocene ($E_{1/2}$=0.1 V v Ag/AgCl) as reference (0.5 mM in THF with 0.1 M TBAHFP using as reference), and of b) polymer PTANBE1 using decamethylferrocene ($E_{1/2}$=0.1 V v Ag/AgCl) as reference (0.5 mM in THF with 0.1 M TBAHFP using as reference).

Although monomer TANBE shows limited solubility in toluene, after a heating and cooling process as described in the experimental part, a gel can be formed. The critical gelation concentration was estimated by a simple tube inversion experiment on freshly prepared gels (Figure 71).
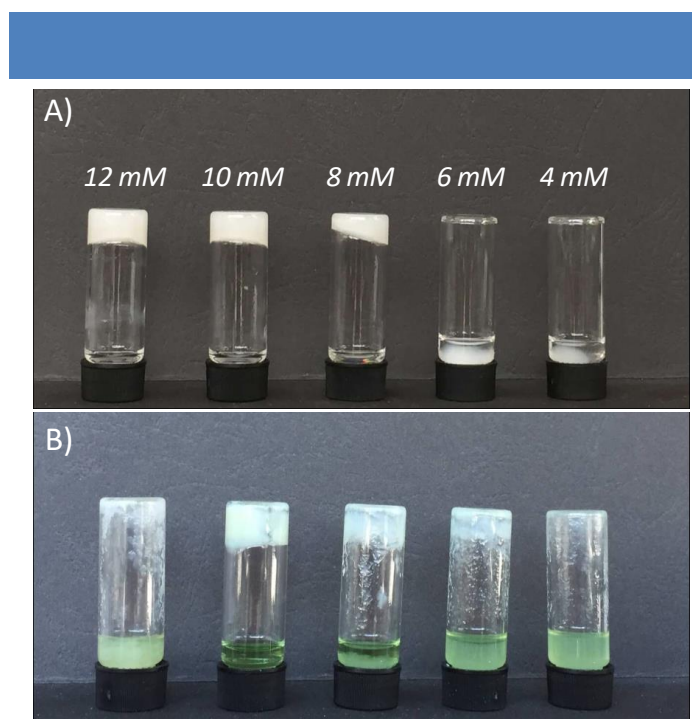

Figure 71 | Tube inversion experiments a) for various concentrations of TANBE gels in toluene, and b) for various concentrations of TANBE gels in a 9:1 mixture of toluene:tetrachloroethane after light irradiation for 60 minutes. Photographs were taken 12 hours after having inverted the tubes.

As shown from Figure 71a, self-supporting gels in toluene are preserved after 12 hours

for concentrations above 8 mM while gels irradiated for 60 minutes in a 9:1 mixture of toluene:tetrachloroethane cannot be preserved even for concentrations of up to 15 mM. This observation might be due to the formation of less entangled fibrous network after light irradiation in the presence of a chlorinated solvent. Organic solvents within the gels can be exchanged *via* several removal and addition processes. A physical gel in toluene (**Gel1'**, Figure 72a) was treated with a solution of Grubbs III in toluene *in situ*. The gel was softly shaken for 12 hours to let the catalyst diffuse through the gel network and then washed thoroughly with methanol to get rid of the catalyst and monomer residues, affording a covalently polymerized gel (**Gel1**, Figure 72b). Moreover, physical gels can also be produced from a 9:1 mixture of toluene:tetrachloroethane, offering the possibility to enhance the self-assembly of TANBE by generating radical cations (Figure 72c and e). Light irradiation for 15 or 60 minutes of physical gels **Gel2'** and **Gel3'** followed by similar polymerization procedures afforded polymerized gels **Gel2** and **Gel3** respectively (Figure 20d and f). Upon light irradiation, the color of the gel changed from white to green which indicates the presence of radical cations. After extensive washing and solvent exchange procedures, **Gel1** showed a grey color while **Gel2** and **Gel3** showed more bluish grey color (Figure 72b, d and f). Interestingly, these three covalently polymerized gels could be easily manipulated and thus analyzed using various physico-chemical techniques.
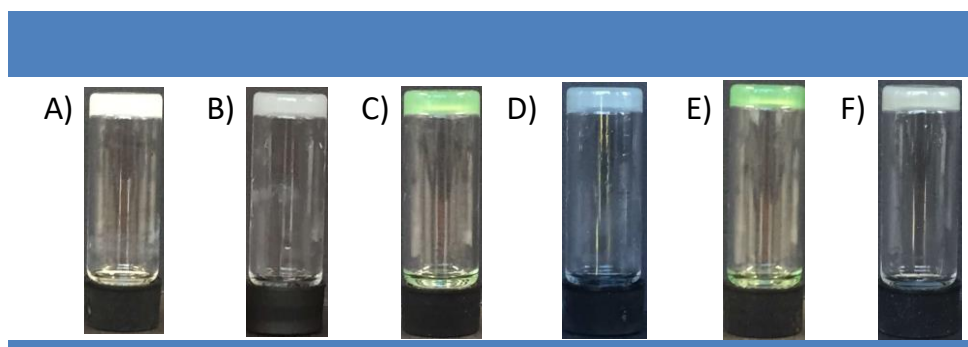

Figure 72 | Tube inversion experiments for gels: a) non-polymerized gel in toluene (15 mM, **Gel1'**); b) covalently polymerized gel (**Gel1**) obtained from **Gel1'**; c) non-polymerized gel in a mixture of 9:1 toluene:tetrachloroethane irradiated for 15 minutes (15 mM, **Gel2'**); d) covalently polymerized gel (Gel2) obtained from **Gel2'**; e) non-polymerized gel in a mixture of 9:1 toluene:tetrachloroethane irradiated for 60 minutes (15 mM, **Gel3'**); f) covalently polymerized gel (**Gel3**) obtained from **Gel3'**. Photographs were taken as soon as the gels were formed.

FT-IR experiments were performed to confirm the polymerization of norbornene groups within the gels. The band at 1335 cm^{-1} which is typical of norbornene (=C-H out of phase in plane bending mode) decreased drastically after polymerization, indicating the conversion of the cyclo-olefinic double bond into an acyclic one, and thus the presence of polymerized norbornene backbones within **Gel1**, **Gel2** and **Gel3** (Figure 73).
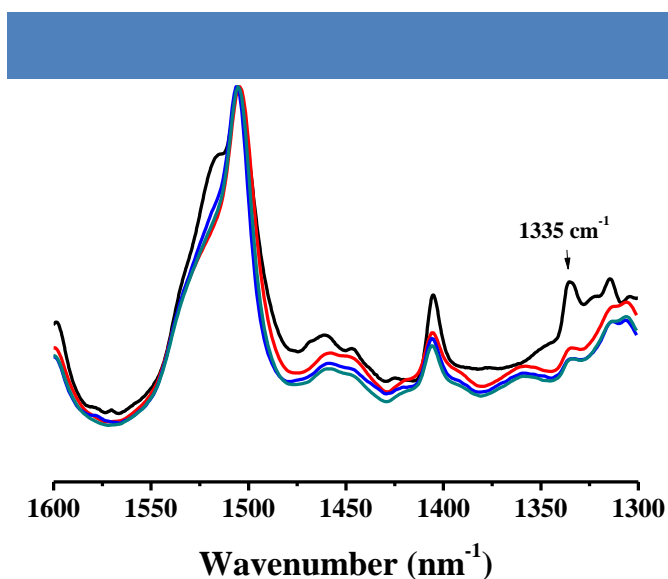
Figure 73 | FT-IR spectra of monomer TANBE (black), **Gel1** (red), **Gel2** (blue) and **Gel3** (green), normalized at 1505 cm⁻¹.

Then, UV-Vis-NIR spectra were performed to study the absorption of the physical gel **Gel2'** obtained from a 9:1 mixture of toluene:tetrachloroethane at 15 mM after 15 minutes light irradiation (Figure 74). Upon light irradiation, the spectra showed the typical features already observed for TANBE monomer: increase of a) the band at around 410 nm due to π-stacking of the triarylamine molecules, b) the band related to the presence of radical cations at 822 nm and c) the broad band related to intermolecular charge transfer at around 1126 nm. As seen from the absorptions at 822 and 1126 nm, their intensity increases upon light irradiation albeit with different kinetics. These experiments suggest that physical **Gel2'** remains light-responsive in the gel state and keeps optical features similar to the light-irradiated solution of TANBE in chloroform.
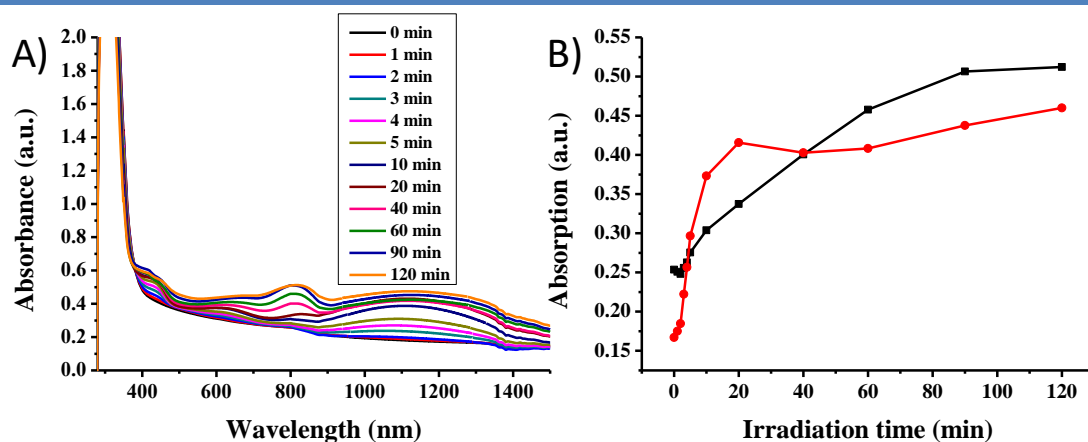

Figure 74 | UV-Vis-NIR spectra of a) **Gel2'** in a 9:1 mixture of toluene:tetrachloroethane (15 mM) during light irradiation, and b) kinetic of the absorption bands at 822 nm (black) and 1126 nm (red).

We then studied the absorption behavior of covalently polymerized **Gel1**, **Gel2** and **Gel3** in a 9:1 mixture of toluene:tetrachloroethane (Figure 75). Interestingly, compared to their non-covalently polymerized counterparts, a broad band at around 630 nm is observed for all three gels while additional broad bands at around 410 nm correlated to triarylamine aromatic stacking and at around 1100 nm correlated to intermolecular charge transfer are observed for the three gels. Furthermore, the localized radical cation band at around 800 nm was found to be quenched for all gels after polymerization. Upon light irradiation, the three gels display increasing radical cation absorption bands at around 800 nm and charge transfer bands at around 1100 nm albeit with different intensities and kinetics depending on the gel preparation.
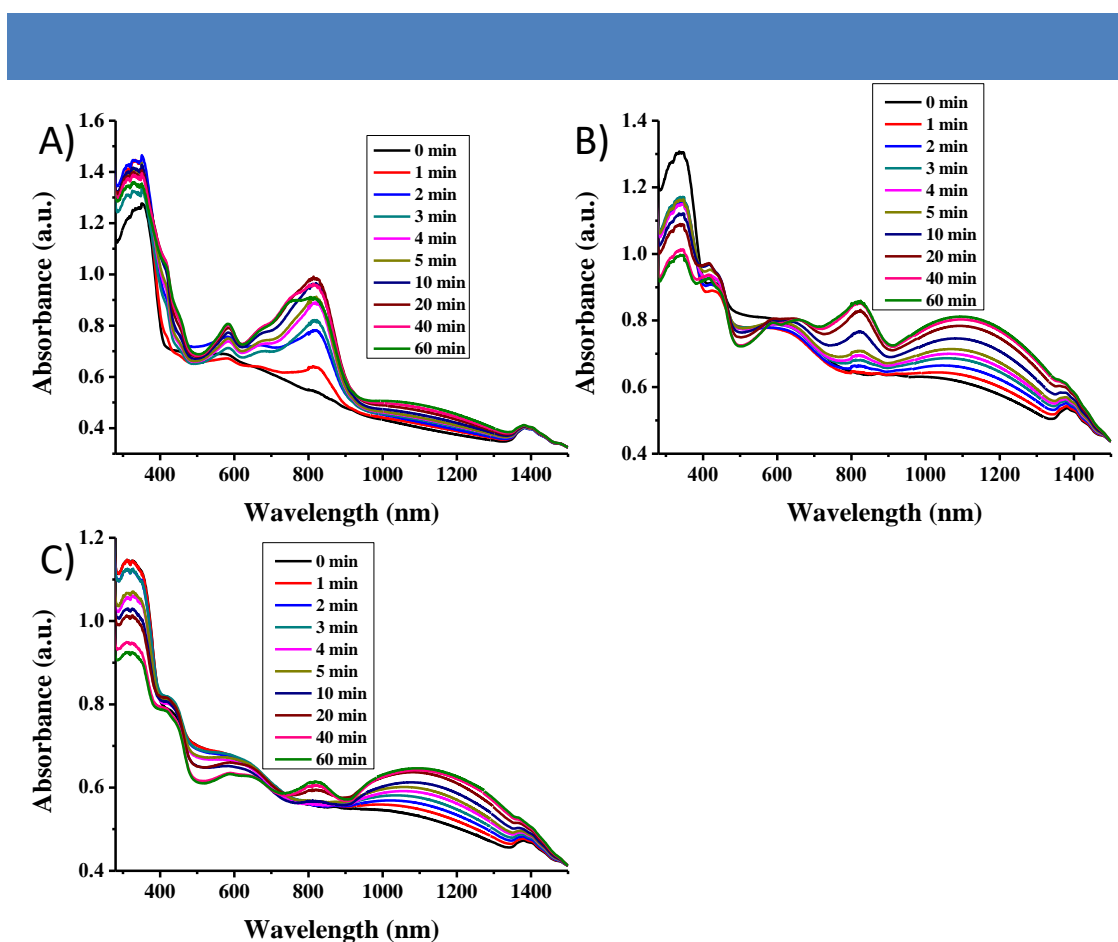

Figure 75 | UV-Vis-NIR spectra of **Gel1**, **Gel2** and **Gel3** in a 9:1 mixture of toluene:tetrachloroethane upon light irradiation.

For **Gel1** prepared from a non-irradiated physical gel, we observe that the intensity of the band at ~800 nm is highly enhanced compared to the one at ~1100 nm upon light irradiation. On the other hand, for **Gel2**, both bands display similar intensities upon light irradiation while, for **Gel3**, the intensity of the band at ~1100 nm is more pronounced compared to the one at ~ 800 nm. These observations suggest that the ordering of the triarylamine units is different in the chemical gels, *i.e.* enhanced by light irradiation of the preorganized physical gels as

already demonstrated by our group.[146] These experiments also demonstrated that chemical gels keep the optical properties of triarylamine self-assemblies even after covalent polymerization.

TEM and SEM techniques were then employed to investigate the morphology of the physical gels and polymerized gels. For physical gel **Gel1'**, networks made of micrometric fiber-like structures are observed by TEM but it proved difficult to image **Gel2'** and **Gel3'** by the same technique (Figure 76a). SEM imaging of the chemical gels revealed dense fibrous networks formed by large and elongated fibers in the three cases (Figure 76b, c and d). However, a pronounced alignment of the fibers over larger distances could be observed for **Gel2** and **Gel3**, which probably result from the light-induced process that favors the formation of fibers with less defects.
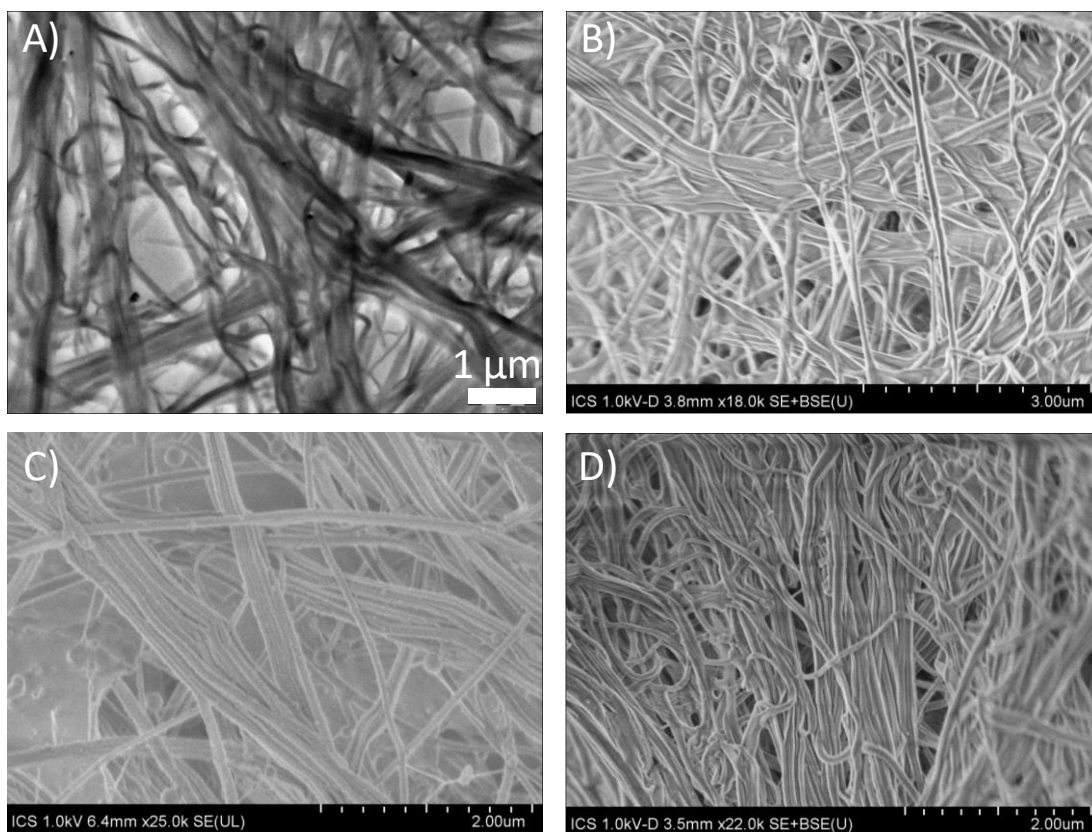

Figure 76 | TEM images of a) TANBE Gel in Toluene/TCE (9/1) without irradiation; SEM images of b) **Gel1**, c) **Gel2** (Cryo-SEM) and d) **Gel3**.

X-ray scattering was then performed on physical and cross-linked gels to determine the packing parameters of the structures within the gels. For all samples, a strong scattering peak at 0.191 Å^{-1} evidenced the typical smectic-type packing with a periodicity of 32.9 Å along the one-dimensional self-assembled structure as already observed by our group.[146] In order to

study the effect of light irradiation on the nanostructures, a Gaussian fit was performed for these scattering peaks on the three chemical gels. A decrease in the peak width at half-maximum is observed for irradiated **Gel2**, **Gel3** in contrast to **Gel1**, suggesting a decrease of structural defects with light (Figure 77). However, it should be mentioned that the time of irradiation does not seem to have an impact on the structural organization.
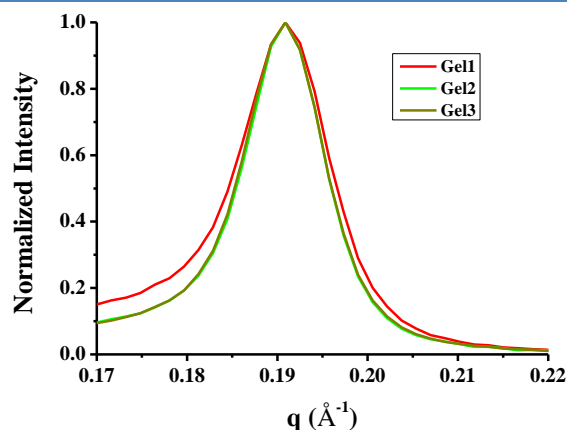

Figure 77 | Normalized peaks at 0.191 Å⁻¹ of **Gel1** (red), **Gel2** (green) and **Gel3** (brown).

TGA experiments were performed to determine the thermal stability of **Gel1**, **Gel2** and **Gel3** (Figure 78). While TANBE monomer shows only one decomposition process related to the degradation of the molecule, all the polymerized gels undergo two identical decomposition processes with the first one probably arising from the loss of solvent and monomer residues. Therefore, the monomer starts to decompose at 249 °C while the gels begin to decompose at ~ 400 °C, indicating an improved thermal stability after polymerization. However, all the samples exhibit bulk decomposition temperature at 600 °C, suggesting the same intrinsic material properties.
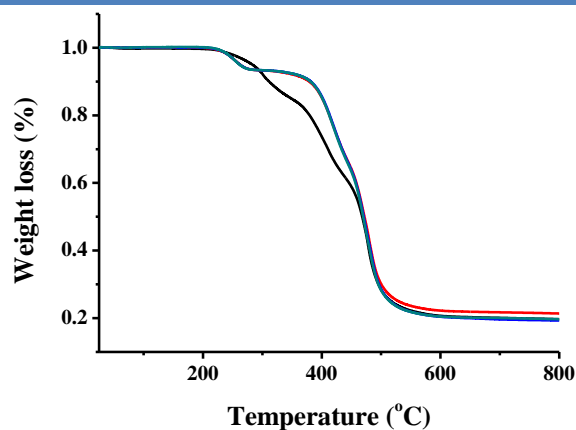

Figure 78 | TGA curves of monomer TANBE (black), **Gel1** (red), **Gel2** (blue) and **Gel3** (green).

Finally, we recently just started to probe the mechanical properties of our physical and chemical gels by rheology. For physical gel **Gel1'**, in the low frequency area, the value of G'' is higher than that of G' indicating the liquid nature of the sample, whereas, in the high frequency region, the value of G' is higher than that of G'', indicating the solid nature of the sample (Figure 79). Hence, the crossover around a frequency at 5 Hz suggests a liquid-solid transition for **Gel1'**, which is typical of a liquid-like phase. In the next steps, rheology experiments will be performed on cross-linked gels to determine their mechanical robustness compared to their physical counterparts.
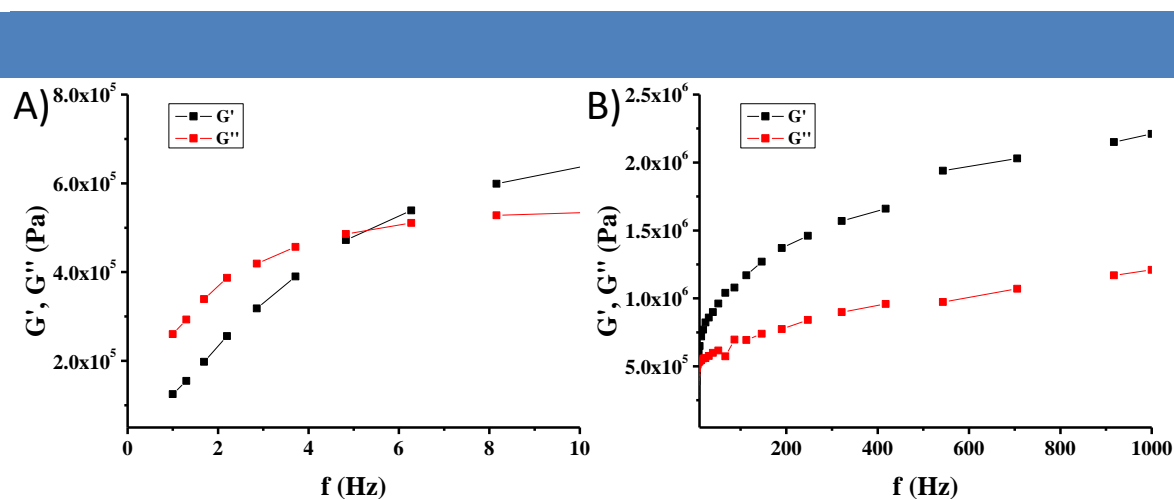

Figure 79 | Behavior of G' and G'' as a function of frequency for physical gel **Gel1'**, a) low frequency area and b) high frequency area.

4. Conclusions

In this chapter, three triarylamine molecules decorated either with siloxane end groups (TAEOS1 and TAEOS2) or with norbornene end units (TANBE) were first designed and successfully synthesized. The self-assembly of all three molecules was first investigated in solution by various physico-chemical techniques including spectroscopies, cyclic voltammetry and microscopy. They all suggest that the presence of functional units as end groups does not affect the self-assembling properties into fibrillar aggregates with optical properties reminiscent of the triarylamine trisamides as already described by our group. Interestingly, UV-Vis-NIR spectroscopy revealed different electronic states between trisurea TAEOS1 self-assemblies and trisamide TAEOS2 self-assemblies probably due to their different self-assembled structures. Gels were then prepared *in situ* from TAEOS1 by sol-gel method and from preorganized TANBE monomers by ring opening metathesis polymerization. Currently, we have only confirmed the formation of covalent gel from TAEOS1 using FT-IR

spectroscopy, TGA analysis and SEM microscopy. More characterizations including UV-Vis-NIR, fluorescence spectroscopy along with rheology and conductivity experiments will be performed in order to determine if functional robust materials built from self-assembled architectures can be obtained by the sol-gel technique. On the other hand, chemical gels prepared by ROMP from TANBE physical gels were fully characterized by means of different techniques, confirming cross-linking within the gels and preservation of charge-transfer processes between the triarylamine units within the covalent network. Finally, first rheology experiments revealed the intrinsic liquid nature of the physical gel and further rheology and conductivity experiments will be performed to determine the mechanical and electrical properties of the chemical gels. Anyway, we expect that this approach will be a useful tool to construct conducting materials combing mechanical robustness with excellent conductivity for promising applications in electronic devices.

CONCLUSIONS AND PERSPECTIVES

In this manuscript, I described the results of my PhD work on two topics related to the self-assembly of well-designed triarylamine molecules, which was pioneered by our group.

In terms of synthetic achievements, we successfully synthesized six novel tris-amide triarylamine molecules decorated with either water-soluble groups (polyethylene glycol, peptide or cyanine dye) or polymerizable groups (siloxane or norbornene). While the synthesis of TAPEG and TAEOS1 was straight forward from the well-known *N,N*-bis(4-aminophenyl)benzene-1,4-diamine derivative, other synthetic route required either specific synthetic tools or advanced multi-step synthetic strategies. For instance, TAPeptide was synthesized directly on solid support which, to the best of our knowledge, represents the first polymer-supported synthesis of a tritopic molecule. On the other hand, complex functional molecules TACy3, TAEOS2 and TANBE were achieved after optimization of multi-step synthetic routes.

In chapter five, we then studied the self-assemblies of triarylamine monomers decorated with polar side chains in either water or methanol. The corresponding supramolecular polymers were characterized following a systematic approach combing ^{1}H NMR, UV-Vis, and fluorescence spectroscopies with small angle neutron scattering and microscopy experiments. In most cases, fibrillar morphologies were evidenced in water and methanol independently of the side chains, demonstrating that the triarylamine core drives the self-assembly process even in polar media and that side chains provide a hydrophilic environment necessary for solubility issues. Interestingly, for TAPeptide, twisted fibers with a single handedness were observed in acidic conditions suggesting transfer of chirality from the peptidic side chain to the self-assembled structures. Overall, the work described in this section demonstrates the potential of the triarylamine building block as a structuring unit for self-assembly processes in polar solvents. To the best of our knowledge, it represents the first example of water-soluble supramolecular polymers based on triarylamine molecules.

In chapter six, we then studied the self-assemblies of three tris-amide triarylamine derivatives with polymerizable side chains in solution upon light irradiation. We demonstrated that these side chains do not hinder the self-assembly process and that the resulting supramolecular polymers diplay optical behaviors similar to the initially reported tris-amide triarylamine compound.[128] We then manage to covalently polymerize these self-assembled fibrillar aggregates either by sol-gel process involving siloxane polymerization or by ring opening metathesis polymerization. While all chemical gels displayed optical

properties reminiscent of the supramolecular polymers and increased thermal stabilities, we still have to demonstrate their enhanced mechanical properties by further rheology experiments and to determine the electrical properties by conductivity measurements.

Overall, these two works enlarge the potential of the triarylamine scaffold as structuring unit to produce supramolecular polymers in a wide range of solvents and as robust functional materials for further applications in electronics and/or plasmonics.

EXPERIMENTAL PART

1. General procedures

a. *Solvent and chemical reagents*

All reagents and solvents were purchased at the highest commercial quality and used without further purification unless otherwise noted. Dry solvents were obtained using a double column SolvTech purification system. Water was deionized by using a milli-gradient system (Millipore, Molsheim, France). Microwave reactions were carried out with a single mode cavity Discover SP Microwave Synthesizer (CEM Corporation, NC, USA), producing continuous irradiation at 2455 MHz and equipped with simultaneous external air-cooling system. Yields refer to spectroscopically purified (^{1}H NMR) homogeneous materials.

b. *Chromatographic methods*

Thin Layer Chromatographies were performed using silica on TLC aluminium foils (silica gel matrix with fluorescent indicator 254 nm, thickness: 500 μm, Sigma-Aldrich). In most cases, irradiation using a *Bioblock VL-4C* UV-Lamp (6W, 254 nm and/or 365 nm) as well as *p*-anisaldehyde, phosphomolybdic acid and Cerium ammonium molybdate stainings were used for visualization. *Ultra Performance Liquid Chromatographies coupled to Mass Spectroscopy* (UPLC-MS) were carried out on a *Waters Acquity UPLC-SQD* apparatus equipped with a PDA detector (190-500 nm, 80 Hz), using a reverse phase column (Water, BEH C_{18} 1.7 μm, 2.1×50 mm), the MassLynx 4.1 - XP software and a gradient (water-acetonitrile + 0.1% TFA) as eluent. *Preparative Adsorption Flash Column Chromatographies* were performed using silica gel (60 Å, 230 – 400 mesh, 40 – 63 μm, Sigma-Aldrich) or aluminium oxide 90 (standardized activity Π, 70 – 230 mesh, Merck). *Preparative High Performance Liquid Chromatographies coupled to Mass Spectroscopy* (HPLC-MS) were performed using a *Waters AutoPurify* system equipped with a UV detector set at 300 nm, a *3100* mass spectrometer, reverse phase columns (Waters, Sun Fire Prep C_{18} 5.0 μm, 19 × 150 mm; Waters, XBridge Prep C_{18} 5.0 μm, 19 × 150 mm) running with a water/methanol gradient as eluent (with 0.1% formic acid for the Sun Fire Prep C_{18}, or 0.05% ammonia for the XBridge Prep C_{18}) and the MassLynx 4.1 – XP software.

c. *Analytical methods and instruments*

i. Nuclear Magnetic Resonance

^{1}H NMR spectra were recorded on a Bruker Avance 400 spectrometer at 400 MHz and ^{13}C spectra at 100 MHz. The spectra were internally referenced to the residual proton solvent

signal (CDCl$_3$: 7.26 ppm, CD$_3$OD: 3.31 ppm, D$_2$O: 4.79 ppm, DMSO-d$_6$: 2.50 ppm, DMF-d$_7$: 8.03, 2.92 and 2.75 ppm, Toluene-d$_8$: 7.09, 7.01, 6.97 and 2.08 ppm and THF-d$_8$: 3.58 and 1.72 ppm for ^{1}H spectrum, and CDCl$_3$: 77.16 ppm, CD$_3$OD: 49.00 ppm, DMSO-d$_6$: 39.52 ppm, DMF-d$_7$: 163.15, 34.89 and 29.76 ppm, Toluene-d$_8$: 137.48, 128.87, 127.96, 125.13 and 20.43 ppm and THF-d$_8$: 67.21 and 25.31 ppm for ^{13}C spectrum). For ^{1}H NMR assignments, the chemical shifts are given in ppm. Coupling constants *J* are given in Hz. Peaks are described as singlet (s), doublet (d), triplet (t), quartet (q), multiplet (m), broad (br), broad singlet (brs) and broad multiplet (brm).

ii.   Mass spectrometry

ESI-MS mass spectra were recorded in a SQD apparatus from Waters.

iii.   UV-vis-NIR experiments

UV-vis-NIR spectra were recorded either on a Varian Vary 5000 apparatus (for far NIR region measurements or integration sphere measurements) or on a Perkin Elmer-Lambda 25 spectrometer.

iv.   Fluorescence experiments

Fluorescence experiments were recorded on a FluoroMax-4 (Horiba Jobin-Yvon) spectro-fluorometer with the general settings: slit width : 5 nm, inc : 1, integration time : 0.1 s.

v.   InfraRed Spectroscopy

InfraRed (I. R.) spectra were recorded on a Fourier transform infrared spectrometer VERTEX 70 (Bruker) by drop-casting a solution on an ATR diamond probe, unless otherwise noted.

vi.   Gel Permeation Chromatography (GPC)

GPC experiments were performed at the Plateforme de caractérisation des polymers, on four PLgel-B columns (particles size: 5 μm, length: 30 cm, diameter: 7.5 mm, separation in the 103 – 2 × 106 g.mol^{-1}). A triple detector from Wyatt Techn was used (light scattering, viscometer, refractometer). A HPLC-grade tetrahydrofuran was used as solvent. Rate of flow: 1 mL/min. The samples were dissolved in the solvent 1 h prior to experiment and filtered on a 0.45 μm filter (Phenex by Phenomenex) and injected.

vii.   Scanning Electron Microscopy (SEM)

SEM experiments were performed using a Hitachi S-4500 microscope (0.5-30 kV).

viii.   Transmission Electron Microscopy (TEM)

TEM experiments were performed using a CM12 Philips microscope equipped with a MVIII (SoftImaging System) CCD camera. Samples were analyzed in Bright Field Mode with a LaB_6 cathode and 120 kV tension. Image treatments were performed by using analySIS (Soft Imaging System) software. Statistical analyses were performed using ImageJ software. For sample preparation, a solution containing the compound of interest was dropped (~5 µL) onto a carbon-coated (glow discharged for aqueous samples) copper grid placed on a Whatman filter paper. The grid was then left to dry at air before analysis.

ix.   Atomic Force Microscopy (AFM)

Atomic force microscopy (AFM) images were obtained by scanning the samples using a Nanoscope 8 (Bruker) operated in Peak-Force tapping mode. Peak-Force AFM is based on Peak force tapping technology, during which the probe is oscillated in a similar fashion as it is in tapping mode, but at far below the resonance frequency. Each time the tip and the sample are brought together, a force curve is captured. These forces can be controlled at levels much lower than contact mode and even lower than tapping mode allowing operation on even the most delicate soft samples, as is the case here. Ultra-sharp silicon tips on nitride levers were used (Bruker, Scanasyst with spring constant of 0.4 N/m). During AFM imaging, the force was reduced in order to avoid dragging of molecules by the tip. All analyses of the images were conducted in integrated software. Images were recorded directly on previously prepared TEM grids.

x.   Small angle neutron scattering (SANS)

SANS experiments were performed on the PACE spectrometer at the Laboratoire Leon Brillouin (LLB, CEA Saclay). Typically, three configurations were used: the first was set with a distance sample to detector of 4.7 m, a wavelength of 13 Å and a collimation distance of 5.00 m, the second at 3 m and 4.6 Å and the last at 1 m and 4.6 Å with a collimation distance of 2.5 m, providing a large accessible q-range from 3×10^{-3} to 0.3 $Å^{-1}$.

xi.   Small angle X-ray scattering (SAXS)

Small angle X-ray scattering experiments were performed at the Institut Charles Sadron by using a diffractometer developed by Molecular Metrology (Elexience in France), and a Nanostar diffractometer from Bruker-Anton Paar. Both instruments operate with a pinhole collimation of the X-ray beam and a two-dimensional gas-filled multiwire detector. For the Elexience diffractometer, a monochromatic (λ= 1.54 Å with Dl/l < 4%) and focused X-ray beam is obtained through a multilayer optic designed and fabricated by Osmic. For the

Nanostar, a monochromatic and almost parallel X-ray beam (divergence better than 0.03º) is obtained through a confocal mirror with advanced W/Si multilayer coating from Xenocs. The size of the incident beam on the sample was close to 600 and 300 μm for the Elexience and Nanostar diffractometers, respectively. The sample to detector distance was set at 0.70 m for the Elexience diffractometer and 0.20 m for the Nanostar one, allowing to explore scattering vectors ranging from $q = 0.01$ Å^{-1} to 0.9 Å^{-1}, with $q = 4\pi\sin(\theta/2)/\lambda$, where λ and θ are the wavelength of the incident beam and the scattering angle, respectively. The q-resolution related to the beam size on the sample and the beam divergence was close to 0.005 Å^{-1}. Cells of 1 mm thickness and calibrated Mica windows were used as sample holders. Measurements were performed at room temperature. All data were treated according to standard procedures for isotropic small angle X-ray scattering. After radial averaging, the spectra were corrected from electronic noise of the detector, empty cell, absorption and sample thickness. A ^{55}Ir source was used for the corrections of the q-calibration. After all these data treatments, the scattered intensities were corrected from the scattering of the solvent. According to such a procedure, the scattered intensity I(q) containing all the structural information is obtained for each solution.

xii. Dynamic light scattering experiments (DLS)

DLS experiments were performed either on a ZetaSizer Nano ZS (Malvern Instruments, Worcestershire, U.K.) or at the University Paris Diderot on the 3D DLS spectrometer (LS Instruments, Fribourg, Switzerland) equipped with a 25 mW HeNe laser (JDS uniphase) operating at λ=632.8 nm, a two channel multiple tau correlator (1088 channels in autocorrelation), a variable-angle detection system, and a temperature-controlled index matching vat (LS Instruments). For experiments performed on the 3D DLS spectrometer, the scattering spectra was measured using two single mode fibre detections and two high sensitivity APD detectors (Perkin Elmer, model SPCM-AQR-13-FC). Solutions were directly filtered through 0.22 μm Millipore filter into the scattering cell.

xiii. Electrochemistry

Prior to analysis, all samples were degassed with argon. Electrochemical measurements were performed on an Autolab PGstat101 (Metrohm, Switzerland). All electrolyte salts were purchased at electrochemical grade from Aldrich. Electrochemical studies were performed on a platinum 2 mm diameter working electrode, a platinum wire counter electrode and a silver wire pseudo-reference electrode. The counter and reference electrodes were separated from solution with a Vicor glass bridge. Reported redox values were internally referenced against

decamethylferrocene.

xiv. Rheology

Measurements of the complex shear modulus $G*$ were performed at the Institut Charles Sadron with a piezoelectric rheometer developed in house.[164] This device is a plate-plate rheometer which operates with piezoelectric ceramics vibrating in the shear mode. As shown in Figure 1, the principle of measurements consists in a very small strain ε applied onto the sample through the glass slide attached to the emitting ceramic, and the stress σ received on the opposite glass slide is measured by the receiving ceramic attached to this glass slide. The complex shear modulus $G*$ is calculated by the stress-strain relationship $G*=\sigma/\varepsilon$.
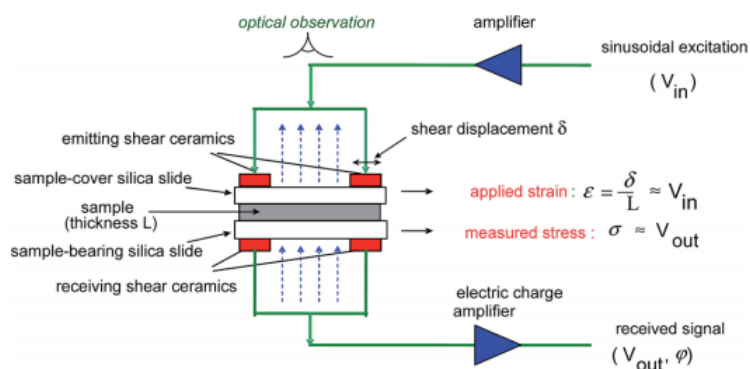
Figure S1 | Block diagram of the piezoelectric rheometer.

The measuring cell is placed in an oven which can be controlled in temperature from -60 to +150 °C within a tenth of a degree Celsius. This device can acquire data in a very wide frequency range from $f = 2 \times 10^{-2}$ to 10^4 Hz, by imposing very low strains ε ranging from 10^{-6} to 10^{-2} to samples with a thickness L which can vary from about ten micrometers (liquid) to a few centimeters (soft solid). Another advantage of this device is related to the very small amount of sample required to perform measurements

---

[164]Sánchez-Ferrer, A., Rogez, D. and Martinoty, P. Influence of the degree of polymerisation and of the architecture on the elastic properties of new polyurea elastomers. *RSC Adv.* **5,** 6758–6770 (2015).

2. Syntheses and analyses of compounds

*N,N-bis(4-nitrophenyl)benzene-1,4-diamine (**1**)*

1
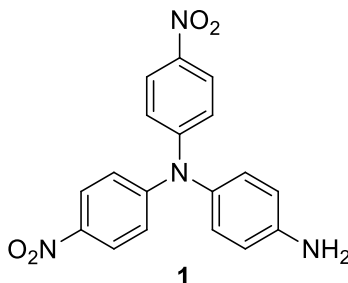
To a solution of *p*-fluoronitrobenzene (2.20 mL, 20 mmol) and *p*-phenylenediamine (1.08 g, 10 mmol) in dimethyl sulfoxide (25 ml) was added potassium carbonate (5.56 g, 40 mmol). The mixture was stirred and heated at 90 °C under argon atmosphere. After four days, the solution was allowed to cool to room temperature and poured into water to give a dark red solid precipitate. This solid crude was washed several times with water and purified by column chromatography (SiO$_2$, dichloromethane/cyclohexane 5:1 → dichloromethane) to provide compound **1** (2.3 g, 66%) as a dark red product.

R_f = 0.25 (cyclohexane/dichloromethane 1:2).

^{1}H NMR (CDCl$_3$, 400 MHz, 25°C): δ = 8.12 (d, ^3J = 9.1 Hz, 4H), 7.13 (d, ^3J = 9.1 Hz, 4H), 6.95 (d, ^3J = 8.5 Hz, 2H), 6.73 (d, ^3J = 8.5 Hz, 2H), 3.85 (s, 2H).

^{13}C NMR (CDCl$_3$, 100 MHz, 25°C): δ = 152.2, 146.2, 142.4, 135.3, 129.2, 125.6, 121.7, 116.7.

ESI-MS: m/z calcd. for C$_{18}$H$_{14}$N$_4$O$_4$: 351.33 [M+H]$^+$, found: 351.32 [M+H]$^+$.

*TAPEG (**2**)*

2
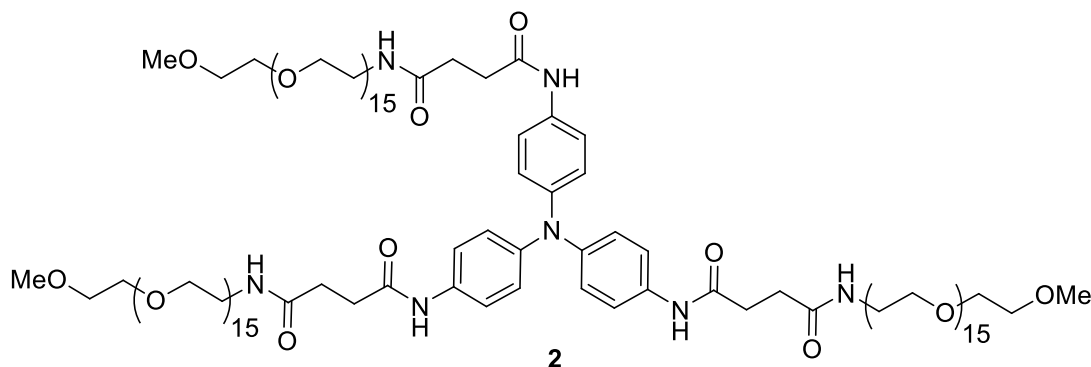
A solution of compound **1** (0.120 g, 0.346 mmol) and tin dichloride (0.874 g, 3.87 mmol) in a mixture of acetonitrile (20 mL) and ethanol (14 mL) was stirred overnight at 80 °C under an
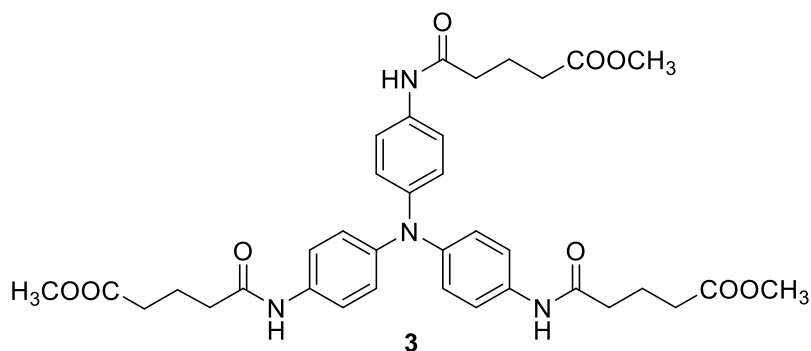
argon atmosphere. The solution was then cooled down to room temperature and diluted with ethyl acetate (150 mL). The organic phase was washed with NaHCO$_{3sat}$ (2 × 100 mL) and brine (100 mL), dried over Na$_2$SO$_4$ and concentrated under reduced pressure to provide *N,N*-bis(4-aminophenyl)benzene-1,4-diamine, which was pure enough to be used as such in the next step. A solution of this tris-amino compound in dichloromethane (18 mL) was added dropwise to a solution of *O*-[(*N*-Succinimidyl)succinyl-aminoethyl]-*O'*-methylpolyethylene glycol (0.875 g, 1.16 mmol) and 4-dimethylaminopyridine (0.140 g, 1.15 mmol) in dichloromethane (5 mL) under an argon atmosphere at room temperature. The reaction was monitored by UPLC-Ms and stopped after stirring for two weeks. The solvent was evaporated under vacuum and the crude residue was purified by reverse-phase preparative HPLC-MS (Column: Sun Fire Prep C$_{18}$) to yield compound **2** (216 mg, 12 %) as a pale brown oil.

^{1}H NMR (CD$_3$OD, 400 MHz, 25°C): δ = 7.46 (d, ^3J = 8.9 Hz, 6H), 6.95 (d, ^3J = 8.9 Hz, 6H), 3.68-3.55 (m, 174H), 3.53 (t, ^3J = 5.5 Hz, 12H), 3.41-3.34 (m, 15H), 2.66 (t, ^3J = 6.6 Hz, 6H), 2.57 (t, ^3J = 6.6 Hz, 6H).

^{13}C NMR (CD$_3$OD, 100 MHz, 25°C): δ = 174.7, 172.6, 145.2, 135.0, 125.2, 122.4, 73.0, 71.6, 71.4, 71.3, 70.6, 59.1, 40.5, 33.1, 32.1.

ESI-MS: m/z calcd. for C$_{129}$H$_{231}$N$_7$O$_{54}$: 1373.288 [M]$^{2+}$, found: 1373.284.

Trimethyl 5,5',5''-((nitrilotris(benzene-4,1-diyl))tris(azanediyl))tris(5-oxopentanoate) (3)

A solution of compound **1** (490 mg, 1.40 mmol) and tin dichloride (3.54 g, 15.7 mmol) in a mixture of acetonitrile (23 mL) and ethanol (19 mL) was stirred overnight at 80 °C under an argon atmosphere. After cooling down to room temperature, the solution was diluted with ethyl acetate (150 mL). The mixture was washed with NaHCO$_{3sat}$ (2 × 100 mL) and brine (100 mL). Then, the organic phase was dried over Na$_2$SO$_4$ and concentrated under reduced pressure to provide *N,N*-bis(4-aminophenyl)benzene-1,4-diamine, which was pure enough to be used as such in the next step. A solution of this crude compound and triethylamine (0.57 mL, 4.2 mmol) in dichloromethane (28 mL) was added dropwise to a solution of methyl

5-chloro-5-oxopentanoate (586 mg, 4.2 mmol) in dichloromethane (5.6 mL) cooled with an ice-bath under an argon atmosphere. The reaction mixture was heated up slowly to room temperature for 12 hours. The solution was then diluted with dichloromethane (100 mL) and the organic phase was washed with NH_4Cl_{sat} (2 × 100 mL) and brine (100 mL), dried over Na_2SO_4 and concentrated under reduced pressure. The crude residue was purified by column chromatography (SiO$_2$, dichloromethane → methanol/dichloromethane 5/100) to yield compound **3** (500 mg, 53%) as a white solid.

R_f = 0.3 (methanol/dichloromethane 5/100).

^{1}H NMR (CD$_3$OD, 400 MHz, 25°C): δ = 7.42 (d, ^3J = 8.7 Hz, 6H), 6.96 (d, ^3J = 8.7 Hz, 6H), 3.67 (s, 9H), 2.45-2.38 (m, 12H), 1.98 (t, ^3J = 7.3 Hz, 6H).

^{13}C NMR (CD$_3$OD, 100 MHz, 25°C): δ = 175.4, 173.6, 145.6, 134.9, 125.3, 122.8, 52.2, 36.9, 34.2, 22.2.

ESI-MS: m/z calcd. for $C_{36}H_{42}N_4O_9$: 675.30 [M+H]$^+$, found: 675.58.

*5,5',5''-((nitrilotris(benzene-4,1-diyl))tris(azanediyl))tris(5-oxopentanoic acid) (**4**)*
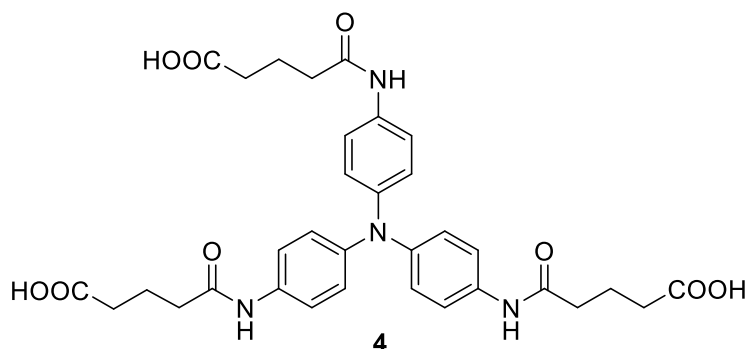

A solution of sodium hydroxide (1 M, 38 mL) was added to a solution of compound **3** (940 mg, 1.49 mmol) in methanol (20 mL). The mixture was stirred at room temperature. The reaction was monitored by UPLC and stopped after 1.5 hours. The mixture was neutralized with 1 M aqueous HCl. The solution was then filtered to recover the precipitate, which was then dissolved in methanol (10 mL) and the solution was further evaporated under reduced pressure to provide compound **4** (430 mg, 46%) as a pure white solid.

^{1}H NMR (CD$_3$OD, 400 MHz, 25°C): δ = 7.42 (d, ^3J = 8.8 Hz, 6H), 6.96 (d, ^3J = 8.8 Hz, 6H), 2.41 (t, ^3J = 7.4 Hz, 6H), 2.37 (t, ^3J = 7.4 Hz, 6H), 1.97 (t, ^3J = 7.3 Hz, 6H).

^{13}C NMR (CD$_3$OD, 100 MHz, 25°C): δ = 178.0, 173.9, 145.6, 134.9, 125.3, 122.8, 37.2, 35.1, 22.7.

ESI-MS: m/z calcd. for $C_{33}H_{36}N_4O_9$: 633.26 [M+H]$^+$, found: 632.59.

*Ala-Ala-Ala-Glu-Glu-Glu amino acid sequence (5)*

5
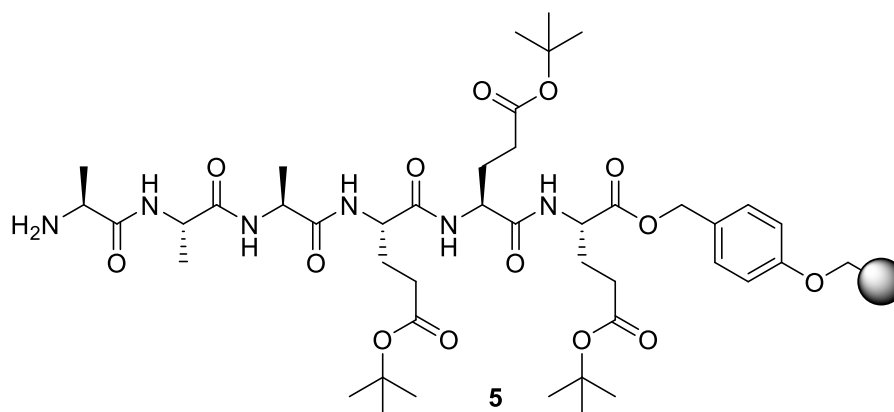
Standard solid phase peptide synthesis was performed using microwave assisted solid phase peptide synthesis with a CEM Liberty 1™ microwave synthesizer starting with a Fmoc-L-Glu-MPPA(Wang) resin (0.62 mmol/g). A typical synthesis was done on a 1.0 mmol scale. For each amino acid, double couplings were performed at 70 ºC and 35 W (microwave power) for 5 min using 4-fold molar excess of each Fmoc L-amino acid (10 mL of a 0.2 M solution in dimethylformamide), HBTU (4 mL of a 0.5 M solution in dimethylformamide) and *N,N*-diisopropylethylamine (2 mL of a 2 M solution in *N*-Methyl-2-pyrrolidone). Fmoc groups were deprotected with 2 successive treatments with 20 vol% piperidine solution in dimethylformamide (15 mL, 70 ºC for 3 min, 55 W). At the end of the synthesis, a small amount of resin was cleaved using a mixture of TFA/H$_2$O/TIPS: 9.5/0.25/0.25 vol% and the purity of the crude peptide was checked after precipitation in diethyl ether.

^{1}H NMR (D$_2$O, 400 MHz, 25°C): δ = 4.45-4.26 (m, 5H), 4.14-4.05 (m, 1H), 2.56-2.44 (m, 6H), 2.28-2.07 (m, 3H), 2.06-1.93 (m, 3H), 1.54 (d, ^3J = 8.6 Hz, 3H), 1.44-1.37 (m, 6H).

ESI-MS: m/z calcd. for C$_{24}$H$_{38}$N$_6$O$_{13}$: 617.25 [M-H]$^-$, found: 617.46.

TAPeptide (6)

6
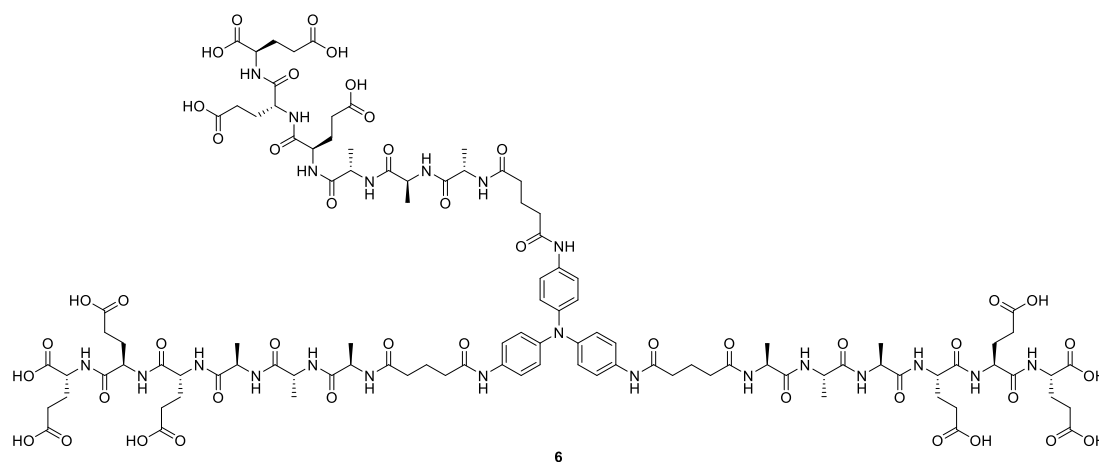
N,N-diisopropylethylamine (DIPEA) (0.42 mL, 2.37 mmol) was added to a solution of compound **4** (200 mg, 0.316 mmol) and PyBop (600 mg, 1.14 mmol) in *N,N*-dimethylformamide (17 mL). The reaction mixture was then stirred thoroughly and further added to the peptidic resin **5** (1.53 g). After shaking for 72 hours, the reaction solution was then drained off and the resulting peptidyl resin was washed with *N,N*-dimethylformamide (5 × 17 mL). Cleavage from the resin and deprotection of compound **6** was performed twice for 1 h with a mixture of TFA, H_2O, and TIPS (16 mL, 95:2.5:2.5). Both cleavage mixtures were filtered into a round-bottom flask. The combined solution was concentrated under reduced pressure and cold diethyl ether was then added to precipitate crude compound **6**. The precipitate was centrifuged, and the supernatant liquid was removed by decantation. After washing with diethyl ether (3 times) to remove residual TFA, the precipitate was dried under vacuum for overnight. Purification of the crude mixture by preparative HPLC (Column: Sun Fire Prep C_{18}) afforded compound **6** (38.9 mg, 4.9%), as a colorless solid.

^{1}H NMR (d_6-DMSO, 400 MHz, 25°C): δ = 10.00 (s, 3H), 8.35 (d, ^3J = 6.2 Hz, 3H), 8.31 (d, ^3J = 5.9 Hz, 3H), 8.09 (d, ^3J = 6.6 Hz, 3H), 7.99 (d, ^3J = 5.8 Hz, 3H), 7.95 (d, ^3J = 7.5 Hz, 3H), 7.89 (d, ^3J = 8.0 Hz, 3H), 7.63 (d, ^3J = 8.8 Hz, 6H), 6.99 (d, ^3J = 8.8 Hz, 6H), 4.50-4.43 (m, 3H), 4.42-4.35 (m, 6H), 4.34-4.27 (m, 9H), 2.54-2.39 (m, 24H), 2.39-2.32 (m, 6H), 2.23-2.10 (m, 9H), 2.04-1.89 (m, 15H), 1.41 (d, ^3J = 7.2 Hz, 9H), 1.37 (d, ^3J = 7.2 Hz, 9H), 1.37 (d, ^3J = 7.2 Hz, 9H).

^{13}C NMR (d_6-DMSO, 100 MHz, 25°C): δ = 173.9, 173.8, 172.9, 172.3, 172.0, 171.9, 171.7, 170.7, 170.5, 142.7, 134.2, 123.5, 120.3, 51.8, 51.7, 51.6, 35.6, 34.3, 30.3, 30.1, 29.9, 27.4, 27.2, 26.5, 21.2, 18.0, 17.9, 17.8.

ESI-MS: m/z calcd. for $C_{105}H_{144}N_{22}O_{45}$: 1215.98 [M-2H]$^{2-}$, found: 1215.71.

*N,N',N''-(nitrilotris(benzene-4,1-diyl)tris(6-bromohexanamide) (**7**)*

7
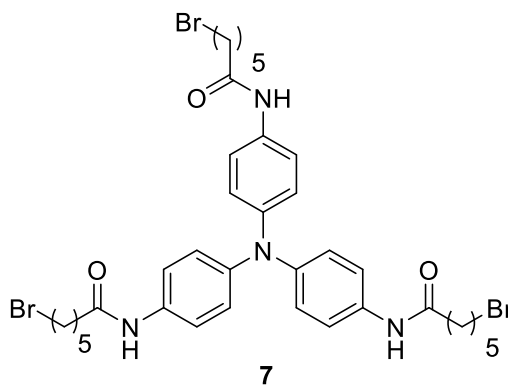
A solution of compound **1** (1.00 g, 2.87 mmol) and tin dichloride (7.22 g, 32.00 mmol) in a mixture of acetonitrile (40 mL) and ethanol (32 mL) was stirred overnight at 80 °C under an argon atmosphere. After cooling down to room temperature, the solution was diluted with ethyl acetate (200 mL). The mixture was washed with $NaHCO_{3sat}$ (2×200 mL) and brine (150 mL). Then, the organic phase was dried over Na_2SO_4 and concentrated under reduced pressure to provide *N,N*-bis(4-aminophenyl)benzene-1,4-diamine, which was pure enough to be used as such in the next step. A solution of this crude compound and triethylamine (1.18 mL, 2.87 mmol) in dichloromethane (60 mL) was added dropwise to a cooled solution of 6-bromohexanoyl chloride (1.30 mL, 8.58 mmol) in dichloromethane (12 mL) at 0 °C under an argon atmosphere. The reaction mixture was heated up slowly to room temperature for 12 hours. Afterwards, solvents were removed under reduced pressure and the resulting crude residue was washed by dichloromethane several times (100 mL) to afford compound **7** (920 mg, 39 %) as a white solid.

^{1}H NMR (CD_3OD:d_8-Toluene 5:3, 400 MHz, 25°C): δ = 7.54 (d, ^3J = 8.8 Hz, 6H), 6.97 (d, ^3J = 8.8 Hz, 6H), 3.23 (t, ^3J = 6.8 Hz, 6H), 2.30 (t, ^3J = 7.4 Hz, 6H), 1.78-1.70 (m, 6H), 1.68-1.61 (m, 6H), 1.45-1.37 (m, 6H).

^{13}C NMR (CD_3OD:d_8-Toluene 5:3, 100 MHz, 25°C): δ = 173.8, 145.3, 134.9, 125.2, 122.4, 37.7, 34.1, 33.6, 28.8, 26.0.

ESI-MS: m/z calcd. for $C_{36}H_{45}Br_3N_4O_3$: 820.10 [M]$^+$, found: 819.80.

N,N',N''-(nitrilotris(benzene-4,1-diyl))tris(6-tritylthio)hexanamide) (8)

8
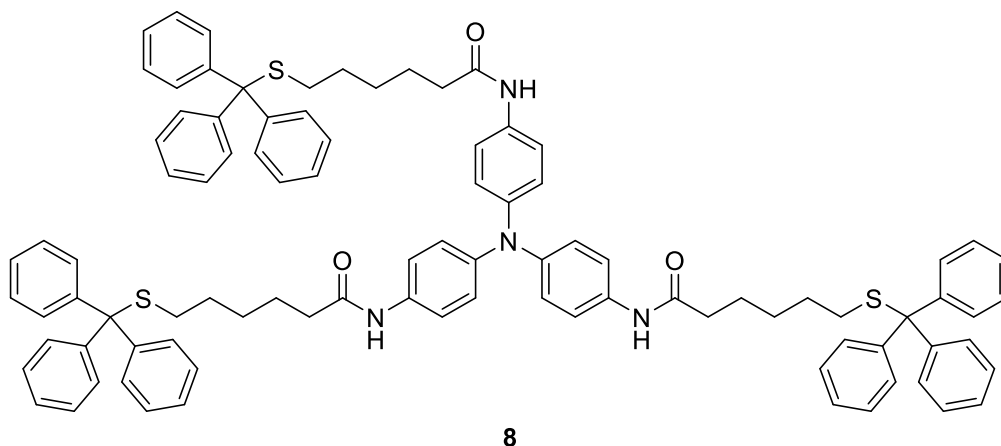
Compound **7** (1.58 g, 1.92 mmol), triphenylmethanethiol (2.13 g, 7.70 mmol) and 1,8-diazabicyclo[5.4.0]undec-7-ene (DBU) (1.17 g, 7.70 mmol) were dissolved in dimethylformamide (30 mL) and the mixture was stirred overnight at 35 °C under an argon atmosphere. After this time, diethyl ether (400 mL) was added and the solution was extracted

with water (3 × 200 mL). The organic phase was dried over Na$_2$SO$_4$, filtered and evaporated under vacuum. The residue was firstly dissolved in dichloromethane (25 mL) and then poured into methanol (100 mL). The resulting precipitate was filtered and dried to yield pure compound **8** (1.49 g, 55%) as a white powder.

^{1}H NMR (d_6-DMSO, 400 MHz, 25°C): δ = 9.76 (s, 3H), 7.47 (d, ^3J = 8.8 Hz, 6H), 7.35-7.28 (m, 36H), 7.26-7.18 (m, 9H), 6.88 (d, ^3J = 8.8 Hz, 6H), 2.19 (t, ^3J = 7.2 Hz, 6H), 2.09 (t, ^3J = 7.2 Hz, 6H), 1.49-1.38 (m, 6H), 1.38-1.27 (m, 6H), 1.27-1.15 (m, 6H).

^{13}C NMR (d_6-DMSO, 100 MHz, 25°C): δ = 170.7, 144.6, 142.7, 134.2, 129.1, 127.9, 126.6, 123.5, 120.3, 66.0, 36.1, 31.3, 28.0, 27.8, 24.7.

ESI-MS: m/z calcd. for C$_{93}$H$_{90}$N$_4$O$_3$S$_3$: 1407.63 [M+H]$^+$, found: 1407.85.

*2,3,3-trimethyl-1-(3-sulfonatopropyl)-3H-indolinium-5-sulfonate (**9**)*

9
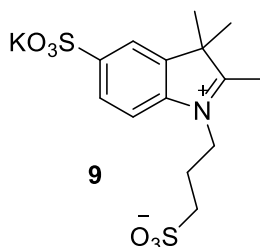
Potassium 2,3,3-trimethyl-3*H*-indole-5-sulfonate (1.49 g, 6.0 mmol) and 1,3-propane sultone (0.8 g, 6.6 mmol) were dissolved in 1,2-dichlorobenzene (10 mL). The reaction mixture was heated to 120 °C and further stirred for 3 days under an argon atmosphere. The mixture was then cooled down to room temperature. The precipitate was then filtered and washed with diethylether (100 mL) to give practically pure compound **9** (0.91 g, 35%) as a red solid.

^{1}H NMR (d_6-DMSO, 400 MHz, 25°C): δ = 8.01 (d, ^4J = 1.2 Hz, 1H), 7.97 (d, ^3J = 8.3 Hz, 1H), 7.81 (dd, ^3J = 8.3 Hz, ^4J = 1.3 Hz, 1H), 4.64 (t, ^3J = 7.9 Hz, 2H), 2.83 (s, 3H), 2.63 (t, ^3J = 6.1 Hz, 2H), 2.20-2.12 (m, 2H), 1.54 (s, 6H).

^{13}C NMR (d_6-DMSO, 100 MHz, 25°C): δ = 197.4, 149.4, 141.6, 141.1, 126.3, 120.7, 114.9, 54.3, 53.5, 47.4, 23.7, 22.0, 13.9.

ESI-MS: m/z calcd. for C$_{14}$H$_{19}$NO$_6$S$_2$: 360.07 [M+H]$^+$, found: 360.08.

*2-((1,3,3-trimethyl-2-methyleneindolin-5-yl)methyl)isoindoline-1,3-dione (**10**)*


10
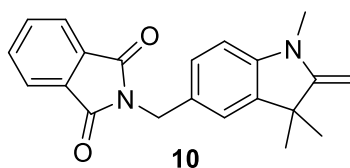
N-hydroxymethylphthalimide (11.80 g, 66 mmol) was added portionwise over a period of 45 min to a stirred solution of Fischer's base (11.53 g, 66 mmol) in concentrated sulphuric acid (60 ml) at room temperature. Upon dissolution of the hydroxymethyl compound, the solution was stirred for 70 hours at room temperature followed by being poured into ice-water. Basification with dilute ammonia (2M, 150 mL) afforded a yellow solid which was shaken up with diethylether (300 mL) to isolate an ether-soluble fraction and an insoluble residue. Both of these fractions were found to be mixtures of two isomeric phthalimides, the ether insoluble fraction consisting predominantly of one isomer. Recrystallization of this solid from ethanol-dichloromethane (100 mL, 4:1) gave compound **10** (11.5 g, 52%) as a yellow powder.

^{1}H NMR (CDCl$_3$, 400 MHz, 25°C): δ = 7.85-7.81 (m, 2H), 7.69-7.67 (m, 2H), 7.26 (dd, ^3J = 8.0 Hz, ^4J = 1.8 Hz, 1H), 7.19 (d, ^4J = 1.7 Hz, 1H), 6.46 (d, ^3J = 8.0 Hz, 1H), 4.76 (s, 2H), 3.82 (s, 2H), 3.00 (s, 3H), 1.31 (s, 6H).

^{13}C NMR (CDCl$_3$, 100 MHz, 25°C): δ = 168.4, 163.1, 146.4, 138.2, 134.0, 132.5, 129.0, 126.7, 123.4, 123.1, 104.8, 73.6, 44.3, 41.9, 30.1, 29.0.

ESI-MS: m/z calcd. for C$_{21}$H$_{20}$N$_2$O$_2$: 333.16 [M+H]$^+$, found: 333.15.

*(1,3,3-trimethyl-2-methyleneindolin-5-yl)methanamine (**11**)*
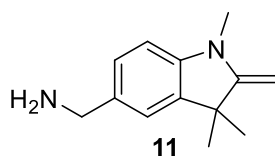
Compound **10** (7.57 g, 22.8 mmol) was heated up to 120 °C in concentrated hydrochloric acid (49 mL). The solution was stirred overnight and then cooled down to room temperature. The precipitate was filtered off and the filtrate was basified with ammonia (120 mL). This aqueous solution was extracted with diethylether (400 mL). The organic phase was evaporated under reduced pressure, yielding compound **11** (4.03 g, 87%) as a yellow viscous oil.

^{1}H NMR (CDCl$_3$, 400 MHz, 25°C): δ = 7.05-7.03 (m, 2H), 6.47 (d, ^3J = 8.4 Hz, 1H), 3.83 (s, 2H), 3.76 (s, 2H), 3.02 (s, 3H), 1.33 (s, 6H).

^{13}C NMR (CDCl$_3$, 100 MHz, 25°C): δ = 163.0, 145.6, 138.1, 132.9, 126.7, 121.2, 104.7, 73.2, 46.3, 44.2, 30.0, 28.9.

ESI-MS: m/z calcd. for C$_{13}$H$_{18}$N$_2$: 203.15 [M+H]$^+$, found: 203.15.

*2-chloro-N-((1,3,3-trimethyl-2-methyleneindolin-5-yl)methyl)acetamide (**12**)*
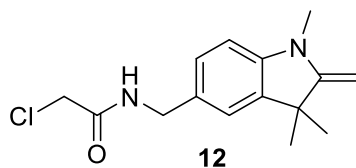
A solution of compound **11** (4.03 g, 19.9 mmol) and triethylamine (2.80 mL, 20.1 mmol) in dichloromethane (125 mL) was added dropwise to a stirred solution of chloroacetyl chloride (1.60 mL, 20.1 mmol) in dichloromethane (20 mL) at 0 °C under an argon atmosphere. After stirring for 90 minutes, the mixture was diluted with dichloromethane (200 mL) and washed twice with 1N hydrochloric acid (1.6 L). Neutralization of the aqueous acidic fraction with a 2N sodium hydroxide solution (800 mL) was followed by extraction with diethylether (2.4 L) and evaporation under vacuum provided compound **12** (4.64 g, 83%) as an oil, which quickly turned reddish purple in air. This oil was used without further purification to prepare compound **14**.

^{1}H NMR (CDCl$_3$, 400 MHz, 25°C): δ = 7.06 (d, ^3J = 8.0 Hz, ^4J = 1.6 Hz, 1H), 7.01 (d, ^3J = 1.4 Hz, 1H), 6.50 (d, ^3J = 7.9 Hz, 1H), 4.40 (d, ^3J = 5.6 Hz, 2H), 4.09 (s, 2H), 3.85 (s, 2H), 3.04 (s, 3H), 1.34 (s, 6H).

ESI-MS: m/z calcd. for C$_{15}$H$_{19}$ClN$_2$O: 279.12 [M+H]$^+$, found: 279.29.

*2-{(E)-2-[Acetyl(phenyl)amino]ethenyl}-3,3-dimethyl-1-(3-sulfonatopropyl)-3H-indolinium-5 -sulfonate (**13**)*
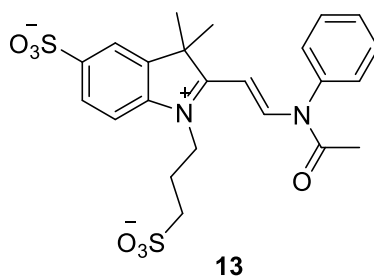
A mixture of compound **9** (1.86 g, 5.2 mmol) and *N,N*-diphenylformamidine (1.86 g, 9.5 mmol) in a 1:2 mixture of acetic acid and acetic anhydride (9.3 mL) was stirred at 120 °C under an argon atmosphere. After two hours, the solvents were evaporated under reduced pressure and the crude residue was washed with acetone until compound **13** was obtained (1.65 g, 63%) as a yellow powder.

^{1}H NMR (d$_6$-DMSO, 400 MHz, 25° C): δ = 8.68 (d, ^3J = 12.2 Hz, 1H), 7.82 (s, 1H), 7.68 (d, ^3J = 7.5 Hz, 1H), 7.58-7.50 (m, 5H), 7.28 (brd, ^3J = 6.8 Hz, 1H), 6.22 (d, ^3J = 12.7 Hz, 1H), 4.23 (brt, ^3J = 6.4 Hz, 2H), 2.62 (t, ^3J = 7.1 Hz, 2H), 2.07-2.03 (m, 2H), 1.71 (s, 6H).

ESI-MS: m/z calcd. for $C_{23}H_{26}N_2O_7S_2$: 507.12 $[M+H]^+$, found: 507.40.

2-{(1E,3Z)-3-[5-(Chloroacetylaminomethyl)-1,3,3-trimethyl-1,3-dihydro-2H-indol-2-ylidene] prop-1-enyl}-1-(3-sulfonatopropyl)-3H-indolium-5-sulfonate (14)


14
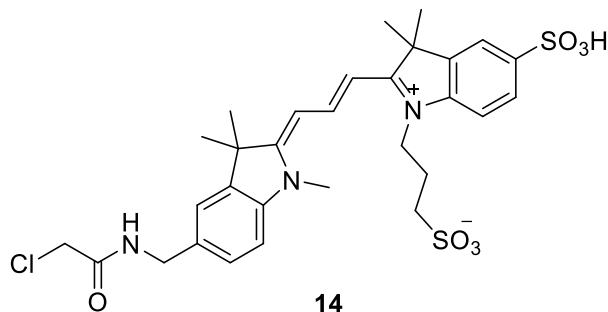
A mixture of compound **13** (1.31 g, 2.6 mmol) and compound **12** (0.72 g, 2.6 mmol) was stirred at 130 ^{o}C in acetic anhydride (24 mL) under argon atmosphere for 45 min. The mixture was then cooled to room temperature, and the resulting precipitate was isolated by filtration. The crude residue was purified by reverse-phase preparative HPLC-MS at a concentration of 100 mg/mL in H_2O to yield pure compound **14** (408 mg, 24%) as a purple solid.

^{1}H NMR (CD$_3$OD, 400 MHz, 25°C): δ=8.54 (t, ^3J = 13.4 Hz, 1H), 7.94-7.88 (m, 2H), 7.52 (d, ^4J = 1.1 Hz, 1H), 7.47-7.39 (m, 2H), 7.37 (d, ^3J = 8.2 Hz, 2H), 6.59 (d, ^3J = 13.3 Hz, 1H), 6.55 (d, ^3J = 13.6 Hz, 1H), 4.49 (s, 2H), 4.35 (brt, ^3J = 7.9 Hz, 2H), 4.11 (s, 2H), 3.73 (s, 3H), 3.00 (t, ^3J = 6.7 Hz, 2H), 2.25 (brt, ^3J = 7.2 Hz, 2H), 1.79 (s, 6H), 1.76 (s, 6H).

^{13}C NMR (CD$_3$OD, 100 MHz, 25°C): δ = 177.8, 175.8, 169.5, 152.6, 144.9, 143.6, 143.4, 142.9, 142.1, 138.2, 129.6, 128.4, 123.0, 121.6, 112.8, 111.8, 105.5, 104.2, 51.0, 50.5, 44.3, 44.1, 43.4, 32.3, 28.5, 28.2, 24.1, 18.5.

ESI-MS: m/z calcd. for $C_{30}H_{36}ClN_3O_7S_2$: 648.15 $[M-H]^-$, found: 648.37.

2-{(1E,3Z)-3-[5-(Iodoacetylaminomethyl)-1,3,3-trimethyl-1,3-dihydro-2H-indol-2-ylidene]pr op-1-enyl}-1-(3-sulfonatopropyl)-3H-indolium-5-sulfonate (15)


15
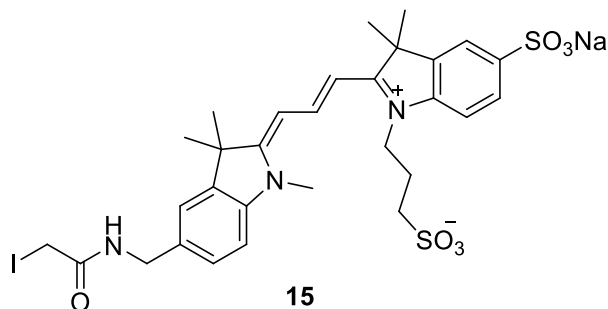
A solution of compound **14** (935 mg, 1.44 mmol) and sodium iodide (1.64 g, 10.92 mmol) in

methanol (67 mL) was heated up to reflux under an argon atmosphere. The reaction was monitored by UPLC-MS. After overnight, the mixture was cooled down to room temperature, filtered and evaporated to provide a purple solid, which was kept under vacuum for the next step.

^{1}H NMR (CD$_3$OD, 400 MHz, 25°C): δ = 8.54 (dd, ^3J = 13.5, 13.5 Hz, 1H), 7.92-7.90 (m, 2H), 7.52 (d, ^3J = 1.1 Hz, 1H), 7.43-7.40 (m, 2H), 7.28 (d, ^3J = 7.7 Hz, 2H), 6.76 (d, ^3J = 13.7 Hz, 1H), 6.76 (d, ^3J = 13.2 Hz, 1H), 4.49 (s, 2H), 4.39 (brt, ^3J = 7.7 Hz, 2H), 3.81 (s, 2H), 3.77 (s, 3H), 3.07 (t, ^3J = 6.9 Hz, 2H), 2.27 (brt, ^3J = 7.6 Hz, 2H), 1.78 (s, 6H), 1.77 (s, 6H).

ESI-MS: m/z calcd. for C$_{30}$H$_{36}$IN$_3$O$_7$S$_2$: 740.09 [M-H]$^-$, found: 740.37.

TACy3 (16)

16
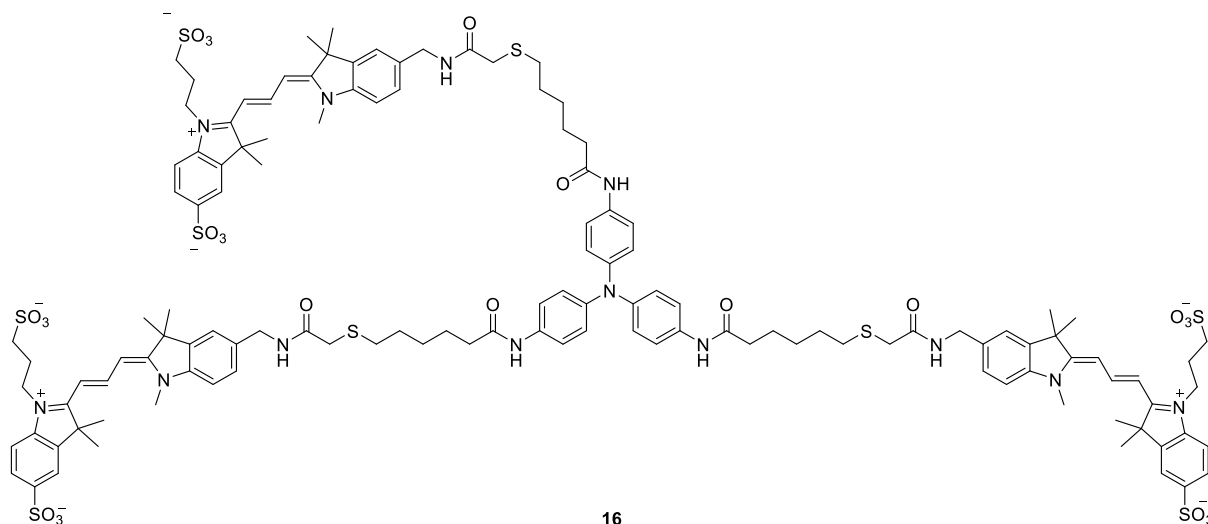
Triethylsilane (12.7 mL) and trifluoroacetic acid (25.4 mL) were added into a solution of compound **8** (507 mg, 0.36 mmol) in dichloromethane (25 mL). The mixture was protected from light and stirred for one hour at room temperature under an argon atmosphere. After that time, solvents were evaporated to give the deprotected tris-thiol triarylamine compound as a white solid. In an oven-dried round bottom flask containing this tris-thiol compound and potassium carbonate (455 mg, 3.30 mmol) was added a solution of crude compound **15** in dimethylformamide (90 mL). The reaction mixture was stirred overnight at room temperature under an argon atmosphere. Further evaporation under reduced pressure followed by reverse-phase preparative HPLC-MS (Column: XBridge Prep C$_{18}$) at concentration of 200 mg/mL in water afforded pure compound **16** (273 mg, 30%) as a purple solid.

^{1}H NMR (CD$_3$OD, 400 MHz, 25°C): δ = 8.47 (dd, ^3J = 13.6 Hz, ^3J = 13.6 Hz, 3H), 7.94-7.88 (m, 6H), 7.52 (s, 3H), 7.44-7.39 (m, 6H), 7.37-7.28 (m, 9H), 6.77 (d, ^3J = 8.9 Hz, 6H), 6.56 (d,

^3J = 6.8 Hz, 3H), 6.52 (d, ^3J = 7.3 Hz, 3H), 4.46 (s, 6H), 4.29 (brt, ^3J = 8.0 Hz, 6H), 3.69 (s, 9H), 2.97 (t, ^3J = 6.6 Hz, 6H), 2.56 (t, ^3J = 7.4 Hz, 6H), 2.31 (t, ^3J = 7.2 Hz, 6H), 2.21 (brt, ^3J = 7.4 Hz, 6H), 1.73 (s, 18H), 1.71 (s, 18 H), 1.63-1.52 (m, 12H), 1.45-1.33 (m, 12H).

^{13}C NMR (CD$_3$OD, 100 MHz, 25°C): δ = 177.8, 175.4, 174.2, 172.9, 152.3, 144.9, 144.3, 143.6, 143.3, 142.8, 142.0, 141.5, 138.8, 129.6, 128.4, 123.2, 121.5, 112.9, 111.7, 105.7, 104.0, 69.0, 51.0, 50.3, 44.2, 37.7, 36.6, 33.5, 32.5, 30.2, 29.4, 28.6, 28.2, 26.4, 24.1.

ESI-MS: m/z calcd. for C$_{126}$H$_{153}$N$_{13}$O$_{24}$S$_9$: 1258.92 [M-2H]$^{2-}$, found: 1258.88.

*TANBE (**17**)*
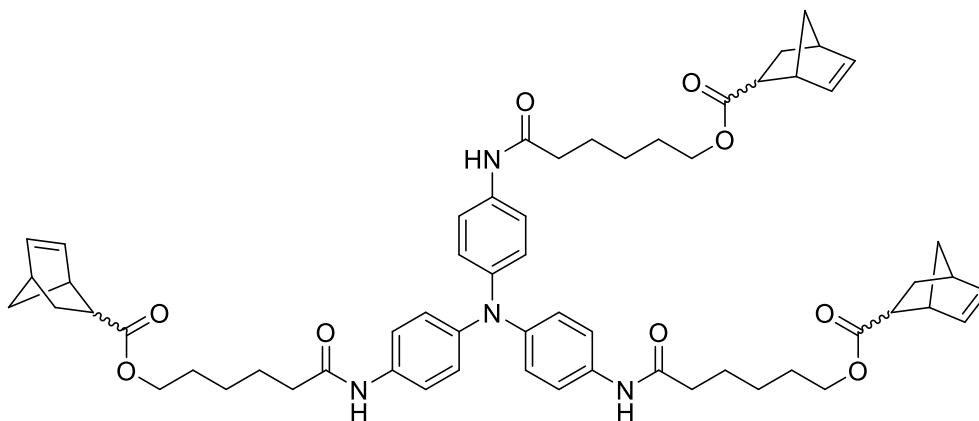
17

An oven-dried flask was charged with 5-norbornene-2-carboxylic acid (0.20 mL, 1.647 mmol) and anhydrous potassium carbonate (0.68 g, 4.941 mmol) in dry dimethylformamide (15 mL) under an argon atmosphere. The reaction mixture was stirred at room temperature for 10 min and then, a solution of compound **7** (150 mg, 0.183 mmol) and a catalytic amount of tetrabutylammonium iodide (20 mg, 0.054 mmol) in dimethylformamide (5 mL) was added. The solution was then stirred at room temperature for 6 hours. After that time, the solvent was evaporated under vacuum. The crude residue was dissolved in ethyl acetate (100 mL) and the organic phase wasextracted with water (200 mL), brine (100 mL) and dried over Na$_2$SO$_4$. Further evaporation under reduced pressure and purification by column chromatography (SiO$_2$, cyclohexane → ethyl acetate/cyclohexane 3:2) provided compound **17** (90 mg, 50%) as a white solid.

R_f = 0.3 (ethyl acetate /cyclohexane 3/2).

^{1}H NMR (CDCl$_3$, 400 MHz, 25°C): δ = 7.43 (s, 3H), 7.33 (d, ^3J = 8.4 Hz, 6H), 6.93 (d, ^3J = 8.4 Hz, 6H), 6.16 (dd, ^3J = 5.6, 3.1 Hz, 2H), 6.13 (dd, ^3J = 5.6, 2.9 Hz, 1H), 6.09 (dd, ^3J = 5.5, 3.0 Hz, 1H), 5.90 (dd, ^3J = 5.7, 2.8 Hz, 2H), 4.08 (t, ^3J = 6.7 Hz, 2H), 4.02 (dd, ^3J = 6.6, 3.1

Hz, 4H), 2.95-2.88 (m, 6H), 2.35 (t, ^3J = 7.4 Hz, 6H), 1.93-1.83 (m, 3H), 1.80-1.71 (m, 6H), 1.71-1.59 (m, 9H), 1.52-1.31 (m, 15H).

^{13}C NMR (CDCl$_3$, 100 MHz, 25°C): δ = 176.5, 175.0, 171.2, 138.2, 137.9, 135.9, 132.5, 64.1, 49.8, 46.8, 46.5, 45.9, 43.5, 43.4, 42.7, 41.8, 37.5, 30.5, 29.4, 28.6, 25.8, 25.4.

ESI-MS: m/z calcd. for C$_{60}$H$_{72}$N$_4$O$_9$: 993.54 [M+H]$^+$, found: 993.68.
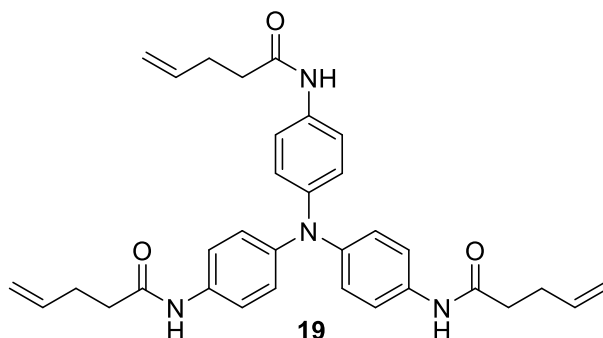
*TAEOS1 (**18**)*

18
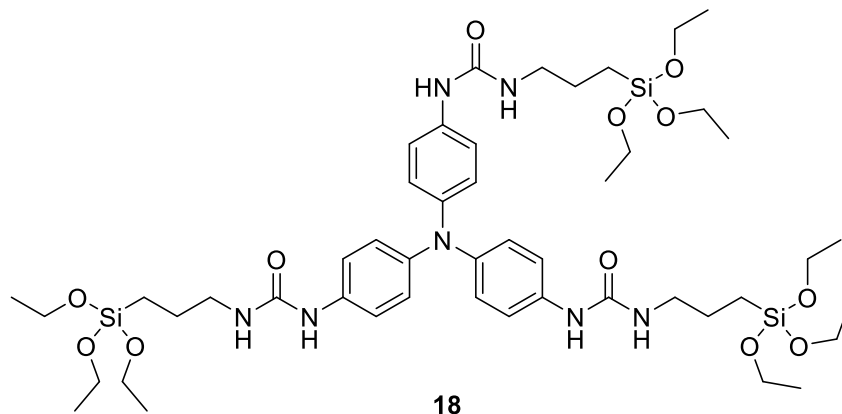
A solution of compound **1** (350 mg, 1.01 mmol) and tin dichloride (2.55 g, 11.3 mmol) in a mixture of acetonitrile (24 mL) and ethanol (16 mL) was stirred overnight at 80 °C under an argon atmosphere. After cooling down to room temperature, the residue was diluted with ethyl acetate (100 mL). The organic phase was extracted with NaHCO$_{3sat}$ (2 × 100 mL) and brine (100 mL), dried over sodium sulfate and then concentrated under vacuum to afford *N,N*-bis(4-aminophenyl)benzene-1,4-diamine, which was pure enough to be used as such in the next step. A solution of this crude compound in dichloromethane (30 mL) was added dropwise to 3-isocyanatopropyltriethoxysilane (1.50 g, 6.06 mmol) under an argon atmosphere. The reaction mixture was stirred overnight at room temperature and then concentrated under vacuum. The crude residue was further purified by column chromatography (SiO$_2$, dichloromethane→ dichloromethane/methanol 10/1) to yield compound **18** (340 mg, 32.6%) as awhite powder.

R_f = 0.3 (dichloromethane /methanol 10/1).

^1H NMR (CD$_3$OD: Toluene 5:3, 400 MHz, 25°C): δ = 7.30 (d, ^3J = 8.8 Hz, 6H), 6.96 (d, ^3J = 8.8 Hz, 6H), 3.78 (q, ^3J = 7.0 Hz, 18H), 3.20 (t, ^3J = 7.0 Hz, 6H), 1.72-1.60 (m, 6H), 1.19 (t, ^3J = 7.0 Hz, 27H), 0.69-0.62 (m, 6H).

^{13}C NMR (CD$_3$OD: Toluene 5:3, 100 MHz, 25°C): δ = 158.5, 144.6, 135.8, 125.5, 121.9, 59.6, 43.5, 24.9, 19.0, 8.6.

ESI-MS: m/z calcd. for C$_{48}$H$_{81}$N$_7$O$_{12}$Si$_3$: 1031.53 [M]$^+$, found: 1031.68.

N,N',N''-(nitrilotris(benzene-4,1-diyl))tris(pent-4-enamide) (19)

A solution of compound **1** (603 mg, 1.72 mmol) and tin dichloride (4.35 g, 19.3 mmol) in a mixture of acetonitrile (23 mL) and ethanol (19 mL) was stirred overnight at 80 °C under an argon atmosphere. After cooling down to room temperature, the solution was diluted with ethyl acetate (150 mL). The organic phase was washed with $NaHCO_{3sat}$ (2 × 100 mL) and brine (100 mL), dried over Na_2SO_4 and then concentrated under reduced pressure to afford *N,N*-bis(4-aminophenyl)benzene-1,4-diamine, which was pure enough to be used as such in the next step. 4-pentenoyl chloride (0.76 mL, 6.9 mmol) was added dropwise to a cooled (0°C) solution of this crude tris-amine and triethylamine (0.95 mL, 5.2 mmol) in dichloromethane (40 mL) under an argon atmosphere. The reaction mixture was heated up slowly to room temperature for 12 hours. The solution was diluted with dichloromethane (100 mL) andthe organic phase was washed with NH_4Cl_{sat} (2 × 100 mL) and brine (100 mL), dried over Na_2SO_4 and concentrated under reduced pressure. The crude residue was washed by dichloromethane (50 mL) yielding compound **19** (872 mg, 94%) as a white solid.

^{1}H NMR (CD$_3$OD, 400 MHz, 25°C): δ = 7.42 (d, ^3J = 8.7 Hz, 6H), 6.96 (d, ^3J = 8.7 Hz, 6H), 5.95-5.83 (m, 3H), 5.10 (d, ^2J = 17.6 Hz, 3H), 5.01 (d, ^2J = 9.9 Hz, 3H), 2.48-2.39 (m, 12H).

^{13}C NMR (CD$_3$OD, 100 MHz, 25°C): δ = 173.7, 145.6, 138.4, 134.9, 125.3, 122.8, 116.0, 37.4, 31.0.

ESI-MS: m/z calcd. for $C_{33}H_{36}N_4O_3$: 536.28 [M+H]$^+$, found: 537.49.

2,5-dioxopyrrolidin-1-yl pent-4-enoate (20)
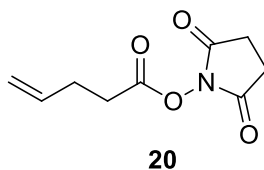
To a solution of *N*-hydroxysuccimide (1.05 g, 9.0 mmol) and triethylamine (1.25 mL, 9.0
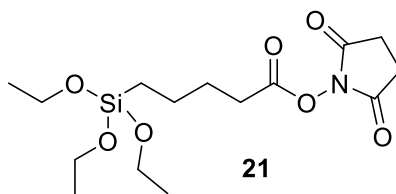
mmol) in dichloromethane (20 mL) cooled at 0 °C was added dropwise 4-pentenoyl chloride (1.0 mL, 9.0 mmol). The reaction mixture was then stirred overnight at room temperature. After evaporation under reduced pressure, the crude residue was purified by column chromatography (SiO$_2$, cyclohexane → dichloromethane/cyclohexane 2:1) to afford compound **20** (1.1 g, 63%) as a colorless oil.

R_f = 0.24 (dichloromethane /cyclohexane 2/1).

^{1}H NMR (CDCl$_3$, 400 MHz, 25°C): δ = 5.85 (ddt, ^3J = 17.0, 10.4, 6.5 Hz, 1H), 5.13 (dd, ^2J = 17.1 Hz, ^3J = 1.5 Hz, 1H), 5.09 (dd, ^2J = 10.2 Hz, ^3J = 1.3 Hz, 1H), 2.82 (s, 4H), 2.71 (t, ^3J = 7.3 Hz, 2H), 2.54-2.45 (m, 2H).

^{13}C NMR (CDCl$_3$, 100 MHz, 25°C): δ = 169.3, 168.2, 135.4, 116.8, 30.5, 28.5, 25.8.

*2,5-dioxopyrrolidin-1-yl 5-(triethoxysilyl)pentanoate (**21**)*

21

To a solution of compound **20** (100 mg, 0.507 mmol) and Karstedt catalyst (10 µL) in dry toluene (5 mL) under an argon atmosphere was added dropwise triethoxysilane (187 µL, 1.014 mmol). The reaction mixture was then stirred overnight at room temperature. After concentration under reduced pressure, the crude residue was purified by column chromatography (SiO$_2$, cyclohexane → dichloromethane/cyclohexane 2:1) to yield compound **21** (125 mg, 68%) as a colorless oil.

R_f = 0.3 (dichloromethane/cyclohexane 2/1).

^{1}H NMR (CDCl$_3$, 400 MHz, 25°C): δ = 3.82 (q, ^3J = 7.0 Hz, 6H), 2.83 (brs, 4H), 2.61 (t, ^3J = 7.6 Hz, 2H), 1.85-1.74 (m, 2H), 1.59-1.49 (m, 2H), 1.22 (t, ^3J = 7.0 Hz, 9H), 0.66 (t, ^3J = 8.3 Hz, 2H).

^{13}C NMR (CDCl$_3$, 100 MHz, 25° C): δ=169.3, 168.8, 59.4, 30.8, 27.9, 25.8, 22.5, 18.3, 10.3.

*TAEOS2 (**22**)*

22
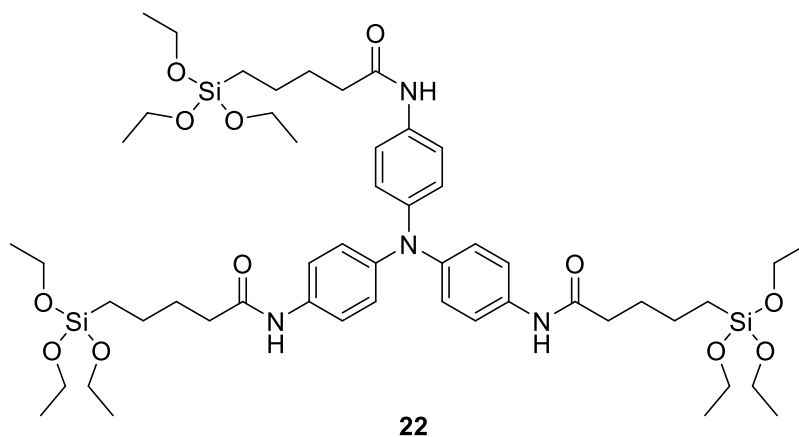
A solution of compound **1** (35.0 mg, 0.101 mmol) and tin dichloride (255 mg, 1.13 mmol) in a mixture of acetonitrile (2.4 mL) and ethanol (1.6 mL) was stirred overnight at 80 °C under an argon atmosphere. After cooling down to room temperature and evaporation under reduced pressure, the residue was diluted with ethyl acetate (10 mL). The organic phase was extracted with NaHCO$_{3sat}$ (2 × 10 mL) and brine (10 mL), dried over sodium sulfate and concentrated under vacuum to afford *N,N*-bis(4-aminophenyl)benzene-1,4-diamine, which was pure enough to be used as such in the next step. To a solution of this crude compound and *N,N*-diisopropylethylamine (58 µL, 0.348 mmol) in tetrahydrofuran (5 mL) was added compound **21** (115 mg, 0.316 mmol). The reaction mixture was stirred at 65 °C under argon atmosphere. The reaction was monitored by UPLC-MS and additional compound **21** (50 mg, 25 mg and 20 mg) was added into the solution every 24 hours. After that time, the reaction mixture was diluted with dichloromethane (50 mL). The organic phase was extracted with NH$_4$Cl$_{sat}$ (2 × 100 mL), NaHCO$_{3sat}$ (2 × 100 mL) and brine (100 mL), dried over sodium sulfate and concentrated under vacuum. The crude residue was washed several times with cyclohexane (50 mL) to yield compound **22** (55 mg, 53 %) as a pale brown solid.

^{1}H NMR (CD$_3$OD, 400 MHz, 25°C): δ = 7.42 (d, ^3J = 8.9 Hz, 6H), 6.94 (d, ^3J = 8.9 Hz, 6H), 3.81 (q, ^3J = 7.0 Hz, 18H), 2.36 (t, ^3J= 7.4 Hz, 6H), 1.79-1.69 (m, 6H), 1.56-1.45 (m, 6H), 1.20 (t, ^3J = 7.0 Hz, 27 H), 0.67 (t, ^3J = 8.2 Hz, 6H).

^{13}C NMR (CD$_3$OD, 100 MHz, 25°C): δ = 174.5, 145.6, 135.0, 125.3, 122.7, 59.6, 37.7, 30.4, 28.1, 23.7, 18.8, 11.2.

ESI-MS: m/z calcd. for C$_{51}$H$_{84}$N$_4$O$_{12}$Si$_3$: 1028.54 [M+H]$^+$, found: 1028.07.

Typical procedure for PTANBE covalent polymer
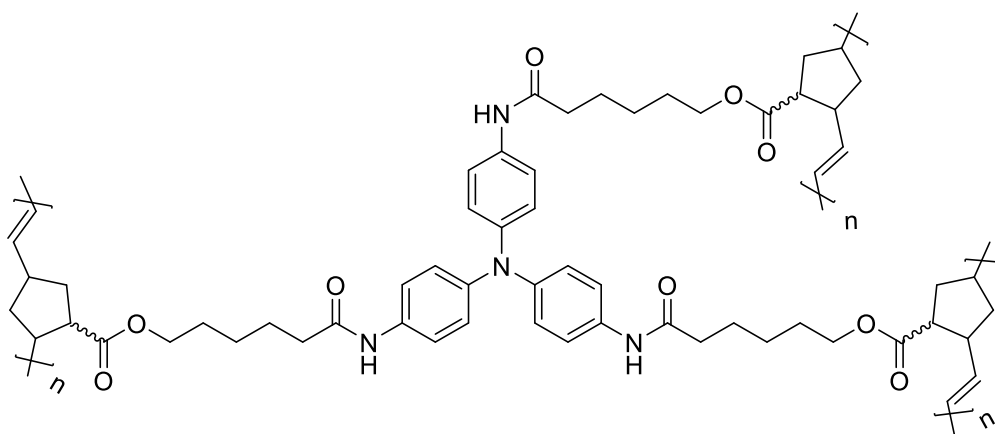
In an oven-dried schlenck tube, a solution of compound **17** (21.1 mg, 0.021 mmol) in dichloromethane (10.6 mL) was stirred under argon atmosphere. This solution was irradiated with white light for one hour. After the addition of benzylidene-bis (tricyclohexylphosphine)dichlororuthenium (first generation Grubbs catalyst) (5.3 mg, 0.0064 mmol), the reaction mixture was stirred at room temperature for another four hours. The reaction was then quenched by adding ethyl vinyl ether (2 mL). The solvent was evaporated under vacuum and washed by methanol to afford covalent polymer PTANBE (15.0 mg, 71%) as a brown solid.

PTANBE1 covalent polymer (23)

^{1}H NMR (d_8-THF, 400 MHz, 25°C): δ = 9.63-8.67 (brs, 3H), 7.79-7.23 (brs, 6H), 7.07-6.66 (brs, 6H), 5.68-5.04 (brs, 6H), 4.28-3.77 (brs, 6H), 3.04-2.62 (brs, 8H), 2.55-2.17 (brs, 7 H), 2.17-1.52 (brm, 14H), 1.52-1.01 (brm, 15 H).

GPC: PDI = 10.31, M_n = 6607, M_w = 68128.

PTANBE2 covalent polymer (24)

Compound **17** (19.9 mg, 0.020 mmol), first generation Grubbs catalyst (5.02 mg, 0.006 mmol) in a 9:1 mixture of tetrahydrofuran/dichloromethane (10 mL) without light irradiation.

PTANBE2 (16.2 mg, 81%).

^{1}H NMR (d_8-THF, 400 MHz, 25°C): δ = 9.42-8.78 (brs, 3H), 7.82-7.37 (brs, 6H), 7.04-6.75 (brs, 6H), 5.62-5.04 (brs, 6H), 4.27-3.67 (brs, 6H), 3.01-2.62 (brs, 8H), 2.44-2.17 (brs, 7 H), 2.17-1.52 (brm, 14H), 1.52-1.03 (brm, 15 H).

GPC: PDI = 3.26, M_n = 4540, M_w = 14807.

PTANBE3 covalent polymer (25)

Compound **17** (19.2 mg, 0.019 mmol), first generation Grubbs catalyst (4.84 mg, 0.0058 mmol) in a 9:1 mixture of toluene/dichloromethane (9.6 mL) with light irradiated for one hour.
PTANBE3 (13.5 mg, 70%), which is insoluble in any solvent.

PTANBE4 covalent polymer (26)

Compound **17** (21.3 mg, 0.0213 mmol), first generation Grubbs catalyst (5.37 mg, 0.0064 mmol) in toluene (10.7 mL) without light irradiation.
PTANBE4 (11.4 mg, 54%), which is insoluble in any solvent.

PTANBE5 covalent polymer (27)

Compound **17** (18.7 mg, 0.019 mmol), first generation Grubbs catalyst (4.72 mg, 0.0056 mmol) in dichloromethane (9.4 mL) without light irradiation.
PTANBE5 (14.4 mg, 77%).
^{1}H NMR (d_8-THF, 400 MHz, 25°C): δ = 9.60-8.77 (brs, 3H), 7.73-7.36 (brs, 6H), 7.03-6.74 (brs, 6H), 5.71-5.02 (brs, 6H), 4.33-3.71 (brs, 6H), 3.20-2.39 (brs, 8H), 2.39-2.11 (brs, 7 H), 2.11-1.52 (brm, 14H), 1.52-1.00 (brm, 15 H).
GPC: PDI = 5.11, M_n = 7340, M_w = 37497.

PTANBE6 covalent polymer (28)

Compound **17** (19.8 mg, 0.019 mmol), first generation Grubbs catalyst (4.99 mg, 0.006 mmol) in tetrahydrofuran (9.95 mL) without light irradiation.
PTANBE6 (12.1 mg, 61%).
^{1}H NMR (d_8-THF, 400 MHz, 25°C): δ = 9.47-8.79 (brs, 3H), 7.89-7.35 (brs, 6H), 7.03-6.74 (brs, 6H), 5.63-5.03 (brs, 6H), 4.38-3.3.69 (brs, 6H), 3.05-2.63 (brs, 8H), 2.42-2.18 (brs, 7 H), 2.13-1.52 (brm, 14H), 1.52-1.01 (brm, 15 H).
GPC: PDI = 5.20, M_n = 5082, M_w = 26423.

PTANBE7 covalent polymer (29)

Compound **17** (22.2 mg, 0.022 mmol), third generation Grubbs catalyst ([1,3-Dimesityl-2-imidazolidinylidene]dichloro(phenylmethylene)bis(3-bromopyridine)ruthenium(II)) (5.92 mg, 0.0067 mmol) in dichloromethane (11 mL) with light irradiation for one hour.
PTANBE7 (11.6 mg, 52%), which is insoluble in any solvent.

*PTANBE8 covalent polymer (**30**)*

Compound **17** (18.7 mg, 0.0187 mmol), third generation Grubbs catalyst (4.99 mg, 0.0056 mmol) in a 9:1 mixture of tetrahydrofuran/dichloromethane (9.4 mL) with light irradiation for one hour.

PTANBE8 (17.2 mg, 92%).

^{1}H NMR (d_8-THF, 400 MHz, 25°C): δ = 9.54-8.87 (brs, 3H), 7.80-7.34 (brs, 6H), 7.10-6.66 (brs, 6H), 5.65-4.92 (brs, 6H), 4.42-3.69 (brs, 6H), 3.24-2.49 (brs, 8H), 2.49-2.14 (brs, 7 H), 2.09-1.52 (brm, 14H), 1.52-1.05 (brs, 15 H).

GPC: PDI = 1.65, M_n = 6828, M_w = 11279.

*PTANBE9 covalent polymer (**31**)*

Compound **17** (20.7 mg, 0.0207 mmol), third generation Grubbs catalyst (5.52 mg, 0.0062 mmol) in tetrahydrofuran (10.4 mL) without light irradiation.

PTANBE9 (12.4 mg, 60%).

^{1}H NMR (d_8-THF, 400 MHz, 25°C): δ = 9.55-8.84 (brs, 3H), 7.82-7.33 (brs, 6H), 7.09-6.66 (brs, 6H), 5.69-4.87 (brs, 6H), 4.40-3.52 (brs, 6H), 3.23-2.40 (brs, 8H), 2.40-2.11 (brs, 7 H), 2.09-1.50 (brm, 14H), 1.50-1.05 (brm, 15 H).

GPC: PDI = 1.88, M_n = 4556, M_w = 8552.

*PTANBE10 covalent polymer (**32**)*

Compound **17** (20.6 mg, 0.0206 mmol), third generation Grubbs catalyst (5.49 mg, 0.0062 mmol) in dichloromethane (10.3 mL) without light irradiation.

PTANBE10 (13.5 mg, 66%), which is insoluble in any solvent.

*PTANBE11 covalent polymer (**33**)*

Compound **17** (23.0 mg, 0.023 mmol), third generation Grubbs catalyst (0.62 mg, 0.0007 mmol) in dichloromethane (11.5 mL) without light irradiation.

PTANBE11 (12.1 mg, 53%), which is insoluble in any solvent.

*PTANBE12 covalent polymer (**34**)*

Compound **17** (18.4 mg, 0.018 mmol), third generation Grubbs catalyst (4.91 mg, 0.0056 mmol) in dichloromethane (92 mL) without light irradiation.

PTANBE12 (15.6 mg, 85%).

^{1}H NMR (d_8-THF, 400 MHz, 25°C): δ = 9.69-8.84 (brs, 3H), 7.85-7.33 (brs, 6H), 7.10-6.69

(brs, 6H), 5.68-4.96 (brs, 6H), 4.40-3.59 (brs, 6H), 3.31-2.48 (brs, 8H), 2.45-2.14 (brs, 7 H), 2.13-1.53 (brm, 14H), 1.53-0.93 (brm, 15 H).

GPC: PDI = 2.33, M_n = 4220, M_w = 9843.

PTANBE13 covalent polymer (35)

Compound **17** (14.6 mg, 0.015 mmol), third generation Grubbs catalyst (3.90 mg, 0.0044 mmol) in dichloromethane (292 mL) without light irradiation.

PTANBE13 (13.4 mg, 92%).

^{1}H NMR (d_8-THF, 400 MHz, 25°C): δ = 9.37-8.70 (brs, 3H), 7.73-7.35 (brs, 6H), 7.10-6.72 (brs, 6H), 5.63-4.85 (brs, 6H), 4.34-3.70 (brs, 6H), 3.00-2.56 (brs, 8H), 2.53-2.10 (brs, 7 H), 1.85-1.36 (brm, 14H), 1.36-0.76 (brm, 15 H).

GPC: PDI = 1.42, M_n = 4816, M_w = 6856.

*Typical synthesis of TANBE Gel (procedure for **Gel1**)*

In a vial, compound **17** (3.8 mg, 0.0038 mmol) in toluene (0.255 mL) was heated up to 90°C for 10 minutes and then cooled down to room temperature, leading to an homogeneous mixture. After addition of a solution of third generation Grubbs catalyst (1.1 mg, 0.00117 mmol) in toluene (0.127 mL), the mixture was shaken overnight at room temperature. Ethyl vinyl ether (0.38 mL) was added into the gel to quench the reaction and the vial was shaken for four hours. The resulting gel was washed several times with methanol (5 mL) and then methanol was exchanged by toluene after several washings.

Gel2: Compound **17** (3.9 mg, 0.0039 mmol) in a 9:1 mixture of toluene/tetrachloroethane (0.262 mL), third generation Grubbs catalyst (1.1 mg, 0.00120 mmol) in toluene (0.130 mL).

Gel3: Compound **17** (3.9 mg, 0.0039 mmol) in a 9:1 mixture of toluene/tetrachloroethane (0.262 mL), third generation Grubbs catalyst (1.1 mg, 0.00120 mmol) in toluene (0.130 mL).

*Synthesis of **Gel4***

In a vial, compound **18** (15 mg, 0.0145 mmol) was dissolved in a 1:1 mixture of dichloromethane/methanol (250 μL). Benzylamine (14.3 μL, 0.131 mmol) and deionized water (4.7 μL, 0.261 mmol) were added into the solution. The mixture was shaken for 10 minutes and then kept at room temperature under static conditions for 5 days to yield **Gel4**.

*Synthesis of **Gel5***

In a vial, compound **18** (15 mg, 0.0145 mmol) was dissolved in a 1:1 mixture of dichloromethane/methanol (250 μL). After exposure to light for 60 minutes, benzylamine (14.3 μL, 0.131 mmol) and deionized water (4.7 μL, 0.261 mmol) were added into the solution. The mixture was shaken for 10 minutes and then kept at room temperature under static conditions for 3 days to yield **Gel5**.

*Synthesis of **Gel6***

In a vial, compound **21** (13.5 mg, 0.0131 mmol) was dissolved in chloroform (225 μL). Benzylamine (12.9 μL, 0.118 mmol) and deionized water (4.2 μL, 0.233 mmol) were added into the solution. The mixture was shaken for 10 minutes and then kept at room temperature under static conditions for 13 days to yield **Gel6**.

*Synthesis of **Gel7***

In a vial, compound **21** (15.7 mg, 0.0152 mmol) was dissolved in chloroform (262 μL). After exposure to light for 60 minutes, benzylamine (13.5 μL, 0.1371 mmol) and deionized water (4.4 μL, 0.274 mmol) were added into the solution. The mixture was shaken for 10 minutes and then kept at room temperature under static conditions for 16 days to yield **Gel7.**